Organically-Modified Clay Minerals in Oil Sands: Characterization and Effect of Hydrothermal Treatment

by

Qiang Chen

A thesis submitted in partial fulfillment of the requirements for the degree of

Doctor of Philosophy

in

Chemical Engineering

Department of Chemical and Materials Engineering
University of Alberta

Abstract

The intimate association between bitumen components and clay minerals is an important feature of oil sands fine solids. These organically-modified clay minerals cause serious problems in Canadian oil sands production: hindering bitumen extraction, stabilizing water-in-bitumen emulsions, fouling upgrading equipment, and contributing to the formation of indefinitely-stable mature fine tailings suspensions. In the present work, the irreversible adsorption of asphaltenes from toluene solutions onto kaolinite was studied as a model system for the unextractable adsorption of bitumen components on clay mineral. Native clay minerals obtained from Athabasca bitumen froth, with and without a hydrothermal treatment (at 300–420°C), were examined by several techniques including quantitative nanomechanical mapping atomic force microscopy (QNM-AFM) and X-ray photoelectron spectroscopy (XPS). The effect of the hydrothermal treatment on the organically-modified clay minerals and the consequent changes in their emulsification and filtration behaviors were investigated.

The adsorption of asphaltenes on kaolinite was confirmed to be a largely irreversible process, based on the observation that circa 80% of asphaltenes remained adsorbed on kaolinite even after thorough toluene washing. The irreversibility of asphaltene adsorption is consistent with the presence of unextractable organic matter by toluene in oil sands fine solids reported in the literature. Thermal dehydroxylation enhanced the adsorption capacity of kaolinite for asphaltenes. The XPS-determined percent surface coverage was 18% and 41% on the untreated and dehydroxylated kaolinite, respectively, corresponding to a maximum adsorption density of 3 and 7 mg/m^2. The incomplete surface coverage even at the highest adsorption density indicated the patchy characteristics of adsorbed asphaltenes on both kaolinite substrates. Analogously, patches

of organic matter were also observed on the native clay minerals in oil sands, as indicated by the inhomogeneous spatial distribution of adhesion force on the surfaces of platy particles (determined by QNM-AFM). The surface coverage and mean domain thickness of the organic coating on the clay basal faces were estimated to be 17±6% and 1.4 nm, respectively. In addition to this patchy organic coating, there were organic materials trapped in the oil-mineral aggregates. These trapped organics were found to be softer (more deformable) than the asphaltene fraction of oil sands bitumen.

Hydrothermal treatment at 390°C increased the surface carbon concentration of the fine solids in bitumen froth from 36 to 47 atom% (determined by XPS), but reduced their total organic carbon content from 15 to 10 wt% (determined by bulk elemental analysis). The hydrothermally-treated fine solids became more uniformly hydrophobic and more active in stabilizing emulsions. The volume of the produced emulsions was found to increase linearly and monotonically with the proportion of a specific sub-fraction of the fine solid particles with a critical surface tension of 27–30 mN/m (determined by the film flotation method), likely because of their intermediate hydrophobicity and thus relatively stronger emulsifying capacity.

The filterability of the bitumen froth fine solids was enhanced after the hydrothermal treatment, as shown by both room-temperature filtration and *in-situ* hot filtration (at ~200°C) tests. Based on this observation, a conceptual bitumen froth cleaning approach is proposed, which combines the hydrothermal treatment of bitumen froth, water separation by venting, and solids removal by *in-situ* hot filtration. The small-scale laboratory tests using 500-mL Parr reactors and 0.5-μm pore size stainless steel filters showed that this procedure was able to reduce the fine solids content from 8 wt% in the original bitumen froth to 0.08 wt% in the bitumen product.

Preface

Below is a statement of my contributions to co-authored papers contained in this thesis.

(1) Q. Chen, J. Liu, T. Thundat, M.R. Gray, Q. Liu, Spatially resolved organic coating on clay minerals in bitumen froth revealed by atomic force microscopy adhesion mapping, *Fuel* 191 (2017) 283-289 (Chapter 4 of this thesis). I contributed to design and perform the experiments, analyze the data, and write the paper draft. J. Liu and T. Thundat provided technical support and contributed to manuscript editing. M.R. Gray and Q. Liu were the supervisory authors and contributed to experiment design, data interpretation, and manuscript composition.

(2) Q. Chen, I. Stricek, M.R. Gray, Q. Liu, Influence of hydrophobicity distribution of particle mixtures on emulsion stabilization, *Journal of Colloid and Interface Science* 491 (2017) 179-189 (Chapter 5 of this thesis). I contributed to the experiment design, data collection/analysis, and manuscript composition. I. Stricek was deeply involved in the hydrothermal treatment experiments. M.R. Gray and Q. Liu were the supervisory authors and significantly contributed to data interpretation and paper critics.

(3) Q. Chen, I. Stricek, M. Cao, M.R. Gray, Q. Liu, Influence of hydrothermal treatment on filterability of fine solids in bitumen froth, *Fuel* 180 (2016) 314-323 (Chapter 6 of this thesis). I contributed to design and perform the experiments, analyze the data, and draft the manuscript. I. Stricek and M. Cao contributed to experiment design and data collection. M.R. Gray and Q. Liu were the supervisory authors and were involved with concept formation and manuscript composition.

(4) Q. Chen, M.R. Gray, Q. Liu, Irreversible adsorption of asphaltenes on kaolinite: Influence of dehydroxylation, submitted to *Energy & Fuels* (Chapter 3 of this thesis). I contributed to experiment design, data collection, and manuscript composition. M.R. Gray and Q. Liu were the supervisory authors and contributed to design the experiments, interpret the data, and edit the manuscript.

Acknowledgements

I express my sincere gratitude and appreciation to my supervisors, Dr. Murray R. Gray and Dr. Qi Liu, for their dedicated advice, encouragement, inspiration, and support. Without their guidance and significant input, this thesis work would have not been possible.

I would like to thank Igor Stricek, Mingli Cao, and Jun Zhao for their contribution in performing hydrothermal reactions. Their suggestions and help on various issues are greatly appreciated.

I am thankful to Dr. Thomas Thundat for allowing me to use the atomic force microscopy equipment in his laboratory. I also would like to thank Jun Liu for the equipment trainings.

I would like to thank Xiaoli Tan, Lisa Brandt, Jeremiah Bryksa, Yahui Zhang, and Brittany Mackinnon for their technical support.

I am grateful to Dimitre Karpuzov and Shihong Xu for their suggestions and technical support in X-ray photoelectron spectroscopy measurements. I thank Paul Concepcion for his help and suggestions in performing cryo-SEM tests.

I would like to acknowledge the financial support from the Institute for Oil Sands Innovation (IOSI) at the University of Alberta and the Natural Sciences and Engineering Research Council of Canada (NSERC).

Finally, I would like to express my heartfelt thanks to my parents, Jifang Zhou and Xiuhe Chen, for their endless support, encouragement, and love.

Table of Contents

List of Tables

List of Figures

1 Introduction

1.1 Background

1.1.1 Alberta Oil Sands

The Alberta oil sands in Canada, the third-largest proven oil reserve in the world after Venezuela and Saudi Arabia, contributed 2.4 million barrels of crude oil per day to global demand in 2016, and the Alberta production is forecasted to increase to 3.7 million barrels per day by 2030 [1]. As reported by Alberta Energy Regulator in May 2017 [2], the Alberta oil sands contain remaining established reserves of 165 billion barrels, of which 32 billion barrels (19%) are considered recoverable by surface mining and warm-water extraction, and 133 billion barrels (81%) can be recovered using *in-situ* techniques, such as steam-assisted gravity drainage (SAGD).

1.1.2 Bitumen Recovery from Oil Sands

Surface mining is applied in relatively shallow oil sands deposits (less than ~75 m of overburden) [3]. The typical surface-mineable oil sands in Alberta contain 9−13 wt% bitumen, 80−85 wt% mineral solids (mainly clays and quartz), and 3−7 wt% water [3, 4]. Bitumen is a highly viscous liquid or semi-solid form of petroleum. As illustrated in Figure 1.1, warm-water extraction is currently commercially used to extract bitumen from the oil sands. In a surface mining operation, the oil sands are mined using shovels and trucks. The mined oil sands are crushed and mixed with caustic warm water (40−55°C [5]) to liberate the bitumen from the sands and clay. The mixed oil sands slurry is sent to a large gravity separation vessel through hydrotransport pipelines where the oil sands ore is “conditioned”. Entrained or introduced air attaches to bitumen and the aerated bitumen floats to the top of the vessel, forming a bitumen

froth layer which typically contains 60 wt% bitumen, 30 wt% water, and 10 wt% fine solids [6]. Meanwhile, most of the inorganic solids settle to the bottom, forming a waste stream known as tailings. A typical overall bitumen recovery in commercial operations is about 88−95% in the warm-water extraction process [5]. After bitumen froth treatment which removes fine solids and water, the bitumen is sent to upgraders to produce a lighter crude oil. This crude oil product is then shipped to refineries for further processing to produce final products such as fuels, lubricants, and petrochemicals [5, 7]. The tailings, on the other hand, are discharged to the tailings pond for solid-liquid separation.

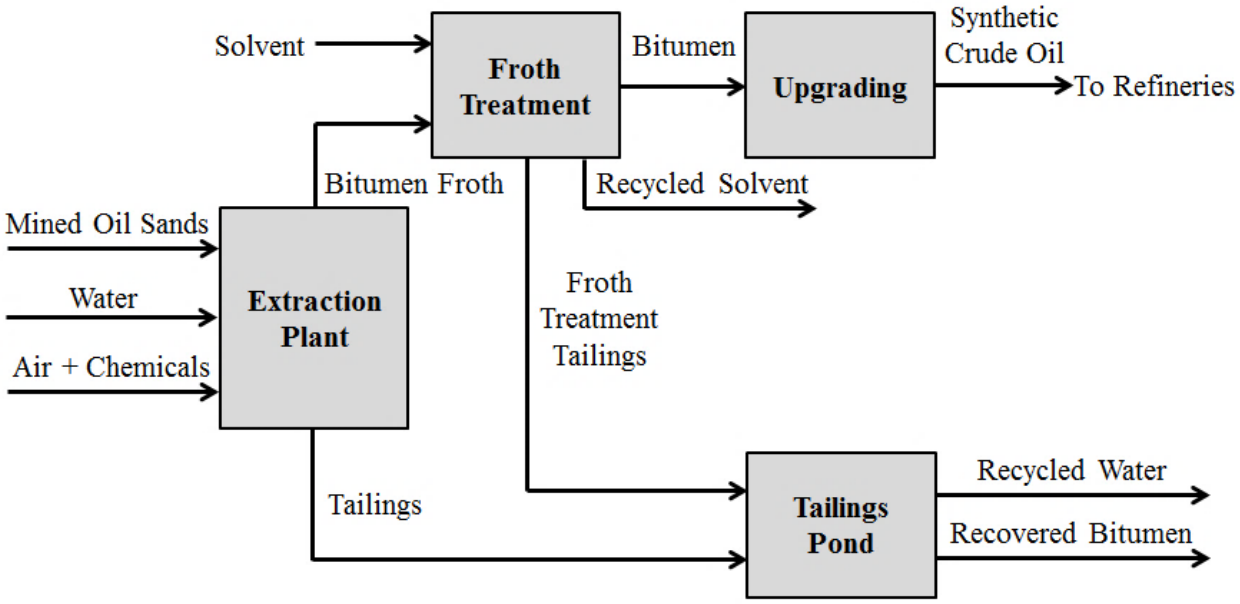

Figure 1.1 Simplified scheme for oil sands processing using a warm-water extraction method (adapted from Masliyah et al. [5]).

Because of the potential advantages such as reduction in fresh water demand, elimination of tailings pond, and high bitumen recovery, non-aqueous bitumen extraction processes have been studied in the past several decades, where organic solvents, such as naphtha and cyclohexane,

were proposed to be used to dissolve and separate the bitumen from oil sands and clays [8-12]. A recent review by Lin et al. [13] presents a comprehensive summary of advances in non-aqueous extraction. Unfortunately, these proposed non-aqueous extraction processes have not been used commercially because of the obstacles such as difficulties in removing the fine solids from extracted bitumen and poor solvent recovery from the extraction gangue [10-13].

In-situ bitumen recovery is used when the overburden above the oil sands formations are too thick for economical mining operations (more than ~75 m) [3]. SAGD is currently used in commercial *in-situ* operations. In this process, a pair of horizontal wells are drilled into the oil sands formation, one a few meters above the other. Steam is injected into the upper well to heat the surrounding oil sands and reduce the viscosity of bitumen. The mobilized bitumen, together with condensed steam, drains into the lower well, where it is pumped to the surface.

1.1.3 Organically-Modified Clay Minerals

The recovered bitumen from oil sands is usually contaminated with solids, which can cause problems in a variety of ways [3]. As reported by Sparks et al. [14], the bulk solids in oil sands, i.e., coarse sand grains (>44 μm), are "inert" as they only inadvertently participate in bitumen separation processes through physical means such as mechanical entrainment. These coarse solids do not cause problems in either surface mining or *in-situ* recovery processes [4, 8]. The fine solids, on the other hand, have a significant detrimental effect [3, 14, 15].

In the oil sands context, fine solids are defined as mineral particles with diameters of less than 44 μm, mainly clay minerals with kaolinite and illite being the most abundant [7, 16]. These fine clay minerals are often associated with a significant amount of irreversibly-adsorbed bitumen-derived organic matter, which is not extractable with common organic solvents (such as toluene)

[14, 17]. The intimate association of bitumen components with clay particles is one of the fundamental features of oil sands fine solids. “How the organic matter is bound to mineral matrix” and “what type of structure is formed” are questions of particular importance but also of great complexity, which will be further discussed in the literature review (Section 2.1).

The irreversible adsorption of bitumen-derived organic matter may dramatically change the clay minerals, both physically and chemically, and hence lead to significantly different particle behaviors. For instance, although inorganic clay minerals are naturally water-wet, their surface wettability is often altered to be bi-wet or even oil-wet by the adsorption of hydrocarbons such as asphaltenes, resins, or humic materials [14, 18, 19]. This alteration of their surface properties can significantly affect the particle separation behavior, since the wettability of the fine particles determines their partition to organic phase, aqueous phase, or organic/aqueous interface [5, 20, 21]. Therefore, cautions need to be taken when applying general knowledge of clay mineral standards to the oil sands-derived clay minerals, due to the organic modification in the latter case.

These organically-modified clay minerals in oil sands cause serious problems during bitumen production. In warm-water extraction, bitumen aeration, a process where bitumen droplets attach to air bubbles to achieve effective flotation, essentially determines the bitumen recovery [5, 15]. The organically-modified clay minerals can adsorb on bitumen droplet surfaces and lower the probability for bitumen-air attachment, thereby hindering bitumen aeration and adversely affecting bitumen recovery and bitumen froth product quality. Formation of stable water-in-oil emulsions poses a major challenge for bitumen cleaning. The emulsified water may cause corrosion problems for pipelines and downstream operations due to the dissolved salts [3, 22]. The organically-modified clay minerals significantly contribute to stabilize these emulsions

because of their bi-wettability [21, 23]. Moreover, the presence of these clay minerals may exacerbate the fouling problems in downstream processes, such as upgrading and refining [7]. In tailings management, the clay minerals are largely responsible for the formation of a stable gel-like structure, resulting in poor dewatering and consolidation of mature fine tailings [24]. Based on these observations, the content of organically-modified fine solids in an oil sands ore is believed to be a good predictor for ore processability [3, 14].

Extensive efforts have been devoted to developing methods capable of removing these problematic clay minerals from bitumen streams [25, 26]. Currently, two processes are used commercially to treat bitumen froth in the Alberta oil sands industry: naphthenic froth treatment (NFT, used by Canadian Natural Resources Limited, Suncor Energy Incorporated, and Syncrude Canada Limited) and paraffinic froth treatment (PFT, used by Shell Canada Limited and Imperial Oil Limited) [26]. Each process has its own disadvantages: NFT cannot generate bitumen product meeting pipeline or market specifications, and PFT gives a significant reduction in bitumen recovery (see Chapter 6 for a more detailed description). Alternative technologies for bitumen froth cleaning are desirable if they can effectively remove the fine solids and reduce hydrocarbon loss.

Thermal conversion is the most popular choice worldwide for processing heavy feedstocks such as bitumen, because of its low operating and capital costs [7]. Although the thermal properties of bitumen have been well documented, the thermal behaviors of organically-modified clay minerals in the presence of bitumen materials are rarely studied [27, 28], much less in the presence of both hydrocarbons and water [29]. Here the term of "hydrothermal treatment" is used to indicate direct thermal processing of bitumen froth (a mixture of bitumen, water, and fine clays) at elevated temperature (up to 450°C) rather than the current approach of a froth treatment

step followed by the upgrading step (Figure 1.1), which reduces the number of process steps. Zhao et al. [29] found that hydrothermal treatment of bitumen froth could make the contained fine clays easier to filter. This observation is encouraging, but many questions still remain unanswered. For example, what is the underlying mechanism for the filterability improvement after hydrothermal treatment of the bitumen froth? How to integrate hydrothermal treatment with commercial solid-liquid separation techniques to generate a viable process for cleaning bitumen froth? Therefore, a more detailed investigation of the properties and behaviors of the organically-modified clay minerals after hydrothermal treatment is required.

1.2 Research Objectives and Working Hypotheses

The research objective of this PhD dissertation is to characterize the organically-modified clay minerals in bitumen froth and to investigate the changes in their structures and behaviors induced by hydrothermal treatment (at 300−420°C for 0−180 min). The emulsification and filtration behaviors of these fine particles were specifically studied, considering their importance in bitumen froth treatment. A conceptual bitumen froth cleaning approach is proposed, which combines the hydrothermal treatment of bitumen froth, water separation by venting at 270°C, and fine solids removal by filtration at 200°C. The feasibility of the above approach was tested at laboratory scale. The working hypotheses and the corresponding testing approaches are as follows:

(1) Hypothesis: thermal dehydroxylation of kaolinite would change its adsorption capacity for asphaltenes. Approach: both single and multiple contacts of untreated or dehydroxylated kaolinite with asphaltene-in-toluene solutions were conducted to evaluate the asphaltene

adsorption capacity on kaolinite in terms of adsorption density, percent surface coverage, and mean domain thickness.

(2) Hypothesis: the organic matter is patchy-coated on the clay surfaces, and this organic coating can be visualized by atomic force microscopy adhesion force mapping due to the different shapes and mechanical properties of the organic materials from the clay minerals. Approach: quantitative nanomechanical mapping atomic force microscopy (QNM-AFM) was used to determine the spatial distribution (or surface coverage), domain thickness, and mechanical property of the organic coating on bitumen froth clay minerals.

(3) Hypothesis: in comparison to the untreated fine solids, the emulsifying capacity of the hydrothermally-treated fine solids would change as their wettability is altered by hydrothermal treatment. Approach: the emulsification behavior of the untreated and hydrothermally-treated fine solids extracted from bitumen froth was investigated using toluene-water emulsification tests.

(4) Hypothesis: hydrothermal treatment would make the fine solids easier to filter, by changing the stacking behavior of clay particles in the filter cake. Approach: the filterability of fine solids was tested by both room-temperature filtration (~25°C) and *in-situ* hot filtration (~200°C); the stacking behavior of clay particles in the filter cake-filter membrane interface is observed by scanning electron microscope.

1.3 Thesis Organization

This thesis is organized into seven chapters:

Chapter 1 provides a general introduction to the background, motivation, objectives, and organization of the thesis work.

Chapter 2 reviews the relevant literature. The current understandings of oil-mineral interactions and hydrothermal technology are discussed.

Chapter 3 investigates the irreversible adsorption of asphaltenes on untreated and dehydroxylated kaolinite. The adsorption density, percent surface coverage, and mean domain thickness of adsorbed asphaltenes on kaolinite substrates were evaluated using X-ray photoelectron spectroscopy (XPS) and elemental analysis.

Chapter 4 discusses the structures and properties of the organic matter associated with the clay minerals extracted from bitumen froth, which were studied by atomic force microscopy adhesion mapping.

Chapter 5 reports the emulsification behavior of the fine solids in bitumen froth, with and without hydrothermal treatments. The results elucidate the influence of hydrophobicity distribution of particle mixtures on the stabilization of water-oil emulsions.

Chapter 6 shows the filtration behavior of bitumen froth fine solids. A mechanism for the filterability improvement after the hydrothermal treatment is proposed based on the observed particle stacking behaviors in the filter cakes.

Chapter 7 contains an overall discussion of this thesis work. The main conclusions, original contributions, and recommendations for future work are also summarized in this chapter.

References

[1] Canadian Association of Petroleum Producers CAPP, 2017, Crude oil forecast, markets and transportation, available at: http://www.capp.ca/publications-and-statistics/publications/303440, retrieved on 8 August 2017.

[2] Alberta Energy Regulator, 2017, Alberta energy regulator 2016/17 annual report, available at: https://www.aer.ca/documents/reports/AER2016-17AnnualReport.pdf, retrieved on 8 August 2017.

[3] J. Masliyah, J. Czarnecki, Z. Xu, Handbook on theory and practice of bitumen recovery from Athabasca oil sands, Volume I: Theoretical basis, Kingsley Knowledge Publishing, Calgary, Alberta, 2011.

[4] U. Romanova, M. Valinasab, E. Stasiuk, H. Yarranton, L. Schramm, W. Shelfantook, The effect of oil sands bitumen extraction conditions on froth treatment performance, Journal of Canadian Petroleum Technology 45 (2006) 36-45.

[5] J. Masliyah, Z.J. Zhou, Z. Xu, J. Czarnecki, H. Hamza, Understanding water-based bitumen extraction from Athabasca oil sands, The Canadian Journal of Chemical Engineering 82 (2004) 628-654.

[6] S. Gao, K. Moran, Z. Xu, J. Masliyah, Role of bitumen components in stabilizing water-in-diluted oil emulsions, Energy & Fuels 23 (2009) 2606-2612.

[7] M.R. Gray, Upgrading oilsands bitumen and heavy oil, The University of Alberta Press, Edmonton, Alberta, 2015.

[8] A. Hooshiar, P. Uhlik, Q. Liu, T.H. Etsell, D.G. Ivey, Clay minerals in nonaqueous extraction of bitumen from Alberta oil sands: Part 1. Nonaqueous extraction procedure, Fuel Processing Technology 94 (2012) 80-85.

[9] X. Li, L. He, G. Wu, W. Sun, H. Li, H. Sui, Operational parameters, evaluation methods, and fundamental mechanisms: Aspects of nonaqueous extraction of bitumen from oil sands, Energy & Fuels 26 (2012) 3553-3563.

[10] H. Nikakhtari, L. Vagi, P. Choi, Q. Liu, M.R. Gray, Solvent screening for non-aqueous extraction of Alberta oil sands, The Canadian Journal of Chemical Engineering 91 (2013) 1153-1160.

[11] K. Pal, L.d.P. Nogueira Branco, A. Heintz, P. Choi, Q. Liu, P.R. Seidl, M.R. Gray, Performance of solvent mixtures for non-aqueous extraction of Alberta oil sands, Energy & Fuels 29 (2015) 2261-2267.

[12] H. Nikakhtari, S. Wolf, P. Choi, Q. Liu, M.R. Gray, Migration of fine solids into product bitumen from solvent extraction of alberta oilsands, Energy & Fuels 28 (2014) 2925-2932.

[13] F. Lin, S.R. Stoyanov, Y. Xu, Recent advances in non-aqueous extraction of bitumen from mineable oil sands: A review, Organic Process Research & Development 21 (2017) 492-510.

[14] B. Sparks, L. Kotlyar, J. O'Carroll, K. Chung, Athabasca oil sands: Effect of organic coated solids on bitumen recovery and quality, Journal of Petroleum Science and Engineering 39 (2003) 417-430.

[15] J. Liu, Z. Xu, J. Masliyah, Role of fine clays in bitumen extraction from oil sands, AIChE Journal 50 (2004) 1917-1927.

[16] P. Bayliss, A. Levinson, Mineralogical review of the Alberta oil sand deposits (Lower Cretaceous, Mannville Group), Bulletin of Canadian Petroleum Geology 24 (1976) 211-224.

[17] S. Wang, Q. Liu, X. Tan, C. Xu, M.R. Gray, Adsorption of asphaltenes on kaolinite as an irreversible process, Colloids and Surfaces A: Physicochemical and Engineering Aspects 504 (2016) 280-286.

[18] L. He, F. Lin, X. Li, H. Sui, Z. Xu, Interfacial sciences in unconventional petroleum production: From fundamentals to applications, Chemical Society Reviews 44 (2015) 5446-5494.

[19] A. Majid, J.A. Ripmeester, Isolation and characterization of humic acids from Alberta oil sands and related materials, Fuel 69 (1990) 1527-1536.

[20] D.M. Sztukowski, H.W. Yarranton, Characterization and interfacial behavior of oil sands solids implicated in emulsion stability, Journal of Dispersion Science and Technology 25 (2004) 299-310.

[21] F. Chen, J. Finch, Z. Xu, J. Czarnecki, Wettability of fine solids extracted from bitumen froth, Journal of Adhesion Science and Technology 13 (1999) 1209-1224.

[22] J. Czarnecki, P. Tchoukov, T. Dabros, Possible role of asphaltenes in the stabilization of water-in-crude oil emulsions, Energy & Fuels 26 (2012) 5782-5786.

[23] T. Jiang, G.J. Hirasaki, C.A. Miller, S. Ng, Wettability alteration of clay in solid-stabilized emulsions, Energy & Fuels 25 (2011) 2551-2558.

[24] R.J. Chalaturnyk, J. Don Scott, B. Özüm, Management of oil sands tailings, Petroleum Science and Technology 20 (2002) 1025-1046.

[25] F. Rao, Q. Liu, Froth treatment in Athabasca oil sands Bitumen recovery process: A review, Energy & Fuels 27 (2013) 7199-7207.

[26] U.G. Romanova, H.W. Yarranton, L.L. Schramm, W.E. Shelfantook, Investigation of oil sands froth treatment, The Canadian Journal of Chemical Engineering 82 (2004) 710-721.

[27] K. Tanabe, M.R. Gray, Role of fine solids in the coking of vacuum residues, Energy & Fuels 11 (1997) 1040-1043.

[28] N. Sanaie, A. Watkinson, B. Bowen, K. Smith, Effect of minerals on coke precursor formation, Fuel 80 (2001) 1111-1119.

[29] J. Zhao, Q. Liu, M.R. Gray, Characterization of fine solids in Athabasca bitumen froth before and after hydrothermal treatment, Energy & Fuels 30 (2016) 1965-1971.

2 Literature Review

2.1 Oil-Mineral Interactions

Interactions between petroleum-derived organic matter and inorganic minerals have attracted considerable research attention due to their ubiquitous occurrence in natural energy resources such as oil sands [1-3]. The irreversible adsorption of components of petroleum or bitumen on clay minerals is essentially determined by the strong interactions at the oil-mineral interface. The scope of this review section, i.e., oil-mineral interactions, is the interactions of bitumen-derived organic components with mineral surfaces. The term of "organic matter" was used to encompass the range of possible bitumen-derived organic components that could occur on the surface of fine mineral solids. Bitumen and humic material from soil share a common set of acidic functional groups, therefore, references from the literature on soil science are included. In the following, the oil-mineral interactions in oil sands are discussed in terms of mineralogy, adsorbed organic matter, interaction mechanisms, aggregation structures, and typical characterization techniques.

2.1.1 Oil Sands Mineralogy

The mineralogy of Alberta oil sands is complex, evidenced by a large number of mineral species identified (over 90), formation of polymorphs of some minerals (e.g., anatase, rutile, and brookite are all polymorphs of one another having the same composition of TiO_2 but significantly different structures), and the presence of ill-defined or poorly-characterized minerals [4-7]. Nevertheless, the primary constituent mineral in the Alberta oil sands is quartz (~90%), with minor amounts of feldspar, clay, and other minerals [8, 9]. The quartz and feldspar grains are relatively easy to separate from bitumen due to their large size (usually >250 μm); however, the clay minerals are very problematic. They tend to enrich in bitumen froth and are the

major constituents of bitumen froth fine mineral solids [4, 10]. Clay minerals are aluminum phyllosilicates with platy shape, having both face (basal plane) and edge surfaces (Figure 2.1A) [11, 12]. Most studies reported that kaolinite and illite are the dominant clay minerals in Alberta oil sands [10, 13, 14].

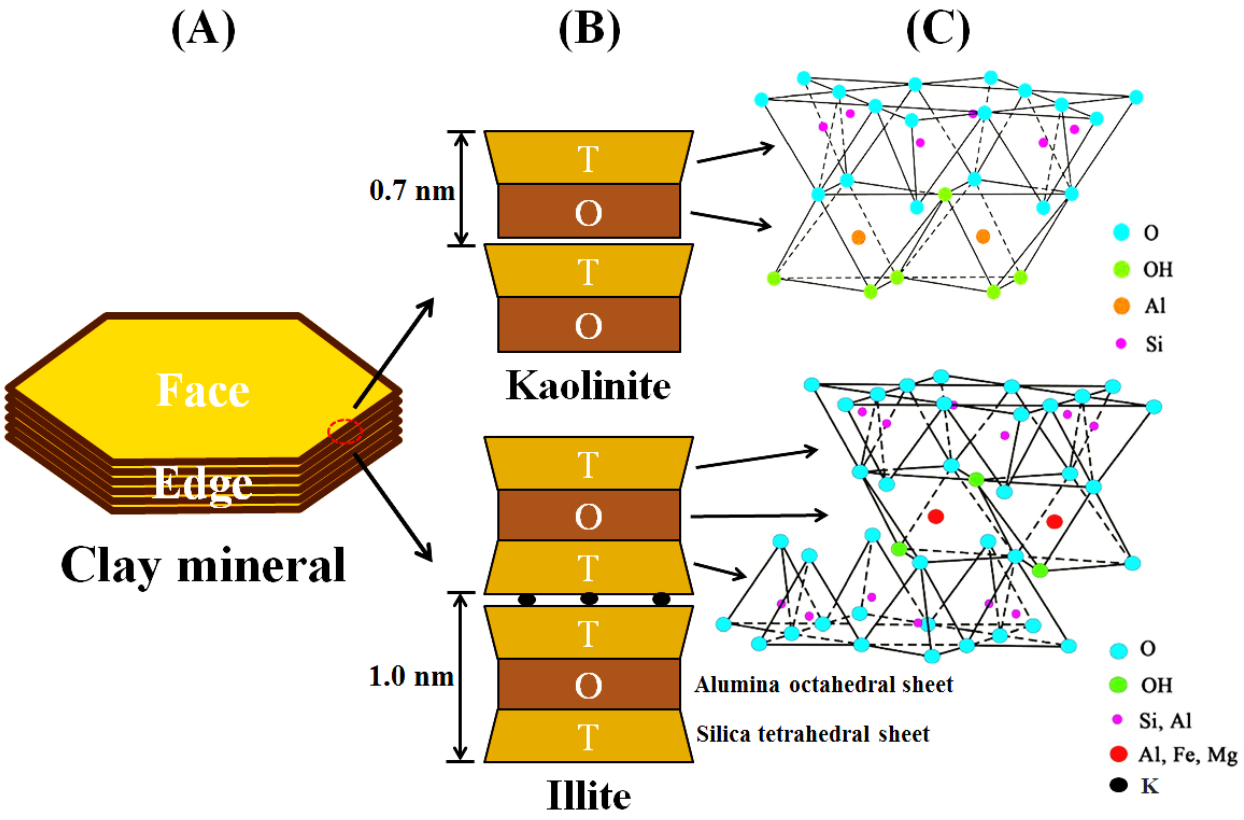

Figure 2.1 Schematic representations of (A) clay mineral showing a stack of clay platelets with face and edge surfaces and (B, C) crystalline structures of 1:1-type kaolinite and 2:1-type illite. Panel C is adapted from Grim [15].

Kaolinite, $Al_2Si_2O_5(OH)_4$, is a 1:1-type clay mineral [4]. As shown in Figure 2.1B, one layer of the mineral consists of a silica tetrahedral sheet (T) and an alumina octahedral sheet (O) with a 0.7-nm basal spacing, and the repeating layers are hydrogen-bonded together [4, 16]. The abundance of these hydrogen bonds makes the binding between the layers so strong that the

kaolinite clay does not delaminate easily (the layers do not swell in water) [4]. Kaolinite has two basal faces: tetrahedral siloxane face of Si-O-Si exposure and octahedral aluminum face of Al-OH exposure (Figure 2.1C) [17]. At the edges of the 1:1 layer, the structure is disrupted and broken bonds occur, which are compensated by water adsorption terminating in -OH groups [17, 18]. The perfect tetrahedral and octahedral sheets are electrically neutral. However, isomorphic substitution of higher valence cations by lower valence cations of similar sizes, such as Si^{4+} substituted by Al^{3+} and Al^{3+} substituted by Mg^{2+}, results in a net negative charge of the corresponding sheets. The net negative charges are balanced by metal cations adsorbed on the clay surfaces. For 1:1 kaolinite, the degree of isomorphic substitution is relatively small, mainly in the tetrahedral sheets where the silicon is substituted [4, 17]. Thus the cation exchange capacity of kaolinite is generally very low (3−5 meq/100 g) [4]. The specific surface area of kaolinite is reported to be in the range of 5−30 m^2/g [4, 19].

Unlike the crystal structure of kaolinite, illite is a 2:1-type clay mineral with two silica tetrahedral sheets and one central alumina octahedral sheet, which are bound together by interlayer cations (mainly K^+), yielding a basal spacing of 1.0 nm (Figure 2.1B) [4, 20]. The degree of isomorphic substitution in illite is usually higher than that of kaolinite, thus making its cation exchange capacity (10−40 meq/100 g) slightly higher in comparison to kaolinite (3−5 meq/100 g). The specific surface area of illite (65−100 m^2/g [4]) is also larger than that of kaolinite (5−30 m^2/g).

Based on the above discussion, the platy shape, the chemical and electrical surface properties, and the relatively large specific surface area of clay minerals may all contribute to their high affinity to organic materials [21-23].

2.1.2 Adsorbed Organic Matter

Adsorption of bitumen-derived organic matter is an important feature of oil sands clay minerals, and the adsorbed organic matter cannot be removed by strong solvents such as toluene [3, 24]. Some researchers defined this organic matter based on solubility [21, 25-27], calling it "toluene-insoluble-organic-matter", which is not justified when such a concept is applied to the phenomenon of adsorption on a solid surface. The non-removal of organic matter by toluene does not necessarily mean that the organic matter is insoluble in toluene, and it only means that the attraction between the organic matter and the solvent molecules could not overcome the adhesion forces between the solid surface and the organic matter, which usually results in irreversible adsorption. For instance, asphaltenes have been demonstrated to irreversibly adsorb on clay minerals [28, 29]. They remain adsorbed even after repeated toluene washing, but are chemically soluble in toluene. Here, the organic material, which is not removable by toluene, is alternately defined as "toluene-unextractable-organic-matter".

In addition, Kotlyar et al. [30-32] defined all the adsorbed organic materials as "humic matter", as a solubility fraction, which posed a fundamental problem of terminology as they ignored the importance of irreversible adsorption of asphaltenes at clay surfaces. In their definition, toluene-soluble asphaltenes that irreversibly adsorb on clay minerals become mis-classified as humic materials because they do not desorb in the toluene solvent.

Although the detailed chemistry and properties of the unextractable organic matter is still unknown, chemical analysis indicated that it was a polar aromatic material with a number of amphiphilic molecules [1, 26, 33]. In essence, this unextractable (or irreversibly-adsorbed)

organic matter could be any hydrocarbon components which have strong binding potential towards minerals, such as humic materials [21, 34], asphaltenes [2, 35], or resins [3, 9].

2.1.3 Interaction Mechanisms at the Oil-Mineral Interface

Extensive studies have been conducted to understand the interaction mechanisms between petroleum- or bitumen-derived organic matter and mineral solids [1, 36, 37]. González et al. [38] claimed that the nature and content of heteroatoms, such as N, O, and S, in the organic molecules played a vital role in the adsorption of organic matter on mineral solid surfaces, mainly by the formation of hydrogen bonds. Wang et al. [39] proposed that the adsorption of bitumen-derived organic matter on hydrophilic solid surfaces (such as silica and alumina) was through polar-polar interactions. As shown by several researchers [40-43], the carboxyl groups were the common and effective chemical species that bound the organics and minerals together. Cations such as Ca^{2+} could also bind at oil-mineral interfaces and bridge between them [43, 44]. In addition, Carbognani et al. [45] suggested that the organic matter could be physically entangled with surfaces of the mineral solids. The strength of oil-mineral interaction is determined by the types of bonds and the surface areas engaged in the contact [46, 47].

Based on these prior studies, Figure 2.2 summarizes the broad range of binding mechanisms at an oil-mineral interface. On surfaces of clay particles, the featured aluminol (Al-OH) and silanol (Si-OH) groups may establish chemical bonding with organic molecules containing carboxyl (R-COOH) groups, forming Si/Al-OOCR bonds (Figure 2.2) [40, 48]. Moreover, cation bridging, acid/base interaction, and hydrogen bonding may occur between active mineral binding sites and organic polar or charged functional groups [1, 49], as shown in Figure 2.2. In addition, some organic macromolecules may be physically entangled with the rough mineral surfaces [50, 51].

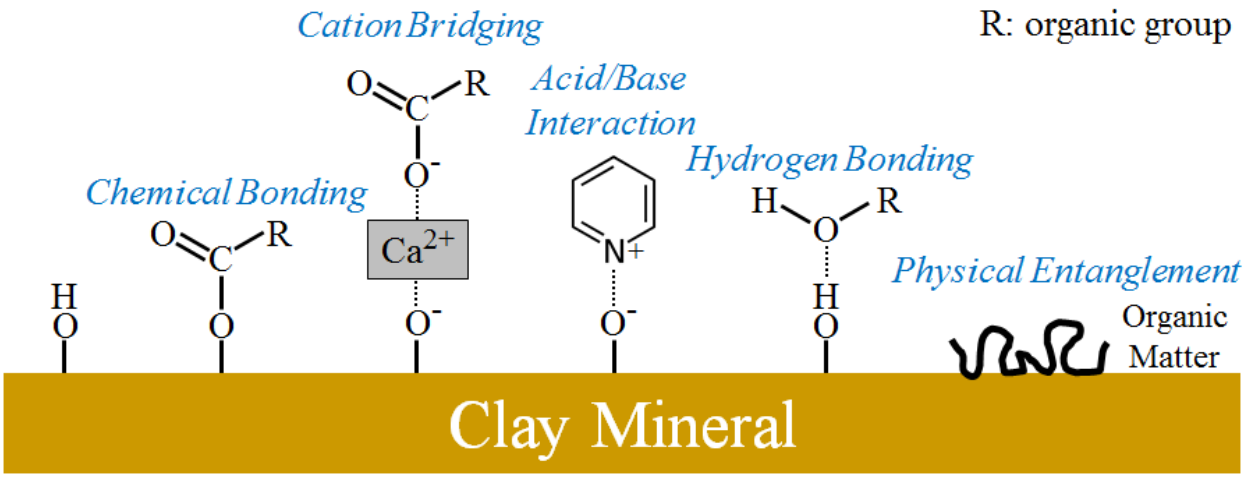

Figure 2.2 Schematic depictions of the mechanisms of oil-mineral interactions as described by Buckley and Liu [49], Gu et al. [52], and Ibraeva et al. [53] (drawing not to scale).

2.1.4 Association between Bitumen-Derived Organic Matter and Clay Minerals

An understanding of the association between bitumen-derived organic matter and clay minerals is of great significance to study the behaviors of the organically-modified clay minerals. In the oil sands, the bitumen-derived organic matter may modify the clay minerals in several ways, thereby leading to different oil-mineral associations. In the following paragraphs, the association of organic matter and mineral solids is discussed in terms of surface coating, aggregation, and intercalation.

Numerous studies [14, 54, 55] suggest that organic material adsorbs on mineral surfaces as an organic coating. One question is whether the organic coating evenly spread over all mineral surfaces or partially coated in discrete spots. Bensebaa et al. [26] characterized the fine solids extracted from oil sands using chemical surface analysis techniques, i.e., X-ray photoelectron spectroscopy (XPS) and time-of-flight secondary ion mass spectroscopy (ToF-SIMS). They concluded that the organic coating was patchy and discontinuous based on the detectable signals

of inorganic elements, e.g., Al and Si, in the topmost layer (~2−5 nm). Similar conclusions were reported for the fine solids derived from soils [56] and marine sediments [57] using techniques such as gas adsorption. The patchy nature of organic matter distribution is also evident in asphaltene-kaolinite model system [58, 59]. However, direct visualization of the spatial distribution of this organic coating is still lacking. The incomplete surface coverage by the adsorbed organics may be partially explained by analogy to the behavior of other colloids such as polymers and proteins, as suggested by Wang et al. [28]. An upper limit to the percent surface coverage exists for polymer colloids even at very high polymer concentrations (which may be 36 to 55% depending on their shapes and sizes), given the fact that even the closest possible arrangement of disks on a planar surface will leave area uncovered [28, 60]. The determination of patchy organic coating (Figure 2.3) provides a structure-based explanation for the observed bi-wet characteristics of the oil sands clay minerals [61, 62], which will be discussed in detail in Chapter 5.

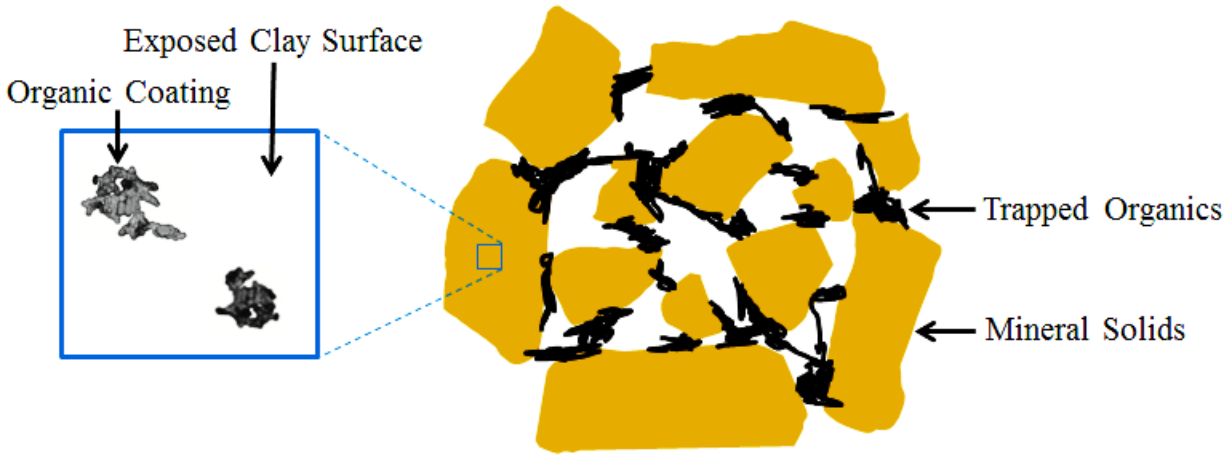

Figure 2.3 Schematic depiction of (left) an organic coating on clay surface and (right) an oil-mineral aggregate where organic matter was trapped between mineral solids acting as “glue”. Adapted from Tisdall et al. [63].

Recent evidences [64-66] also suggest that a significant amount of organic matter may be trapped between mineral particles acting as "glue", leading to the formation of oil-mineral aggregates (Figure 2.3). Bensebaa et al. [64] characterized the oil sands fine solids using step-scan photoacoustic Fourier transform infrared spectroscopy, and concluded that there were colloidal organic particles trapped inside the mineral particle aggregates. Couillard and Mercier [67] also observed clay aggregates containing organic carbon by using energy-dispersive X-ray spectroscopy mapping. Similarly, in soil science, the degraded aromatic humic materials, which constituted 52−98% of the total organic matter in soil, were found to act as binding agents to aluminosilicates, resulting in large oil-mineral aggregates [68, 69]. Bulk density fractionation appeared to be a suitable approach to isolate oil-mineral aggregates that have different organic matter loadings, due to the density difference between organic matter (~1 g/cm^3) and minerals (~2.6 g/cm^3) [21, 65, 66, 70]. The presence of materials with a density in the range of 1−2.6 g/cm^3 provides an indirect evidence for the aggregation of organic matter and mineral solids. The trapped organics in the aggregates was difficult to recover by conventional techniques; therefore, any technology that can break these aggregates and release these trapped organics will potentially increase the recovery of hydrocarbons.

Another possibility is that the organic matter intercalated into clay interlayer spaces. The organic-clay composites can be artificially prepared by intercalation of organic molecules into clay interlayers, and these composites have attracted increasing attention in recent years since they frequently exhibit unexpected hybrid properties synergistically derived from two components [71, 72]. For example, Yano et al. [73] successfully synthesized an organic-clay composite by intercalating dodecylamine into montmorillonite clay. However, under natural conditions, intercalation of organic matter in clay minerals has rarely been found [74-76]. By

electron energy-loss spectroscopy analysis, Couillard and Mercier [67] reported that the organic matter associated with oil sands clay minerals was present on the clay surface, rather than intercalated between individual clay mineral layers within the crystal structure. Eusterhues et al. [76] characterized two German acid forest soils and found no indications of intercalation of organic matter into internal phyllosilicates. One reason for the lack of natural intercalation may be that the size of the indigenous organic molecules was larger than the clay interlayer spaces [77, 78]. The stability of the bitumen-derived organic matter present in oil sands clay minerals, therefore, cannot be attributed to its intercalation into clay interlayers.

2.1.5 Characterization Techniques

A wide range of characterization techniques have been used to examine the organically-modified clay minerals extracted from oil sands, including Fourier transform infrared spectroscopy (FTIR) [64], X-ray photoelectron spectroscopy (XPS) [21], electron energy-loss spectroscopy (EELS) [67], and total internal reflection fluorescence (TIRF) [79]. This section summarizes the main techniques that were used in this work for investigation of the oil-mineral interactions. The introduction below highlights the purposes and features of their use, without attempting to elaborate the fundamental principles behind each technique.

2.1.5.1 Mineralogical and Structural Analysis

Powder X-ray diffraction (XRD) has been used to determine the mineralogical composition of oil sands clay minerals. Generally, various mineral phases in the sample can be identified by comparing peak positions with standard powder XRD databases; however, this is not the case for clay minerals since they have a similar crystal structure in the X and Y dimensions. To identify clay minerals by XRD, oriented samples must be used to increase basal (001) reflection [80]. A

glass slide method [80] was used in this study where oriented samples were prepared from a dispersed suspension of clay minerals. Based on the peak intensities present in XRD pattern, quantitative analysis is theoretically possible for any sample. However, in practice, quantification of clay minerals by XRD requires extensive experience. Computer programs such as RockJock or Rietveld are available for quantitative XRD (Q-XRD) determination of clay minerals, by comparing the integrated XRD intensities of individual minerals in complex mineral mixtures to the XRD intensities of an internal standard (e.g. corundum). A detailed introduction of the principles and procedures for Q-XRD can be found elsewhere [81, 82].

Inferring from absorption band analysis, FTIR can provide information on molecular structures of the organically-modified clay minerals. Frost and Vassallo [83] studied the dehydroxylation process of kaolinite by analyzing FTIR intensities of the hydroxyl bands. Hannisdal et al. [84] investigated the adsorption of crude oil components (mainly asphaltenes and resins) on silica particles using FTIR, and demonstrated that the spectral range between 2800 and 3000 cm^{-1} showing characteristic C-H stretching bands can be used as a measure of hydrocarbons at the silica surface. By comparing FTIR spectra at different modulation frequencies, Bensebaa et al. [64] proposed a new structural image of oil sands fine solids (i.e. a model of oil-mineral aggregates). In the present study, FTIR spectroscopic analysis was used to investigate the kaolinite dehydroxylation (Chapter 3) and the oil-mineral associations (Chapter 5).

2.1.5.2 Degree of Organic Modification

In this thesis work, the degree of organic modification of oil sands clay minerals, with and without hydrothermal treatment, was characterized both at the surface and in the bulk.

X-ray photoelectron spectroscopy (XPS) and time of flight secondary ion mass spectrometry (ToF-SIMS) are two of the most popular techniques for surface analysis, both of which can reveal the nature of chemical species present on the sample surface [22, 85]. XPS can measure the composition and chemical states of elements within the top 2−10 nm surface region, on an area average basis (usually ~1 mm^2) [86, 87]. In contrast, ToF-SIMS is featured by recognition of molecules through their characteristic fragments within the top ~2 nm surface region, on a particle-by-particle basis [88, 89]. Wang et al. [22] and Abdallah and Taylor [90] applied these two techniques to study asphaltene adsorption on kaolinite and metal surfaces, respectively. Both studies proved that a combination of XPS and ToF-SIMS is a promising method in analysis of organic-coated surface. In the present work, therefore, XPS and ToF-SIMS (particularly XPS) were used to quantify the coverage of organic matter on mineral surface.

Total carbon content determined by elemental analysis can provide referential information on total organic content of the organically-modified clay minerals, considering that the organic matter is mainly composed of carbon while the pure clay mineral has negligible carbon content. In this work, the total organic content in asphaltene-coated kaolinite (Chapter 3) and organically-modified clay minerals (Chapter 6) were evaluated by carbon elemental content analysis.

2.1.5.3 Mechanical Property

To the author's knowledge, no studies have yet examined the mechanical property of the bitumen-derived organic matter associated with oil sands clay minerals. In this work, the quantitative nanomechanical mapping atomic force microscopy (QNM-AFM) was applied for the first time to investigate these organic matter fractions in terms of their spatial distribution and

mechanical property (more specifically, adhesion force with an AFM tip). A more detailed introduction of this method is presented in Chapter 4.

2.2 Hydrothermal Technology

Hydrothermal technology has been applied to treat unconventional hydrocarbon resources, including heavy oil [91-93], biomass [94], oil sands bitumen [95-97], oil shale [98], coal [99], asphalt [100], and wastes [101]. The term "hydrothermal" is of geological origin and was first used by the British geologist, Roderick Murchison (1792−1871), to describe the action of water at elevated temperature and pressure in bringing about changes in the crust of the Earth and leading to the formation of various rocks and minerals [102]. Hydrothermal treatment can be broadly defined as chemical and physical transformations using the combination of water (hydro) and thermal energy (high temperature) to convert a feedstock into valuable products. In the present study, hydrothermal cleaning of bitumen froth, i.e., a complex mixture of water, bitumen, and fine solids (mainly clay minerals), was investigated. The behaviors of these components under hydrothermal conditions are discussed in the following sections.

2.2.1 High-Temperature Water

The hydrothermal treatment has attracted considerable attention, largely because of the unique inherent properties of high-temperature water (from liquid water at about 200°C to supercritical water up to 600°C) [103, 104]. Water is inexpensive, non-toxic, readily available, and environmentally friendly [103]. These advantages motivate the use of high-temperature water for the purpose of creating safer, cleaner, and more environmentally benign chemical processes. Furthermore, high-temperature water exhibits properties that are significantly different from those of ambient liquid water. At ambient conditions, the dielectric constant of water is

comparatively large (approximately 80) due to the strong effect of hydrogen bonds. However, the dielectric constant decreases sharply as temperature and pressure increase, reaching a value of 5 at the critical point (T_c = 374°C, P_c = 22.1 MPa) [103]. The low dielectric constant increases its dissolution power for nonpolar organic compounds. Consequently, small organic molecules, which are insoluble in ambient liquid water, become highly soluble in high-temperature water and are completely miscible in supercritical water [104]. The ion product of high-temperature water is about three orders of magnitude higher than that of ambient liquid water. Thus, high concentrations of H^+ and OH^- can be obtained in high-temperature water, providing a good environment for acid- or base-catalyzed reactions [104, 105]. In fact, many studies have shown that water molecules may participate in chemical reactions, including hydrogen donation [106, 107], hydrolysis [108, 109], and hydration [110, 111]. In summary, the high-temperature water may participate in the hydrothermal treatment both physically and chemically as a medium, catalyst, and reactant [94, 103, 104, 112].

2.2.2 Behavior of Bitumen under Hydrothermal Conditions

Bitumen is a representative unconventional heavy-oil resource. The behavior of bitumen under thermal conditions has been well documented [113, 114]. Thermal reactions are known to occur spontaneously in bitumen at sufficiently high temperatures, producing distillation products and often coke as a byproduct [114]. The aim of bitumen upgrading is to produce crude oil product with a better quality. This quality improvement can have different forms: reducing bitumen viscosity to enable pipeline transportation without the use of diluents, reducing the density, and/or removing contaminating elements such as sulfur. A more detailed introduction of upgrading can be found in the literature [114].

Prior studies have suggested that hydrothermal treatment of bitumen can bring several advantages, such as increase of liquid product yield and suppression of coke formation [95, 115-118]. Wahyudiono et al. [119] proposed that upgrading of bitumen in supercritical water at 400°C is a potential technique to transform high-molecular-weight bitumen components into useful bitumen-derived chemical compounds. Zhu et al. [120] reported that pyrolysis of heavy oil can be initiated at low temperature (380°C) in the presence of subcritical water. By using a continuous hydrothermal extraction method, Vilcáez et al. [95] argued that simultaneous upgrading of bitumen and suppression of coke formation was possible. Dutta et al. [121] investigated thermal cracking of Athabasca bitumen over a range of reaction severity (350−530°C and 10−60 min) in the presence or absence of water. The chemical influence of water on thermal reactions was tested by doping water with deuterium oxide (D_2O) and analyzing liquid and coke products by nuclear magnetic resonance and stable isotope mass spectrometry. They observed hydrogen transfer from water to thermally cracked bitumen molecules and thus demonstrated that the presence of water steam could chemically influence the reaction pathway. However, the above advantages were usually achieved under high water contents (~44−80 wt% [122, 123]).

2.2.3 Behavior of Clay Minerals under Hydrothermal Conditions

The thermal and hydrothermal behaviors of the two predominant clay minerals in oil sands, i.e., kaolinite and illite, are discussed below.

The effect of thermal treatment on kaolinite has been studied extensively [124-126]. When kaolinite is heated, it loses any physically absorbed water between 100 and 200°C, i.e., dehydration occurs. Dehydroxylation begins after dehydration, usually in a temperature range

between 350 and 700°C. By losing the chemically bonded water molecules, structural changes take place during dehydroxylation, in which kaolinite transforms into "metakaolin" [127, 128]:

$$Al_2Si_2O_5(OH)_4 \rightarrow Al_2O_3 \cdot 2SiO_2 + 2H_2O \quad (2.1)$$

This process is accompanied by a mass loss of circa 14 wt% as estimated from the theoretical composition (46.54 wt% SiO_2, 39.50 wt% Al_2O_3, and 13.96 wt% H_2O). Currently, no unanimous conclusion can be drawn on the mechanism of the dehydroxylation reaction. There are two explanations which are relatively accepted [127, 129]. The homogeneous mechanism suggests that in two neighboring hydroxyl groups having different acidities, the proton of the more acidic one will react with the less acidic hydroxyl group to form water. This water molecule would diffuse through the interlayer spaces until being eliminated from the particle. In contrast, the heterogeneous mechanism suggests that free protons are produced in some regions of the structure, which can migrate to elimination regions where they react with hydroxyl groups forming water. Frost et al. [130] studied the dehydroxylation of kaolinite using infrared emission spectroscopy, and they proposed that both the above two mechanisms are involved in the dehydroxylation process. The dehydroxylation reaction may result in a strained structure of dehydroxylated kaolinite [131], which will be discussed in detail in Chapter 3. After dehydroxylation at ~350−700°C, cubic spinel and amorphous silica will be produced in a temperature range between 700 and 950°C. A further increase of temperature to 1100°C leads to the formation of the thermodynamically stable mullite phase [127, 132].

In addition to thermal treatment, many studies have also been conducted to examine the behavior of kaolinite under hydrothermal conditions, i.e., thermal treatment of kaolinite in the presence of water [133-135]. The dehydration, dehydroxylation, and recrystallization processes were found

to be not only temperature dependent but also a function of the partial pressure of water, particularly for the dehydroxylation process [83, 136]. The results of Nahdi et al. [133], Levy [136], and Yeskis et al. [137] all indicated that the increase in water vapor pressure increased the onset temperature of dehydroxylation and reduced the dehydroxylation reaction rate.

The thermal transformation of illite is similar to that of kaolinite, following the dehydration, dehydroxylation, and recrystallization processes. Generally, illite dehydroxylates between 350 and 700°C [124, 138, 139]. As observed using X-ray diffraction (XRD), the original crystal structure of illite could be maintained until ~700°C, whereas the XRD reflections of kaolinite were lost upon dehydroxylation below 500°C [124, 138]. Yau et al. [140] studied the hydrothermal behavior of illite over the temperature range of 360−460°C at 30 MPa for 92 days, and they found no significant changes to the illite samples after this hydrothermal treatment. These observations suggest that illite is a stable clay mineral, or at least more stable than kaolinite [141, 142].

The proposed temperature range of hydrothermal treatment in this study, i.e., 300−420°C, falls in or stays very close to the dehydroxylation temperatures of these typical clay minerals. Thus, dehydroxylation may occur during hydrothermal treatment of bitumen froth, even as the degree of dehydroxylation may be limited due to the high water vapor pressure in the treatment system. Currently, the organic adsorption on dehydroxylated minerals is rarely studied. Chapter 3 of this thesis focuses on this research gap and presents an investigation of asphaltene adsorption on dehydroxylated kaolinite.

A number of studies [143-145] have examined the effect of fine solids on bitumen conversions under thermal conditions (in the absence of water). Tanabe and Gray [143] observed that the

presence of fine solids in the Athabasca bitumen vacuum residue delayed the onset of coking and reduced the yield of coke. Sanaie et al. [144] investigated the thermal behavior of bitumen with different solid additives, and they found that the presence of native clays derived from Athabasca oil sands could reduce the coke yield while having no effect on light hydrocarbon formation. These results suggest that the presence of fine solids may have beneficial effects on thermal processing of bitumen.

2.2.4 Hydrothermal Treatment of Bitumen Froth

Direct thermal treatment of bitumen froth leads to hydrothermal reaction conditions because of the naturally present water in bitumen froth (averagely 30 wt%). One of the most important advantages of hydrothermal treatment is that it can use wet-feedstocks without the need for pre-drying, in comparison to conventional pyrolysis processes [146]. Although the behavior of water, bitumen, and clay minerals under hydrothermal conditions has been studied individually, the collective hydrothermal behavior of the mixture of water-oil-mineral (which is the case of bitumen froth) is very rarely studied. However, such a study is crucial to determine whether or not the presence of both water and mineral solids can have beneficial effects on oil upgrading.

To understand the collective effect of water-oil-mineral interactions under hydrothermal conditions, several recent studies in our research group have been carried out [10, 122, 147]. Nhieu et al. [122] examined the effect of water and fine solids on coke formation during thermal treatment of an Athabasca bitumen vacuum residue with 0−33.3 wt% water at 410°C for up to 80 min, and they concluded that the presence of fine solids has a beneficial effect as they delayed the onset of coke formation, while the presence of water has no significant impact within the tested concentration range (i.e. 0−33.3 wt%). Zhao et al. [10] treated the mixtures of Athabasca

bitumen and fine solids extracted from bitumen froth hydrothermally at 392°C for 30 min using a 15 mL micro-reactor. They found that the fine solids turned more oil-wet and were easier to filter after the hydrothermal treatment. Using a micro-reactor equipped with a sapphire window, Dinh [148] and Laborde-Boutet et al. [147] observed the fouling behavior of a variety of heavy oil feedstocks including Athabasca bitumen vacuum residue (~2 wt% fine solids) *in-situ* and in real-time. They observed that the addition of water resulted in the formation of a dark film before the onset of mesophase, and they attributed it to the fine solids deposition caused by subcritical water. This dissertation is based on those previous studies and continues to investigate the water-oil-mineral interactions under hydrothermal conditions, particularly focusing on the properties and behaviors of the clay mineral component.

References

[1] M. Kleber, P. Sollins, R. Sutton, A conceptual model of organo-mineral interactions in soils: Self-assembly of organic molecular fragments into zonal structures on mineral surfaces, Biogeochemistry 85 (2007) 9-24.

[2] L. Kotlyar, B. Sparks, J. Woods, K. Chung, Solids associated with the asphaltene fraction of oil sands bitumen, Energy & Fuels 13 (1999) 346-350.

[3] F. Dongbao, J.R. Woods, J. Kung, D.M. Kingston, L.S. Kotlyar, B.D. Sparks, P.H. Mercier, T. McCracken, S. Ng, Residual organic matter associated with toluene-extracted oil sands solids and its potential role in bitumen recovery via adsorption onto clay minerals, Energy & Fuels 24 (2010) 2249-2256.

[4] J. Masliyah, J. Czarnecki, Z. Xu, Handbook on theory and practice of bitumen recovery from Athabasca oil sands, Volume I: Theoretical basis, Kingsley Knowledge Publishing, Calgary, Alberta, 2011.

[5] H.A. Kaminsky, T.H. Etsell, D.G. Ivey, O. Omotoso, Distribution of clay minerals in the process streams produced by the extraction of bitumen from Athabasca oil sands, The Canadian Journal of Chemical Engineering 87 (2009) 85-93.

[6] P. Bayliss, A. Levinson, Mineralogical review of the Alberta oil sand deposits (Lower Cretaceous, Mannville Group), Bulletin of Canadian Petroleum Geology 24 (1976) 211-224.

[7] W.A. Deer, R.A. Howie, J. Zussman, An introduction to the rock-forming minerals, Longman, London, 1992.

[8] L.L. Schramm, E.N. Stasiuk, M. MacKinnon, Surfactants in Athabasca oil sands slurry conditioning, flotation recovery, and tailings processes, Cambridge University Press, Cambridge, 2000.

[9] E. Czarnecka, J. Gillott, Formation and characterization of clay complexes with bitumen from Athabasca oil sand, Clays and Clay minerals 28 (1980) 197-203.

[10] J. Zhao, Q. Liu, M.R. Gray, Characterization of fine solids in Athabasca bitumen froth before and after hydrothermal treatment, Energy & Fuels 30 (2016) 1965-1971.

[11] S. Guggenheim, R. Martin, Definition of clay and clay mineral: Joint report of the AIPEA nomenclature and CMS nomenclature committees, Clays and Clay Minerals 43 (1995) 255-256.

[12] L. Heller-Kallai, F. Bergaya, B. Theng, G. Lagaly, Handbook of Clay Science. Developments in Clay Science, Elsevier, Amsterdam, 2006.

[13] T. Jiang, G.J. Hirasaki, C.A. Miller, S. Ng, Wettability alteration of clay in solid-stabilized emulsions, Energy & Fuels 25 (2011) 2551-2558.

[14] A. Hooshiar, P. Uhlik, D.G. Ivey, Q. Liu, T.H. Etsell, Clay minerals in nonaqueous extraction of bitumen from Alberta oil sands: Part 2. Characterization of clay minerals, Fuel Processing Technology 96 (2012) 183-194.

[15] R.E. Grim, Applied clay mineralogy, Geologiska Föreningen iStockholm Förhandlingar 84 (1962) 533.

[16] F. Bergaya, G. Lagaly, General introduction: Clays, clay minerals, and clay science, Developments in Clay Science 1 (2006) 1-18.

[17] E. Tombácz, M. Szekeres, Surface charge heterogeneity of kaolinite in aqueous suspension in comparison with montmorillonite, Applied Clay Science 34 (2006) 105-124.

[18] L. Alagha, S. Wang, L. Yan, Z. Xu, J. Masliyah, Probing adsorption of polyacrylamide-based polymers on anisotropic basal planes of kaolinite using quartz crystal microbalance, Langmuir 29 (2013) 3989-3998.

[19] E. Castellini, R. Andreoli, G. Malavasi, A. Pedone, Deflocculant effects on the surface properties of kaolinite investigated through malachite green adsorption, Colloids and Surfaces A: Physicochemical and Engineering Aspects 329 (2008) 31-37.

[20] A.J. Fuller, S. Shaw, M.B. Ward, S.J. Haigh, J.F.W. Mosselmans, C.L. Peacock, S. Stackhouse, A.J. Dent, D. Trivedi, I.T. Burke, Caesium incorporation and retention in illite interlayers, Applied Clay Science 108 (2015) 128-134.

[21] B. Sparks, L. Kotlyar, J. O'Carroll, K. Chung, Athabasca oil sands: Effect of organic coated solids on bitumen recovery and quality, Journal of Petroleum Science and Engineering 39 (2003) 417-430.

[22] S. Wang, Q. Liu, X. Tan, C. Xu, M.R. Gray, Study of asphaltene adsorption on kaolinite by X-ray photoelectron spectroscopy and time-of-flight secondary ion mass spectroscopy, Energy & Fuels 27 (2013) 2465-2473.

[23] K. Wang, B. Xing, Structural and sorption characteristics of adsorbed humic acid on clay minerals, Journal of Environmental Quality 34 (2005) 342-349.

[24] J.J. Adams, Asphaltene adsorption, a literature review, Energy & Fuels 28 (2014) 2831-2856.

[25] L. Kotlyar, B. Sparks, J. Woods, S. Raymond, Y. Le Page, W. Shelfantook, Distribution and types of solids associated with bitumen, Petroleum Science and Technology 16 (1998) 1-19.

[26] F. Bensebaa, L.S. Kotlyar, B.D. Sparks, K.H. Chung, Organic coated solids in Athabasca bitumen: Characterization and process implications, Canadian Journal of Chemical Engineering 78 (2000) 610-616.

[27] A. Majid, B.D. Sparks, J.A. Ripmeester, Characterization of solvent-insoluble organic matter isolated from Alberta oil sands, Fuel 70 (1991) 78-83.

[28] S. Wang, Q. Liu, X. Tan, C. Xu, M.R. Gray, Adsorption of asphaltenes on kaolinite as an irreversible process, Colloids and Surfaces A: Physicochemical and Engineering Aspects 504 (2016) 280-286.

[29] S. Dubey, M. Waxman, Asphaltene adsorption and desorption from mineral surfaces, SPE Reservoir Engineering 6 (1991) 389-395.

[30] L. Kotlyar, H. Kodama, B. Sparks, P. Grattan-Bellew, Non-crystalline inorganic matter-humic complexes in Athabasca oil sand and their relationship to bitumen recovery, Applied Clay Science 2 (1987) 253-271.

[31] L.S. Kotlyar, J.A. Ripmeester, B.D. Sparks, D.S. Montgomery, Characterization of oil sands solids closely associated with Athabasca bitumen, Fuel 67 (1988) 808-814.

[32] L.S. Kotlyar, J.A. Ripmeester, B.D. Sparks, D.S. Montgomery, Characterization of organic-rich solids fractions isolated from Athabasca oil sand using a cold water agitation test, Fuel 67 (1988) 221-226.

[33] D.M. Sztukowski, H.W. Yarranton, Characterization and interfacial behavior of oil sands solids implicated in emulsion stability, Journal of Dispersion Science and Technology 25 (2004) 299-310.

[34] A. Majid, J.A. Ripmeester, Isolation and characterization of humic acids from Alberta oil sands and related materials, Fuel 69 (1990) 1527-1536.

[35] Y. Tu, D. Kingston, J. Kung, L.S. Kotlyar, B.D. Sparks, K.H. Chung, Adsorption of pentane insoluble organic matter from oilsands bitumen onto clay surfaces, Petroleum Science and Technology 24 (2006) 327-338.

[36] J. Masliyah, Z.J. Zhou, Z. Xu, J. Czarnecki, H. Hamza, Understanding water-based bitumen extraction from Athabasca oil sands, The Canadian Journal of Chemical Engineering 82 (2004) 628-654.

[37] E.H. Owens, K. Lee, Interaction of oil and mineral fines on shorelines: Review and assessment, Marine Pollution Bulletin 47 (2003) 397-405.

[38] M.F. González, C.S. Stull, F. López-Linares, P. Pereira-Almao, Comparing asphaltene adsorption with model heavy molecules over macroporous solid surfaces, Energy & Fuels 21 (2007) 234-241.

[39] S. Wang, N. Segin, K. Wang, J.H. Masliyah, Z. Xu, Wettability control mechanism of highly contaminated hydrophilic silica/alumina surfaces by ethyl cellulose, The Journal of Physical Chemistry C 115 (2011) 10576-10587.

[40] S. Ren, T. Dang-Vu, H. Zhao, J. Long, Z. Xu, J. Masliyah, Effect of weathering on surface characteristics of solids and bitumen from oil sands, Energy & Fuels 23 (2008) 334-341.

[41] E.M. Murphy, J.M. Zachara, S.C. Smith, Influence of mineral-bound humic substances on the sorption of hydrophobic organic compounds, Environmental Science & Technology 24 (1990) 1507-1516.

[42] D.E. Axelson, R.J. Mikula, Z.M. Potoczny, Characterization of oil sands mineral components and clay-organic complexes, Fuel Science & Technology International 7 (1989) 659-673.

[43] P. Gilbert, M. Abrecht, B.H. Frazer, The organic-mineral interface in biominerals, Reviews in Mineralogy and Geochemistry 59 (2005) 157-185.

[44] J. Liu, Z. Xu, J. Masliyah, Role of fine clays in bitumen extraction from oil sands, AIChE Journal 50 (2004) 1917-1927.

[45] L. Carbognani, M. Orea, M. Fonseca, Complex nature of separated solid phases from crude oils, Energy & Fuels 13 (1999) 351-358.

[46] R. Wershaw, Model for humus in soils and sediments, Environmental Science & Technology 27 (1993) 814-816.

[47] A. Adegoroye, L. Wang, O. Omotoso, Z. Xu, J. Masliyah, Characterization of organic-coated solids isolated from different oil sands, The Canadian Journal of Chemical Engineering 88 (2010) 462-470.

[48] R.C. Surdam, L.J. Crossey, E.S. Hagen, H.P. Heasler, Organic-inorganic interactions and sandstone diagenesis, AAPG Bulletin 73 (1989) 1-23.

[49] J. Buckley, Y. Liu, Some mechanisms of crude oil/brine/solid interactions, Journal of Petroleum Science and Engineering 20 (1998) 155-160.

[50] J.J. Pignatello, Soil organic matter as a nanoporous sorbent of organic pollutants, Advances in Colloid and Interface Science 76 (1998) 445-467.

[51] A. Golchin, J.A. Baldock, J. Oades, A model linking organic matter decomposition, chemistry, and aggregate dynamics, Soil Processes and the Carbon Cycle, CRC Press, Boca Raton, 1997.

[52] B. Gu, J. Schmitt, Z. Chen, L. Liang, J.F. McCarthy, Adsorption and desorption of natural organic matter on iron oxide: Mechanisms and models, Environmental Science & Technology 28 (1994) 38-46.

[53] Z.E. Ibraeva, A.A. Zhumaly, E. Blagih, S.E. Kudaibergenov, Preparation and characterization of organic-inorganic composite materials based on poly (acrylamide) hydrogels and clay minerals, Macromolecular Symposia 351 (2015) 97-111.

[54] M. Osacky, M. Geramian, D.G. Ivey, Q. Liu, T.H. Etsell, Mineralogical and chemical composition of petrologic end members of Alberta oil sands, Fuel 113 (2013) 148-157.

[55] J. Liang, F. Tumpa, L.P. Estrada, M.G. El-Din, Y. Liu, Impact of ozonation on particle aggregation in mature fine tailings, Journal of Environmental Management 146 (2014) 535-542.

[56] M. Kahle, M. Kleber, R. Jahn, Carbon storage in loess derived surface soils from Central Germany: Influence of mineral phase variables, Journal of Plant Nutrition and Soil Science 165 (2002) 141-149.

[57] L. Mayer, Extent of coverage of mineral surfaces by organic matter in marine sediments, Geochimica et Cosmochimica Acta 63 (1999) 207-215.

[58] A.W. Marczewski, M. Szymula, Adsorption of asphaltenes from toluene on mineral surface, Colloids and Surfaces A: Physicochemical and Engineering Aspects 208 (2002) 259-266.

[59] S. Wang, Q. Liu, X. Tan, C. Xu, M.R. Gray, Adsorption of asphaltenes on kaolinite as an irreversible process, Colloids and Surfaces A: Physicochemical and Engineering Aspects 504 (2016) 280-286.

[60] X. Jin, N.H. Wang, G. Tarjus, J. Talbot, Irreversible adsorption on nonuniform surfaces: The random site model, Journal of Physical Chemistry 97 (1993) 4256-4258.

[61] K. Darcovich, L. Kotlyar, W. Tse, J. Ripmeester, C. Capes, B. Sparks, Wettability study of organic-rich solids separated from Athabasca oil sands, Energy & Fuels 3 (1989) 386-391.

[62] S. Fujii, Y. Yokoyama, Y. Miyanari, T. Shiono, M. Ito, S.I. Yusa, Y. Nakamura, Micrometer-sized gold–silica Janus particles as particulate emulsifiers, Langmuir 29 (2013) 5457-5465.

[63] J. Tisdall, J.M. Oades, Organic matter and water-stable aggregates in soils, Journal of Soil Science 33 (1982) 141-163.

[64] F. Bensebaa, A. Majid, Y. Deslandes, Step-scan photoacoustic Fourier transform and X-rays photoelectron spectroscopy of oil sands fine tailings: New structural insights, Spectrochimica Acta Part A: Molecular and Biomolecular Spectroscopy 57 (2001) 2695-2702.

[65] M.J. Bock, L.M. Mayer, Mesodensity organo–clay associations in a near-shore sediment, Marine Geology 163 (2000) 65-75.

[66] T.S. Arnarson, R.G. Keil, Organic–mineral interactions in marine sediments studied using density fractionation and X-ray photoelectron spectroscopy, Organic Geochemistry 32 (2001) 1401-1415.

[67] M. Couillard, P.H. Mercier, Analytical electron microscopy of carbon-rich mineral aggregates in solvent-diluted bitumen products from mined Alberta oil sands, Energy & Fuels 30 (2016) 5513-5524.

[68] R. Haynes, M. Beare, Influence of six crop species on aggregate stability and some labile organic matter fractions, Soil Biology and Biochemistry 29 (1997) 1647-1653.

[69] P. Nelson, J.A. Baldock, P. Clarke, J. Oades, G. Churchman, Dispersed clay and organic matter in soil: their nature and associations, Australian Journal of Soil Research 37 (1999) 289-290.

[70] I. Turcotte, S.A. Quideau, S.W. Oh, Organic matter quality in reclaimed boreal forest soils following oil sands mining, Organic Geochemistry 40 (2009) 510-519.

[71] X. Liu, Q. Wu, PP/clay nanocomposites prepared by grafting-melt intercalation, Polymer 42 (2001) 10013-10019.

[72] P. Maiti, K. Yamada, M. Okamoto, K. Ueda, K. Okamoto, New polylactide/layered silicate nanocomposites: Role of organoclays, Chemistry of Materials 14 (2002) 4654-4661.

[73] K. Yano, A. Usuki, A. Okada, T. Kurauchi, O. Kamigaito, Synthesis and properties of polyimide–clay hybrid, Journal of Polymer Science Part A: Polymer Chemistry 31 (1993) 2493-2498.

[74] H.R. Schulten, P. Leinweber, Characterization of humic and soil particles by analytical pyrolysis and computer modeling, Journal of Analytical and Applied Pyrolysis 38 (1996) 1-53.

[75] H.R. Schulten, P. Leinweber, New insights into organic-mineral particles: Composition, properties and models of molecular structure, Biology and Fertility of Soils 30 (2000) 399-432.

[76] K. Eusterhues, C. Rumpel, M. Kleber, I. Kögel-Knabner, Stabilisation of soil organic matter by interactions with minerals as revealed by mineral dissolution and oxidative degradation, Organic Geochemistry 34 (2003) 1591-1600.

[77] H.R. Schulten, P. Leinweber, B. Theng, Characterization of organic matter in an interlayer clay-organic complex from soil by pyrolysis methylation-mass spectrometry, Geoderma 69 (1996) 105-118.

[78] B.K. Theng, K.R. Tate, P. Becker-Heidmann, Towards establishing the age, location, and identity of the inert soil organic matter of a spodosol, Journal of Plant Nutrition and Soil Science 155 (1992) 181-184.

[79] S.S. Shende, S. Pendharker, Z. Jacob, N. Nazemifard, Total internal reflection fluorescence microscopy to investigate the distribution of residual bitumen in oil sands tailings, Energy & Fuels 30 (2016) 5537-5546.

[80] D.M. Moore, R.C. Reynolds, X-ray diffraction and the identification and analysis of clay minerals, Oxford University Press, Oxford, 1989.

[81] D. Eberl, User guide to RockJock-A program for determining quantitative mineralogy from X-ray diffraction data, US Geological Survey, 2003.

[82] J. Środoń, V.A. Drits, D.K. McCarty, J.C. Hsieh, D.D. Eberl, Quantitative X-ray diffraction analysis of clay-bearing rocks from random preparations, Clays and Clay Minerals 49 (2001) 514-528.

[83] R.L. Frost, A.M. Vassallo, The dehydroxylation of the kaolinite clay minerals using infrared emission spectroscopy, Clays and Clay minerals 44 (1996) 635-651.

[84] A. Hannisdal, M.H. Ese, P.V. Hemmingsen, J. Sjöblom, Particle-stabilized emulsions: Effect of heavy crude oil components pre-adsorbed onto stabilizing solids, Colloids and Surfaces A: Physicochemical and Engineering Aspects 276 (2006) 45-58.

[85] J. O'Connor, B. Sexton, R.S. Smart, Surface analysis methods in materials science, Springer-Verlag, Berlin, 2013.

[86] D. Briggs, M. Seah, H. Bubert, Practical surface analysis. Vol. 1: Auger and X-ray photoelectron spectroscopy, Angewandte Chemie-German Edition 107 (1995) 1367.

[87] E. Kleimenov, H. Bluhm, M. Hävecker, A. Knop-Gericke, A. Pestryakov, D. Teschner, J.A. Lopez-Sanchez, J.K. Bartley, G.J. Hutchings, R. Schlögl, XPS investigations of VPO catalysts under reaction conditions, Surface Science 575 (2005) 181-188.

[88] A. Benninghoven, Surface analysis by secondary ion mass spectrometry (SIMS), Surface Science 299 (1994) 246-260.

[89] R.N. Sodhi, Time-of-flight secondary ion mass spectrometry (TOF-SIMS): Versatility in chemical and imaging surface analysis, Analyst 129 (2004) 483-487.

[90] W.A. Abdallah, S.D. Taylor, Study of asphaltenes adsorption on metallic surface using XPS and TOF-SIMS, The Journal of physical chemistry C 112 (2008) 18963-18972.

[91] M. Dejhosseini, T. Aida, M. Watanabe, S. Takami, D. Hojo, N. Aoki, T. Arita, A. Kishita, T. Adschiri, Catalytic cracking reaction of heavy oil in the presence of cerium oxide nanoparticles in supercritical water, Energy & Fuels 27 (2013) 4624-4631.

[92] G.P. Kayukova, A.T. Gubaidullin, S.M. Petrov, G.V. Romanov, N.N. Petrukhina, A.V. Vakhin, Changes of asphaltenes' structural phase characteristics in the process of conversion of heavy oil in the hydrothermal catalytic system, Energy & Fuels 30 (2016) 773-783.

[93] R.O. Canıaz, C. Erkey, Process intensification for heavy oil upgrading using supercritical water, Chemical Engineering Research and Design 92 (2014) 1845-1863.

[94] K. Tekin, S. Karagöz, S. Bektaş, A review of hydrothermal biomass processing, Renewable and Sustainable Energy Reviews 40 (2014) 673-687.

[95] J. Vilcáez, M. Watanabe, N. Watanabe, A. Kishita, T. Adschiri, Hydrothermal extractive upgrading of bitumen without coke formation, Fuel 102 (2012) 379-385.

[96] M. Morimoto, Y. Sugimoto, S. Sato, T. Takanohashi, Bitumen cracking in supercritical water upflow, Energy & Fuels 28 (2014) 858-861.

[97] M. Subramanian, Supercritical fluid extraction of oil sand bitumens from the Uinta basin, Utah, The University of Utah, 1996.

[98] R. Veski, V. Palu, K. Kruusement, Co-liquefaction of kukersite oil shale and pine wood in supercritical water, Oil Shale 23 (2006) 236-249.

[99] M. Sakaguchi, K. Laursen, H. Nakagawa, K. Miura, Hydrothermal upgrading of Loy Yang Brown coal-effect of upgrading conditions on the characteristics of the products, Fuel Processing Technology 89 (2008) 391-396.

[100] T. Sato, T. Adschiri, K. Arai, G.L. Rempel, F.T. Ng, Upgrading of asphalt with and without partial oxidation in supercritical water, Fuel 82 (2003) 1231-1239.

[101] I. Pavlovič, Z.e. Knez, M. Škerget, Hydrothermal reactions of agricultural and food processing wastes in sub-and supercritical water: A review of fundamentals, mechanisms, and state of research, Journal of Agricultural and Food Chemistry 61 (2013) 8003-8025.

[102] K. Byrappa, T. Adschiri, Hydrothermal technology for nanotechnology, Progress in Crystal Growth and Characterization of Materials 53 (2007) 117-166.

[103] Y. Guo, S. Wang, D. Xu, Y. Gong, H. Ma, X. Tang, Review of catalytic supercritical water gasification for hydrogen production from biomass, Renewable and Sustainable Energy Reviews 14 (2010) 334-343.

[104] N. Akiya, P.E. Savage, Roles of water for chemical reactions in high-temperature water, Chemical Reviews 102 (2002) 2725-2750.

[105] P. Kritzer, Corrosion in high-temperature and supercritical water and aqueous solutions: A review, The Journal of Supercritical Fluids 29 (2004) 1-29.

[106] O.M. Ogunsola, Decomposition of isoquinoline and quinoline by supercritical water, Journal of Hazardous Materials 74 (2000) 187-195.

[107] T. Moriya, H. Enomoto, Conversion of polyethylene to oil using supercritical water and donation of hydrogen in supercritical water, Japanese Journal of Polymer Science and Technology 58 (2001) 661-673.

[108] C. Fromonteil, P. Bardelle, F. Cansell, Hydrolysis and oxidation of an epoxy resin in sub- and supercritical water, Industrial & Engineering Chemistry Research 39 (2000) 922-925.

[109] M. Sasaki, Z. Fang, Y. Fukushima, T. Adschiri, K. Arai, Dissolution and hydrolysis of cellulose in subcritical and supercritical water, Industrial & Engineering Chemistry Research 39 (2000) 2883-2890.

[110] J. An, L. Bagnell, T. Cablewski, C.R. Strauss, R.W. Trainor, Applications of high-temperature aqueous media for synthetic organic reactions, The Journal of Organic Chemistry 62 (1997) 2505-2511.

[111] A.R. Katritzky, F.J. Luxem, M. Siskin, Aqueous high-temperature chemistry of carbo-and heterocycles. 6. Monosubstituted benzenes with two carbon atom side chains unsubstituted or oxygenated at the α-position, Energy & Fuels 4 (1990) 518-524.

[112] M. Siskin, A.R. Katritzky, Reactivity of organic compounds in superheated water: General background, Chemical Reviews 101 (2001) 825-836.

[113] A. Shah, R. Fishwick, J. Wood, G. Leeke, S. Rigby, M. Greaves, A review of novel techniques for heavy oil and bitumen extraction and upgrading, Energy & Environmental Science 3 (2010) 700-714.

[114] M.R. Gray, Upgrading oilsands bitumen and heavy oil, The University of Alberta Press, Edmonton, Alberta, 2015.

[115] N. Li, B. Yan, X.M. Xiao, A review of laboratory-scale research on upgrading heavy oil in supercritical water, Energies 8 (2015) 8962-8989.

[116] O.N. Fedyaeva, A.V. Shatrova, A.A. Vostrikov, Effect of temperature on bitumen conversion in a supercritical water flow, The Journal of Supercritical Fluids 95 (2014) 437-443.

[117] M. Morimoto, Y. Sugimoto, Y. Saotome, S. Sato, T. Takanohashi, Effect of supercritical water on upgrading reaction of oil sand bitumen, The Journal of Supercritical Fluids 55 (2010) 223-231.

[118] T. Sato, T. Tomita, P.H. Trung, N. Itoh, S. Sato, T. Takanohashi, Upgrading of bitumen in the presence of hydrogen and carbon dioxide in supercritical water, Energy & Fuels 27 (2013) 646-653.

[119] S. Wahyudiono, T. Shiraishi, M. Sasaki, M. Goto, Non-catalytic liquefaction of bitumen with hydrothermal/solvothermal process, The Journal of Supercritical Fluids 60 (2011) 127-136.

[120] C.C. Zhu, C. Ren, X.C. Tan, G. Chen, P.Q. Yuan, Z.M. Cheng, W.K. Yuan, Initiated pyrolysis of heavy oil in the presence of near-critical water, Fuel processing technology 111 (2013) 111-117.

[121] R.P. Dutta, W.C. McCaffrey, M.R. Gray, K. Muehlenbachs, Thermal cracking of Athabasca bitumen: Influence of steam on reaction chemistry, Energy & Fuels 14 (2000) 671-676.

[122] P. Nhieu, Q. Liu, M.R. Gray, Role of water and fine solids in onset of coke formation during bitumen cracking, Fuel 166 (2016) 152-156.

[123] L.Q. Zhao, Z.M. Cheng, Y. Ding, P.Q. Yuan, S.X. Lu, W.K. Yuan, Experimental study on vacuum residuum upgrading through pyrolysis in supercritical water, Energy & Fuels 20 (2006) 2067-2071.

[124] C.J. McConville, W.E. Lee, Microstructural development on firing illite and smectite clays compared with that in kaolinite, Journal of the American Ceramic Society 88 (2005) 2267-2276.

[125] N. Osornio-Rubio, J. Torres-Ochoa, M. Palma-Tirado, H. Iménez-Islas, R. Rosas-Cedillo, J. Fierro-Gonzalez, G. Martínez-González, Study of the dehydroxylation of kaolinite and alunite from a Mexican clay with DRIFTS-MS, Clay Minerals 51 (2016) 55-68.

[126] H. Wang, C. Li, Z. Peng, S. Zhang, Characterization and thermal behavior of kaolin, Journal of Thermal Analysis and Calorimetry 105 (2011) 157-160.

[127] H. Cheng, Q. Liu, J. Yang, S. Ma, R.L. Frost, The thermal behavior of kaolinite intercalation complexes-A review, Thermochimica Acta 545 (2012) 1-13.

[128] P. Zemenová, A. Kloužková, M. Kohoutková, R. Král, Investigation of the first and second dehydroxylation of kaolinite, Journal of Thermal Analysis and Calorimetry 116 (2014) 633-639.

[129] G. Brindley, J. Kao, Relation between the structural disorder and other characteristics of kaolinites and dickites, Clays and Clay Minerals, Citeseer, 1986.

[130] R.L. Frost, E. Horvath, É. Makó, J. Kristóf, Á. Rédey, Slow transformation of mechanically dehydroxylated kaolinite to kaolinite-an aged mechanochemically activated formamide-intercalated kaolinite study, Thermochimica Acta 408 (2003) 103-113.

[131] C.E. White, J.L. Provis, T. Proffen, D.P. Riley, J.S. van Deventer, Combining density functional theory (DFT) and pair distribution function (PDF) analysis to solve the structure of metastable materials: The case of metakaolin, Physical Chemistry Chemical Physics 12 (2010) 3239-3245.

[132] A.K. Chakraborty, New data on thermal effects of kaolinite in the high temperature region, Journal of Thermal Analysis and Calorimetry 71 (2003) 799-808.

[133] K. Nahdi, P. Llewellyn, F. Rouquérol, J. Rouquérol, N. Ariguib, M. Ayedi, Controlled rate thermal analysis of kaolinite dehydroxylation: Effect of water vapour pressure on the mechanism, Thermochimica Acta 390 (2002) 123-132.

[134] P. Ptáček, D. Kubátová, J. Havlica, J. Brandštetr, F. Šoukal, T. Opravil, Isothermal kinetic analysis of the thermal decomposition of kaolinite: The thermogravimetric study, Thermochimica Acta 501 (2010) 24-29.

[135] I. Lapides, S. Yariv, N. Lahav, M. Dvorachek, Stabilizing of aqueous kaolinite suspensions by thermal vapour-pressure shock explosion treatment, Thermochimica Acta 318 (1998) 251-263.

[136] J.H. Levy, Effect of water vapor pressure on the dehydration and dehydroxylation of kaolinite and smectite isolated from Australian tertiary oil shales, Energy & Fuels 4 (1990) 146-151.

[137] D. Yeskis, A.K. Van Groos, S. Guggenheim, Dehydroxylation of kaolinite, American Mineralogist 70 (1985) 1-2.

[138] T. Jiang, G. Li, G. Qiu, X. Fan, Z. Huang, Thermal activation and alkali dissolution of silicon from illite, Applied Clay Science 40 (2008) 81-89.

[139] V.A. Drits, D.K. McCarty, The nature of structure-bonded H_2O in illite and leucophyllite from dehydration and dehydroxylation experiments, Clays and Clay Minerals 55 (2007) 45-58.

[140] Y.C. Yau, D.R. Peacor, E.J. Essene, J.H. Lee, L.C. Kuo, M.A. Cosca, Hydrothermal treatment of smectite, illite, and basalt to 460°C comparison of natural with hydrothermally formed clay minerals, Clays and Clay Minerals 35 (1987) 241-250.

[141] J.K. Edzwald, J.B. Upchurch, C.R. O'Melia, Coagulation in estuaries, Environmental Science & Technology 8 (1974) 58-63.

[142] B. Fritz, Multicomponent solid solutions for clay minerals and computer modeling of weathering processes, The Chemistry of Weathering, Springer Netherlands, 1985.

[143] K. Tanabe, M.R. Gray, Role of fine solids in the coking of vacuum residues, Energy & Fuels 11 (1997) 1040-1043.

[144] N. Sanaie, A. Watkinson, B. Bowen, K. Smith, Effect of minerals on coke precursor formation, Fuel 80 (2001) 1111-1119.

[145] P. Rahimi, T. Gentzis, C. Fairbridge, Interaction of clay additives with mesophase formed during thermal treatment of solid-free Athabasca bitumen fraction, Energy & Fuels 13 (1999) 817-825.

[146] M.T. Timko, A.F. Ghoniem, W.H. Green, Upgrading and desulfurization of heavy oils by supercritical water, The Journal of Supercritical Fluids 96 (2015) 114-123.

[147] C. Laborde-Boutet, D. Dinh, F. Bender, M. Medina, W.C. McCaffrey, In situ observation of fouling behavior under thermal cracking conditions: Hue, saturation, and intensity image analyses, Energy & Fuels 30 (2015) 3666-3675.

[148] D. Dinh, In-situ observation of heavy-oil cracking using backscattering optical techniques, University of Alberta, Master thesis, 2015.

3 Irreversible Adsorption of Asphaltenes on Kaolinite: Influence of Dehydroxylation

3.1 Introduction

Adsorption of petroleum-derived organic matter at various surfaces or interfaces impacts the entire chain of oil production, from reservoir recovery to pipeline transport and oil refining [1, 2]. Asphaltenes, as the heaviest and most polar fraction of crude oil, significantly contribute to such adsorption, particularly on mineral and metal surfaces [2]. Extensive efforts have been devoted to understanding the adsorption behavior of asphaltenes from solvent solution onto clay minerals [3, 4], silica [5, 6], metals [7], and glasses [8]. In each case, a significant amount of asphaltenes was found to either irreversibly adsorb, or give undetectable rates of desorption [2, 4, 9]. Conventional adsorption isotherms such as the Langmuir type or Freundlich type are often used to model the dependence of the adsorption density on asphaltene concentration in bulk solution. However, as reported by Wang et al. [4], such adsorption isotherms are merely curve fittings with no fundamental validity or predictive value, because of the irreversible attachment of asphaltenes on adsorbent surfaces. Consequently, asphaltene adsorption is dominated by unbalanced adsorption/desorption kinetics, and as such it is not a true equilibrium process [4, 10]. The amount and surface coverage of adsorbed asphaltenes can be influenced by many factors, including surface properties of adsorbent [2], source of asphaltenes [11], concentration of asphaltene solution [8], time period of contact [9], solvent [12], and moisture content [13]. The adsorption density of asphaltenes can range from 0.2 to 100 mg/m^2 [2, 14], and both monolayer [5, 9] and multilayer [2, 8] adsorption have been reported.

The oil industry is increasingly relying on unconventional oil resources such as oil sands bitumen, which contain a significant amount of mineral solids [15], for oil production. Thermal

treatment (up to 550°C) is a popular choice worldwide for processing heavy oil such as bitumen [15], under which conditions the entrained mineral solids may be thermally altered. Although the adsorption behavior of asphaltenes on naturally occurring minerals has been extensively studied [2, 6], information on asphaltene adsorption on thermally-altered minerals is scarce. The potential importance of such a study can be seen from a number of problems such as coke formation, equipment fouling, and catalyst deactivation that are encountered during upgrading and refining of heavy oil [15]. For instance, asphaltenes are well known to act as coke precursors during thermal processing of heavy oil. Prior studies showed that the addition of specific minerals such as kaolinite can suppress coke formation [15]. The present work will provide insights in understanding the coking suppression mechanisms by investigating the adsorption behavior of asphaltenes on thermally-treated minerals.

Kaolinite has been widely used for the study of asphaltene adsorption because of its abundance in petroleum reservoirs and oil sands and its strong affinity for organic compounds [3, 4, 15]. As mentioned in Section 2.2.3, kaolinite dehydroxylates at 350−700°C to form metakaolin, which is widely used in ceramic processing, as a geopolymer precursor, and in manufacture of molecular sieves [16-18]. Rahier et al. [17] found that the amount of metakaolin increases linearly with the degree of dehydroxylation as determined by thermogravimetric analysis (TGA). Currently, no study has yet examined the influence of kaolinite dehydroxylation on its adsorption capacity for asphaltenes.

The working hypothesis is that the adsorption of asphaltenes on kaolinite would be enhanced after thermal treatment due to dehydroxylation. The influence of kaolinite dehydroxylation on asphaltene adsorption was investigated using both single- and multiple-contact adsorption

methods. The adsorption density, percent surface coverage, and mean domain thickness were evaluated based on the total and surface carbon content analysis.

3.2 Materials and Methods

3.2.1 Materials

The kaolinite was supplied by ACROS Organics and used as received for the adsorption experiments. The C_7 asphaltenes were extracted from Athabasca bitumen (provided by Imperial Oil Limited) following the method of ASTM D6560-12 [19]. The total carbon content of the asphaltene sample is 82 wt%, as determined by a Thermo Scientific Flash 2000 elemental analyzer. Reagent-grade toluene was purchased from Fisher Scientific and used to prepare asphaltene solutions.

3.2.2 Thermal Treatment

The thermal treatment of the kaolinite was carried out in a Model 3-550 Ney Vulcan programmable muffle furnace. The kaolinite samples were heated in air at a rate of 5°C/min from room temperature (~25°C) to 300−700°C and then held for 2 h. Afterwards, the samples were cooled down to ambient temperature and kept in dry bottles. All the thermally-treated samples were prepared immediately before being used for adsorption, to avoid atmospheric moisture uptake.

3.2.3 Single-Contact Adsorption

The single-contact adsorption experiments were carried out following the procedures of Wang et al. [4]. One gram of the untreated or thermally-treated kaolinite sample was added into 50 mL

asphaltene-in-toluene solution. In this work, all the adsorption tests were conducted using asphaltene-in-toluene solutions with a fixed concentration of 2 g/L. The effect of solution concentration on the asphaltene adsorption has been reported in a prior work [4]. The mixture was shaken by an elliptical shaker for 24 h at room temperature and then filtered using 0.22-μm Millipore filter membrane. To test the irreversibility of asphaltene adsorption, small quantity (~30 mg) of the filter cake from the untreated and 500°C-treated kaolinite were collected after all the liquid had passed through (the amount of unadsorbed asphaltenes left in this filter cake was negligible). The remaining filter cake was washed repeatedly with fresh toluene until the filtrate was colorless. All the other filter cakes were directly washed with fresh toluene. All cake solids were placed in an oven at 65°C to dry.

3.2.4 Multiple-Contact Adsorption

The untreated and 700°C-treated kaolinite samples were selected for the multiple-contact adsorption experiments. The method of Wang et al. [4] was used, following the same procedures as described in Section 3.2.3 for each successive adsorption contact. One gram of kaolinite was contacted with 50 mL asphaltene-in-toluene solution (2 g/L). After 24 h of contact, the kaolinite-asphaltene suspension was filtered and the separated kaolinite was washed with toluene until the filtrate was colorless. After toluene washing, the kaolinite sample was placed in an oven. The dried kaolinite from the first contact were mixed into a fresh 50 mL asphaltene-in-toluene solution, followed by 24 h shaking, filtration, and repeated cake washing with fresh toluene. The steps were repeated for up to five times and the kaolinite after each contact was analyzed by several techniques which are described below.

3.2.5 Analytical Methods

The transmission Fourier transform infrared (FTIR) spectra of the kaolinite samples were obtained in a Nicolet 6700 FTIR spectrometer (Thermo Scientific, USA) within the wavenumber range of 4000−400 cm^{-1}, using a KBr pressed disk technique [20]. The KBr pellet was prepared by mixing 0.5 mg of kaolinite powder in 200 mg KBr and then pressing at 27.6 MPa into a 1-cm-diameter disk.

Thermogravimetric analysis (TGA) was performed with a Thermo Cahn TherMax 400 thermogravimetric analyser by heating approximately 10 mg of the kaolinite samples at a rate of 10°C/min to 900°C under argon atmosphere. The data of weight was normalized by the weight of the sample at 250°C to eliminate the effects of moisture and gaseous species [21].

The particle size of the kaolinite was determined by laser diffraction using a Malvern Mastersizer 3000 particle size analyzer. De-ionized water was used as the dispersing medium in the measurements. The kaolinite-water solutions were treated in an ultrasonic bath for 30 seconds and the particle size data were collected immediately after the treatment. The BET specific surface area was determined from N_2 adsorption isotherms using a Quantachrome Autosorb 1MPa instrument. Prior to analysis, the kaolinite samples were outgassed for 3 h at 280°C.

A Zeiss Sigma 300 VP field emission scanning electron microscope (SEM) was used to analyze the morphology of the kaolinite samples. A suspension of kaolinite particles was prepared by mixing about 50 mg kaolinite in 1 mL water. A droplet of the mixed suspension was cast on an aluminum SEM sample holder. After evaporation of water, a Leica EM SCD005 Coater was used to deposit a thin carbon coating onto the particles to avoid sample charging.

A Thermo Scientific Flash 2000 elemental analyzer was used to determine the total carbon contents of the kaolinite samples. X-ray photoelectron spectroscopy (XPS) measurements were conducted with a Kratos AXIS 165 X-ray photoelectron spectrometer to determine the surface concentration of carbon as well as other elements. For XPS measurements, monochromatic Al Kα source (hν = 1486.6 eV) was used at a power of 210 W. Survey scan spectra were acquired at 160 eV pass-energy to analyze the surface chemical composition.

The wettability of the asphaltene-coated kaolinite was characterized by three methods: contact angle measurements, film flotation technique, and toluene-water emulsification tests.

The contact angles of the samples were determined by the sessile drop method [22], i.e., water drops were placed on the pressed pellets and the contact angles were measured by the outline of the water drops in air. Each kaolinite sample (~100 mg) was pressed at 34 MPa into a 1-cm diameter pellet by an ICL 12 TON E-Z Press^{TM} pellet presser for contact angle measurements using a FTA200 contact angle goniometer equipped with an optical microscope and illumination system.

The procedures of film flotation tests used by Wang et al. [23] were followed in this study. Circa 0.03 g of kaolinite was slowly and evenly sprinkled on the surface of methanol-water solutions with surface tension ranging from 22.51 to 72.01 mN/m [24], which were prepared by mixing different volumes of methanol with deionized water at 10 vol% increments. The floating particles were collected when particle settling stopped, and then dried and weighed. The critical surface tension of the kaolinite sample should be in the range of surface tensions of the two neighboring probing solutions where the kaolinite particles just floated or sank. A more detailed

introduction on the principles and procedures of film flotation technique is presented in Chapter 5 (Section 5.2.2).

In emulsification tests, 0.1 g of the kaolinite was mixed with 20 mL toluene and 20 mL water. The toluene-water-kaolinite mixture was hand-shaken for 2 min and subsequently left to stand to phase separate. The volume of the produced emulsions after 24 h standing was recorded. More information on the method of emulsion preparation can be found in Chapter 5 (Section 5.2.3).

The filterability was characterized by membrane filtration using the 0.22-μm Millipore GVWP filter paper. One gram of the kaolinite sample was mixed with 50 mL toluene to form a suspension. The suspension was then mixed and filtered at 55 kPa vacuum pressures under room temperature (~25°C). When all the liquid had passed through the filter, the total time was recorded as the filtration time. More details on room-temperature filtration can be found in Chapter 6 (Section 6.2.3).

3.3 Results

3.3.1 Degree of Dehydroxylation

Molecular structural changes during thermal treatment of kaolinite at 300−700°C were examined with FTIR (Figure 3.1). All the peak assignments are based on the published data [17, 25, 26]. The band at 912 cm^{-1} is assigned to the bending mode of structural Al_2OH groups. The bands at 3620 and 3652 cm^{-1} are assigned to the inner OH stretching modes. The band at 3697 cm^{-1} reflects both the inner- and outer-surface OH groups, including hydroxyl groups at the edges. All of these OH bands gradually disappeared as the treatment temperature increased, indicating the

occurrence of kaolinite dehydroxylation (particularly when the treatment temperature was higher than 500°C).

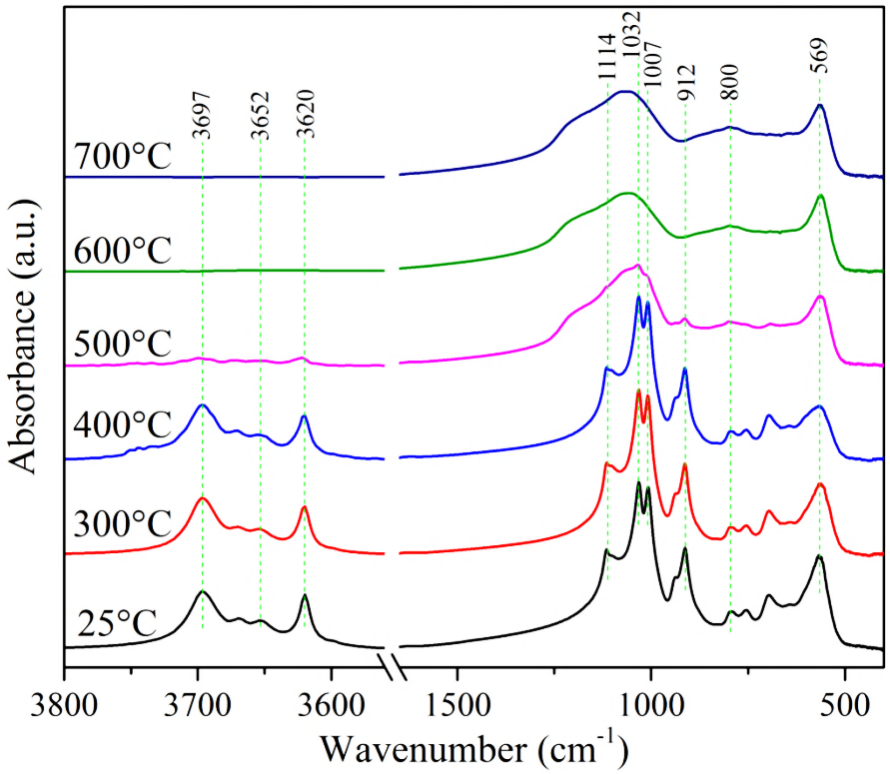

Figure 3.1 FTIR spectra of the untreated (25°C) and thermally-treated (300−700°C) kaolinite.

The weight loss in TGA gives direct information on the degree of dehydroxylation of thermally-treated clay mineral [17, 27]. Figure 3.2 shows the typical TGA curves of the untreated and dehydroxylated kaolinite before and after single contact with asphaltene-in-toluene solutions. The TGA weight of the untreated kaolinite became constant after ~650°C, indicating complete dehydroxylation of the sample. However, the observed maximum weight loss, ~10 wt%, is lower than the theoretical weight loss (i.e. 14 wt% [28]) for an idealized kaolinite following complete dehydroxylation, likely due to the impurity of the kaolinite sample [27]. The weight losses of the dehydroxylated kaolinite samples were significantly lower than that of the untreated kaolinite,

due to the dehydroxylation reactions during thermal treatment [17, 27]. In particular, the 700°C-dehydroxylated kaolinite showed negligible weight loss in TGA test (up to 900°C). After asphaltene adsorption, the weight losses of all the samples were increased, which is attributed to the presence of irreversibly-adsorbed asphaltene materials (all the asphaltene-coated kaolinite samples in Figure 3.2 have been thoroughly washed with toluene). The similar additional weight losses, ~2% as presented in Figure 3.2, indicated the similar asphaltene adsorption densities on these samples, which will be further studied by carbon content analysis.

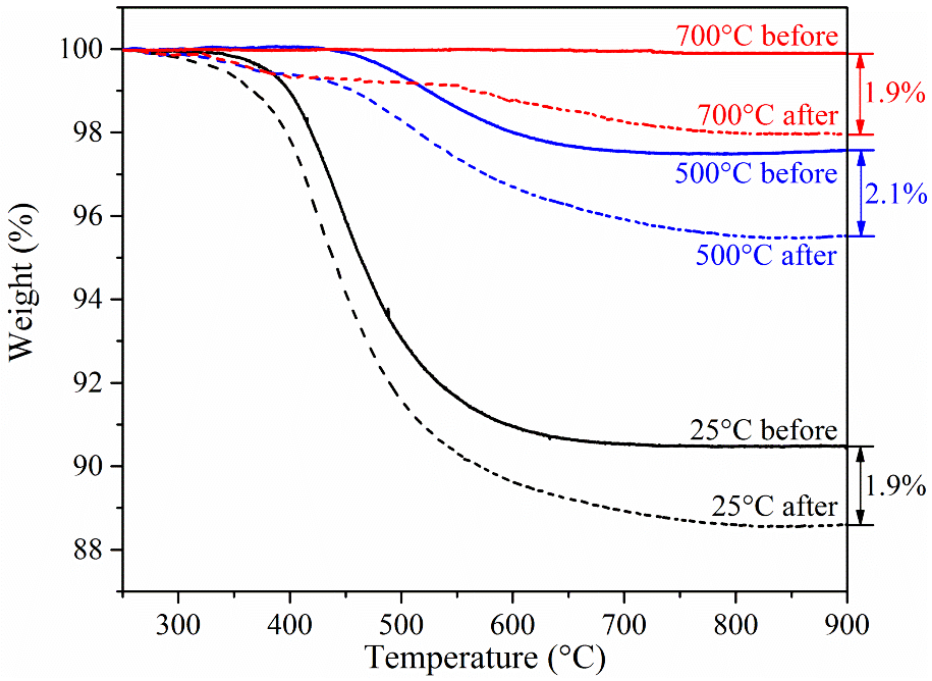

Figure 3.2 TGA curves of the untreated (25°C), 500°C-dehydroxylated, and 700°C-dehydroxylated kaolinite before and after asphaltene adsorption using single-contact method. All the asphaltene-coated kaolinite samples were toluene washed.

To quantitatively estimate the degree of dehydroxylation (D), the following equation was used based on the TGA data [17, 27]:

$$D = 1 - m / m_0 \tag{3.1}$$

where m is the TGA weight loss at 900°C of the kaolinite samples (%), and m_0 is the maximum weight loss where a value of 10% was used, corresponding to the weight loss of the untreated kaolinite when heated to 900ºC. For instance, when a kaolinite sample previously heated at 700ºC for 2 h was tested in the TGA analysis, the weight loss *m* was circa zero, so the degree of dehydroxylation of this sample was circa one.

Figure 3.3 shows the degree of dehydroxylation (D) of the kaolinite samples as a function of the treatment temperature. In Figure 3.3, three regions can be distinguished: (i) below 400°C, where no significant dehydroxylation reaction occurs and D is close to zero; (ii) in the range of 400−600°C, where D increases sharply from ~0 to ~1; (iii) above 600°C, where D remains almost constant and close to one. This trend is consistent with the observations of Shvarzman et al. [27] and Rahier et al. [17]. The results indicate that dehydroxylation of the kaolinite started above 400°C and was largely completed by 600°C.

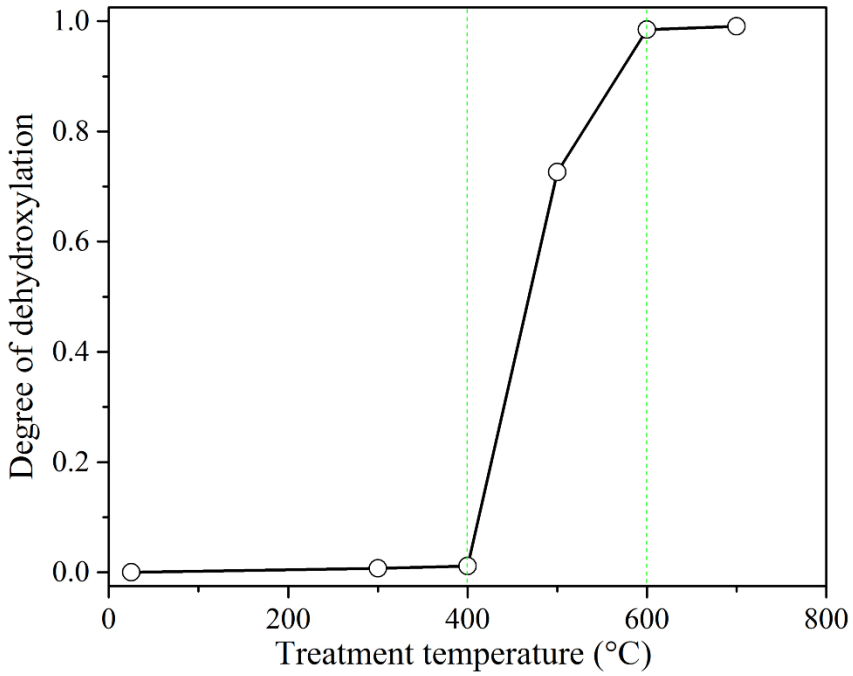

Figure 3.3 Degree of kaolinite dehydroxylation (determined by TGA weight loss using Equation 3.1) as a function of the treatment temperature. The untreated kaolinite is denoted as treatment temperature at 25°C.

3.3.2 Particle Size, Specific Surface Area, and Particle Morphology

The mean particle size of the untreated kaolinite was ~3 μm (D_{50}), as determined by a Mastersizer 3000 particle size analyzer. No significant change in particle size was observed after thermal treatment at temperatures up to 700°C followed by asphaltene adsorption (Table 3.1). The BET specific surface area of the kaolinite samples also remained constant at ~11 m^2/g over the range of temperatures studied, as presented in Table 3.1.

Table 3.1 Particle size and specific surface area of the untreated and dehydroxylated kaolinite.

Kaolinite		Untreated	Dehydroxylated at 500°C	Dehydroxylated at 700°C
Mean particle size (D_{50}) (μm)	Before adsorption	2.8	3.1	2.6
	After adsorption	3.0	3.3	2.5
BET specific surface area (m^2/g)		11.0	10.9	10.9

The morphology of the kaolinite particles was observed by scanning electron microscopy (SEM). The images in Figure 3.4 clearly show the platy crystals of kaolinite. Neither thermal treatment at up to 700°C (Figures 3.4B and 3.4C) nor asphaltene adsorption (Figure 3.4D) significantly changed the particle size and shape of the kaolinite, consistent with the data in Table 3.1. The adsorbed asphaltenes on kaolinite particles could not be identified on the SEM image (Figure 3.4D).

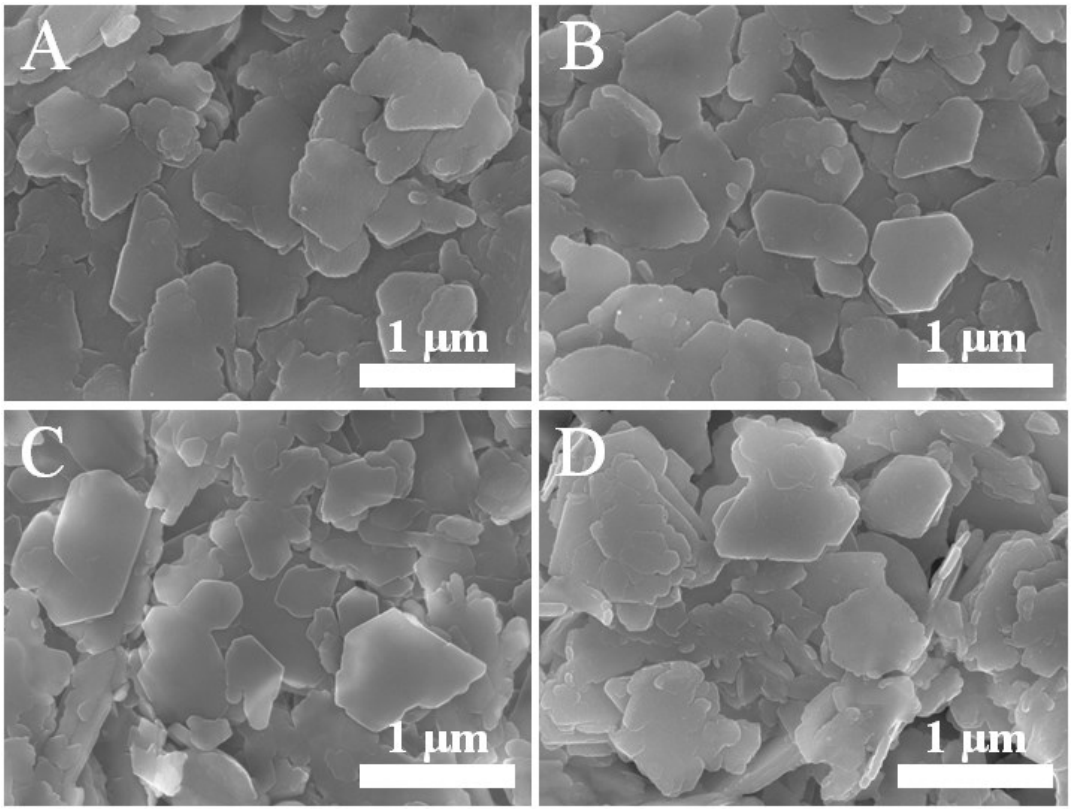

Figure 3.4 Typical SEM images of (A) untreated kaolinite, (B) dehydroxylated kaolinite at 500°C, (C) dehydroxylated kaolinite at 700°C, and (D) dehydroxylated kaolinite at 700°C followed by asphaltene adsorption.

3.3.3 Irreversibility of Asphaltene Adsorption

Before asphaltene adsorption, the total carbon contents of the untreated and dehydroxylated kaolinite were negligible (Table 3.2). After single contact with the asphaltene-in-toluene solution, the carbon contents were significantly increased for both the untreated and dehydroxylated kaolinite. To estimate the adsorption density of asphaltenes on kaolinite, the following equation was used based on total carbon content analysis:

$$\Gamma = \frac{TC_{coated} - TC_k}{TC_a - TC_{coated}} \times \frac{1000}{S} \tag{3.2}$$

where Γ is the adsorption density of asphaltenes (mg/m^2), TC_{coated}, TC_k, and TC_a are the total carbon contents (wt%) of the asphaltene-coated kaolinite, uncoated kaolinite, and bulk asphaltenes (TC_a = 82 wt%) respectively, and S is the specific surface area of the kaolinite (11 m^2/g). The carbon contribution from the kaolinite was deducted in Equation 3.2.

Table 3.2 Effect of toluene washing on the adsorption density of asphaltenes on kaolinite.

Kaolinite	Before adsorption	After adsorption without toluene washing		After adsorption with toluene washing		Asphaltenes remaining adsorbed (%)
	Total carbon (wt%)	Total carbon (wt%)	Adsorption density (mg/m^2)	Total carbon (wt%)	Adsorption density (mg/m^2)	
Untreated	0.04	1.95	2.17	1.58	1.75	81
Dehydroxylated (at 500°C)	0.04	2.09	2.34	1.66	1.84	79

As presented in Table 3.2, the asphaltene adsorption density was estimated to be 1.8−2.3 mg/m^2 (corresponding to 20−25 mg/g) for the asphaltene-coated kaolinite materials with a total carbon content of 1.6−2.1 wt%. This relatively low adsorption density likely explained why there was no detectable asphaltenes in SEM images of the less than 10 μm^2 sample area. The result is in good agreement with the linear correlation between asphaltene adsorption density and total carbon content reported by Wang et al. [3], where an asphaltene sample with similar carbon content was used and the asphaltene adsorption density was determined by ultraviolet-visible spectrophotometric technique. Such a consistency confirms the validity of the calculated results for asphaltene adsorption density using the method of total carbon content analysis.

The irreversibility of asphaltene adsorption was confirmed with toluene as the reference solvent. After thorough washing with toluene, circa 80% of the asphaltenes remained adsorbed (Table 2). This portion of adsorbed asphaltenes cannot be desorbed even after further contacting with fresh toluene for 24 hours. These observations confirm the conclusion that the adsorption of asphaltenes on mineral surfaces is largely an irreversible process [4, 5]. This strongly-bound sub-fraction of asphaltenes significantly contributes to modify the particle behaviors [6, 29]. Therefore, in the following sections, the behavior of this irreversibly-adsorbed asphaltene sub-fraction on toluene-washed samples of kaolinite was specifically analyzed.

3.3.4 Adsorption Behavior with Single Contact

After single contact with asphaltene-in-toluene solution, the adsorption density of asphaltenes (calculated from Equation 3.2) on the untreated and dehydroxylated kaolinite was similar (Table 3.3), which is consistent with the previous conclusion from the TGA data (Figure 3.2). However, a significant difference was observed in surface chemical composition. After thermal treatment followed by asphaltene adsorption, the concentrations of carbon and sulfur at kaolinite surfaces were increased while the concentrations of aluminum, silicon, and oxygen showed a slight decreasing trend, particularly when the treatment temperature was higher than 500°C. Sánchez et al. [18] investigated the surface transformations on kaolinite induced by thermal treatment using XPS, and they observed that thermal treatment did not change the concentration ratio SC_{Al}/SC_{Si} on kaolinite surface. Indeed, in the present study, the SC_{Al}/SC_{Si} ratio remained unchanged even after asphaltene adsorption (Table 3.3), indicating that neither the alumina nor the silica regions were preferentially covered by the asphaltenes, consistent with the conclusion of Wang et al. [3].

Table 3.3 Effect of thermal treatment on the adsorption density and percent surface coverage of asphaltenes on kaolinite (single-contact adsorption method). The untreated kaolinite is denoted as treatment temperature at 25°C.

Treatment temperature (°C)	Adsorption density (mg/m^2)	Surface composition (atom%)[a]					$\frac{SC_{Al}}{SC_{Si}}$	Surface coverage (%)[b]
		C	S	Al	Si	O		
25	1.75	22.5	0.2	12.0	15.4	50.0	0.8	15
300	1.76	23.4	0.1	12.7	16.0	47.9	0.8	16
400	1.79	23.4	0.1	12.5	16.0	47.9	0.8	16
500	1.84	30.6	0.6	10.6	15.1	43.1	0.7	25
600	1.87	35.4	1.0	11.0	14.4	38.2	0.8	31
700	1.87	35.2	0.8	10.9	14.3	38.8	0.8	31

[a] Determined by XPS.

[b] Calculated from Equation 3.3.

Following the method of Wang et al. [3], the percent surface coverage by adsorbed asphaltenes on kaolinite was estimated based on the surface carbon concentration determined by XPS:

$$\theta = \frac{SC_{coated} - SC_k}{SC_a - SC_k} \times 100\% \tag{3.3}$$

where θ is the percent surface coverage by adsorbed asphaltenes, and SC_{coated}, SC_k, and SC_a are the carbon concentrations on the surface of asphaltene-coated kaolinite, uncoated kaolinite (10.3 atom%), and bulk asphaltenes (90.6 atom%), respectively. As shown in Table 3.3, the calculated percent surface coverage by adsorbed asphaltenes on the untreated kaolinite was 15%,

while that on the dehydroxylated kaolinite (at 600−700°C) was doubled (31%). This result was not expected, considering that the adsorption density of asphaltenes was similar for all the kaolinite samples (Table 3.3). To understand this unexpected result, multiple-contact adsorption experiments were conducted and the results are presented in the following section.

3.3.5 Adsorption Behavior with Multiple Contacts

The multiple-contact adsorption results are illustrated in Figure 3.5 in terms of (A) adsorption density (calculated from Equation 3.2 using the total carbon content data), (B) percent surface coverage (calculated from Equation 3.3 using the XPS surface carbon concentration data), and (C) mean thickness of adsorbed asphaltene domains on the kaolinite surface. The mean domain thickness was estimated by the following equation, using the data for adsorption density and percent surface coverage:

$$\delta = \frac{\Gamma}{\rho_a \times \theta} \times 10^5 \tag{3.4}$$

where δ is the mean thickness of adsorbed asphaltene domains (nm), Γ is the adsorption density (mg/m^2), ρ_a is the density of the asphaltenes (assumed to be 1200 kg/m^3 [30]), and θ is the percent surface coverage by adsorbed asphaltenes (%). The value of 10^5 was the result of unit conversion.

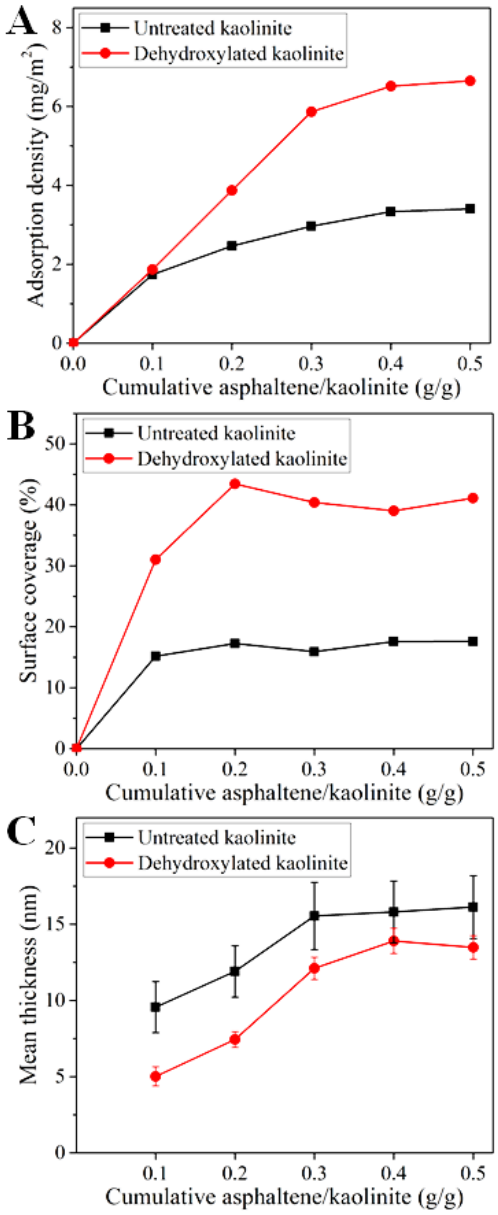

Figure 3.5 (A) Adsorption density, (B) percent surface coverage, and (C) mean thickness of adsorbed asphaltene domains on the untreated and dehydroxylated kaolinite (at 700°C) in multiple-contact adsorption experiments. The horizontal axis indicates the cumulative amount of asphaltenes contacted with the kaolinite sample, with values of 0.1 to 0.5 g/g corresponding to the first to fifth contact respectively. The error bars in panel C indicate the estimated errors based on the propagation of errors in adsorption density (±0.2 mg/m^2) and surface coverage (±2%).

The data in Figure 3.5A show that the adsorption density of asphaltenes on both the untreated and dehydroxylated kaolinite increased with the cumulative amount of asphaltenes in toluene solutions contacted with the kaolinite sample (i.e. the number of contacts). However, the adsorption density on the dehydroxylated kaolinite was higher than that on the untreated kaolinite, particularly after the second contact. The percent surface coverage by adsorbed asphaltenes on the untreated kaolinite did not change significantly with the number of contacts (Figure 3.5B), although an increasing adsorption density was observed (Figure 3.5A), an observation consistent with that of Wang et al. [4]. The percent surface coverage on the dehydroxylated kaolinite increased from ~30% to ~40% after the second contact, and thereafter a plateau was reached. A continuous increasing trend in domain thickness of adsorbed asphaltenes was observed for both the untreated and dehydroxylated kaolinite up to the fourth contact (Figure 3.5C). A discussion of these results is given in the following section.

3.3.6 Wettability and Filterability

Table 3.4 presents the wettability and filterability of the kaolinite with different degrees of asphaltene surface coverage (0−41%). The increase of surface coverage significantly increased the hydrophobicity of kaolinite particles, as indicated by the increasing contact angle and decreasing critical surface tension. All the kaolinite particles in each sample behaved the same on different methanol-water solutions (i.e., they all floated or sank at the same time, depending on the solution surface tension), suggesting their homogeneity in surface wettability. Before asphaltene adsorption, neither the untreated kaolinite nor the dehydroxylated kaolinite could stabilize emulsions (emulsion volume = 0). However, after asphaltene adsorption, both kaolinite samples were capable of stabilizing emulsions, and the volumes of the produced emulsions increased with the increasing asphaltene surface coverage, as indicated in Table 3.4. In contrast,

no significant change in filtration time was observed between all the investigated samples (Table 3.4), indicating that neither thermal treatment nor asphaltene adsorption altered the filtration behavior of the kaolinite particles.

Table 3.4 Effect of asphaltene surface coverage on the wettability and filterability of kaolinite samples. From A to E, the sample was untreated kaolinite, 700°C-dehydroxylated kaolinite, untreated kaolinite after single contact with asphaltene solution, 700°C-dehydroxylated kaolinite after single contact with asphaltene solution, and 700°C-dehydroxylated kaolinite after five contacts with asphaltene solutions, respectively.

Sample	A	B	C	D	E
Surface coverage (%)	0	0	15	31	41
Contact angle (deg.)	15	27	86	99	102
Critical surface tension (mN/m)	>72	>72	33−37	30−33	27−30
Emulsion volume (%)	0	0	22	34	47
Filtration time (s)	68	70	68	70	69

3.4 Discussion

Asphaltenes are known to form nanoaggregates even in a good solvent such as toluene, and the nanoaggregates are the prevalent species in an asphaltene-toluene solution at concentrations higher than 0.1−0.2 g/L [31-33]. Consequently, the adsorption behavior observed in the present study is essentially a reflection of the behavior of colloidal asphaltene nanoaggregates. The structure and size of the asphaltene nanoaggregates have been widely studied using a range of

analytical techniques, such as nuclear magnetic resonance and small angle scattering [31, 33, 34]. Although it still remains a subject of intense debate [33, 34], these nanoaggregates are believed to have a complex bridged and porous structures with a mean aggregate size in the range of 2−20 nm [31, 34, 35].

Extensive studies have been conducted to understand the interaction mechanisms of organic matter adsorption on mineral surfaces [36, 37]. Gray et al. [33] proposed a supramolecular assembly model for asphaltene aggregates, combing cooperative bindings by acid-base interactions, hydrogen bonding, metal coordination complexes, and π−π stacking. These binding forces are also believed to play a role in asphaltene-mineral interactions [2, 38, 39]. Several studies have shown that the functional groups with heteroatoms (such as N, O, and S) allow asphaltenes to interact with a mineral surface containing polar sites (such as aluminol and silanol), thus initiating adsorption [2, 38, 40]. Andrieux et al. [41] proposed that the interactions between the aromatic π system and surface siloxane groups are responsible for the 2,4,6-trimethylpyridine adsorption on silica.

As a 1:1 aluminosilicate clay mineral, kaolinite has two basal faces: tetrahedral siloxane face of Si-O-Si exposure and octahedral aluminum face of Al-OH exposure [42]. At the edge surfaces of the 1:1 layer, the structure is disrupted and broken bonds occur, which are accommodated as −OH groups [42, 43]. Consequently, the aluminol, silanol, and siloxane groups present at kaolinite surfaces can all contribute as potential binding sites for asphaltenes, by a variety of interaction forces as mentioned earlier. The adsorption data in the present study revealed the average behavior of kaolinite, i.e., a combined effect of adsorption from both basal and edge surfaces [44, 45]. The adsorbed asphaltene nanoaggregates can orient at the kaolinite surface in a variety of ways and can deposit at multiple active sites, due to their pronounced heterogeneity [2,

33]. They can also provide additional sites for adsorption, leading to the asphaltene-on-asphaltene deposition [2, 4, 9].

XPS measurement can detect elements at depths up to 10 nm on sample surface but the signal intensities follow an exponential attenuation with the penetration depth [46]. Thus, the elements within the top ~2 nm surface region normally dominate the XPS signals [47, 48]. In the present study, the asphaltene domain thicknesses on all the kaolinite samples were larger than 5 nm (Figure 3.5C), which is sufficient to significantly attenuate the XPS signals of underlying Al and Si. This argument is supported by the observation that the percent surface coverage (calculated based on the XPS data using Equation 3.3) of the untreated kaolinite remained unchanged upon subsequent multiple contacts (Figure 3.5B), even as the asphaltene adsorption density was significantly increased from 1.7 up to 3.4 mg/m^2 (Figure 3.5A). Such an observation also suggests that the additional adsorbed asphaltenes preferentially and primarily deposited on the asphaltenes already on the surface (rather than on the exposed kaolinite), which is consistent with the conclusion of Wang et al. [4]. The percent surface coverage by adsorbed asphaltenes was well below 50% even at the highest level of adsorption (Figure 3.5), indicating that the asphaltenes only patchily adsorbed on the kaolinite surfaces. Such an adsorption characteristic is consistent with the observed patchy organic coating on oil sands fine solids [1, 49].

Based on these observations, the XPS-determined percent surface coverage by adsorbed asphaltenes indicated the density of active binding sites on kaolinite surfaces over a wide range of adsorption densities. As illustrated in Figure 3.6, the percent surface coverage increased with the increasing degree of kaolinite dehydroxylation, particularly revealed by the single-contact adsorption data. This result suggests that the adsorption of asphaltenes on kaolinite, more specifically, the density of active binding sites on kaolinite surface, was strongly affected by the

degree of dehydroxylation. In comparison to single contact, multiple contacts of 700°C-dehydroxylated kaolinite (degree of dehydroxylation = 1) with asphaltene-in-toluene solutions resulted in a further increase in the percent surface coverage. However, the multiple contacts did not significantly change the percent surface coverage on the untreated kaolinite (degree of dehydroxylation = 0). Acevedo et al. [8] observed stepwise adsorption of asphaltenes on glass surfaces, and they proposed that the coverage of the first asphaltene layer is limited by surface saturation and afterwards one or two further layers can be adsorbed leading to multilayer adsorption. The adsorption process in the present study is believed to follow similar pathways. The results in Figure 3.6 suggest that after single contact, surface saturation was not achieved on the dehydroxylated kaolinite, while the saturation state had already been reached on the untreated kaolinite due to the limited density of binding sites on its surface.

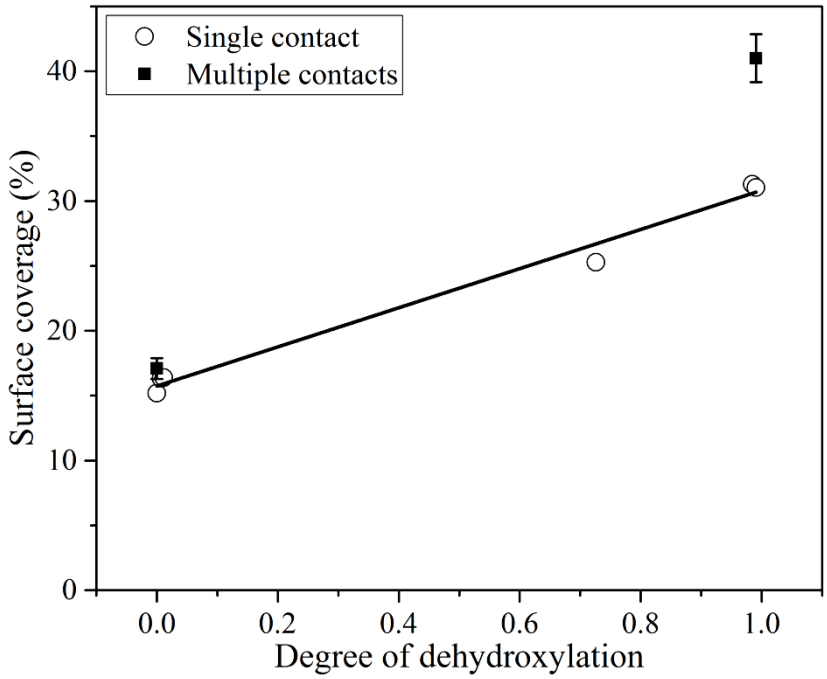

Figure 3.6 Relationship between percent surface coverage by adsorbed asphaltenes (determined by XPS using Equation 3.3) and degree of dehydroxylation (determined by TGA weight loss using Equation 3.1). The line shows a linear fit to the single-contact adsorption data with R^2 = 0.985.

White et al. [16] studied the structure of dehydroxylated kaolinite by combining density functional theory and pair distribution function analysis. They proposed that the strained nature of this dehydroxylated material was responsible for its high activity. As kaolinite undergoes dehydroxylation, water molecules are released from the alumina layers, resulting in strained Al-O-Al bonds. The slightly growing and broadening peak at 800 cm^{-1} (Al-O) in the FTIR spectra of Figure 3.1 supports the above argument. As proposed by White et al. [16], these aluminium atoms reorganize to relieve as much of the strain as possible, which, in turn, requires all atoms to shift in position, leading to the buckling of both alumina and silica layers. These kinds of strained structures are rare on the untreated kaolinite, and they are proved to be extremely active

[16, 50, 51]. For example, Dubois and Zegarski [52] demonstrated that such strained structures are more active than surface hydroxyl groups in binding with alkoxysilanes. Bauer et al. [51] reported that the strained sites are active towards adsorption of organic materials such as naphthalene and pyrene. Consequently, the exposure of these active strained sites on dehydroxylated kaolinite likely provided additional binding sites for asphaltenes, leading to the increased percent surface coverage (Table 3.3 and Figure 3.5B).

Bich et al. [53] reported that physical parameters of dehydroxylated kaolinite remained very close to those of the untreated kaolinite, consistent with the observations in this study that the particle size, specific surface area, and particle morphology (Table 3.1 and Figure 3.4) did not change significantly after thermal treatment at 300−700°C. These physical characteristics, therefore, cannot be responsible for the observed increased percent surface coverage by adsorbed asphaltenes.

The dehydroxylated kaolinite had higher density of stronger binding sites than the untreated kaolinite, thus enabling more asphaltenes to adsorb on its surface, as clearly revealed in multiple-contact adsorption experiments (Figure 3.5A). However, such a trend was not observed in single-contact adsorption: the untreated and dehydroxylated kaolinite showed similar adsorption density, as presented in Table 3.3. Wang et al. [4] proposed that the adsorption of asphaltenes was governed by the kinetics of the irreversible adsorption, rather than equilibrium thermodynamics, which was supported by many experimental evidences [5, 7]. For example, Zahabi et al. [7] reported that the adsorption of asphaltenes on gold and silica showed multilayer adsorption, without reaching equilibrium even after 16 h. Xie and Karan [12] studied the asphaltene adsorption on metal surfaces, and they reported that no equilibrium can be achieved

in asphaltene solutions and the initial adsorption process is controlled by the diffusion of asphaltenes from the bulk solution to the adsorption surfaces.

In such a kinetically controlled process, the adsorption is mainly constrained by the time allowed for contact, the density of "active" asphaltenes with strong binding potential, and the density of active surface sites for binding. The first two conditions were the same for the untreated and dehydroxylated kaolinite, in either single- or multiple-contact adsorption experiments. After single contact of the kaolinite with the asphaltene-in-toluene solution, the similar asphaltene adsorption densities on the surfaces of the untreated and dehydroxylated kaolinite suggest that the single-contact adsorption was limited by the contact time and the density of "active" asphaltenes. By increasing both the cumulative time (up to five days) for contact and the cumulative density of "active" asphaltenes and thoroughly washing the asphaltene-coated samples with toluene after each successive contact (the toluene wash may potentially enhance the irreversible adsorption process by removing the reversibly-adsorbed asphaltenes before the next contact), a significantly higher adsorption density on both the untreated and dehydroxylated kaolinite was observed after multiple contacts in comparison to single contact (Figure 3.5A). After multiple contacts, the dehydroxylated kaolinite gave much higher adsorption density than the untreated kaolinite, consistent with the increasing density of kaolinite binding sites after dehydroxylation as discussed earlier. An apparent adsorption plateau was observed after the fourth contact (Figure 3.5), likely because that any further adsorbed asphaltenes was completely reversible and subsequently removed by toluene washing.

In comparison to the untreated kaolinite, the initial thickness of asphaltene domains on the dehydroxylated kaolinite was significantly lower; however, this difference gradually diminished with increasing adsorption density (Figure 3.5). The results suggest a different structural

organization of adsorbed asphaltenes on the two materials at low adsorption density. The higher density of stronger binding sites on the dehydroxylated kaolinite would enable more intense interactions with each adsorbed asphaltene nanoaggregate (i.e. possibly more binding sites for one nanoaggregates than the untreated kaolinite), potentially resulting in a more deformed and flattened asphaltene profile [39, 54] and hence giving a smaller domain thickness. This hypothesis could potentially be tested by calorimetric titration methods, where the initial contact of asphaltenes with dehydroxylated kaolinite would give a larger magnitude of enthalpy of adsorption than natural kaolinite. Such a thickness difference only happened in the initial adsorption of asphaltenes in immediate contact with the kaolinite surfaces. As the kaolinite surface reached saturation, the subsequent asphaltene-on-asphaltene deposition largely diminished this difference, as indicated by the equivalent final domain thickness between the untreated and dehydroxylated kaolinite (Figure 3.5C).

A 10-nm-thick asphaltene film was formed on the untreated kaolinite after single contact (Figure 3.5C), which is comparable with the reported thickness for adsorbed asphaltenes where the adsorption was conducted under similar conditions and the thickness was determined by surface forces apparatus [39] and quartz crystal microbalance [55]. The adsorption data reported by Wang et al. [3] indicated that the mean domain thickness was unchanged even at much lower adsorption densities in the range of 0.3 to 1.2 mg/m^2. The results suggest that a single layer of asphaltene colloids was most likely formed after single contact of the untreated kaolinite with asphaltene-in-toluene solution, giving 15% coverage of the total surface (Table 3.3). The mean thickness of the asphaltene domains on the dehydroxylated kaolinite was reduced to 5 nm (Figure 3.5C), likely due to the more flattened structure as discussed earlier. A final domain thickness of ~15 nm was observed on both the untreated and dehydroxylated kaolinite. Given an

asphaltene colloid dimension on the surface in the range of 5 to 10 nm, the final mean thickness of the domains corresponds to 1.5 to 3 layers of adsorption. Any further adsorption became reversible as defined by desorption during the toluene wash.

The adsorption of asphaltenes on kaolinite surface rendered the particles more hydrophobic and enabled the particles to stabilize water-oil emulsions. As the surface coverage by adsorbed asphaltenes increased from 0 to 41%, the emulsion volume progressively increased from 0 to 47% (Table 3.4), indicating that the emulsification behavior was very sensitive to surface chemical compositions of the kaolinite particles. However, asphaltene adsorption over a wide range of surface coverage (from 0 up to 41%) did not change the particle filterability, which could be explained by several possibilities: (1) the small quantities of adsorbed asphaltenes (up to 7 mg/m^2) were unable to significantly change the particle filtration behavior, or (2) the filtration behavior of kaolinite particles was insensitive to their surface properties. These results will be further discussed in Chapter 7, together with the observations for native clay minerals extracted from bitumen froth.

3.5 Conclusions

The adsorption behavior of Athabasca asphaltenes on the untreated and dehydroxylated kaolinite was investigated in this study. Both the adsorption density and percent surface coverage on the dehydroxylated kaolinite were higher than those on the untreated material, particularly after multiple contacts with asphaltene-in-toluene solutions. The percent surface coverage by adsorbed asphaltenes increased with the increasing degree of dehydroxylation, likely because the strained nature of the dehydroxylated kaolinite provided additional binding sites. When irreversible adsorption was completed upon multiple contacts, 15-nm-thick domains were formed on both the

untreated and dehydroxylated kaolinite, which corresponded to 1.5 to 3 layers of asphaltene colloids. The asphaltene adsorption enabled the kaolinite particles to stabilize water-oil emulsion; in contrast, such adsorption did not significantly change the filterability of the kaolinite.

References

[1] B. Sparks, L. Kotlyar, J. O'Carroll, K. Chung, Athabasca oil sands: Effect of organic coated solids on bitumen recovery and quality, Journal of Petroleum Science and Engineering 39 (2003) 417-430.

[2] J.J. Adams, Asphaltene adsorption, a literature review, Energy & Fuels 28 (2014) 2831-2856.

[3] S. Wang, Q. Liu, X. Tan, C. Xu, M.R. Gray, Study of asphaltene adsorption on kaolinite by X-ray photoelectron spectroscopy and time-of-flight secondary ion mass spectroscopy, Energy & Fuels 27 (2013) 2465-2473.

[4] S. Wang, Q. Liu, X. Tan, C. Xu, M.R. Gray, Adsorption of asphaltenes on kaolinite as an irreversible process, Colloids and Surfaces A: Physicochemical and Engineering Aspects 504 (2016) 280-286.

[5] S. Acevedo, M.A. Ranaudo, C. García, J. Castillo, A. Fernández, Adsorption of asphaltenes at the toluene−silica interface: A kinetic study, Energy & Fuels 17 (2003) 257-261.

[6] S. Dubey, M. Waxman, Asphaltene adsorption and desorption from mineral surfaces, SPE Reservoir Engineering 6 (1991) 389-395.

[7] A. Zahabi, M.R. Gray, T. Dabros, Kinetics and properties of asphaltene adsorption on surfaces, Energy & Fuels 26 (2012) 1009-1018.

[8] S. Acevedo, J. Castillo, A. Fernández, S. Goncalves, M.A. Ranaudo, A study of multilayer adsorption of asphaltenes on glass surfaces by photothermal surface deformation. Relation of this adsorption to aggregate formation in solution, Energy & Fuels 12 (1998) 386-390.

[9] S. Acevedo, M.A. Ranaudo, C. García, J. Castillo, A. Fernández, M. Caetano, S. Goncalvez, Importance of asphaltene aggregation in solution in determining the adsorption of this sample on mineral surfaces, Colloids and Surfaces A: Physicochemical and Engineering Aspects 166 (2000) 145-152.

[10] S. Saraji, L. Goual, M. Piri, Adsorption of asphaltenes in porous media under flow conditions, Energy & Fuels 24 (2010) 6009-6017.

[11] D. Dudášová, A. Silset, J. Sjöblom, Quartz crystal microbalance monitoring of asphaltene adsorption/deposition, Journal of Dispersion Science and Technology 29 (2008) 139-146.

[12] K. Xie, K. Karan, Kinetics and thermodynamics of asphaltene adsorption on metal surfaces: A preliminary study, Energy & Fuels 19 (2005) 1252-1260.

[13] S. Collins, J. Melrose, Adsorption of asphaltenes and water on reservoir rock minerals, Proceedings of the SPE Oilfield and Geothermal Chemistry Symposium, Denver, CO, June 1-3, 1983, DOI: 10.2118/11800-MS.

[14] J. Mendoza, I. Castellanos, A. Ortiz, E. Buenrostro, C. Durán, S. López, Study of monolayer to multilayer adsorption of asphaltenes on reservoir rock minerals, Colloids and Surfaces A: Physicochemical and Engineering Aspects 340 (2009) 149-154.

[5] M.R. Gray, Upgrading oilsands bitumen and heavy oil, The University of Alberta Press, Edmonton, Alberta, 2015.

[16] C.E. White, J.L. Provis, T. Proffen, D.P. Riley, J.S. van Deventer, Combining density functional theory (DFT) and pair distribution function (PDF) analysis to solve the structure of metastable materials: The case of metakaolin, Physical Chemistry Chemical Physics 12 (2010) 3239-3245.

[17] H. Rahier, B. Wullaert, B. Van Mele, Influence of the degree of dehydroxylation of kaolinite on the properties of aluminosilicate glasses, Journal of Thermal Analysis and Calorimetry 62 (2000) 417-427.

[18] R.T. Sánchez, E. Basaldella, J. Marco, The effect of thermal and mechanical treatments on kaolinite: Characterization by XPS and IEP measurements, Journal of Colloid and Interface Science 215 (1999) 339-344.

[19] ASTM D 6560-12, Standard test method for determination of asphaltenes (heptane insolubles) in crude petroleum and petroleum products, ASTM, West Conshohocken, PA, 2012.

[20] J. Madejová, FTIR techniques in clay mineral studies, Vibrational Spectroscopy 31 (2003) 1-10.

[21] C. Hedley, G. Yuan, B. Theng, Thermal analysis of montmorillonites modified with quaternary phosphonium and ammonium surfactants, Applied Clay Science 35 (2007) 180-188.

[22] T. Chau, A review of techniques for measurement of contact angles and their applicability on mineral surfaces, Minerals Engineering 22 (2009) 213-219.

[23] C. Wang, M. Geramian, Q. Liu, D.G. Ivey, T.H. Etsell, Comparison of different methods to determine the surface wettability of fine solids isolated from Alberta oil sands, Energy & Fuels 29 (2015) 3556-3565.

[24] G. Vazquez, E. Alvarez, J.M. Navaza, Surface tension of alcohol water+water from 20 to 50°C, Journal of Chemical & Engineering Data 40 (1995) 611-614.

[25] L. Edomwonyi-Otu, B.O. Aderemi, A.S. Ahmed, N.J. Coville, M. Maaza, Influence of thermal treatment on kankara kaolinite, Opticon1826 5 (2013) 1-5.

[26] R.L. Frost, A.M. Vassallo, The dehydroxylation of the kaolinite clay minerals using infrared emission spectroscopy, Clays and Clay minerals 44 (1996) 635-651.

[27] A. Shvarzman, K. Kovler, G. Grader, G. Shter, The effect of dehydroxylation/amorphization degree on pozzolanic activity of kaolinite, Cement and Concrete Research 33 (2003) 405-416.

[28] H. Cheng, Q. Liu, J. Yang, S. Ma, R.L. Frost, The thermal behavior of kaolinite intercalation complexes-A review, Thermochimica Acta 545 (2012) 1-13.

[29] S. Subramanian, S. Simon, B. Gao, J. Sjöblom, Asphaltene fractionation based on adsorption onto calcium carbonate: Part 1. Characterization of sub-fractions and QCM-D measurements, Colloids and Surfaces A: Physicochemical and Engineering Aspects 495 (2016) 136-148.

[30] K. Akbarzadeh, A. Hammami, A. Kharrat, D. Zhang, S. Allenson, J. Creek, S. Kabir, A. Jamaluddin, A.G. Marshall, R.P. Rodgers, Asphaltenes−problematic but rich in potential, Oilfield Review 19 (2007) 22-43.

[31] J. Eyssautier, D. Frot, L. Barré, Structure and dynamic properties of colloidal asphaltene aggregates, Langmuir 28 (2012) 11997-12004.

[32] Y.M. Ganeeva, T.N. Yusupova, G.V. Romanov, Asphaltene nano-aggregates: Structure, phase transitions and effect on petroleum systems, Russian Chemical Reviews 80 (2011) 993-1008.

[33] M.R. Gray, R.R. Tykwinski, J.M. Stryker, X. Tan, Supramolecular assembly model for aggregation of petroleum asphaltenes, Energy & Fuels 25 (2011) 3125-3134.

[34] Z. Hosseini-Dastgerdi, S. Tabatabaei-Nejad, E. Khodapanah, E. Sahraei, A comprehensive study on mechanism of formation and techniques to diagnose asphaltene structure; molecular and aggregates: A review, Asia-Pacific Journal of Chemical Engineering 10 (2015) 1-14.

[35] H. Yarranton, D. Ortiz, D. Barrera, E. Baydak, L. Barré, D. Frot, J. Eyssautier, H. Zeng, Z. Xu, G. Dechaine, On the size distribution of self-associated asphaltenes, Energy & Fuels 27 (2013) 5083-5106.

[36] M. Kleber, P. Sollins, R. Sutton, A conceptual model of organo-mineral interactions in soils: Self-assembly of organic molecular fragments into zonal structures on mineral surfaces, Biogeochemistry 85 (2007) 9-24.

[37] E.H. Owens, K. Lee, Interaction of oil and mineral fines on shorelines: Review and assessment, Marine Pollution Bulletin 47 (2003) 397-405.

[38] M.L. Chacón-Patiño, C. Blanco-Tirado, J.A. Orrego-Ruiz, A. Gómez-Escudero, M.Y. Combariza, High resolution mass spectrometric view of asphaltene–SiO_2 interactions, Energy & Fuels 29 (2015) 1323-1331.

[39] A. Natarajan, N. Kuznicki, D. Harbottle, J. Masliyah, H. Zeng, Z. Xu, Understanding mechanisms of asphaltene adsorption from organic solvent on mica, Langmuir 30 (2014) 9370-9377.

[40] A. Abudu, L. Goual, Adsorption of crude oil on surfaces using quartz crystal microbalance with dissipation (QCM-D) under flow conditions, Energy & Fuels 23 (2008) 1237-1248.

[41] D. Andrieux, J. Jestin, N. Kervarec, R. Pichon, M. Privat, R. Olier, Adsorption mechanism of substituted pyridines on silica suspensions: An NMR study, Langmuir 20 (2004) 10591-10598.

[42] E. Tombácz, M. Szekeres, Surface charge heterogeneity of kaolinite in aqueous suspension in comparison with montmorillonite, Applied Clay Science 34 (2006) 105-124.

[43] L. Alagha, S. Wang, L. Yan, Z. Xu, J. Masliyah, Probing adsorption of polyacrylamide-based polymers on anisotropic basal planes of kaolinite using quartz crystal microbalance, Langmuir 29 (2013) 3989-3998.

[44] L. Yan, A.H. Englert, J.H. Masliyah, Z. Xu, Determination of anisotropic surface characteristics of different phyllosilicates by direct force measurements, Langmuir 27 (2011) 12996-13007.

[45] H. Zhao, S. Bhattacharjee, R. Chow, D. Wallace, J.H. Masliyah, Z. Xu, Probing surface charge potentials of clay basal planes and edges by direct force measurements, Langmuir 24 (2008) 12899-12910.

[46] D. Briggs, M. Seah, H. Bubert, Practical Surface Analysis. Volume 1: Auger and X-ray Photoelectron Spectroscopy, Angewandte Chemie-German Edition 107 (1995) 1367.

[47] E. Kleimenov, H. Bluhm, M. Hävecker, A. Knop-Gericke, A. Pestryakov, D. Teschner, J.A. Lopez-Sanchez, J.K. Bartley, G.J. Hutchings, R. Schlögl, XPS investigations of VPO catalysts under reaction conditions, Surface Science 575 (2005) 181-188.

[48] Z. Lu, J. McCaffrey, B. Brar, G. Wilk, R. Wallace, L.C. Feldman, S. Tay, SiO_2 film thickness metrology by X-ray photoelectron spectroscopy, Applied Physics Letters 71 (1997) 2764-2766.

[49] M. Couillard, P.H. Mercier, Analytical electron microscopy of carbon-rich mineral aggregates in solvent-diluted bitumen products from mined Alberta oil sands, Energy & Fuels 30 (2016) 5513-5524.

[50] C.E. White, J.L. Provis, T. Proffen, D.P. Riley, J.S. van Deventer, Density functional modeling of the local structure of kaolinite subjected to thermal dehydroxylation, The Journal of Physical Chemistry A 114 (2010) 4988-4996.

[51] R.K. Bauer, P. de Mayo, L.V. Natarajan, W.R. Ware, Surface photochemistry: The effect of surface modification on the photophysics of naphthalene and pyrene adsorbed on silica gel, Canadian Journal of Chemistry 62 (1984) 1279-1286.

[52] L.H. Dubois, B.R. Zegarski, Bonding of alkoxysilanes to dehydroxylated silica surfaces: A new adhesion mechanism, The Journal of Physical Chemistry 97 (1993) 1665-1670.

[53] C. Bich, J. Ambroise, J. Péra, Influence of degree of dehydroxylation on the pozzolanic activity of metakaolin, Applied Clay Science 44 (2009) 194-200.

[54] R. Cadena-Nava, A. Cosultchi, J. Ruiz-Garcia, Asphaltene behavior at interfaces, Energy & Fuels 21 (2007) 2129-2137.

[55] D. Harbottle, Q. Chen, K. Moorthy, L. Wang, S. Xu, Q. Liu, J. Sjoblom, Z. Xu, Problematic stabilizing films in petroleum emulsions: Shear rheological response of viscoelastic asphaltene films and the effect on drop coalescence, Langmuir 30 (2014) 6730-6738.

4 Spatially Resolved Organic Coating on Clay Minerals in Bitumen Froth Revealed by Atomic Force Microscopy Adhesion Mapping[1]

4.1 Introduction

The adsorption of organic matter on mineral surfaces is a subject of interest in a variety of disciplines, such as petroleum geology, pharmacy, cosmetics, and ceramics [1, 2]. In oil sands processing, the organic matter associated with the oil sands fine solids can significantly affect the behavior of the fine solids, significantly impacting the bitumen production process [3, 4]. For example, the fine solids in the bitumen froth (an intermediate product during warm-water oil sands extraction process) are believed to play a vital role in stabilizing water-in-oil emulsions and thus degrading bitumen quality as the emulsions are difficult to separate from the bitumen froth [4, 5]. The emulsion stabilizing property of the fine solids is caused by their bi-wet characteristics, due to hydrocarbon coating [6]. Therefore, an understanding of the properties and structures of the organic matter associated with these fine solids is essential for oil sands processing.

Chemical analysis in prior studies [4, 6, 7] indicated that the organic matter associated with the fine solids derived from oil sands was polar, aromatic material which was similar to asphaltene fraction of oil sands bitumen, as mentioned in literature review chapter (Section 2.1.2). However, no studies compared the mechanical properties of the two aforementioned materials. Clay minerals are the main components of the mineral solids in Alberta oil sands [8, 9]. The organic matter can modify the clay minerals either by adsorbing on the clay surfaces as an organic

[1] A version of this chapter has been published as Q. Chen, J. Liu, T. Thundat, M.R. Gray, Q. Liu, Spatially resolved organic coating on clay minerals in bitumen froth revealed by atomic force microscopy adhesion mapping, Fuel 191 (2017) 283-289.

coating, or by cementing the mineral particles into oil-mineral aggregates as "glue" (see Section 2.1.4 for more details) [10-13]. As the organic matter may appear as nano- or submicron domains on clay surfaces [3, 14], ultra-high resolution techniques are needed to study the organic coating on the clay surfaces. Scanning electron microscopy (SEM) and transmission electron microscopy (TEM) have been used [4, 15]. However, the thin film thickness of organic coating [3] and the poor conductivity of clay minerals (a carbon or metal coating is needed to avoid sample charging) make it challenging to visualize the organic coating on mineral solids by these imaging techniques. The surface analysis techniques such as X-ray photoelectron spectroscopy (XPS) and time-of-flight secondary ion mass spectroscopy (ToF-SIMS) have also been applied, and the organic coverage on clay surfaces is proposed to be patchy and discontinuous based on the detectable signals of inorganic elements (such as Al and Si) in the topmost layer (2−5 nm) [4, 16], as discussed in Section 2.1.4. However, determination of the spatial distribution and thickness of the organic matter adsorbed on the clay minerals has not been possible.

Another challenge in imaging of organic-clay mixtures is their tendency to aggregate. Six et al. [17] and Sohi et al. [18] successfully disrupted the oil-mineral aggregates in soil by ultrasonic treatment and then separated the organic matter by centrifugation. Their approach suggested that ultrasonication followed by centrifugation was a practical way to separate the organic matter in the fine solids aggregates.

Atomic force microscopy (AFM), invented in the early 1980s, is a powerful tool for surface analysis with nano- or even atomic resolution [19, 20], but measurement of the mechanical properties of materials is difficult using contact or tapping mode of AFM [21]. PeakForce Quantitative Nanomechanical Mapping (QNM) mode of AFM, recently developed by Pittenger et al. [22], can quantitatively and unambiguously measure the mechanical properties (e.g.

adhesion and modulus) [23]. This method is particularly useful for analyzing samples with different material components showing variations in mechanical properties, such as shales [24], polymers [25], and biological materials [26].

In this study, QNM-AFM was applied for the first time to study the organic matter associated with the clay minerals extracted from bitumen froth. Different components (i.e. platy clays, organic coating, separated organics, and submicron particles) were identified by topographic imaging and adhesion force mapping. The spatial distribution of organic coating on clay minerals was directly visualized, and its surface coverage and adsorption domain thickness on the clay basal faces were quantitatively determined. This study shows that QNM-AFM can be a useful technique in analyzing the organic contamination of a mineral surface. The results lead to a better understanding of the structures and properties of the organic matter associated with the oil sands clay minerals.

4.2 Materials and Methods

4.2.1 Materials

Four samples were analyzed to enable quantitative comparisons: a model mineral (kaolinite), a model organic (C_7 asphaltenes), bitumen froth fine solids, and hydrothermally-treated bitumen froth fine solids. The kaolinite powders were purchased from ACROS organics. The C_7 asphaltenes were precipitated from Athabasca bitumen (obtained from Imperial Oil Limited) using ASTM D6560-12 method [27]. The bitumen froth sample was acquired from CanmetENERGY, Devon, Alberta. The fine solids in the bitumen froth were extracted by filtration using 0.22-μm pore size GVWP Millipore filter membrane. The filtration was conducted at 55 kPa vacuum pressure under room temperature. To obtain the fine solids, one

gram of the bitumen froth was diluted by 100 mL toluene to form a suspension for filtration. When all the liquid passed through the filter, the filter cake was washed by toluene until the filtrate became colorless. The filter cake solids was dried at 65°C for 24 h and then collected for AFM measurements. The fine solids were mainly composed of organically-modified clay minerals with a total organic carbon content of 15 wt%. Detailed information on the mineralogical and chemical compositions of these fine solids can be found in Chapter 6 of this thesis. The bitumen froth was hydrothermally treated at 390°C for 30 min. The detailed information on equipment and operating procedures is given in Chapter 6 (Section 6.2.2). After hydrothermal treatment, the fine solids were extracted from treated bitumen froth following the same procedures as described above for the untreated bitumen froth fine solids.

4.2.2 Sample Preparation for AFM Measurements

The solutions of kaolinite, bitumen froth fine solids, and hydrothermally-treated fine solids were prepared by mixing the solids particles with the deionized water (Milli-Q, Millipore) at a concentration of 1 mg/mL, followed by 30 min ultrasonication (Model FB15064, Fisher Scientific). After 2 h of standing, a drop of the solution (~10 μL) was cast on a 1 cm^2 SiO_2 substrate (nanoFAB, University of Alberta) which had been prewashed successively in 10 mL methanol and 10 mL water and blown dry with N_2 gas to remove any contaminants and impurities from the surface. The drop was allowed to dry at ambient conditions for 2 h and kept inside a petri dish before AFM measurements to avoid contamination by ambient particles.

The asphaltene sample was dissolved in toluene by ultrasonication to make 0.005 wt% asphaltene solution. A drop of this solution was cast on the SiO_2 substrate. The drop was allowed to dry at ambient conditions for 2 h. After toluene evaporation, only the solid asphaltenes

adhered to the substrate. The substrate with the asphaltenes was kept inside a petri dish before AFM measurements.

To separate the organic matter in the bitumen froth fine solids aggregates, the fine solids sample was mixed with toluene at a concentration of 1 mg/mL, followed by 30 min ultrasonication. The solution was centrifuged for 3 h at 2000 × g using a Model C1301 Spectrafuge Mini Centrifuge (Labnet international, Korea). After centrifugation, the organic matter was expected to concentrate in the supernatant due to its lower density than the minerals. A drop of the supernatant solution was cast on the SiO_2 substrate. The drop was allowed to dry at ambient conditions for 2 h and kept inside a petri dish before AFM measurements.

4.2.3 Adhesion Characterization by PeakForce QNM Mode of AFM

The AFM measurements were performed in PeakForce QNM mode using Bruker Icon AFM (Santa Barbara, CA) at ambient conditions (temperature 22±1°C, relative humidity 15±4%). A Pt-Ir coated silicon probe (SCM-PIT, Bruker) with tip radius of 20 nm and cantilever spring constant of 2.8 N/m was used to obtain the topography and adhesion images. Detailed description for the working principles of QNM-AFM can be found elsewhere [22, 28]. Briefly, the sample surface is measured by the deflection of the cantilever, and a force-distance curve is obtained for each image pixel. The z-piezo in PeakForce QNM mode is driven with a sinusoidal waveform (rather than a triangular waveform in conventional modes), which allows direct force control of damaging lateral forces. Figure 4.1 shows the schematic force-distance curves of a typical PeakForce QNM-AFM measurement during approach and retraction of the tip. The peak force value of the force-distance curves is used as the imaging feedback parameter, and the maximum pull-off force during the retraction of the tip is designated as adhesion force. The

topography and adhesion images were captured with a resolution of 512×512 pixels, a scan rate of 1.0 Hz, and a peak-force frequency of 2 kHz. All the images were processed using Nanoscope analysis software (V1.50, Bruker).

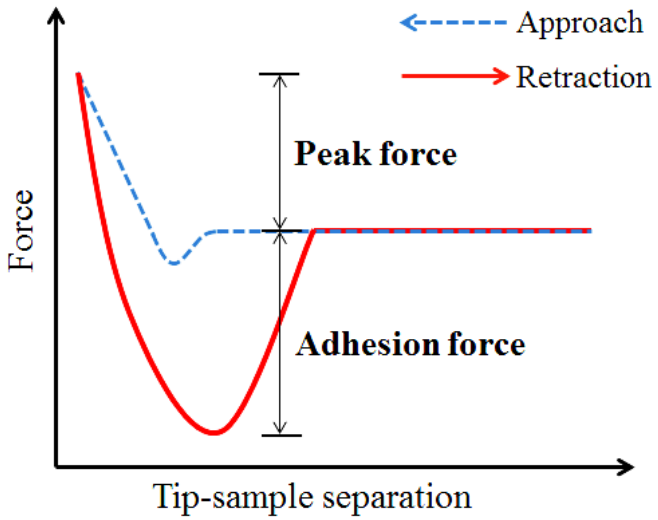

Figure 4.1 Schematic force-distance curves obtained from a typical PeakForce QNM-AFM measurement during approach and retraction of the tip.

4.3 Results and Discussion

4.3.1 Topographic Imaging and Adhesion Force Mapping of Kaolinite

Kaolinite, a major type of clay mineral present in the bitumen froth fine solids [29], was chosen as the reference clay for this study. Figure 4.2A shows a typical topographic image of the pure kaolinite particles deposited on SiO_2 substrate, and Figure 4.2B is the corresponding tip-sample adhesion force map. The platy kaolinite particles with layer thickness of 4−6 nm (Figure 4.2C) can be clearly identified, and they exhibited a lower adhesion force compared to the substrate. The average adhesion forces for the kaolinite and the substrate were 4.0±0.2 nN and 7.5±0.2 nN, respectively, obtained by fitting the frequency distribution of adhesion force in Figure 4.2D with

a Gaussian function (R^2 = 0.99) [21, 30]. From the cross-section analysis shown in Figure 4.2C, the kaolinite particles with different layer thickness exhibited identical adhesion force, indicating that the observed adhesion force was not sensitive to the layer thickness of the rigid kaolinite clay particles, consistent with the observation of Morozov et al. [31] using palygorskite clay.

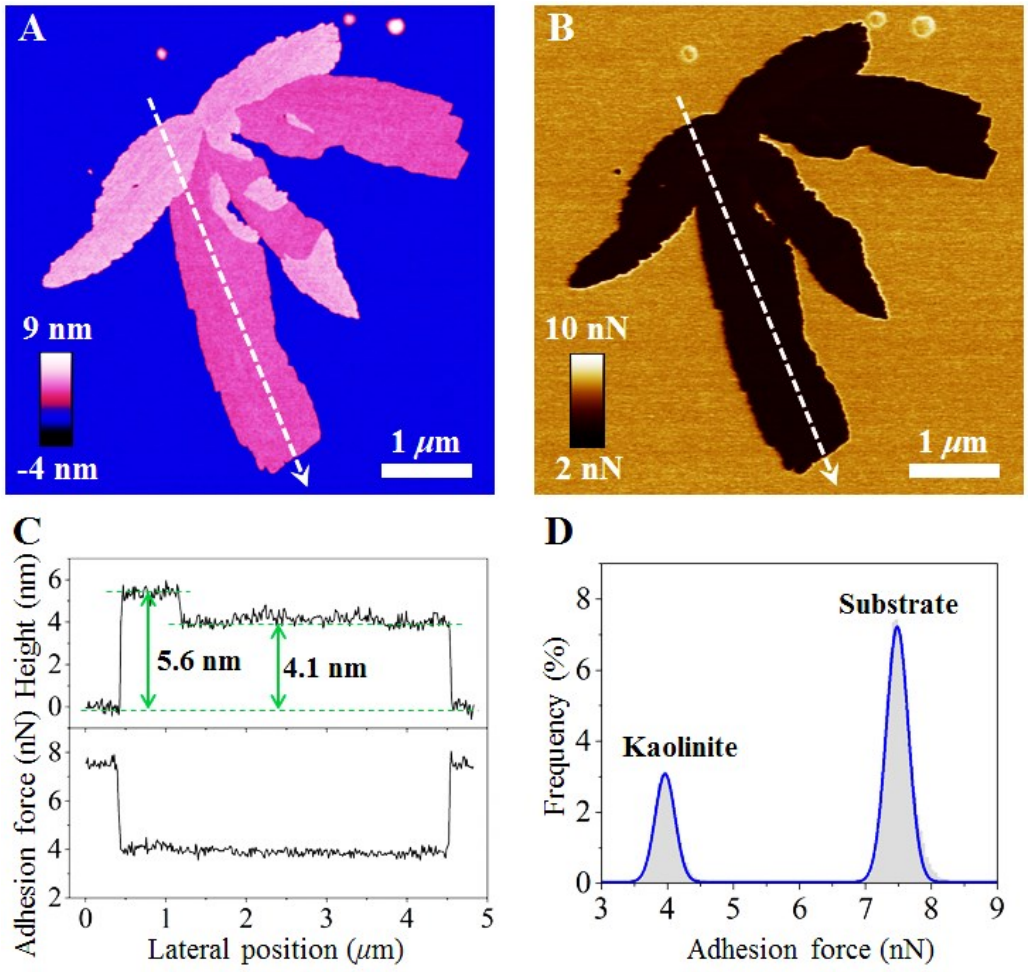

Figure 4.2 (A) Topographic image and (B) corresponding tip-sample adhesion force map of kaolinite particles on SiO_2 substrate. (C) Cross-section analysis of height and adhesion force corresponding to the white dash arrows in panels A and B. (D) Frequency distribution of adhesion force corresponding to panel B. The blue solid line in panel D shows a Gaussian fit to the data with R^2 = 0.99.

4.3.2 Topographic Imaging and Adhesion Force Mapping of Asphaltenes

Asphaltenes are surface-active components of oil sands bitumen, which can irreversibly adsorb on mineral surfaces [32, 33]. Here, the adhesive behavior of the asphaltenes extracted from oil sands bitumen was studied in parallel to kaolinite. Figure 4.3 shows the topographic image (A) and the corresponding adhesion force map (B) of the asphaltene aggregates. As described in Section 4.2.2, the asphaltene aggregates were obtained at ambient conditions by evaporating toluene in which the asphaltenes were dissolved. The asphaltene aggregates formed fractal structures and exhibited higher adhesion force than the SiO_2 substrate, which is consistent with the observation of Mehranfar et al. [34]. Unlike the kaolinite particles, the adhesion force of the asphaltenes showed variations corresponding closely with their thickness, as indicated by the cross-section analysis in Figure 4.3C. Figure 4.3D shows the frequency distribution of adhesion force corresponding to the adhesion force map in Figure 4.3B. By Gaussian fitting ($R^2 = 0.92$), the average tip-asphaltene and tip-substrate adhesion forces were calculated to be 20.2±3.6 nN and 9.5±1.3 nN, respectively. Here, the adhesion force of the asphaltene-deposited substrate (9.5±1.3 nN) is slightly higher than that of the kaolinite-deposited substrate (7.5±0.2 nN), probably due to substrate contamination caused by a thin film of spread asphaltenes on the substrate surface in the former case [21, 35]. The adhesion force of the organic asphaltenes (20.2 nN) is much higher than that of the inorganic kaolinite (4.0 nN), suggesting that the organic materials could be distinguished from the inorganic minerals by their different tip-sample adhesion forces using QNM-AFM.

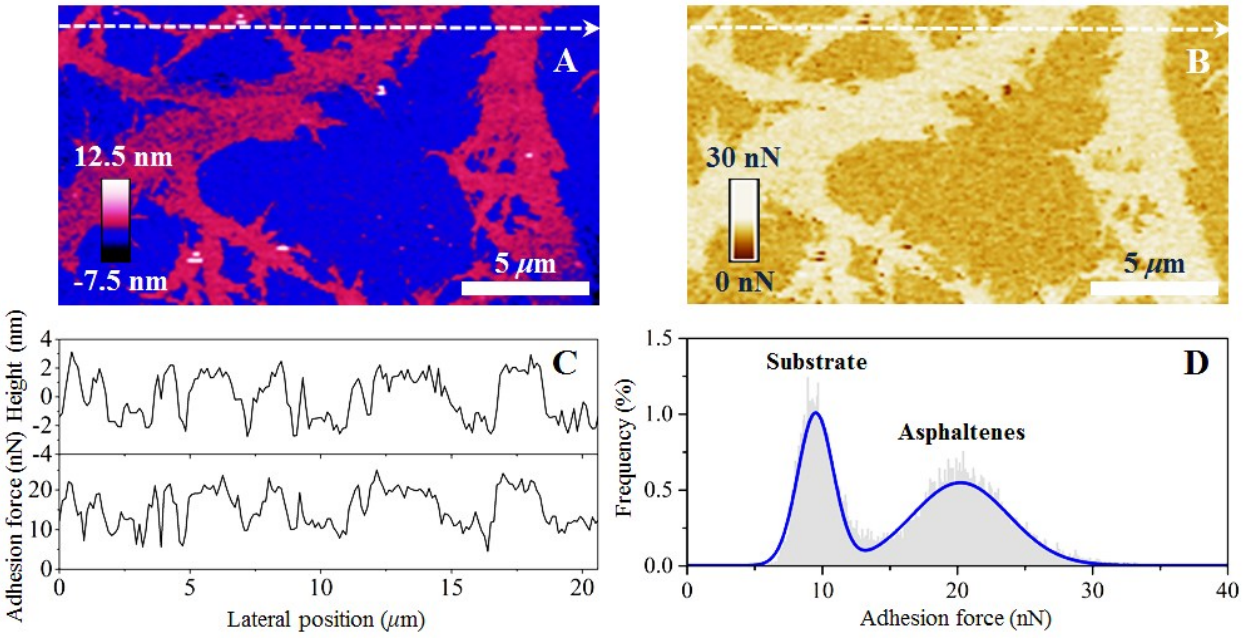

Figure 4.3 (A) Topographic image and (B) corresponding adhesion force map of the asphaltene aggregates on SiO_2 substrate. (C) Cross-section analysis of height and adhesion force corresponding to the white dash arrows in panels A and B. (D) Frequency distribution of adhesion force corresponding to panel B. The blue solid line in panel D shows a Gaussian fit to the data with $R^2 = 0.92$.

4.3.3 Characterization of the Bitumen Froth Fine Solids

Figure 4.4A shows a typical topographic image of the bitumen froth fine solids, and Figure 4.4B is the corresponding adhesion force map. Platy clay particles with layer thickness of 5−6 nm (Figure 4.4C) can be clearly identified. These platy clays exhibited lower adhesion force than the substrate, which is consistent with the observation of the kaolinite in Figure 4.2B. As highlighted by the green dash boxes in Figures 4.4A and 4.4B, two particles with similar heights exhibited significantly different adhesion forces: the lower particle shows a very high adhesion force (~75 nN), while the upper particle shows a low adhesion force similar to the platy clay particles (~10

nN). This indicates that the lower particle is most likely organic in nature, corresponding to the "separated organics" from oil-mineral aggregates after ultrasonic treatment [17, 18]. Similarly, several featured domains with particularly high adhesion forces, as highlighted by the yellow dash circles in Figure 4.4B, can be readily found in the adhesion force map (Figure 4.4B). In addition, a significant number of submicron particles can be identified (Figure 4.4A). The organic coating on the platy clay particles could not be clearly discriminated in Figure 4.4B (if there are any), likely due to the relatively large scanning area (20 μm × 20 μm) and the large range in adhesion forces (0−70 nN).

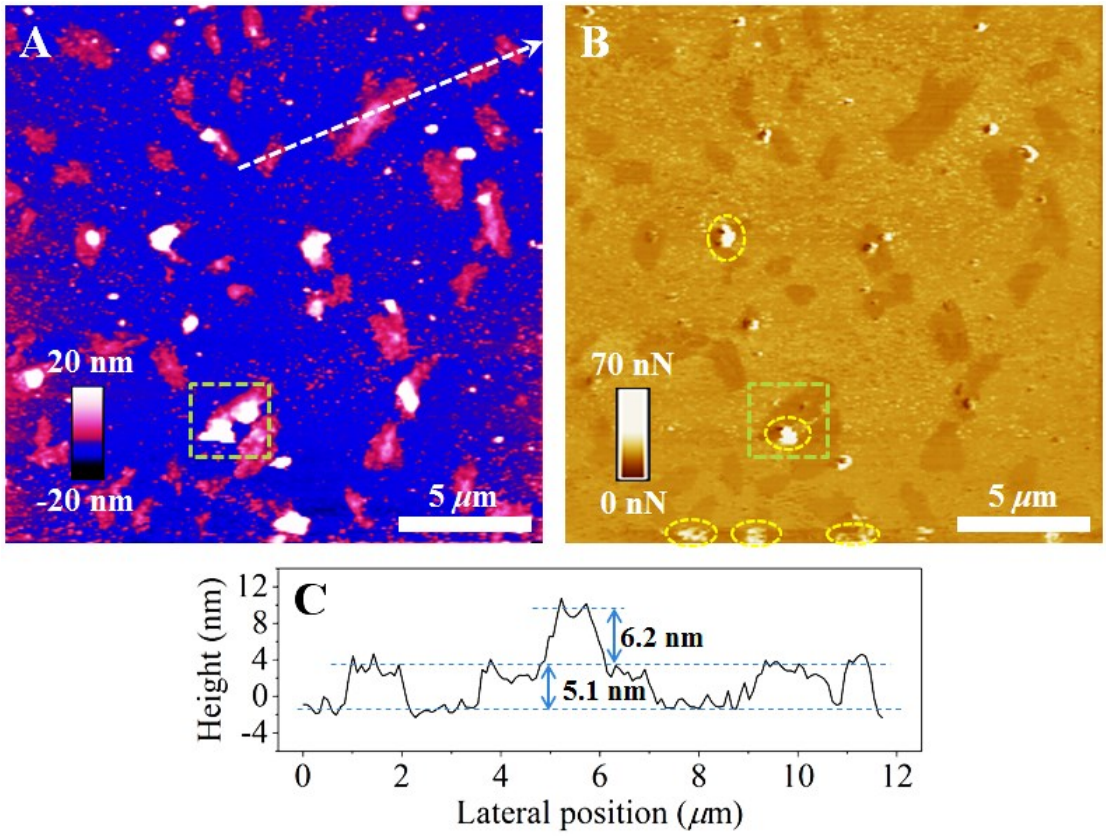

Figure 4.4 (A) Topographic image and (B) corresponding adhesion force map of the bitumen froth fine solids. (C) Height cross-section analysis corresponding to the white dash arrow in panel A.

More detailed adhesion force distributions of the different components of the bitumen froth fine solids (indicated in Figure 4.4) were revealed on the magnified images as shown in Figure 4.5. A number of patchy-distributed domains on the platy clays exhibited relatively high adhesion force (Figure 4.5D), indicating the existence of organic coating on clay minerals [4, 36]. These domains cannot be discriminated from the topographic image in Figure 4.5A, suggesting that the organic coating was very thin and thus did not give significant changes in particle topography or thickness. The presence of such features highlights the complementary role of force-of-adhesion measurements in the study of multi-domain structures [37]. The area percentage of surface organic coverage on the clay basal faces was calculated to be 17±6%, based on analysis of 30 platy clay particles using ImageJ software. These solid samples were highly diluted in the present study to minimize particle stacking; therefore, the clay particles were predominantly horizontally-orientated (which is their preferential orientation), and only showed their basal faces in AFM images. Consequently, any organic coating on the edge faces of clays was not considered in the above calculation of surface coverage. In addition, larger errors in adhesion force values have been reported at particle edges due to tip artifacts [37, 38]. Therefore, the high adhesion-force areas at the particle edges were also excluded from the calculation.

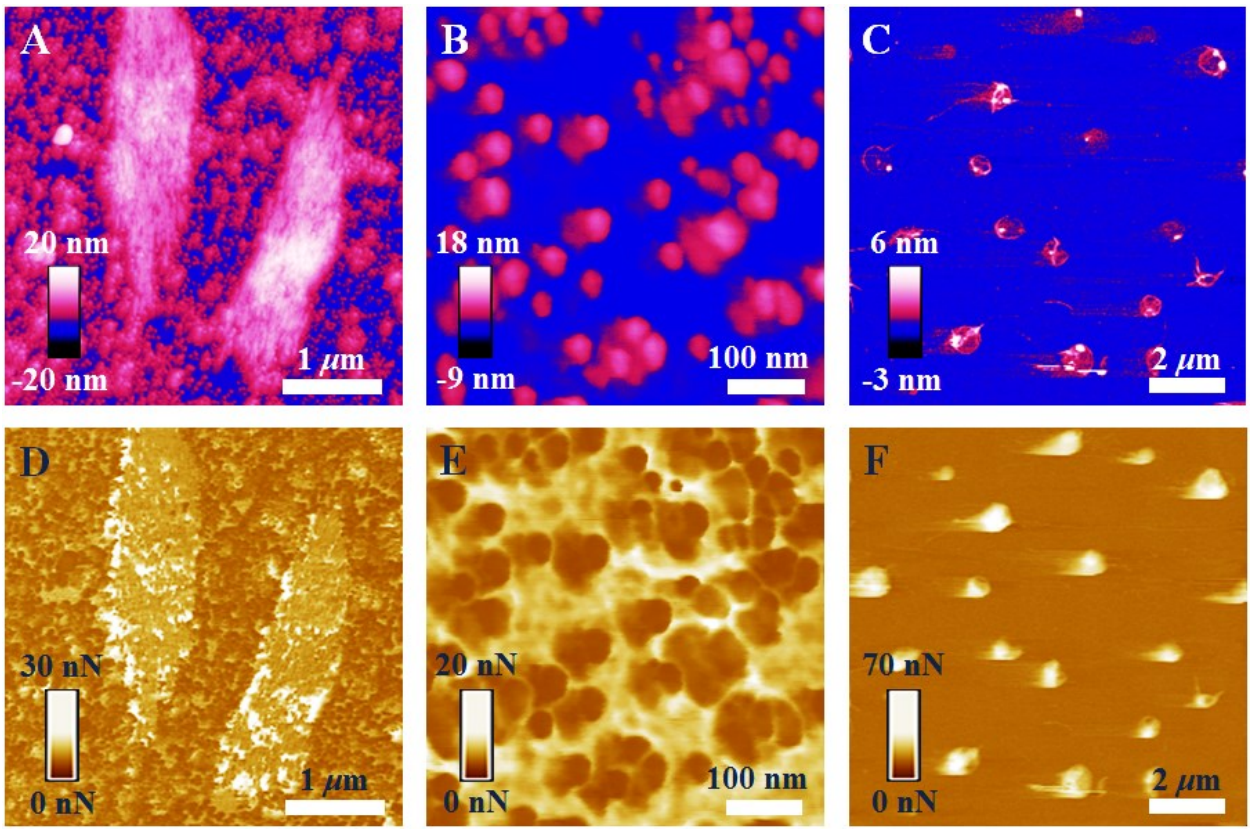

Figure 4.5 (A−C) Topographic images and (D−F) corresponding adhesion force maps of the different components in the bitumen froth fine solids: platy clays with organic coating (A, D), submicron particles (B, E), and separated organics (C, F).

As shown in Figures 4.5B and 4.5E, the low adhesion force (~3 nN) of the submicron particles (30−100 nm) suggests their mineral origin. Figures 4.5C and 4.5F show the topography and adhesion images of the separated materials collected by the ultrasonication and centrifugation procedures described in Section 4.2.2. The particularly high adhesion force of these materials suggests their organic nature. The presence of these sticky "separated organics" supports the argument that there are organic materials trapped in the oil-mineral aggregates as "glue" (Section 2.1.4).

The "stickiness" of the different components (i.e. platy clays, organic coating, separated organics, and submicron particles) was quantitatively assessed by the tip-sample adhesion force (Figure 4.6). The adhesion force of a domain of each component was obtained by fitting its frequency adhesion force distribution with a Gaussian function. The average adhesion forces and the standard deviations reported in Figure 4.6 are based on at least 70 domains for each component.

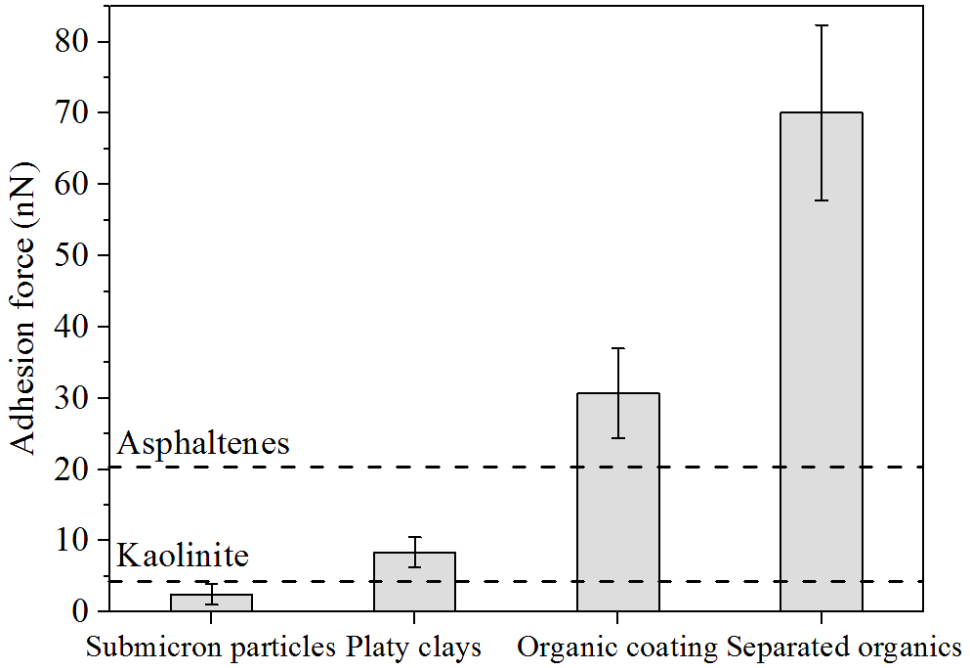

Figure 4.6 Tip-sample adhesion forces of the different components in the bitumen froth fine solids. The dash horizontal lines show the adhesion forces of the kaolinite and the asphaltenes.

The strength of the adhesion force holding two materials together is a function of attractive forces at their interfaces [39]. In general, such forces between AFM tip and the sample may include contributions from van der Waals forces, electrostatic forces, capillary forces, chemical bonding forces, and mechanical interlocking [30, 39-42]. In the present study, the contribution from electrostatic forces to the net tip-sample adhesion force is assumed to be negligible because

the Pt/Ir coated silicon tip is not expected to accumulate surface charges under the ambient conditions of this study. Capillary forces can result from condensation of water vapor between the sample surface and the AFM tip, which tend to occur on hydrophilic surfaces [43]. However, the capillary forces became significant only when the relative humidity is over 40% [30, 44, 45]. Thus, in this study, they are assumed to be very low due to the low relative humidity (~15%). The chemical bonding forces can also be neglected, since the surfaces of the tip and sample are saturated with chemical bonds and no ionic, covalent, or metallic bonds are expected to form during contact [30]. Mechanical interlocking between the tip and the sample is well documented in literature, resulting from structural surface features (e.g. hooks and loops) [39, 46-49]. This mechanical interaction can be an important contributor to the adhesion force, which is greater for soft surfaces than for rigid surfaces [50-52].

The adhesion forces of the submicron particles and platy clays were close to that of the kaolinite (Figure 4.6). For these rigid mineral solids, the van der Waals interactions most probably dominate the net adhesion force [53, 54]. Indeed, the observed adhesion forces of 2−10 nN fall well in a typical adhesion force range of 1−20 nN [21, 55-58] for the tip-mineral contact, in cases when van der Waals forces dominate. The adhesion forces of the organic components, i.e., organic coating and separated organics, were much higher than those of the mineral components (Figure 4.6). Similar observations have been reported by Morozov et al. [31] using polyethylene-palygorskite composites, Ihalainen et al. [21] using latex-kaolinite composites, and Martínez-Tong et al. [57] using polylactic acid-natural rubber-organoclay composites. The higher adhesion forces of the organic components can be attributed to their enhanced mechanical interlocking, resulting from the increased tip-sample contact area due to indentation [47, 59].

The typical thickness of the separated organics with the corresponding adhesion force (Figures 4.5C and 4.5F) is shown in Figure 4.7, together with the data of asphaltenes (Figure 4.3) for comparison. A linear correlation between the adhesion force and the thickness was observed for both the separated organics ($R^2 = 0.97$) and the asphaltenes ($R^2 = 0.99$). Ihalainen et al. [21] studied the mechanical properties of polymer latex coated kaolinite by AFM, and observed that the adhesion force increased linearly with the thickness of the latex film (up to 17 nm) on kaolinite particles. They attributed it to the increased indentation depth with the increased film thickness. Similar observations were reported by Landoulsi et al. [60] using proteins and Yu et al. [61] using asphalt binders. The results suggest that the observed tip-sample adhesion force for soft organic materials is proportional to their thickness.

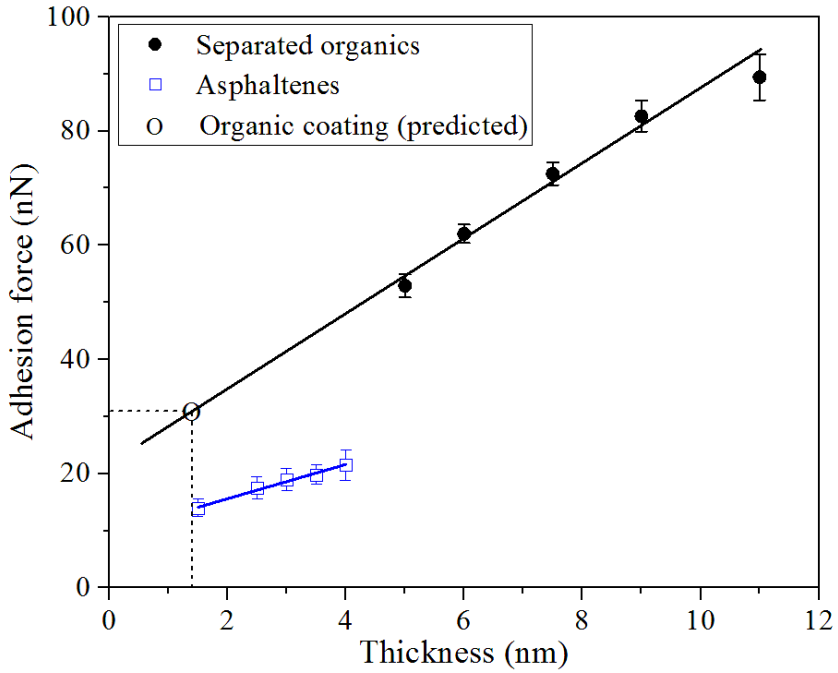

Figure 4.7 Tip-sample adhesion forces as a function of the thickness of the organic materials. The solid lines show a linear fit to the data.

The organic coating and the separated organics are expected to be chemically similar [3, 11]. However, the adhesion force of the organic coating was found to be much lower than that of the separated organics (Figure 4.6). This result was most likely due to its relatively smaller thickness. Quantification of the thickness of organic coating on the unsmooth clay surfaces is difficult (Figure 4.4C); however, by extrapolating the linear fit for the separated organics in Figure 4.7, the average thickness of the organic coating was estimated to be 1.4 nm based on its average adhesion force (Figure 4.6). Such a thin thickness is consistent with the observations in Figure 4.5A, where the organic domains did not give any obvious changes in topography. For a mineral surface with a 1.4-nm-thick organic coating, the conventional surface analysis techniques such as XPS (~2−10 nm probing depth) may underestimate the fraction of the mineral surface that is organically modified.

As mentioned in the introduction (Section 4.1), the organic matter associated with the fine solids was found to be polar, aromatic material similar to asphaltene fraction of oil sands bitumen based on chemical analysis [4, 6, 7]. However, the comparison of mechanical properties between the associated organic matter and asphaltenes was rare. The adhesion force value of the separated organics is larger than that of the asphaltenes at the same thickness (Figure 4.7), indicating that the separated organic material was “softer” (more deformable) than the asphaltene sample. This difference in mechanical properties implies a difference in composition. The softness of asphaltene materials is affected by the amount of “resin” present, which is heptane-soluble material [62]. The layers of organic matter in the fine solids aggregates may retain more soluble components during sample preparation than the asphaltenes precipitated from heptane, making it softer. Alternately, the organic matter associated with the clay minerals may include humic components which are not characteristic of bitumen, as suggested by Bensebaa et al. [3].

4.3.4 Hydrothermally-Treated Fine Solids

Figure 4.8 shows the topographic image (A) and the corresponding adhesion force map (B) of the hydrothermally-treated fine solids. The inhomogeneous adhesion force distribution on hydrothermally-treated clays indicates that the organic coating on the clay surface remained patchy and discontinuous even after hydrothermal treatment. In Figure 4.8, the area coverage of surface organic coating on the hydrothermally-treated clays and the magnitude of the adhesion force were similar to those on the untreated material (Figure 4.5). Due to the pronounced heterogeneity of the bitumen froth clay minerals (as evidenced from Figures 4.4–4.6 and literature [9, 36, 63, 64]), the difference between the untreated and hydrothermally-treated particles was not quantified by using QNM-AFM, which is an imaging technique in the level of individual submicron/micron particles and thus is challenging in obtaining statistical implications. Instead, the effect of hydrothermal treatment on the oil-mineral association will be analyzed in-depth in Chapters 5 and 6 using techniques such as elemental analysis, XPS, and FTIR, which reflect the average characteristics of particles.

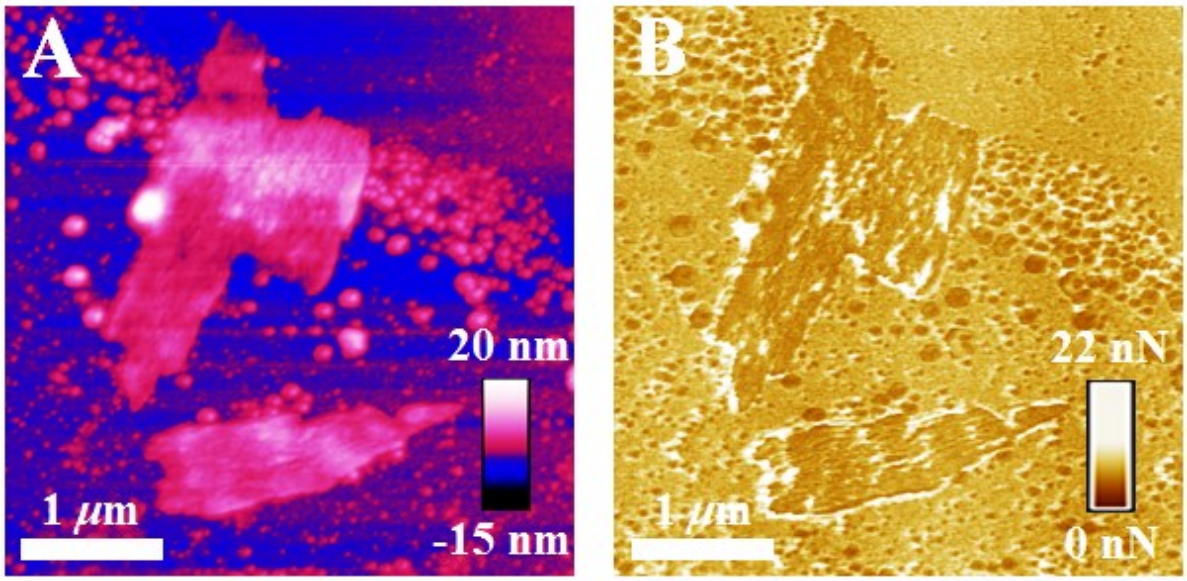

Figure 4.8 (A) Topographic image and (B) corresponding adhesion force map of the hydrothermally-treated fine solids.

4.4 Conclusions

The organic matter associated with the fine solids extracted from Athabasca bitumen froth was studied by QNM-AFM. By topographic imaging and adhesion force mapping, several different components, i.e., platy clays, organic coating, separated organics, and submicron particles, were identified due to their variations in shapes and mechanical properties. The organic coating on the clay minerals was clearly visualized on the adhesion force maps, showing a patchy-distributed structure. Its surface coverage and average adsorbed layer thickness on the clay basal faces were 17±6% and 1.4 nm, respectively. The organic matter associated with the bitumen froth fine solids, which cannot be washed off by toluene, was found to be softer than the asphaltene fraction of oil sands bitumen. Hydrothermal treatment of bitumen froth did not alter the patchy character of the organic coating on clay surface.

References

[1] R. Fuhrer, I.K. Herrmann, E.K. Athanassiou, R.N. Grass, W.J. Stark, Immobilized β-cyclodextrin on surface-modified carbon-coated cobalt nanomagnets: Reversible organic contaminant adsorption and enrichment from water, Langmuir 27 (2011) 1924-1929.

[2] A.E. Wiącek, K. Dul, Effect of surface modification on starch/phospholipid wettability, Colloids and Surfaces A: Physicochemical and Engineering Aspects 480 (2015) 351-359.

[3] F. Bensebaa, L.S. Kotlyar, B.D. Sparks, K.H. Chung, Organic coated solids in Athabasca bitumen: Characterization and process implications, The Canadian Journal of Chemical Engineering 78 (2000) 610-616.

[4] B. Sparks, L. Kotlyar, J. O'Carroll, K. Chung, Athabasca oil sands: Effect of organic coated solids on bitumen recovery and quality, Journal of Petroleum Science and Engineering 39 (2003) 417-430.

[5] N. Yan, M.R. Gray, J.H. Masliyah, On water-in-oil emulsions stabilized by fine solids, Colloids and Surfaces A: Physicochemical and Engineering Aspects 193 (2001) 97-107.

[6] L. Kotlyar, B. Sparks, J. Woods, K. Chung, Solids associated with the asphaltene fraction of oil sands bitumen, Energy & Fuels 13 (1999) 346-350.

[7] L. Kotlyar, B. Sparks, J. Woods, S. Raymond, Y. Le Page, W. Shelfantook, Distribution and types of solids associated with bitumen, Petroleum Science and Technology 16 (1998) 1-19.

[8] H.A. Kaminsky, T.H. Etsell, D.G. Ivey, O. Omotoso, Distribution of clay minerals in the process streams produced by the extraction of bitumen from Athabasca oil sands, The Canadian Journal of Chemical Engineering 87 (2009) 85-93.

[9] J. Masliyah, J. Czarnecki, Z. Xu, Handbook on theory and practice of bitumen recovery from Athabasca oil sands, Volume I: Theoretical basis, Kingsley Knowledge Publishing, Calgary, Alberta, 2011.

[10] P. Nelson, J.A. Baldock, P. Clarke, J. Oades, G. Churchman, Dispersed clay and organic matter in soil: Their nature and associations, Australian Journal of Soil Research 37 (1999) 289-290.

[11] F. Bensebaa, A. Majid, Y. Deslandes, Step-scan photoacoustic Fourier transform and X-rays photoelectron spectroscopy of oil sands fine tailings: New structural insights, Spectrochimica Acta Part A: Molecular and Biomolecular Spectroscopy 57 (2001) 2695-2702.

[12] A. Majid, S. Argue, V. Boyko, G. Pleizier, P. L'Ecuyer, J. Tunney, S. Lang, Characterization of sol–gel-derived nano-particles separated from oil sands fine tailings, Colloids and Surfaces A: Physicochemical and Engineering Aspects 224 (2003) 33-44.

[13] A. Majid, B.D. Sparks, J.A. Ripmeester, Characterization of solvent-insoluble organic matter isolated from Alberta oil sands, Fuel 70 (1991) 78-83.

[14] Y. Tu, D. Kingston, J. Kung, L.S. Kotlyar, B.D. Sparks, K.H. Chung, Adsorption of pentane insoluble organic matter from oilsands bitumen onto clay surfaces, Petroleum Science and Technology 24 (2006) 327-338.

[15] A. Hooshiar, P. Uhlik, D.G. Ivey, Q. Liu, T.H. Etsell, Clay minerals in nonaqueous extraction of bitumen from Alberta oil sands: Part 2. Characterization of clay minerals, Fuel processing technology 96 (2012) 183-194.

[16] S. Wang, Q. Liu, X. Tan, C. Xu, M.R. Gray, Study of asphaltene adsorption on kaolinite by X-ray photoelectron spectroscopy and time-of-flight secondary ion mass spectroscopy, Energy & Fuels 27 (2013) 2465-2473.

[17] J. Six, G. Guggenberger, K. Paustian, L. Haumaier, E. Elliott, W. Zech, Sources and composition of soil organic matter fractions between and within soil aggregates, European Journal of Soil Science 52 (2001) 607-618.

[18] S.P. Sohi, N. Mahieu, J.R. Arah, D.S. Powlson, B. Madari, J.L. Gaunt, A procedure for isolating soil organic matter fractions suitable for modeling, Soil Science Society of America Journal 65 (2001) 1121-1128.

[19] G. Binnig, C.F. Quate, C. Gerber, Atomic force microscope, Physical Review Letters 56 (1986) 930.

[20] G. Binnig, C. Gerber, E. Stoll, T. Albrecht, C. Quate, Atomic resolution with atomic force microscope, Europhysics Letters 3 (1987) 1281.

[21] P. Ihalainen, J. Järnström, A. Määttänen, J. Peltonen, Nano-scale mapping of mechanical and chemical surface properties of pigment coated surfaces by torsional harmonic atomic force microscopy, Colloids and Surfaces A: Physicochemical and Engineering Aspects 373 (2011) 138-144.

[22] B. Pittenger, N. Erina, C. Su, Quantitative mechanical property mapping at the nanoscale with PeakForce QNM. Application Note Veeco Instruments Incorporated, 2010.

[23] M.E. Dokukin, I. Sokolov, Quantitative mapping of the elastic modulus of soft materials with HarmoniX and PeakForce QNM AFM modes, Langmuir 28 (2012) 16060-16071.

[24] M. Eliyahu, S. Emmanuel, R.J. Day-Stirrat, C.I. Macaulay, Mechanical properties of organic matter in shales mapped at the nanometer scale, Marine and Petroleum Geology 59 (2015) 294-304.

[25] T. Young, M. Monclus, T. Burnett, W. Broughton, S. Ogin, P. Smith, The use of the PeakForce^{TM} quantitative nanomechanical mapping AFM-based method for high-resolution Young's modulus measurement of polymers, Measurement Science and Technology 22 (2011) 125703.

[26] G. Pletikapić, A. Berquand, T.M. Radić, V. Svetličić, Quantitative nanomechanical mapping of marine diatom in seawater using peak force tapping atomic force microscopy, Journal of Phycology 48 (2012) 174-185.

[27] ASTM D 6560-12, Standard test method for determination of asphaltenes (heptane insolubles) in crude petroleum and petroleum products, ASTM, West Conshohocken, PA, 2012.

[28] H. Fischer, H. Stadler, N. Erina, Quantitative temperature-depending mapping of mechanical properties of bitumen at the nanoscale using the AFM operated with PeakForce Tapping^{TM} mode, Journal of microscopy 250 (2013) 210-217.

[29] J. Zhao, Q. Liu, M.R. Gray, Characterization of fine solids in Athabasca bitumen froth before and after hydrothermal treatment, Energy & Fuels 30 (2016) 1965-1971.

[30] X. Xiao, L. Qian, Investigation of humidity-dependent capillary force, Langmuir 16 (2000) 8153-8158.

[31] I.A. Morozov, O.K. Garishin, V.V. Shadrin, V.A. Gerasin, M.A. Guseva, Atomic force microscopy of structural-mechanical properties of polyethylene reinforced by silicate needle-shaped filler, Advances in Materials Science and Engineering 2016 (2016) Article ID 8945978.

[32] S. Dubey, M. Waxman, Asphaltene adsorption and desorption from mineral surfaces, SPE Reservoir Engineering 6 (1991) 389-395.

[33] S. Wang, Q. Liu, X. Tan, C. Xu, M.R. Gray, Adsorption of asphaltenes on kaolinite as an irreversible process, Colloids and Surfaces A: Physicochemical and Engineering Aspects 504 (2016) 280-286.

[34] M. Mehranfar, R. Gaikwad, S. Das, S.K. Mitra, T. Thundat, Effect of temperature on morphologies of evaporation-triggered asphaltene nanoaggregates, Langmuir 30 (2014) 800-804.

[35] R. Gaikwad, A. Hande, S. Das, S.K. Mitra, T. Thundat, Determination of charge on asphaltene nanoaggregates in air using electrostatic force microscopy, Langmuir 31 (2015) 679-684.

[36] M. Couillard, P.H. Mercier, Analytical electron microscopy of carbon-rich mineral aggregates in solvent-diluted bitumen products from mined Alberta oil sands, Energy & Fuels 30 (2016) 5513-5524.

[37] P. Eaton, J.R. Smith, P. Graham, J.D. Smart, T.G. Nevell, J. Tsibouklis, Adhesion force mapping of polymer surfaces: Factors influencing force of adhesion, Langmuir 18 (2002) 3387-3389.

[38] T. Stifter, E. Weilandt, O. Marti, S. Hild, Influence of the topography on adhesion measured by SFM, Applied and Environmental Microbiology 66 (1998) S597-S605.

[39] M. Larsson, M. Ahmad, Improved polymer–glass adhesion through micro-mechanical interlocking, Journal of Micromechanics and Microengineering 16 (2006) S161.

[40] L. Heepe, S.N. Gorb, Biologically inspired mushroom-shaped adhesive microstructures, Annual Review of Materials Research 44 (2014) 173-203.

[41] S.J. Marshall, S.C. Bayne, R. Baier, A.P. Tomsia, G.W. Marshall, A review of adhesion science, Dental Materials 26 (2010) e11-e16.

[42] T.P. Chou, G. Cao, Adhesion of sol-gel-derived organic-inorganic hybrid coatings on polyester, Journal of Sol Gel Science and Technology 27 (2003) 31-41.

[43] D.L. Sedin, K.L. Rowlen, Adhesion forces measured by atomic force microscopy in humid air, Analytical Chemistry 72 (2000) 2183-2189.

[44] L. Zhang, L. Li, S. Chen, S. Jiang, Measurements of friction and adhesion for alkyl monolayers on Si (111) by scanning force microscopy, Langmuir 18 (2002) 5448-5456.

[45] M. Fuji, K. Machida, T. Takei, T. Watanabe, M. Chikazawa, Effect of wettability on adhesion force between silica particles evaluated by atomic force microscopy measurement as a function of relative humidity, Langmuir 15 (1999) 4584-4589.

[46] H. Brodowsky, E. Mäder, Jute fibre/epoxy composites: surface properties and interfacial adhesion, Composites Science and Technology 72 (2012) 1160-1166.

[47] W.S. Kim, I.H. Yun, J.J. Lee, H.T. Jung, Evaluation of mechanical interlock effect on adhesion strength of polymer–metal interfaces using micro-patterned surface topography, International Journal of Adhesion and Adhesives 30 (2010) 408-417.

[48] J.A. Warner, B. Forsyth, F. Zhou, J. Myers, C. Frethem, G. Haugstad, Characterization of Pebax angioplasty balloon surfaces with AFM, SEM, TEM, and SAXS, Journal of biomedical materials research. Part B, Applied biomaterials 104 (2016) 470-475.

[49] C. Lee, S.M. Kim, Y.J. Kim, Y.W. Choi, K.-Y. Suh, C. Pang, M. Choi, Robust microzip fastener: Repeatable interlocking using polymeric rectangular parallelepiped arrays, ACS Applied Materials & Interfaces 7 (2015) 2561-2568.

[50] Y. Rahmawan, S.M. Kang, S.Y. Lee, K.Y. Suh, S. Yang, Enhanced shear adhesion by mechanical interlocking of dual-scaled elastomeric micropillars with embedded silica particles, Macromolecular Reaction Engineering 7 (2013) 616-623.

[51] C.A. Rezende, L.T. Lee, F. Galembeck, Surface mechanical properties of thin polymer films investigated by AFM in pulsed force mode, Langmuir 25 (2009) 9938-9946.

[52] H. Shulha, A. Kovalev, N. Myshkin, V.V. Tsukruk, Some aspects of AFM nanomechanical probing of surface polymer films, European Polymer Journal 40 (2004) 949-956.

[53] F. Leite, A. Riul, P. Herrmann, Mapping of adhesion forces on soil minerals in air and water by atomic force spectroscopy (AFS), Journal of Adhesion Science and Technology 17 (2003) 2141-2156.

[54] T. Eastman, D.M. Zhu, Adhesion forces between surface-modified AFM tips and a mica surface, Langmuir 12 (1996) 2859-2862.

[55] O. Noel, M. Brogly, G. Castelein, J. Schultz, In situ determination of the thermodynamic surface properties of chemically modified surfaces on a local scale: An attempt with the atomic force microscope, Langmuir 20 (2004) 2707-2712.

[56] M. Sababi, J. Kettle, H. Rautkoski, P.M. Claesson, E. Thormann, Structural and nanomechanical properties of paperboard coatings studied by peak force tapping atomic force microscopy, ACS Applied Materials & Interfaces 4 (2012) 5534-5541.

[57] D.E. Martínez-Tong, A. Najar, M. Soccio, A. Nogales, N. Bitinis, M. López-Manchado, T. Ezquerra, Quantitative mapping of mechanical properties in polylactic acid/natural rubber/organoclay bionanocomposites as revealed by nanoindentation with atomic force microscopy, Composites Science and Technology 104 (2014) 34-39.

[58] J. Liu, R. Gaikwad, A. Hande, S. Das, T. Thundat, Mapping and quantifying surface charges on clay nanoparticles, Langmuir 31 (2015) 10469-10476.

[59] A. Weisenhorn, P. Maivald, H.J. Butt, P. Hansma, Measuring adhesion, attraction, and repulsion between surfaces in liquids with an atomic-force microscope, Physical Review B 45 (1992) 11226.

[60] J. Landoulsi, V. Dupres, Direct AFM force mapping of surface nanoscale organization and protein adsorption on an aluminum substrate, Physical Chemistry Chemical Physics 15 (2013) 8429-8440.

[61] X. Yu, N.A. Burnham, R.B. Mallick, M. Tao, A systematic AFM-based method to measure adhesion differences between micron-sized domains in asphalt binders, Fuel 113 (2013) 443-447.

[62] D. Lesueur, The colloidal structure of bitumen: Consequences on the rheology and on the mechanisms of bitumen modification, Advances in Colloid and Interface Science 145 (2009) 42-82.

[63] T. Dang-Vu, R. Jha, S.Y. Wu, D.D. Tannant, J. Masliyah, Z. Xu, Wettability determination of solids isolated from oil sands, Colloids and Surfaces A: Physicochemical and Engineering Aspects 337 (2009) 80-90.

[64] M. Osacky, M. Geramian, D.G. Ivey, Q. Liu, T.H. Etsell, Mineralogical and chemical composition of petrologic end members of Alberta oil sands, Fuel 113 (2013) 148-157.

5 Influence of Hydrophobicity Distribution of Particle Mixtures on Emulsion Stabilization[2]

5.1 Introduction

Particle-stabilized emulsions are often encountered in products including foods, pharmaceuticals, and crude oils [1, 2]. While formation of stable emulsions is desirable in some of the food and pharmaceutical industries [3, 4], the presence of water-in-oil emulsions poses major problems for oil production such as oil sands bitumen processing, crude oil de-watering, and cleaning of coal-derived liquids [5, 6]. For example, the emulsified water in the hydrocarbon phase, typically stabilized by fine particles [6], causes serious corrosion problems in the downstream upgrading/refining units due to the salts dissolved in the water [6, 7]. Consequently, a study of the emulsification behavior of the native fine particles in these energy-related systems is crucial.

Intensive efforts [1, 2, 8, 9] have been devoted to understanding the mechanism of particle-stabilized emulsions using well-defined particles such as silica. As is well known, the particles can adsorb at oil/water interfaces in the form of a densely-packed layer, creating a steric barrier against droplet coalescence [10-12]. Several factors influencing emulsion stability have been identified, including oil phase composition, emulsification technique, storage conditions, particle characteristics, and particle-particle interactions [13-17]. However, arguably the most important factors are concerned with the particle characteristics, more specifically particle size and wettability [8, 18].

Generally, particles of sizes ranging from nanometers to microns are ideal for stabilizing emulsions [19]. Sztukowski and Yarranton [12] observed that particles of 1−10 μm in diameter

[2] A version of this chapter has been published as Q. Chen, I. Stricek, M.R. Gray, Q. Liu, Influence of hydrophobicity distribution of particle mixtures on emulsion stabilization, Journal of Colloid and Interface Science 491 (2017) 179-189.

could stabilize water-in-hydrocarbon emulsions. Yan et al. [20] reported that particles of about 2 μm were responsible for the stabilization of water-in-diluted-bitumen emulsions. Meanwhile, numerous experimental studies [8, 16, 21] have demonstrated that the wettability of particles can dominantly affect the formation and stability of particle-stabilized emulsions. From a thermodynamic point of view, only particles with bi-wet characteristics can stabilize oil-water emulsions [16, 19]. In terms of contact angle θ which solid particles make at oil/water interfaces, particles of contact angles close to 90° can strongly adsorb at the interfaces and thus effectively stabilize emulsions. If $\theta>90°$ (hydrophobic) or $\theta<90°$ (hydrophilic), particles can still reside at the interfaces but the resulting emulsions are less stable. Under strong wetting or non-wetting conditions, that is for $\theta>160°$ (strongly hydrophobic) or $\theta<20°$ (strongly hydrophilic), no stable emulsions can be formed [8, 19, 22].

The natural emulsifying agents are usually complex particle mixtures, such as the fine particles derived from oil sands which contribute to the formation of bitumen emulsions [6]. However, the study of emulsion stabilization using native oil sands fine solids is rare [6, 12]. Few studies have examined the emulsification behavior of particle mixtures where the constituent particles possess a wide range of hydrophobicity, much less the emulsifying capacities of the entire particle mixtures versus the sub-fractions of particles with defined hydrophobicity [23, 24]. This lack of work is possibly due to the complexity and heterogeneity of oil sands fine solids and the difficulty in preparing populations of particles with different distributions of hydrophobicity.

The oil sands fine solids are mainly composed of clay minerals such as kaolinite and illite [25, 26]. These clay minerals are organically modified [27-29]. As discussed in the literature review chapter (Section 2.1.4), the presence of an organic coating on mineral surfaces has been revealed using surface analysis techniques such as X-ray photoelectron spectroscopy (XPS) and time-of-

flight secondary ion mass spectroscopy (ToF-SIMS), and the coating is found to be patchy and discontinuous [28, 30]. Recent evidence [29, 31] also suggests that there was organic matter trapped between mineral particles acting as “glue”, forming oil-mineral aggregates. Given the above features, the oil sands fine solids exhibit pronounced heterogeneities: mixed mineralogical composition [26, 32], patchy organic coating [27, 28], and oil-mineral aggregation [29, 33].

Due to their heterogeneities, quantification of the wettability of the oil sands fine solids is difficult. Contact angle has been commonly used to evaluate the wettability. However, the contact angle of fine particles cannot be unambiguously determined, especially for heterogeneous fine particles [34]. Critical surface tension of a solid particle, as defined by Zisman [35], is an important parameter that can be used as a wettability index [36]. The estimation of critical surface tension by Zisman plot [35] relies on the contact angle measurements, which are nontrivial task as mentioned earlier. Film flotation, developed by Fuerstenau et al. [37], permits determination of the critical surface tension distribution of particle mixtures and gives some appreciable information about the extent of heterogeneity in terms of surface properties. Wang et al. [38] compared different methods in wettability determination for Alberta oil sands fine solids, and concluded that the film flotation is the more appropriate method.

In the present study, the fine solids from the Alberta oil sands bitumen froth were subjected to hydrothermal treatment at different temperatures (300−420°C). The treated fine particles were then characterized using the film flotation technique to assess their wettability, and used in the emulsification of toluene-water system. Cold stage scanning electron microscopy (SEM) was applied to visualize the interfacial structure of the resulting emulsions. The results demonstrate the influence of hydrophobicity distribution of particle mixtures on their emulsification behavior.

5.2 Materials and Methods

5.2.1 Hydrothermal Treatment and Fine Solids Sample Preparation

The bitumen froth sample, which contained 78 wt% bitumen, 14 wt% water and 8 wt% fine solids as determined by Dean-Stark extraction analysis, was obtained from CanmetENERGY, Devon, Alberta, courtesy of Imperial Oil Limited. The steps of the hydrothermal treatment of bitumen froth are described in detail in Chapter 6 (Section 6.2.2) and are only briefly summarized here: a bitumen froth sample weighing 165 g was loaded into a 500 mL Model 4575B Series Parr Reactor. The hydrothermal treatment was carried out at 300−420°C for 30 min. The pressure under different reaction conditions was in the range of 8.6−19.3 MPa. After the reaction, the reactor was cooled to 270°C and subsequently the vapors inside the reactor were vented off. The venting was operated at 270°C to maintain the water in vapor form. Afterwards, the reactor content was allowed to cool under ambient conditions overnight to room temperature (~25°C).

Four samples were prepared to examine the emulsification behavior of fine particles in the presence of bitumen. The residue of the bitumen froth after hydrothermal treatment at 390°C and vapor-venting at 270°C was designated as “treated bitumen-fine solids mixture”. For comparison, the bitumen froth was heated to 270°C and then the vapor was vented off to obtain the dewatered bitumen froth, which was designated as “untreated bitumen-fine solids mixture”. To remove the fine solids, the untreated and treated bitumen-fine solids mixtures were diluted with toluene to form a suspension for filtration using a 0.22-μm pore size GVWP Millipore filter membrane. When all the liquid had passed through the filter, the filter cake was washed with toluene until the filtrate was colorless. The filtrate was then collected and toluene in the filtrate

was allowed to evaporate. After toluene evaporation, the residues from "untreated bitumen-fine solids mixture" and "treated bitumen-fine solids mixture" were designated as "untreated bitumen" and "treated bitumen", respectively.

The fine solids in the original bitumen froth and the treated bitumen-fine solids mixtures at 300−420°C were also obtained by filtration following the same procedures described above. The filter cakes were placed in a vacuum oven and dried at 65°C for 24 h to collect the fine solids for analysis. The filtered solids from the original bitumen froth and treated bitumen-fine solids mixture were designated as untreated and treated fine solids, respectively.

5.2.2 Wettability Characterization

A film flotation technique was used to assess the wettability of the untreated and treated fine solids. The effect of particle size (up to 425 μm), particle density (up to 5 g/cm^3), and particle shape is sensibly negligible for practical film flotation, which has been demonstrated both experimentally [37] and theoretically [39]. The experiment procedures for film flotation tests described by Wang et al. [38] were followed in the present study. Briefly, eleven methanol-water solutions with surface tension ranging from 22.51 to 72.01 mN/m [40] were prepared by mixing 0−100 vol% of methanol at 10 vol% increments with pure water and kept in a 25°C constant-temperature water bath. Approximately 0.03 g of fine solids (accurately weighed to 4 decimal places) was slowly and evenly sprinkled on the surface of each solution in an ascending sequence based on surface tension (i.e. from the lowest to the highest probing solution surface tension). After waiting for ~2 min when particle settling stopped, the floating particles were collected using a sheet of paper, which was then dried and weighed.

The weight percentage of the floating particles on each solution surface was recorded as a function of probing solution surface tension. The increase in the weight percentage of the floating particles due to the increasing solution surface tension was calculated, and the critical surface tensions (γ_c) of the incremental particles should be in the range of surface tensions of these two neighboring probing solutions. To calculate the mean critical surface tension ($\bar{\gamma}_c$), the γ_c of each sub-fraction (i.e. each group of incremental particles) was designated as the surface tension of the probing solution where they just floated. For example, the floating particles increased from 54 to 86 wt% as the solution surface tension increased from 37 to 41 mN/m for the untreated fine solids, so the critical surface tension for this sub-fraction, i.e., the incremental 32 wt% particles, should be in the range of 37−41 mN/m and was designated as 41 mN/m to calculate $\bar{\gamma}_c$. Similar method was used by Wang et al. [38]. The mean critical surface tension ($\bar{\gamma}_c$) of all particles and its standard deviation (σ_{γ_c}) were calculated by Equations 5.1 and 5.2, respectively [37, 39]:

$$\bar{\gamma}_c = \sum_{i=1}^{11} (\gamma_c)_i w_i \tag{5.1}$$

$$\sigma_{\gamma_c} = \left\{ \sum_{i=1}^{11} \left[(\gamma_c)_i - \bar{\gamma}_c \right]^2 w_i \right\}^{1/2} \tag{5.2}$$

Here $(\gamma_c)_i$ is the critical surface tension for the *i*th methanol-water solution, and w_i is its corresponding incremental weight fraction of floating particles. The standard deviation, σ_{γ_c}, reflects the spread of the critical surface tension for the separated sub-fractions from the mean value of the population of measured particles. Therefore, σ_{γ_c} was used to assess the

heterogeneity of the particle mixtures [37, 38]. Wang et al. [38] observed good repeatability of the film flotation results using 0.2−1 μm fine particles from the clay fraction of oil sands. Dang-Vu et al. [41] reported that the film flotation results were highly reproducible using 100−200 μm oil sands coarse solids. In the present study, the film flotation experiments for the untreated and treated fine solids at 390°C were conducted four times, while those of the other samples were conducted two times. The average values were reported and the uncertainties of the percentage of floating particles and mean critical surface tension were estimated to be within ±4 wt% and ±0.3 mN/m, respectively.

The contact angle measurements followed the same method as described in Chapter 3 (Section 3.2.5). Circa 100 mg of each fine solids sample was pressed into a 1-cm diameter pellet by an ICL 12 TON E-Z Press^{TM} pellet presser (at 34 MPa) [42]. The contact angles were measured by a FTA200 contact angle goniometer equipped with an optical microscope and illumination system.

5.2.3 Preparation of Emulsions

Using the four samples mentioned in Section 5.2.1, the emulsification tests were conducted as follows. 0.2 g of the "untreated bitumen-fine solids mixture", "treated bitumen-fine solids mixture", "untreated bitumen", or "treated bitumen" was diluted by 20 mL toluene and then mixed with 20 mL water in a 50 mL test bottle. The mixtures were hand-shaken for 2 min (frequency ~1 Hz, amplitude ~20 cm) and left to stand to phase separate for 24 h. Li et al. [43] compared the emulsion stability prepared by different methods, including hand-shaking or using a homogenizer. They found that the emulsions prepared by the above two methods showed

similar characteristics. In the present study, the hand-shaking method was used due to its simplicity and relatively low energy input.

In the cases where bitumen is absent, similarly, the emulsions were prepared by first mixing 0.2 g of fine solids sample with 20 mL toluene, and then 20 mL water was added. The toluene-water-solids mixture was hand-shaken for 2 min and subsequently left to stand to phase separate for at least 24 h. The positions of toluene/emulsion and water/emulsion interfaces were recorded as a function of time until no visible changes could be observed. The internal structures and the type of the emulsions were observed and imaged using a Zeiss Axiovert 200M microscope. The emulsion type was also inferred by a dilution method [8], i.e., a drop of each emulsion was added to a volume of either pure toluene or pure water. Water continuous emulsions would disperse in water and remain as an intact drop in toluene, while toluene continuous emulsions would disperse in toluene and remain as an intact drop in water. A cold stage scanning electron microscopy (SEM, Hitachi S-3000N) was used to visualize the interfacial structure of the particle-stabilized emulsions. A drop of the resulting emulsions (~20 μL) was cast on the cold stage (–19°C). The structure of the emulsion droplets was observed and imaged at different magnifications.

Particle partitioning tests were also carried out following the procedures of Wang et al. [38]. One gram of the untreated or treated fine solids at 390°C was placed in a glass bottle together with 50 mL water and 50 mL toluene. The mixture was hand-shaken for 2 min and left to phase separate. The toluene layer, emulsion layer, and aqueous layer were separated 40 min after preparation to minimize the interference of sedimentation. The separated layers were dried, and the fine particles in each layer were weighed.

5.2.4 Characterization of Fine Solids

The particle size distribution of the fine solids was determined by laser diffraction using a Malvern Mastersizer 3000 particle size analyzer. It is capable of measuring particles in size range of 0.01 to 3500 μm. Toluene was used as the dispersing medium in the measurements.

The transmission Fourier transform infrared (FTIR) spectra of the solids samples were obtained in a Nicolet 6700 FTIR spectrometer (Thermo Scientific, USA) within the wavenumber range of 4000−400 cm^{-1}. The KBr pellet was prepared by mixing 0.5 mg of fine solids in 200 mg of KBr and then pressing at 27.6 MPa into a 1-cm-diameter disk.

The surface chemical composition of the fine solids was analyzed by X-ray photoelectron spectroscopy (XPS) and time-of-flight secondary ion mass spectroscopy (ToF-SIMS). Pellet samples for the XPS and ToF-SIMS measurements were prepared by the same method as described previously for contact angle measurements.

The XPS measurements were conducted with a Kratos AXIS 165 X-ray photoelectron spectrometer. Survey scan spectra (160 eV pass-energy) were obtained to detect all the elements possibly present and high resolution scan spectra (20 eV pass-energy) were obtained for more detailed information about carbon, oxygen, sulfur, aluminum, and silicon.

The ToF-SIMS spectra were obtained using a ToF-SIMS IV instrument (ION-ToF GmbH). Bi^+ ions were used as analytical source, operated at 25 kV in a static mode. The *n*-heptane asphaltenes used for ToF-SIMS measurements were precipitated from Athabasca bitumen, courtesy of Imperial Oil Limited.

5.3 Results

5.3.1 Distribution of Particle Hydrophobicity

Figure 5.1 shows the film flotation results of the untreated fine solids and typical hydrothermally-treated fine solids. Figure 5.1A shows the cumulative percentage of floating particles versus the solution surface tension, while Figure 5.1B shows their frequency distributions extracted from the data in Figure 5.1A. The cumulative percentage curves have a similar shape, and shifted to lower surface tension with increasing severity of the hydrothermal treatment, indicating the increased hydrophobicity of the fine solids. The data in Figure 5.1B clearly show that both the untreated and treated fine solids samples were mixtures of particles with varying degrees of hydrophobicity, which could be separated into several sub-fractions based on critical surface tension (γ_c). The γ_c of the untreated bitumen froth fine solids fell in the range of 26−56 mN/m, which agrees with the reported range of γ_c for oil sands particles [41, 44] and soil particles [45]. The calculated mean critical surface tension ($\bar{\gamma}_c$) of 39 mN/m for the untreated fine solids sample was lower than the value of ~45 mN/m reported by Darcovich et al. [44], and higher than the value of ~25 mN/m reported by Dang-Vu et al. [41]. This inconsistency may be due to the differences in the extraction methods and the sources of the oil sands samples. After the hydrothermal treatments, $\bar{\gamma}_c$ progressively decreased from 39 mN/m for the untreated fine solids to 30 mN/m for the treated fine solids at 420°C. At the same time, the standard deviation of the critical surface tension σ_{γ_c} became smaller (Table 5.1), indicating that overall the fine solids became more uniformly hydrophobic as a result of the hydrothermal treatment. The sessile drop contact angle, measured on pressed pellets of the fine solids, increased from 57°

for the untreated fine solids to 109° for the treated fine solids at 420°C (Table 5.1), which is consistent with the observations from film flotation.

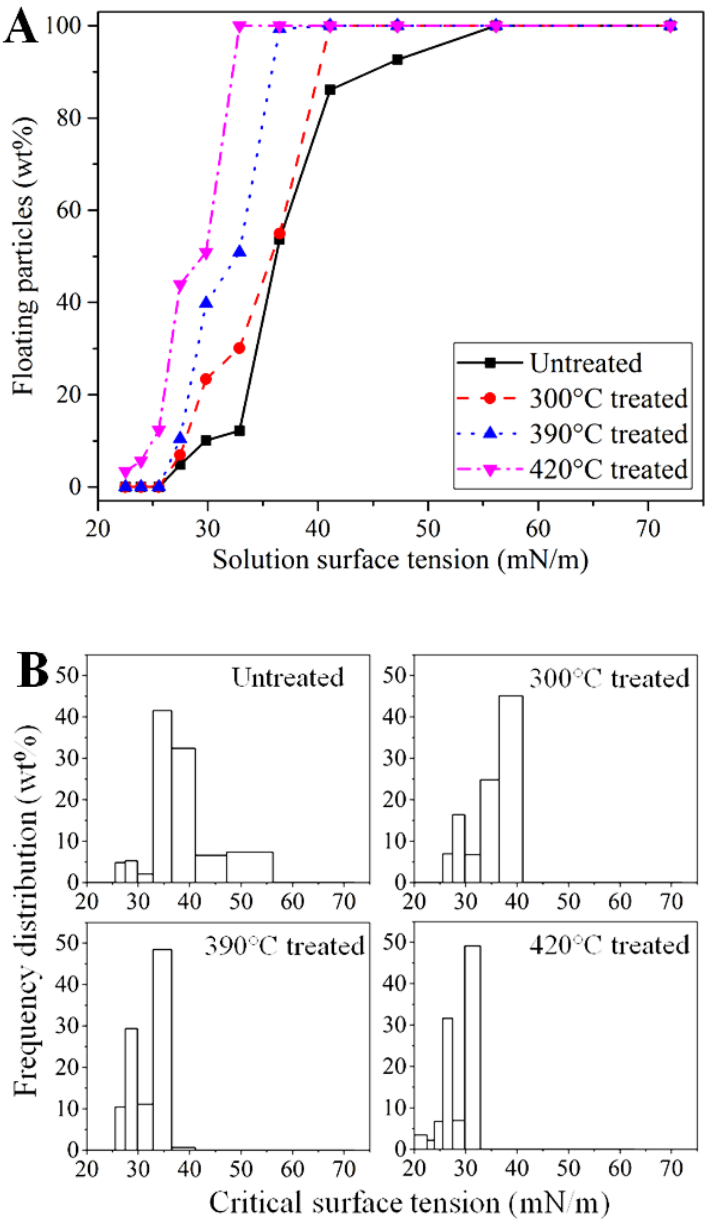

Figure 5.1 Film flotation results of the untreated and treated fine solids: (A) weight percentage of floating particles as a function of the surface tension of methanol-water solution and (B) frequency distribution of the critical surface tension of the fine solids.

Table 5.1 Wetting parameters of the untreated and treated fine solids (at 300−420°C).

Fine solids	Untreated	Hydrothermal treatment temperature (°C)							
		300	330	350	370	390	400	410	420
$\bar{\gamma}_c$ (mN/m)	39.3	36.6	35.6	34.4	33.7	33.2	32.9	30.9	29.9
σ_{γ_c} (mN/m)	6.5	4.8	4.6	3.9	3.5	3.5	3.7	3.3	3.2
Sessile drop contact angle (deg.)	56.8 ± 2.9	75.9 ± 1.1	76.4 ± 0.5	76.3 ± 3.0	82.2 ± 1.2	82.8 ± 1.9	83.0 ± 2.6	89.7 ± 3.2	109.0 ± 3.8

5.3.2 Emulsion Stabilization

The emulsification behavior of the dewatered product (i.e. bitumen-fine solids mixture), with or without a hydrothermal treatment, was examined and shown in Figure 5.2. The fact that both fine solids [2, 6] and asphaltene fraction of oil sands bitumen [20, 46] can stabilize water-in-oil emulsions has been well recognized. As expected, in all cases, an emulsion phase was formed, together with a toluene-diluted bitumen phase on the top and an aqueous phase at the bottom, as shown in Figure 5.2. However, the emulsion volume formed by the treated bitumen-fine solids mixture (Figure 5.2B) was much larger than that formed by the untreated bitumen-fine solids mixture (Figure 5.2A). After removing the fine solids by filtration, the "untreated bitumen" and "treated bitumen" produced similar emulsion volumes (Figures 5.2C and 5.2D), both of which were reduced compared to the emulsion volumes before fine solids removal (Figures 5.2A and 5.2B). These results confirm the conclusion that both the fine solids and the bitumen components (typically asphaltenes) could contribute to emulsion stabilization [20, 47]. Furthermore, the results indicate that the hydrothermal treatment significantly enhanced the emulsifying capacity

of the fine solids, while it did not significantly change the emulsifying capacity of the bitumen components.

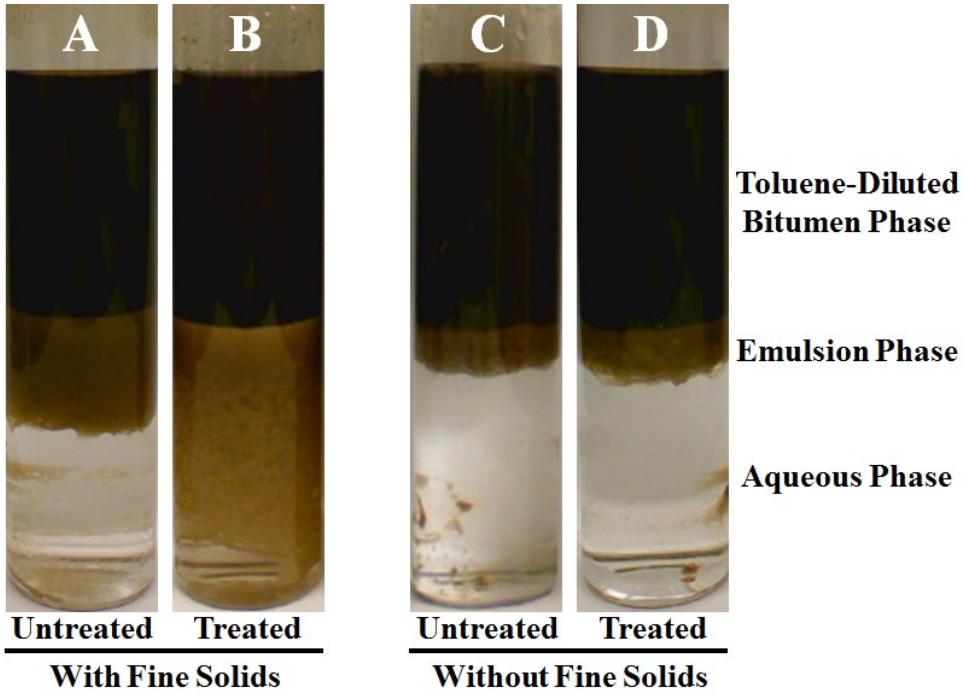

Figure 5.2 Role of fine solids and bitumen components in stabilizing emulsions. From left to right, the emulsions were formed by (A) untreated bitumen-fine solids mixture, (B) treated bitumen-fine solids mixture, (C) untreated bitumen, and (D) treated bitumen. A description of how these terms were defined is provided in Section 5.2.1. All photographs were taken 24 h after preparation.

To eliminate the interference of the bitumen components and to explore the underlying mechanism of the enhanced emulsifying capacity of the hydrothermally-treated fine solids, the emulsification behavior of the fine solids in the absence of bitumen was further investigated by toluene-water emulsification tests. After emulsion preparation, the toluene-water-solids mixture again separated into three distinct phases, with a toluene phase on the top, an aqueous phase at

the bottom, and an emulsion phase in the middle stabilized by fine solid particles (Figure 5.3), consistent with the observations in Figure 5.2. The emulsion stability was assessed by the volume percentage of the produced emulsions (V_E) as a function of time [6, 8]:

$$V_E = \frac{H_U - H_L}{H_T} \times 100\% \tag{5.3}$$

Here H_U is the height of upper toluene/emulsion interface, H_L is the height of lower water/emulsion interface, and H_T is the height of total toluene-water-solids mixture (Figure 5.3).

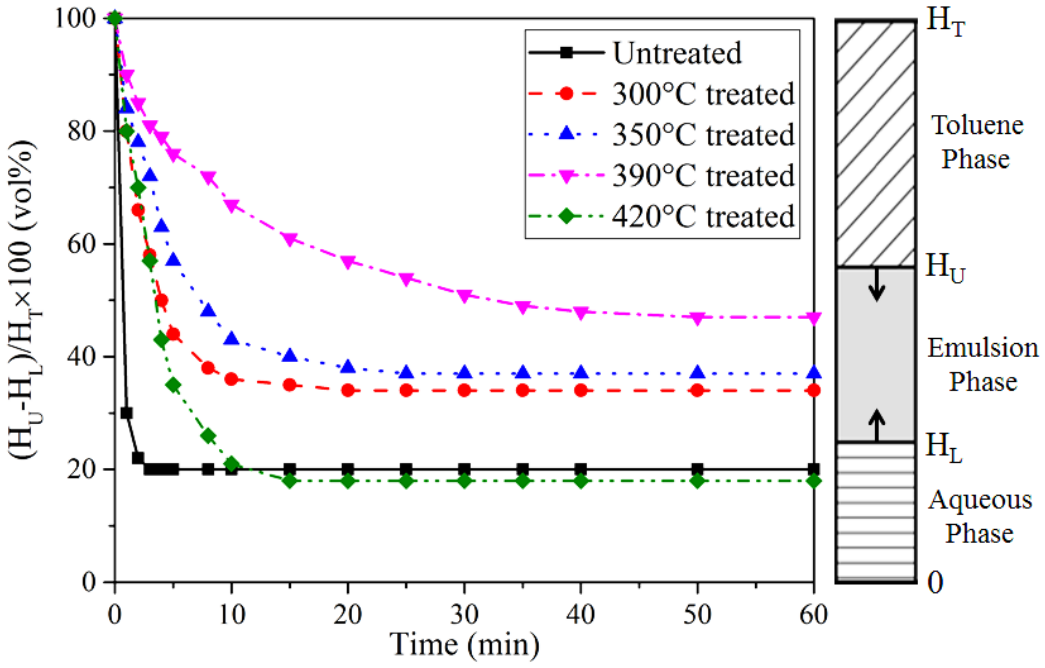

Figure 5.3 Volume percentage of the produced emulsions as a function of time. The arrows in the schematic appearance (right) indicate the moving directions of the interfaces with time.

Both the volume of the produced emulsions and the time to reach this volume are significantly altered by hydrothermal treatment, as can be seen in Figure 5.3. For the untreated fine solids (most hydrophilic), the volume percentage of the produced emulsions dropped sharply to a

constant value of 20% within 3 min and remained stable for the duration of observation (1 h). For the fine solids treated at 300−390°C, the volume percentage of the stable emulsions was higher at 35−50% and the time required to reach this stable emulsion volume increased to 20−40 min. For the fine solids treated at 420°C (most hydrophobic), the volume of the stable emulsions was close to the most hydrophilic sample (i.e. 20% for the untreated fine solids), but with a longer time of about 15 min to reach the final emulsion volume. When the observation time was increased from 1 to 24 h, the emulsion volume did not change, but the fine particles settled in both the toluene and the water phases giving clear fluids. Extensive washing of the fine particles with both toluene and water did not alter the emulsion formation; therefore, the stabilization was by particles rather than any soluble species.

To understand the internal structures and the type of the produced emulsions, the emulsion phase was examined under an optical microscope. The produced emulsions from all the investigated samples showed similar characteristics (Figure 5.4). As shown in Figure 5.4A, spherical droplets with diameters of 10−50 μm are observed, consistent with the observation of Sztukowski and Yarranton [12] who reported emulsions with 1−50 μm droplet size stabilized by 1−10 μm platy clay particles. The enlarged image (Figure 5.4B) shows inner smaller drops entrapped in the outer bigger globule, indicating the presence of multiple emulsions. When drops of the emulsion were removed and placed in toluene, the drops dispersed in toluene; when the drops were placed in water, they remained as intact drops in water. This indicates that toluene was the continuous phase and the produced emulsion was mainly an o/w/o emulsion. When emulsions are stabilized by surfactants, two different surfactants are normally required to prepare such multiple emulsions [48]. Sekine et al. [49] found that the combination of clay minerals and surfactants could enhance the formation of o/w/o emulsions, and they attributed it to the external oil/water

interface which was partially coated with a layer of clay particles making it rigid. The observation of multiple emulsions is consistent with Barthel et al. [50] and Binks [51], who prepared multiple emulsions using a binary mixture of silica particles, with different hydrophobicity (25% difference in Si-OH content). Therefore, the observation of multiple emulsions is consistent with the heterogeneity of particle surface properties illustrated in Figure 5.1.

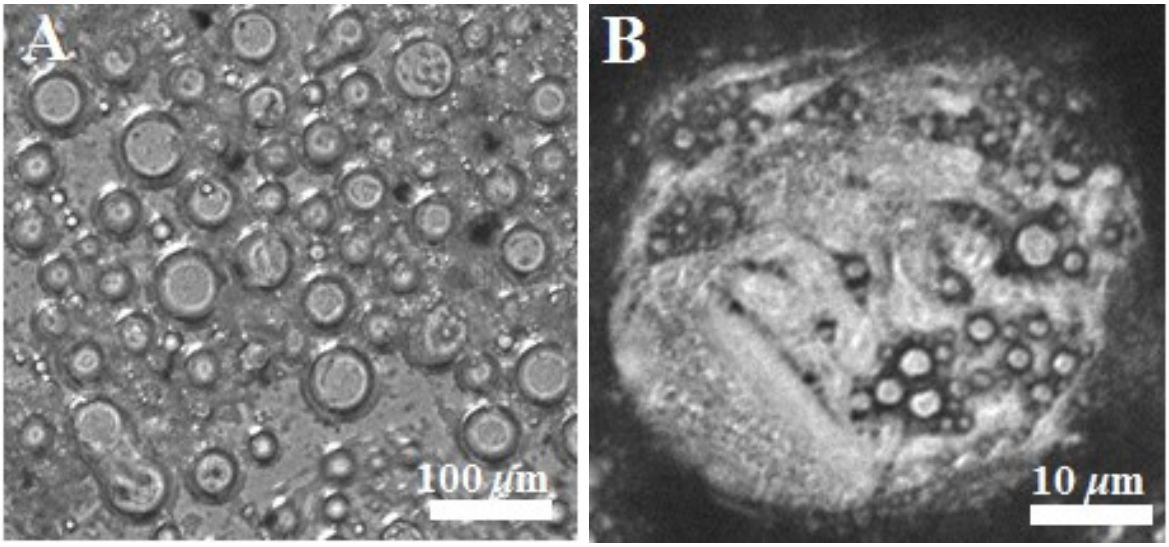

Figure 5.4 (A) Typical optical microscopy image of the produced emulsions, and (B) enlarged image showing a single multiple emulsion globule.

To understand the emulsion stabilizing mechanisms of the fine particles, a cold stage SEM was used to visualize the interfacial structure of the emulsions droplets. Figure 5.5 shows the typical SEM images of (A) an emulsion droplet coated by fine particles, (B) a droplet edge, and (C) an interface between two adjacent droplets. Under the testing condition (–19°C), the water was expected to be in solid phase [52] and the toluene was expected to be in liquid phase or evaporate [53]. The presence of iced spherical water droplets (Figure 5.5A) is consistent with the previous

conclusion that toluene was the continuous phase in the produced emulsions. The image of Figure 5.5A clearly shows that how the micron/submicron sized fine particles coated on the surface of water droplet and thus stabilized it. As shown in an enlarged image (Figure 5.5B), individual particles are seen to form a close-packed monolayer at surface, consistent with the observations of Binks and Kirkland [54]. Such a layer of particles created a steric barrier against droplet coalescence (Figure 5.5C).

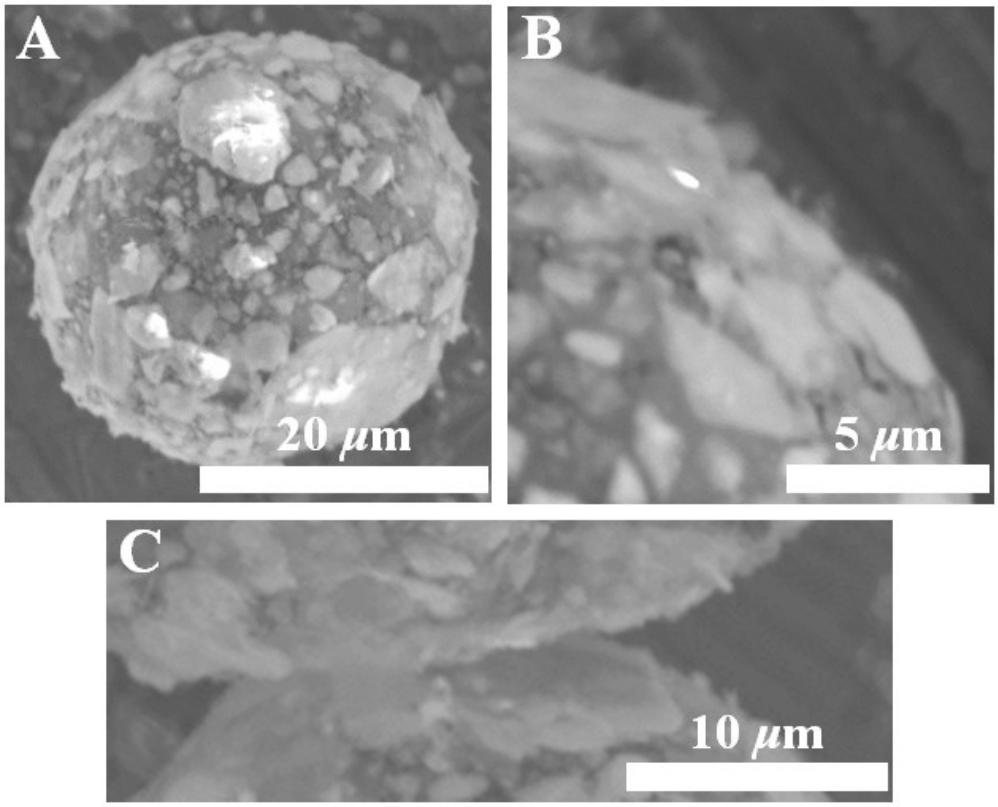

Figure 5.5 Typical SEM images at different magnifications showing (A) an emulsion droplet coated by fine particles, (B) a droplet edge, and (C) an interface between two adjacent droplets.

Based on prior work [19, 41], the fine particles located in emulsion phase were expected to be more bi-wet, while those in water and toluene phases were expected to be more water-wet and oil-wet, respectively. The data of Figure 5.3 show that the fine solids treated at 390°C gave the

largest volume of stable emulsions. At this temperature of treatment, the fraction of fine solids located in the emulsion phase was significantly increased from 30 to 70% after hydrothermal treatment (Figure 5.6), which was proportional to the volume of the produced emulsions from the untreated fine solids and those treated at 390°C (Figure 5.3). The range of particle surface hydrophobicity was broader in the untreated fine solids, with the critical surface tensions in the range of 26−56 mN/m. After the hydrothermal treatment at 390°C, the range of critical surface tension narrowed to 26−41 mN/m (Figure 5.1B), because most of the initial water-wet particles were converted to bi-wet material (Figure 5.6). The increase in the fraction of particles in the emulsion phase suggests that a specific sub-fraction of bi-wet particles in the critical surface tension range of 26−41 mN/m was responsible for the emulsion stabilization, and that the proportion of this sub-fraction was increased by the hydrothermal treatment.

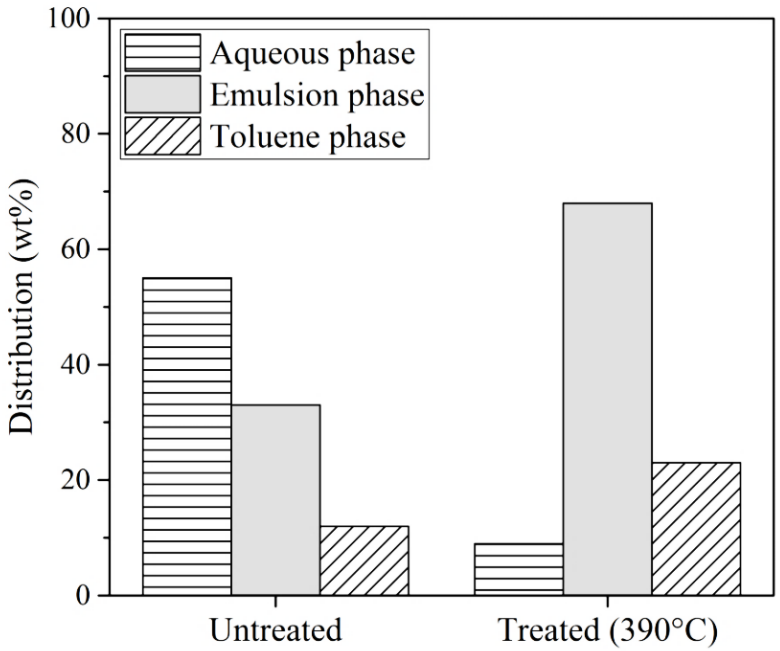

Figure 5.6 Distribution of fine particles in the different phases determined by particle partitioning tests.

The strong emulsifying capacity of the fine solids treated at 390°C contradicted the observations of Zhao et al. [32], who found that the emulsifying capacity of fine solids was reduced after hydrothermal treatment. The original fine solids sample used by Zhao et al. [32] contained much less water-wet particles (10 wt%) than the sample in the present study (55 wt%). Hydrothermal treatment likely altered the originally water-wet particles to bi-wet (Figure 5.6), but due to the lack of water-wet particles in the initial sample of Zhao et al. [32], such a transformation did not increase the net yield of bi-wet particles. Instead, their originally dominant bi-wet particles (65 wt%) were made more oil-wet and the proportion of the bi-wet particles was reduced to 25 wt% after hydrothermal treatment, giving a corresponding reduction in the volume of the produced emulsions. This inconsistency highlights the significant impact of hydrophobicity distribution of particle mixtures on their overall emulsification performance.

5.3.3 Solids Characterization

5.3.3.1 Particle Size

All the untreated and treated fine solids show a particle size distribution mostly between 0.3 and 30 μm, with a mean value (D_{50}) of ~5 μm, as determined by a Mastersizer 3000 particle size analyzer. Figure 5.7 shows the size-frequency distribution curves of the untreated and a typical treated fine solids (at 390°C). The similar shape of the curves implies that hydrothermal treatment did not significantly change the particle size of the fine solids. The results suggest that particle size was not the reason for the difference in emulsification behavior between different fine solids samples (Figures 5.2 and 5.3).

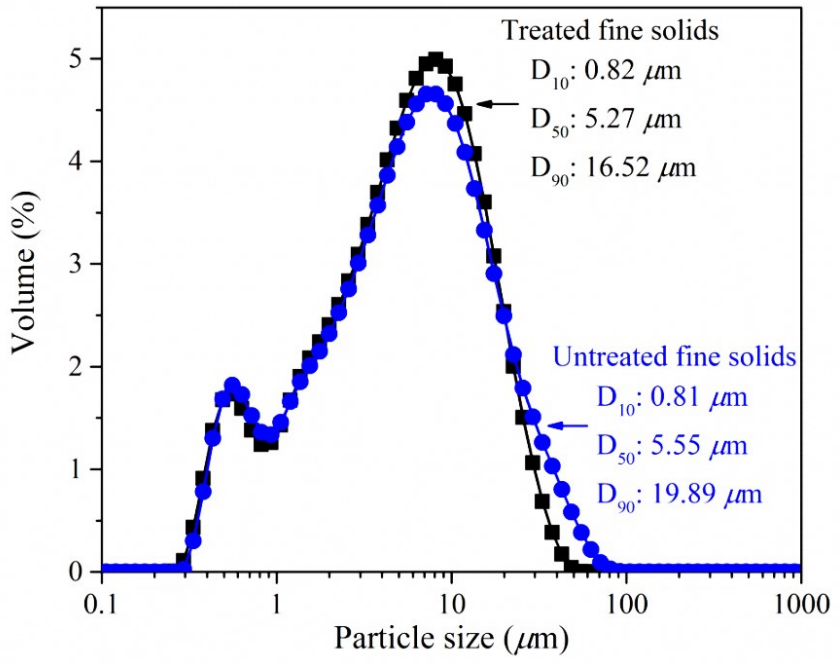

Figure 5.7 Particle size distributions of untreated and treated fine solids (at 390°C).

5.3.3.2 FTIR Spectra

Figure 5.8 shows the FTIR spectra of the untreated and treated fine solids in the temperature range of 300−420°C. All the peak assignments are based on published data [27, 38, 55]. The vibrational peaks can be separated into two groups: organic based modes and inorganic based modes. For the organic based modes, the peaks at 2922 and 1456 cm^{-1} could be assigned to C-H asymmetrical stretching and C-H deformation in $-CH_2$, respectively. The peaks at 2852 and 1377 cm^{-1} corresponded to C-H symmetrical stretching and C-H deformation in $-CH_3$. The C=C stretching mode was observed at 1612 cm^{-1}. For the inorganic based modes, the Si-O stretching modes were detected at 1105, 1031, 1008, and 696 cm^{-1}. The three peaks at 3697, 3650, and 3620 cm^{-1} were assigned to free O-H stretching. The peak at 913 cm^{-1} corresponded to the O-H bending mode from Al-OH and Si-OH groups. The peak intensities of these hydroxyl groups remained unchanged after hydrothermal treatment at temperatures up to 410°C, indicating that

the dehydroxylation reaction was insignificant for the treated samples at 300−410°C. The 420°C treated sample gave reduced hydroxyl intensities in comparison to the other samples, indicating the occurrence of dehydroxylation in this sample with relatively high treatment temperature. These results are consistent with the observation in Chapter 3 that dehydroxylation of kaolinite only happened when the treatment temperature was higher than ~400°C. The peaks at 1419, 860 and 736 cm^{-1}, which were only observed in the untreated fine solids, were assigned to carbonates. The disappearance of carbonates peaks in the treated fine solids is likely due to the conversion of carbonate into some mixture of oxides in high temperature hydrothermal environment. The co-existence of organic and inorganic modes in the FTIR spectra confirms that the toluene-washed fine solids isolated from bitumen froth are complex oil-mineral mixture.

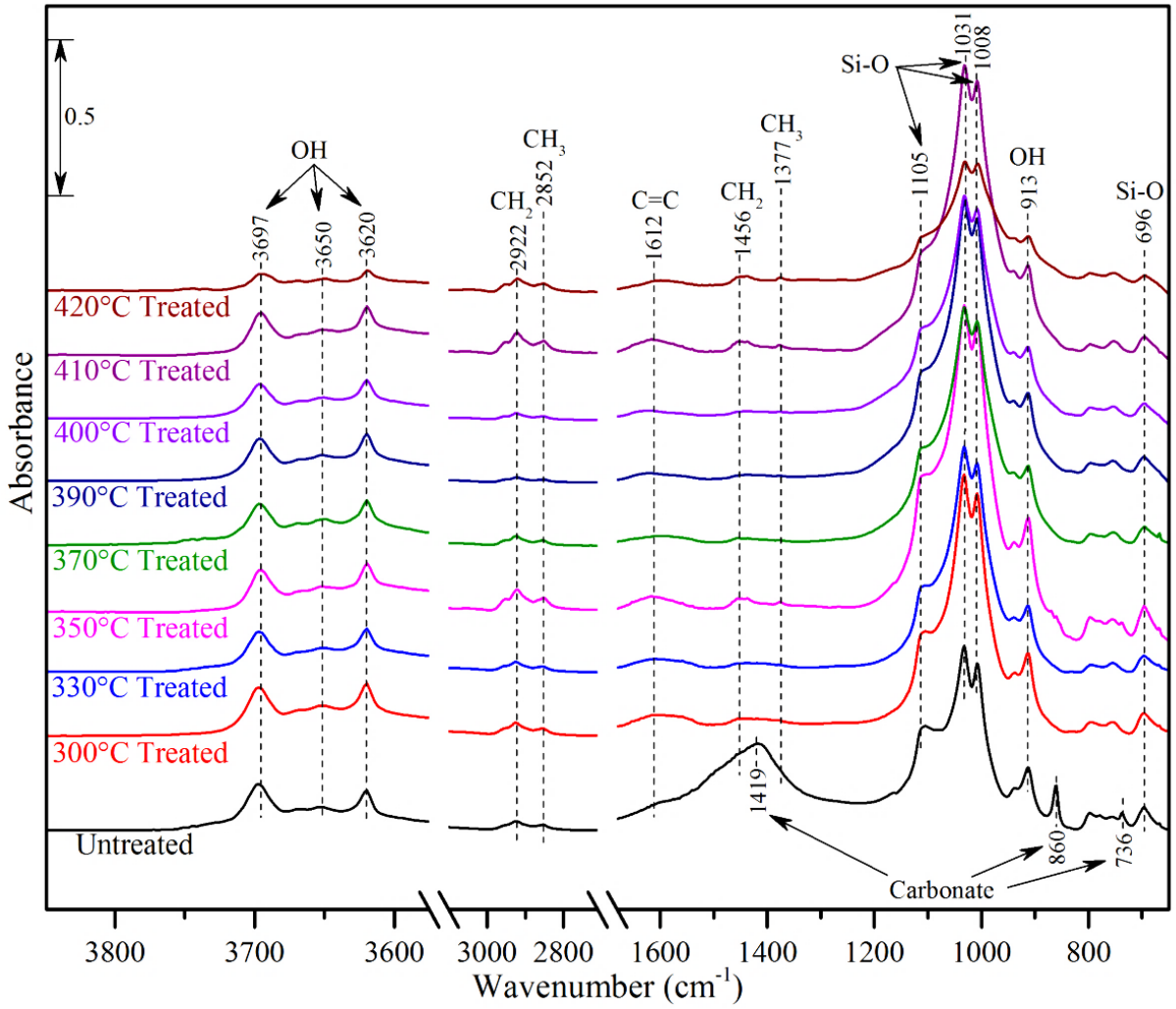

Figure 5.8 FTIR spectra of the untreated and treated fine solids (at 300−420°C).

5.3.3.3 Coverage of Organic Coating on Solids Surfaces

Both the particle hydrophobicity and emulsifying capacity are sensitive to the surface properties of particles. Here, the surface chemical composition of the fine particles was determined by XPS and the results are presented in Table 5.2. Carbon and sulfur indicate the presence of organic components, while aluminum, silicon and oxygen are the main elements of the clay minerals [56, 57]. The data of Table 5.2 show that the atomic concentrations of C and S increased after the

hydrothermal treatment, while the concentrations of Al, Si and O decreased, consistent with the observations of Zhao et al. [32]. To compare the relative ratio of organics and minerals on the solids surfaces, an organics/minerals ratio (OMR) was defined as

$$OMR = \frac{C_c}{C_{Al} + C_{Si}} \tag{5.4}$$

where C_C, C_{Al}, and C_{Si} are the surface atomic concentrations of elements carbon, aluminum, and silicon, respectively. The larger the OMR, the more extensive the organic coating of solids surfaces. Hydrothermal treatment at 300−390°C for 30 min did not change the coverage of surface organic coating significantly, based on the OMR values in Table 5.2. However, a more severe treatment temperature at 420°C dramatically increased the organic coating on the solids surfaces, with the OMR increasing from 2 to 10. Kayukova et al. [58] found that asphaltenes could lose their solubility in aromatic solvents after hydrothermal treatment at 360°C for 5 h, likely due to oligomerization. In the present study, the increased reaction-induced organic coating after hydrothermal treatment at 400−420°C for 30 min may be attributed to the formation of insoluble asphaltenes or mesophase coke materials [58, 59]. The Al/Si ratio was similar for all the fine solids samples, indicating that neither the alumina nor the silica regions were preferentially coated by the organic materials, a conclusion similar to Wang et al. [57] and Chapter 3 of this thesis where samples of asphaltene-coated kaolinite were used.

Table 5.2 Surface chemical composition of the untreated and treated fine solids (at 300−420°C) determined by XPS.

Sample		Untreated	Hydrothermal treatment temperature (°C)							
			300	330	350	370	390	400	410	420
Atomic concentration of elements (atom%)	C	35.5	44.1	43.0	43.7	49.5	47.2	55.0	64.5	70.9
	S	0.5	0.8	0.9	0.9	0.9	1.2	1.4	4.3	5.2
	Al	7.3	7.0	6.8	6.5	6.4	5.3	5.2	3.0	2.4
	Si	12.1	11.4	12.3	12.3	10.8	9.8	10.3	6.7	4.8
	O	44.6	36.7	36.9	36.6	32.4	36.5	28.1	21.5	16.7
Organics/minerals ratio (OMR)		1.8	2.4	2.2	2.3	2.9	3.1	3.6	6.6	9.8
Al/Si		0.6	0.6	0.6	0.5	0.6	0.5	0.5	0.4	0.5

For higher sensitivity of detection within the topmost layer (~2 nm) [60], ToF-SIMS measurements were performed. Positive ion ToF-SIMS spectra in the m/z range of 0−300 were acquired. Characteristic peaks with significant intensity were observed only in the m/z range of 0−50. The peak intensity values in each spectrum were normalized by the respective total secondary ion yields in the m/z range of 0−50, and two normalized spectra were averaged for each sample. Figure 5.9 shows the characteristic peaks of the samples in this range, together with a mass spectrum of an asphaltene sample for comparison. The peak assignments are based on published data in related studies [27, 57]. The possible organic fragments detected in the samples were $C_2H_3^+$ (higher peak at m/z = 27), $C_2H_5^+$ (m/z = 29), $C_3H_3^+$ (higher peak at m/z = 39), $C_3H_5^+$ (m/z = 41) and $C_3H_7^+$ (m/z = 43). These fragments correlated well with the appearance in the asphaltene spectrum, indicating that the organic coating on the mineral surfaces was chemically

similar to asphaltenes. The peaks at m/z = 27 (lower), 28, 39 (lower) and 40 were assigned to inorganic fragments Al^+, Si^+, K^+ and Ca^+, respectively. The coexistence of organic and inorganic peaks in the topmost layer detected by ToF-SIMS was consistent with the XPS data in Table 5.2 and FTIR data in Figure 5.8. The inorganic peaks were significantly smaller than the organic peaks in the treated fine solids at 420°C, suggesting that its topmost layer was almost completely organic materials.

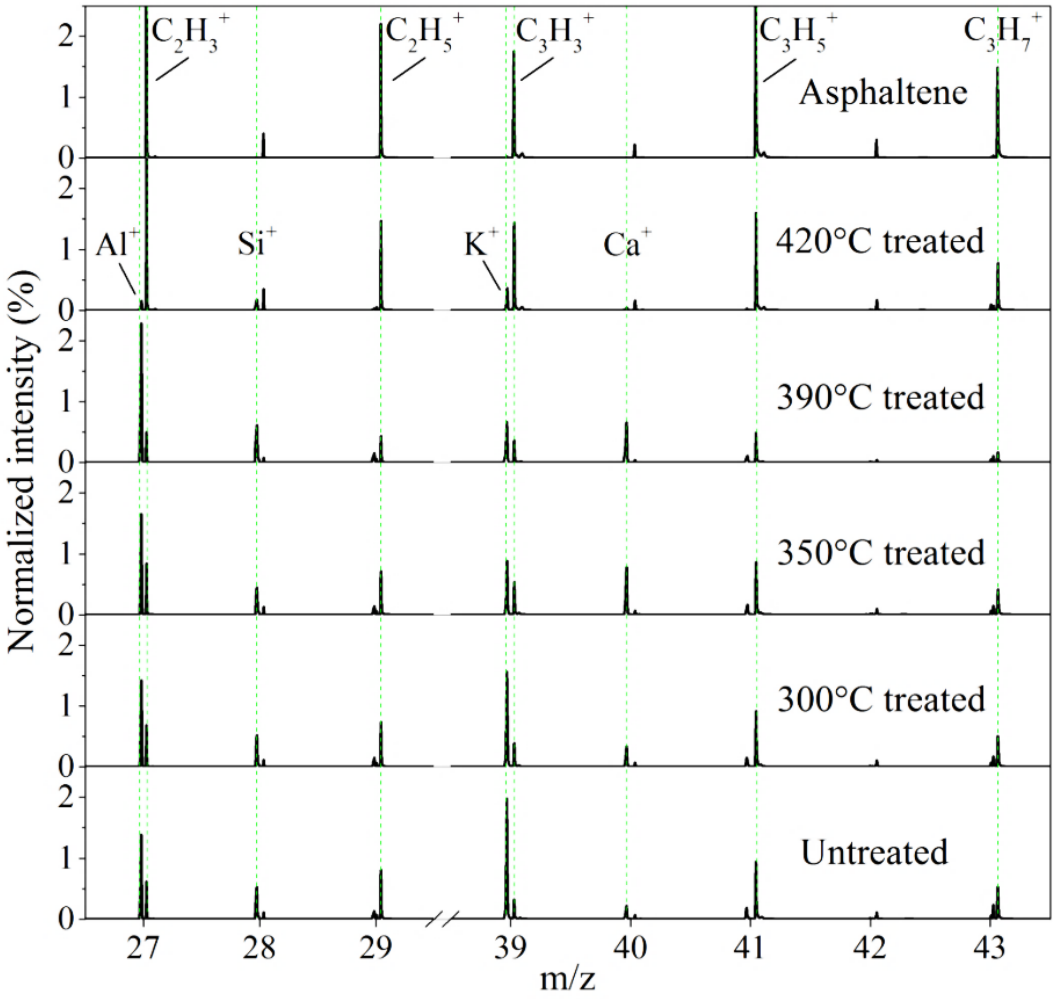

Figure 5.9 ToF-SIMS spectra of the asphaltenes, untreated and treated fine solids.

5.4 Discussion

5.4.1 Correlation between Particle Hydrophobicity and Surface Chemical Composition

The data of Figure 5.10 show that the mean critical surface tension ($\bar{\gamma}_c$) of the fine solids decreased with the surface organics/minerals ratio (OMR), indicating that the increase in organic coating on the solids surfaces was responsible for the increase in particle hydrophobicity. The effect was particularly pronounced when the concentration of surface organics was low. The result is consistent with the correlation between contact angles versus surface carbon concentration reported by Nikakhtari et al. [61] using fine particles extracted from oil sands ores.

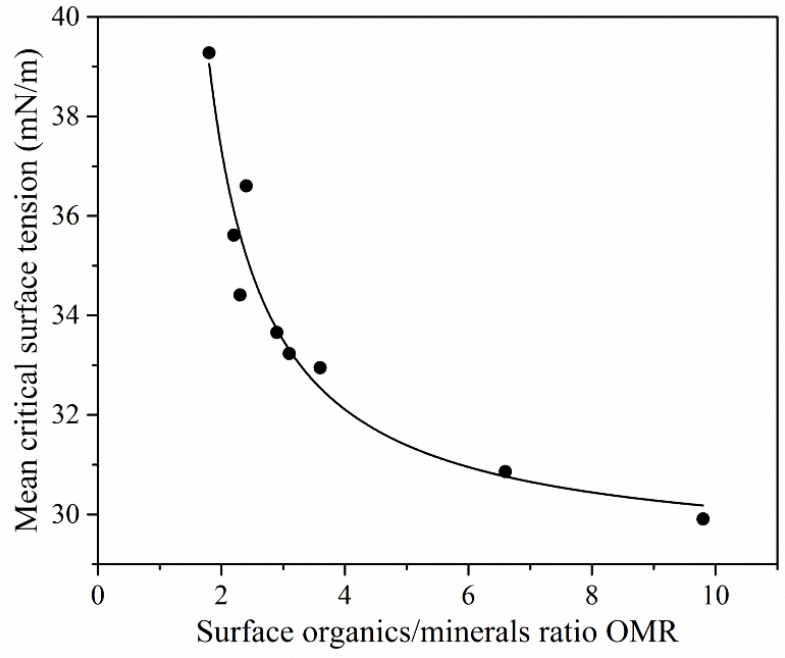

Figure 5.10 Relationship between mean critical surface tension $\bar{\gamma}_c$ determined by film flotation and surface organics/minerals ratio OMR determined by XPS. The trend line shows an exponential fit to the data with $R^2 = 0.92$.

5.4.2 Correlation between Emulsifying Capacity and Particle Hydrophobicity

In Figure 5.11A, the volume percentage of the produced emulsions (1 h after preparation) is plotted against the weight percentage of particles with a critical surface tension of 27−30 mN/m (one of the sub-fractions in Figure 5.1B) and a linear correlation was observed ($R^2 = 0.94$). In contrast, no correlation was observed between the emulsion volume and the mean critical surface tension of the entire particle mixtures (Figure 5.11B), any other single sub-fraction, or any combination of sub-fractions shown in Figure 5.1B. The results suggest that the produced emulsions were stabilized most strongly by the sub-fraction of particles with the critical surface tension of 27−30 mN/m.

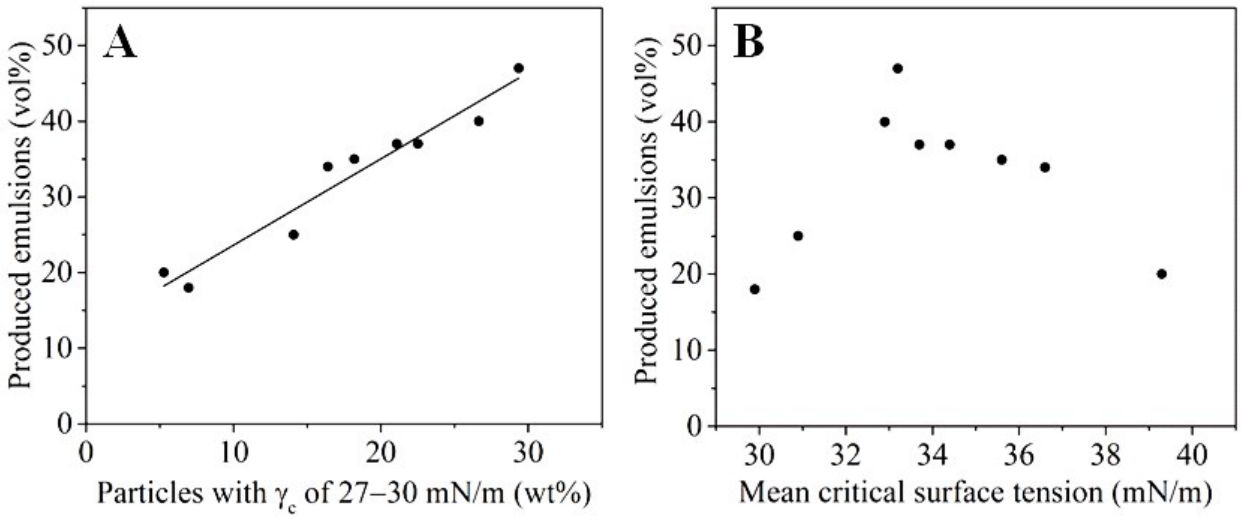

Figure 5.11 Relationship between the emulsifying capacity denoted by the volume percentage of the produced emulsions 1 h after preparation and the weight percentage of particles with the critical surface tension of 27−30 mN/m (A), or the mean critical surface tension (B). The line in (A) shows a linear fit to the data with $R^2 = 0.94$.

As mentioned in the introduction (Section 5.1), thermodynamic considerations suggest that particles with a contact angle of 90° have the strongest ability to stabilize oil-water emulsions [8, 16]. Some experimental results support this conclusion [62, 63], while others do not [6, 64], possibly due to the difficulty in obtaining precise contact angle values of particles at oil/water interfaces, or because of the heterogeneity in the particle populations. The contact angle for the particles with a critical surface tension of 27−30 mN/m, the sub-fraction most active for stabilizing emulsions, was estimated using a modified version of Neumann's equation of state [65]. The method was originally proposed by Fuerstenau et al. [36] and verified experimentally for particles such as coal and ZnS [36, 66, 67]. By this approach, the contact angle was calculated to be 88−93° for the critical surface tension of 27−30 mN/m, which is consistent with the experimental result by Bhushan et al. [68], who measured a contact angle of ~95° for alkylsilane-coated SiO_2 with a critical surface tension of ~28 mN/m. This result suggests that the particles with the critical surface tension of 27−30 mN/m have intermediate hydrophobicity.

5.4.3 Overall Effect of Hydrothermal Treatment on Fine Solids Surface Composition, Particle Hydrophobicity and Emulsifying Capacity

As discussed in the introduction, the fine particles in bitumen froth are a complex mixture of inorganic minerals and carbonaceous materials (Table 5.2) [32]. Each particle in such a mixture may have its own unique set of surface properties, resulting in heterogeneity of shape and surface coating at the level of individual particles. A particle in such a complex mixture can be platy clay mineral, particulate organic matter, or an oil-mineral aggregate [29, 33, 69]. The strong emulsifying capacity of particles with intermediate hydrophobicity can be attributed to their effective adsorption at the oil/water interfaces [70, 71], which may be controlled by the balanced distribution of hydrophobic/hydrophilic areas/groups on particle surfaces [44, 63]. Binks and

Fletcher [70] suggested that the strongest possible adsorption would be for a Janus particle with an oil-wet face and a water-wet face. Fujii et al. [63] experimentally showed that Au-SiO_2 Janus particles adsorbed at the oil/water interfaces as a monolayer with the Au and SiO_2 surfaces facing the oil and water phases, respectively. Unlike the synthetic Janus particles with two distinct faces, the fine particles in this study must exhibit a random distribution of nano-scale organic and inorganic domains on their heterogeneous surfaces [27, 28, 44]. The organic domains (such as hydrocarbon groups) contribute to the hydrophobic character of the particle, while the inorganic domains (such as Si-OH groups) contribute to the hydrophilic character of the particle [8, 44]. This heterogeneity of the particle surfaces enables particles from the bitumen froth to be bi-wet.

Film flotation allows a separation of particle mixtures based on the degree of hydrophobicity at a single particle level, giving sub-fractions that were still an ensemble of heterogeneous particles but with similar particle-average hydrophobicity. The hydrothermal treatment reduced the heterogeneity of the particle mixtures by increasing the coverage of organic coating on solids surfaces (Table 5.2 and Figure 5.9) and thus making them more uniformly hydrophobic (Figure 5.1 and Table 5.1). Even small changes in surface chemistry induced by hydrothermal treatment can change the critical surface tension of solid particles due to its high sensitivity (Figure 5.10) [72].

The toluene-water emulsions in the present study were stabilized by such heterogeneous mixtures of particles with varying degrees of hydrophobicity controlled by different extents of surface organic coverage (Figure 5.12). Binks and Kirkland [54] observed the interfacial structure around droplets in particle-stabilized emulsions using low temperature field emission scanning electron microscopy, and they found a close-packed layer of aggregates of silica

particles at the surface of emulsion droplets. In the present study, the emulsion structure was studied by a similar technique and a close-packed layer of clay particles at the surface of emulsified water droplets was observed (Figure 5.5). These consistent results support the coating mechanism of fine particles in stabilizing emulsions [1, 73].

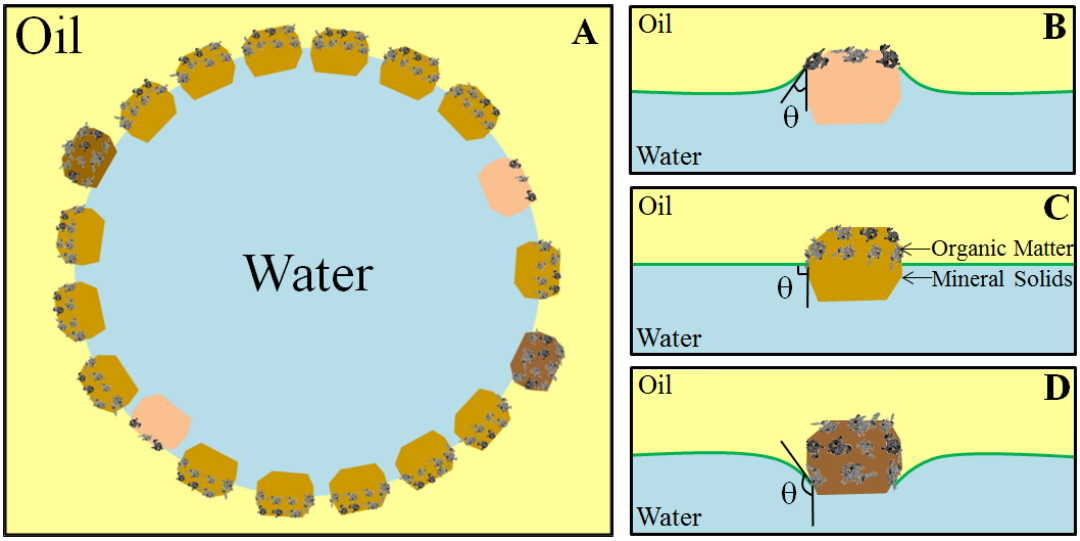

Figure 5.12 (A) Schematic depiction of a water-in-oil emulsion stabilized by mixtures of particles with varying degrees of hydrophobicity. (B−D) Positions of a particle at an oil/water interface with different extents of surface organic coverage. The drawing is not to scale.

Hydrothermal treatment of increasing severity progressively altered the distribution of particle hydrophobicity (Figure 5.1B) and thus altered their emulsification behavior (Figure 5.3). The volume of the produced emulsions was found to depend linearly and monotonically on the percentage of particles with a critical surface tension of 27−30 mN/m (Figure 5.11A). As schematically depicted in Figure 5.12A, these particles, with an intermediate hydrophobicity (Figure 5.12C), dominate the oil/water interface and dictate the emulsification behavior of the entire particle mixtures.

The maximum yield of this interfacially-active sub-fraction of particles was obtained after a hydrothermal treatment at 390°C. A more severe treatment at 420°C significantly increased the organic coating on solids surfaces (Table 5.2 and Figure 5.9), converting the particles to a more oil-wet range of critical surface tension, making them less effective in attaching to the toluene/water interfaces (Figure 5.12D) [2, 8], thereby decreasing the volume of the produced emulsions (Figure 5.3). Here, the particle-particle interaction may also be a contributor to the decreased emulsion volume. Whitby et al. [17] proposed an emulsion destabilization mechanism caused by strong particle-particle interaction using water-in-oil emulsions stabilized by hydrocarbons-modified montmorillonite clay particles. The particle-particle interaction is expected to be stronger between particles which are heavily coated by organic materials like the treated fine solids at 420°C in the present study. The observation of reduced emulsions formed by the treated fine solids at 420°C suggests that "over-treating" (i.e. hydrothermal treatment at relatively high severity) of the bi-wet particles in bitumen froth, making them more completely hydrophobic, may be a potential way to destabilize the bitumen emulsions.

5.5 Conclusions

The influence of hydrophobicity distribution of particle mixtures on their emulsification behavior was investigated using a series of populations of particles with different distributions of hydrophobicity enabled by hydrothermal treatment at different severities. The fine solids in bitumen froth were mixtures of particles with varying degrees of hydrophobicity, with critical surface tension ranging from 26 to 56 mN/m and a mean critical surface tension of 39 mN/m. Hydrothermal treatment in the temperature range from 300°C to 420°C decreased the mean critical surface tension of the fine solids to 37 mN/m to 30 mN/m, respectively, and narrowed the distribution of the critical surface tension. The volume of the produced toluene-water emulsions

had no discernable relationship to the mean critical surface tension of the particle mixtures, but depended linearly and monotonically on the percentage of particles with a critical surface tension of 27−30 mN/m. The results suggest that this active sub-fraction of particles, with an intermediate hydrophobicity, dominated the emulsification behavior of the particle mixtures. In previous studies [2, 8, 9] uniform particles with controlled hydrophobicity, either by chemical grafting organosilanes [8, 74] or by adsorption of different types of macromolecules [68, 75], were used to study the emulsion stabilization mechanisms. Few studies examined the emulsification performance of heterogeneous mixtures of particles with varying hydrophobicity [23, 24]. The present work fills this knowledge gap and the findings may aid in analysis of future studies of emulsion formation by heterogeneous particle mixtures in a variety of industrial sectors.

References

[1] F. Leal-Calderon, V. Schmitt, Solid-stabilized emulsions, Current Opinion in Colloid & Interface Science 13 (2008) 217-227.

[2] Y. Chevalier, M.A. Bolzinger, Emulsions stabilized with solid nanoparticles: Pickering emulsions, Colloids and Surfaces A: Physicochemical and Engineering Aspects 439 (2013) 23-34.

[3] C. Charcosset, Preparation of emulsions and particles by membrane emulsification for the food processing industry, Journal of Food Engineering 92 (2009) 241-249.

[4] P. Shah, D. Bhalodia, P. Shelat, Nanoemulsion: A pharmaceutical review, Systematic Reviews in Pharmacy 1 (2010) 24.

[5] P.K. Kilpatrick, Water-in-crude oil emulsion stabilization: Review and unanswered questions, Energy & Fuels 26 (2012) 4017-4026.

[6] N. Yan, M.R. Gray, J.H. Masliyah, On water-in-oil emulsions stabilized by fine solids, Colloids and Surfaces A: Physicochemical and Engineering Aspects 193 (2001) 97-107.

[7] M.R. Gray, Upgrading oilsands bitumen and heavy oil, The University of Alberta Press, Edmonton, Alberta, 2015.

[8] B. Binks, S. Lumsdon, Influence of particle wettability on the type and stability of surfactant-free emulsions, Langmuir 16 (2000) 8622-8631.

[9] N. Ashby, B. Binks, Pickering emulsions stabilised by Laponite clay particles, Physical Chemistry Chemical Physics 2 (2000) 5640-5646.

[10] A. Walther, M. Hoffmann, A.H. Müller, Emulsion polymerization using Janus particles as stabilizers, Angewandte Chemie 120 (2008) 723-726.

[11] N. Glaser, D.J. Adams, A. Böker, G. Krausch, Janus particles at liquid-liquid interfaces, Langmuir 22 (2006) 5227-5229.

[12] D.M. Sztukowski, H.W. Yarranton, Oilfield solids and water-in-oil emulsion stability, Journal of Colloid and Interface Science 285 (2005) 821-833.

[13] D.E. Tambe, M.M. Sharma, Factors controlling the stability of colloid-stabilized emulsions: I. An experimental investigation, Journal of Colloid and Interface Science 157 (1993) 244-253.

[14] B. Binks, S. Lumsdon, Effects of oil type and aqueous phase composition on oil–water mixtures containing particles of intermediate hydrophobicity, Physical Chemistry Chemical Physics 2 (2000) 2959-2967.

[15] B. Binks, J. Rodrigues, Types of phase inversion of silica particle stabilized emulsions containing triglyceride oil, Langmuir 19 (2003) 4905-4912.

[16] R. Aveyard, B.P. Binks, J.H. Clint, Emulsions stabilised solely by colloidal particles, Advances in Colloid and Interface Science 100 (2003) 503-546.

[17] C.P. Whitby, H.K. Anwar, J. Hughes, Destabilising Pickering emulsions by drop flocculation and adhesion, Journal of Colloid and Interface Science 465 (2016) 158-164.

[18] L.J. Duffus, J.E. Norton, P. Smith, I.T. Norton, F. Spyropoulos, A comparative study on the capacity of a range of food-grade particles to form stable o/w and w/o Pickering emulsions, Journal of Colloid and Interface Science 473 (2016) 9-21.

[19] L. He, F. Lin, X. Li, H. Sui, Z. Xu, Interfacial sciences in unconventional petroleum production: From fundamentals to applications, Chemical Society Reviews 44 (2015) 5446-5494.

[20] Z. Yan, J.A. Elliott, J.H. Masliyah, Roles of various bitumen components in the stability of water-in-diluted-bitumen emulsions, Journal of Colloid and Interface Science 220 (1999) 329-337.

[21] V.N. Paunov, O.J. Cayre, P.F. Noble, S.D. Stoyanov, K.P. Velikov, M. Golding, Emulsions stabilised by food colloid particles: Role of particle adsorption and wettability at the liquid interface, Journal of Colloid and Interface Science 312 (2007) 381-389.

[22] L. Torres, R. Iturbe, M. Snowden, B. Chowdhry, S. Leharne, Preparation of o/w emulsions stabilized by solid particles and their characterization by oscillatory rheology, Colloids and Surfaces A: Physicochemical and Engineering Aspects 302 (2007) 439-448.

[23] B. Binks, S. Lumsdon, Transitional phase inversion of solid-stabilized emulsions using particle mixtures, Langmuir 16 (2000) 3748-3756.

[24] Z.G. Cui, K.Z. Shi, Y.Z. Cui, B. Binks, Double phase inversion of emulsions stabilized by a mixture of $CaCO_3$ nanoparticles and sodium dodecyl sulphate, Colloids and Surfaces A: Physicochemical and Engineering Aspects 329 (2008) 67-74.

[25] H.A. Kaminsky, T.H. Etsell, D.G. Ivey, O. Omotoso, Distribution of clay minerals in the process streams produced by the extraction of bitumen from Athabasca oil sands, The Canadian Journal of Chemical Engineering 87 (2009) 85-93.

[26] J. Masliyah, J. Czarnecki, Z. Xu, Handbook on theory and practice of bitumen recovery from Athabasca oil sands, Volume I: Theoretical basis, Kingsley Knowledge Publishing, Calgary, Alberta, 2011.

[27] F. Bensebaa, L.S. Kotlyar, B.D. Sparks, K.H. Chung, Organic coated solids in Athabasca bitumen: Characterization and process implications, The Canadian Journal of Chemical Engineering 78 (2000) 610-616.

[28] B. Sparks, L. Kotlyar, J. O'Carroll, K. Chung, Athabasca oil sands: Effect of organic coated solids on bitumen recovery and quality, Journal of Petroleum Science and Engineering 39 (2003) 417-430.

[29] F. Bensebaa, A. Majid, Y. Deslandes, Step-scan photoacoustic Fourier transform and X-rays photoelectron spectroscopy of oil sands fine tailings: New structural insights, Spectrochimica Acta Part A: Molecular and Biomolecular Spectroscopy 57 (2001) 2695-2702.

[30] Y. Tu, D. Kingston, J. Kung, L.S. Kotlyar, B.D. Sparks, K.H. Chung, Adsorption of pentane insoluble organic matter from oilsands bitumen onto clay surfaces, Petroleum Science and Technology 24 (2006) 327-338.

[31] T.S. Arnarson, R.G. Keil, Organic–mineral interactions in marine sediments studied using density fractionation and X-ray photoelectron spectroscopy, Organic Geochemistry 32 (2001) 1401-1415.

[32] J. Zhao, Q. Liu, M.R. Gray, Characterization of fine solids in Athabasca bitumen froth before and after hydrothermal treatment, Energy & Fuels 30 (2016) 1965-1971.

[33] M. Couillard, P.H. Mercier, Analytical electron microscopy of carbon-rich mineral aggregates in solvent-diluted bitumen products from mined Alberta oil sands, Energy & Fuels 30 (2016) 5513-5524.

[34] G. Wolansky, A. Marmur, The actual contact angle on a heterogeneous rough surface in three dimensions, Langmuir 14 (1998) 5292-5297.

[35] W.A. Zisman, Relation of the equilibrium contact angle to liquid and solid constitution, contact angle, wettability, and adhesion, Advances in Chemistry Series 43 (1964) 1-51.

[36] D. Fuerstenau, J. Diao, J. Hanson, Estimation of the distribution of surface sites and contact angles on coal particles from film flotation data, Energy & Fuels 4 (1990) 34-37.

[37] D. Fuerstenau, J. Diao, M. Williams, Characterization of the wettability of solid particles by film flotation 1. Experimental investigation, Colloids and Surfaces 60 (1991) 127-144.

[38] C. Wang, M. Geramian, Q. Liu, D.G. Ivey, T.H. Etsell, Comparison of different methods to determine the surface wettability of fine solids isolated from Alberta oil sands, Energy & Fuels 29 (2015) 3556-3565.

[39] J. Diao, D. Fuerstenau, Characterization of the wettability of solid particles by film flotation 2. Theoretical analysis, Colloids and Surfaces 60 (1991) 145-160.

[40] G. Vazquez, E. Alvarez, J.M. Navaza, Surface tension of alcohol water+water from 20 to 50°C, Journal of Chemical & Engineering Data 40 (1995) 611-614.

[41] T. Dang-Vu, R. Jha, S.Y. Wu, D.D. Tannant, J. Masliyah, Z. Xu, Wettability determination of solids isolated from oil sands, Colloids and Surfaces A: Physicochemical and Engineering Aspects 337 (2009) 80-90.

[42] T. Chau, A review of techniques for measurement of contact angles and their applicability on mineral surfaces, Minerals Engineering 22 (2009) 213-219.

[43] Z. Li, D. Harbottle, E. Pensini, T. Ngai, W. Richtering, Z. Xu, Fundamental study of emulsions stabilized by soft and rigid particles, Langmuir 31 (2015) 6282-6288.

[44] K. Darcovich, L. Kotlyar, W. Tse, J. Ripmeester, C. Capes, B. Sparks, Wettability study of organic-rich solids separated from Athabasca oil sands, Energy & Fuels 3 (1989) 386-391.

[45] J. Bachmann, G. Arye, M. Deurer, S.K. Woche, R. Horton, K.H. Hartge, Y. Chen, Universality of a surface tension-contact angle relation for hydrophobic soils of different texture, Journal of Plant Nutrition and Soil Science 169 (2006) 745-753.

[46] F. Yang, P. Tchoukov, E. Pensini, T. Dabros, J. Czarnecki, J. Masliyah, Z. Xu, Asphaltene subfractions responsible for stabilizing water-in-crude oil emulsions. Part 1: Interfacial behaviors, Energy & Fuels 28 (2014) 6897-6904.

[47] G. Gu, Z. Xu, K. Nandakumar, J. Masliyah, Influence of water-soluble and water-insoluble natural surface active components on the stability of water-in-toluene-diluted bitumen emulsion, Fuel 81 (2002) 1859-1869.

[48] C. Goubault, K. Pays, D. Olea, P. Gorria, J. Bibette, V. Schmitt, F. Leal-Calderon, Shear rupturing of complex fluids: Application to the preparation of quasi-monodisperse water-in-oil-in-water double emulsions, Langmuir 17 (2001) 5184-5188.

[49] T. Sekine, K. Yoshida, F. Matsuzaki, T. Yanaki, M. Yamaguchi, A novel method for preparing oil-in-water-in-oil type multiple emulsions using organophilic montmorillonite clay mineral, Journal of Surfactants and Detergents 2 (1999) 309-315.

[50] H. Barthel, B.P. Binks, A. Dyab, P. Fletcher, Multiple emulsions, US Patent 7722891, May 25, 2010.

[51] B.P. Binks, Particles as surfactants-similarities and differences, Current Opinion in Colloid & Interface Science 7 (2002) 21-41.

[52] IFA, GESTIS Substance Database, http://gestis-en.itrust.de/nxt/gateway.dll/gestis_en/000000.xml?f=templates$fn=default.htm$vid=gestiseng:sdbeng$3.0, keyword: water (accessed on May 1, 2017).

[53] IFA, GESTIS Substance Database, http://gestis-en.itrust.de/nxt/gateway.dll/gestis_en/000000.xml?f=templates$fn=default.htm$vid=gestiseng:sdbeng$3.0, keyword: toluene (accessed on May 1, 2017).

[54] B. Binks, M. Kirkland, Interfacial structure of solid-stabilised emulsions studied by scanning electron microscopy, Physical Chemistry Chemical Physics 4 (2002) 3727-3733.

[55] D. Lin-Vien, N.B. Colthup, W.G. Fateley, J.G. Grasselli, The handbook of infrared and Raman characteristic frequencies of organic molecules, Academic Press, San Diego, California, 1991.

[56] S. Ren, T. Dang-Vu, H. Zhao, J. Long, Z. Xu, J. Masliyah, Effect of weathering on surface characteristics of solids and bitumen from oil sands, Energy & Fuels 23 (2008) 334-341.

[57] S. Wang, Q. Liu, X. Tan, C. Xu, M.R. Gray, Study of asphaltene adsorption on kaolinite by X-ray photoelectron spectroscopy and time-of-flight secondary ion mass spectroscopy, Energy & Fuels 27 (2013) 2465-2473.

[58] G. Kayukova, A. Kiyamova, G. Romanov, Hydrothermal transformations of asphaltenes, Petroleum Chemistry 52 (2012) 5-14.

[59] I.A. Wiehe, A phase-separation kinetic model for coke formation, Industrial & Engineering Chemistry Research 32 (1993) 2447-2454.

[60] H. Ota, T. Akai, H. Namita, S. Yamaguchi, M. Nomura, XAFS and ToF-SIMS analysis of SEI layers on electrodes, Journal of Power Sources 119 (2003) 567-571.

[61] H. Nikakhtari, S. Wolf, P. Choi, Q. Liu, M.R. Gray, Migration of fine solids into product bitumen from solvent extraction of alberta oilsands, Energy & Fuels 28 (2014) 2925-2932.

[62] N. Yan, J.H. Masliyah, Characterization and demulsification of solids-stabilized oil-in-water emulsions Part 2. Demulsification by the addition of fresh oil, Colloids and Surfaces A: Physicochemical and Engineering Aspects 96 (1995) 243-252.

[63] S. Fujii, Y. Yokoyama, Y. Miyanari, T. Shiono, M. Ito, S.i. Yusa, Y. Nakamura, Micrometer-sized gold–silica Janus particles as particulate emulsifiers, Langmuir 29 (2013) 5457-5465.

[64] N. Yan, J.H. Masliyah, Characterization and demulsification of solids-stabilized oil-in-water emulsions Part 1. Partitioning of clay particles and preparation of emulsions, Colloids and Surfaces A: Physicochemical and Engineering Aspects 96 (1995) 229-242.

[65] D. Li, A. Neumann, Contact angles on hydrophobic solid surfaces and their interpretation, Journal of Colloid and Interface Science 148 (1992) 190-200.

[66] D. Janssen, R. De Palma, S. Verlaak, P. Heremans, W. Dehaen, Static solvent contact angle measurements, surface free energy and wettability determination of various self-assembled monolayers on silicon dioxide, Thin Solid Films 515 (2006) 1433-1438.

[67] M. Holuszko, J. Franzidis, E. Manlapig, M. Hampton, B. Donose, A. Nguyen, The effect of surface treatment and slime coatings on ZnS hydrophobicity, Minerals Engineering 21 (2008) 958-966.

[68] B. Bhushan, T. Kasai, G. Kulik, L. Barbieri, P. Hoffmann, AFM study of perfluoroalkylsilane and alkylsilane self-assembled monolayers for anti-stiction in MEMS/NEMS, Ultramicroscopy 105 (2005) 176-188.

[69] R. Haynes, M. Beare, Influence of six crop species on aggregate stability and some labile organic matter fractions, Soil Biology and Biochemistry 29 (1997) 1647-1653.

[70] B. Binks, P. Fletcher, Particles adsorbed at the oil-water interface: A theoretical comparison between spheres of uniform wettability and “Janus” particles, Langmuir 17 (2001) 4708-4710.

[71] C. Snoeyink, S. Barman, G.F. Christopher, Contact angle distribution of particles at fluid interfaces, Langmuir 31 (2015) 891-897.

[72] R.M.Š. Sokolovic, S.M. Sokolovic, Effect of the nature of different polymeric fibers on steady-state bed coalescence of an oil-in-water emulsion, Industrial & Engineering Chemistry Research 43 (2004) 6490-6495.

[73] T.S. Horozov, B.P. Binks, Particle-stabilized emulsions: A bilayer or a bridging monolayer? Angewandte Chemie International Edition 45 (2006) 773-776.

[74] J. Brzoska, I.B. Azouz, F. Rondelez, Silanization of solid substrates: A step toward reproducibility, Langmuir 10 (1994) 4367-4373.

[75] M. Hato, Attractive forces between surfaces of controlled “hydrophobicity” across water: A possible range of “hydrophobic interactions” between macroscopic hydrophobic surfaces across water, The Journal of Physical Chemistry 100 (1996) 18530-18538.

6 Influence of Hydrothermal Treatment on Filterability of Fine Solids in Bitumen Froth[3]

6.1 Introduction

The current oil sands operations in the Fort McMurray region in northern Alberta, Canada, use a warm-water extraction process which generates a bitumen froth as an intermediate product. Typical bitumen froth contains 60 wt% bitumen, 30 wt% water and 10 wt% fine solids [1]. The water may carry dissolved salts, which contribute to corrosion hazards in downstream operations [2]. The fine solids not only stabilize water-in-oil emulsions, but are also detrimental to downstream processes like upgrading and refining [3, 4]. Transport of the bitumen by pipeline requires that contents of basic sediment and water (BS&W) be lower than 0.5 vol%, while water alone is limited to 0.3−0.5 vol% [5]. In order to be acceptable for pipeline transport, the water and fine solids in the bitumen froth must be removed.

Two technologies are currently used for cleaning bitumen froth, depending on the solvent used to dilute the bitumen froth and lower its viscosity [4, 6]. When naphtha distillate is used, the emulsion is only partly broken and significant amounts of solids and water remain even after using inclined-plate settlers and centrifuges (Figure 6.1A). In this case, the resulting bitumen can still contain 2−5 wt% water and 0.5−1 wt% fine solids [7] and cannot be transported by pipelines unless it is first processed by coking-type upgrading plants. When a poor solvent such as hexane is used, 4−10% of the bitumen fraction, mostly asphaltene, precipitates, flocculating and removing with it almost all water and fine solids [8] (Figure 6.1B). The rejection of the asphaltene fraction in paraffinic froth treatment (PFT) may potentially lower the oil yield;

[3] A version of this chapter has been published as Q. Chen, I. Stricek, M. Cao, M.R. Gray, Q. Liu, Influence of hydrothermal treatment on filterability of fine solids in bitumen froth, Fuel 180 (2016) 314-323.

however, some companies, such as Shell, deliberately reject the asphaltenes using PFT because their refinery does not have a coking unit and asphaltenes are known as a coke precursor. Both the froth cleaning processes require distillation to remove the large volumes of solvent from the bitumen product, and solvent recovery units to recover the residual solvents from the fine solids and water. Inefficiencies in solvent recovery are a major contribution to solvent losses into the tailings ponds [4].

Alternative technologies for froth cleaning are desirable if they can reduce the equipment cost, reduce energy consumption, and reduce environmental impact. The bi-wettable fine solids stabilize water-in-oil emulsions, which, in turn, makes solids and water removal from bitumen froth extremely difficult [9]. Hence, any technology which can alter the surface properties of the fine solids may be a potential choice for froth cleaning. Hydrothermal treatment is direct thermal processing of bitumen froth at elevated temperature rather than the current approach of froth treatment followed by upgrading. After the hydrothermal treatment, the wide range of the surface properties of the initial fine solids particles with a high disparity of wettability was made uniformly hydrophobic [10].

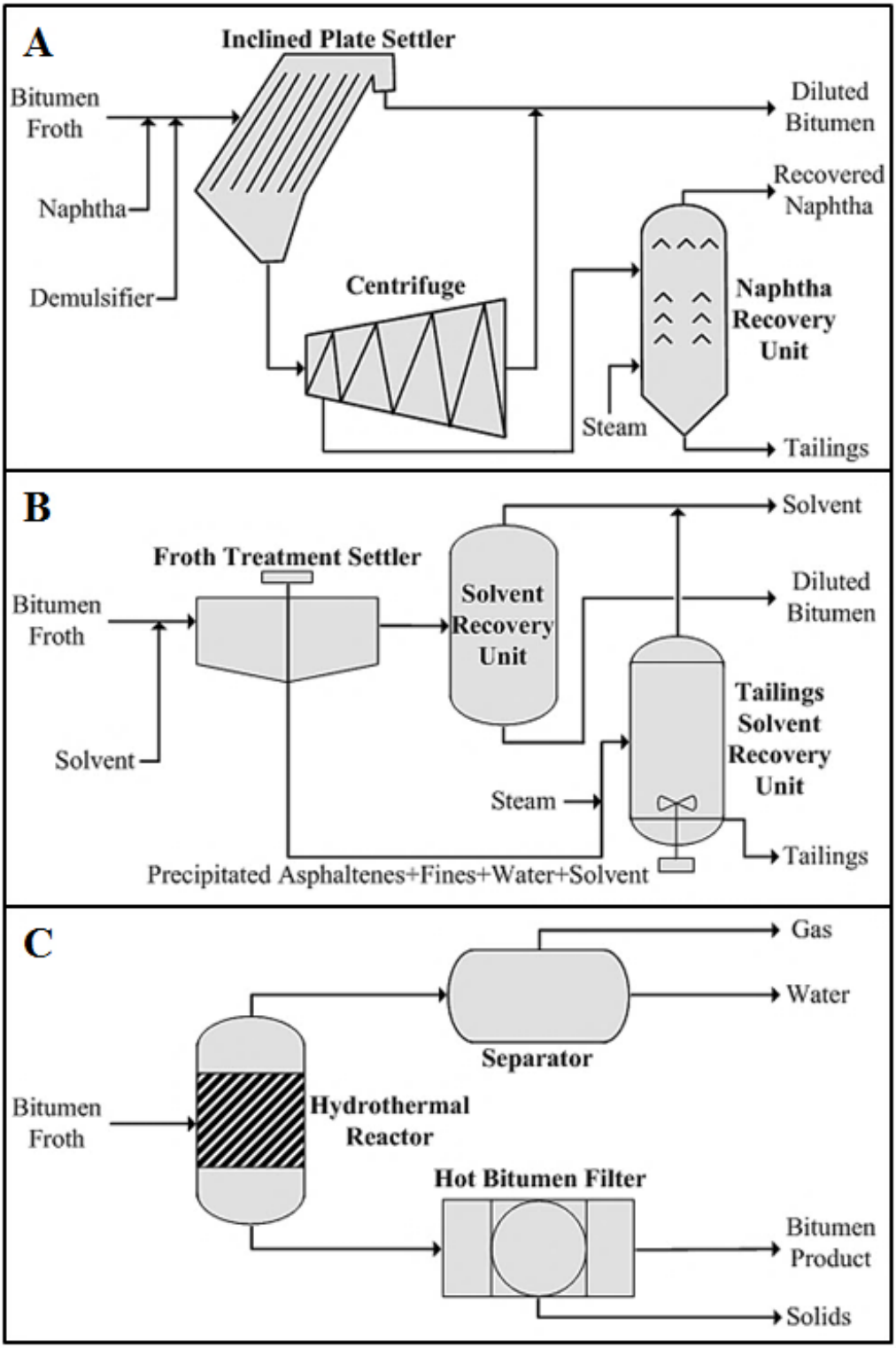

Figure 6.1 Schematics of bitumen froth treatment processes: (A) simplified naphthenic froth treatment, (B) simplified paraffinic froth treatment, and (C) conceptual hydrothermal treatment.

Filtration is a well-established method for solid-liquid separation [11]. Although bitumen is viscous at room temperature, at the elevated temperatures that follow hydrothermal treatment its lowered viscosity may enable filtration. In related studies, Yoshida et al. [12] performed hot filtration of coal liquids at 360°C by using 0.5-μm pore size stainless steel filters to produce ash-free material. They found that a high extraction yield can be achieved under hot filtration with addition of organic solvents such as methylnaphthalene. Filtration at high temperature offers many advantages, such as increased overall efficiency, improved product quality, recovery of thermal energy, and integration of filtration into the overall process [13, 14]. Advances in filter media have provided materials such as sintered metal and porous ceramic filter media that are readily available and suitable for hot filtration at temperatures up to 900°C [15-17].

To employ filtration in bitumen froth cleaning process, the filterability of the fine solids is of great significance. No systematic studies have examined the filtration behavior of the fine solids after hydrothermal treatment. A filter cake can be described as a packed bed of particles with a complex system of interconnected inter-particle voids [18]. The stacking of microscopic particles inside the filter cake is directly related to the macroscopic filtration performance. In this regard, any changes in the pore structure of the filter cake due to particle rearrangement will affect the flow behavior within the filter cake and in turn change the filterability.

The working hypothesis is that hydrothermal treatment would improve the filterability of the fine solids in bitumen froth by disrupting the original stacking of clay particles. A conceptual bitumen froth cleaning approach is proposed, as shown in Figure 6.1C, which combines the hydrothermal treatment of bitumen froth, water separation by venting and solids removal by hot filtration. The objectives were to study the influence of hydrothermal treatment at 300−420°C for up to 180 min on the filterability of the fine solids in bitumen froth and to test the feasibility of

solids removal from bitumen froth by hydrothermal treatment followed by hot filtration at the laboratory scale.

6.2 Materials and Methods

6.2.1 Bitumen Froth

The bitumen froth sample was obtained from CanmetENERGY, Devon, Alberta, courtesy of Imperial Oil Limited. The sample contained 78 wt% bitumen, 14 wt% water and 8 wt% fine solids as determined by Dean-Stark extraction.

6.2.2 Hydrothermal Treatment and Water Removal

The hydrothermal treatment, venting and solids hot filtration were carried out using the laboratory set up shown in Figure 6.2. The treatment temperature and time are optimized by conducting hydrothermal treatment at 300−420°C for 0−180 min. The hydrothermal treatment was performed using a 500 mL 4575B Series Parr reactor (Figure 6.2A). To carry out the hydrothermal treatment, a bitumen froth sample weighing 165 g was loaded into the Parr reactor for each run. The reactor was then pressurized with nitrogen to 0.7 MPa and placed in a heating mantle to heat to the desired temperature. When the temperature reached 100°C, the stirring was turned on and fixed at 300 rpm. Circa 40 min were taken for the reactor to reach the target temperature. The reactor was left at the target temperature for certain treatment time (the heat-up time was not included in the reported treatment time). The following conditions were investigated: 300, 330, 350, 370, 390, 400, 410, and 420°C for 30 min, and 390°C for 0, 10, 30, 60, and 180 min. In this context, a treatment time of 0 min means heating the reactor to 390°C then immediately cooling it without holding the temperature at 390°C. The pressure under

different treatment conditions was in the range of 8.6−19.3 MPa. After the hydrothermal treatment, the reactor was cooled down to 270°C by turning off the heating mantle and circulating cooling water in the coil inside the Parr reactor. The vapors inside were vented out at 270°C and subsequently condensed (Figure 6.2B). The amount of hydrocarbon vented off at 270°C was insignificant unless the hydrothermal treatment was carried out at higher than 400°C. Afterwards, the reactor contents were further cooled down to 200°C with stirring. Then both the cooling water and stirring were turned off. The contents in the reactor were either *in-situ* filtered at 200°C (hot filtration), or cooled overnight to room temperature, then diluted with solvent and filtered (room-temperature filtration).

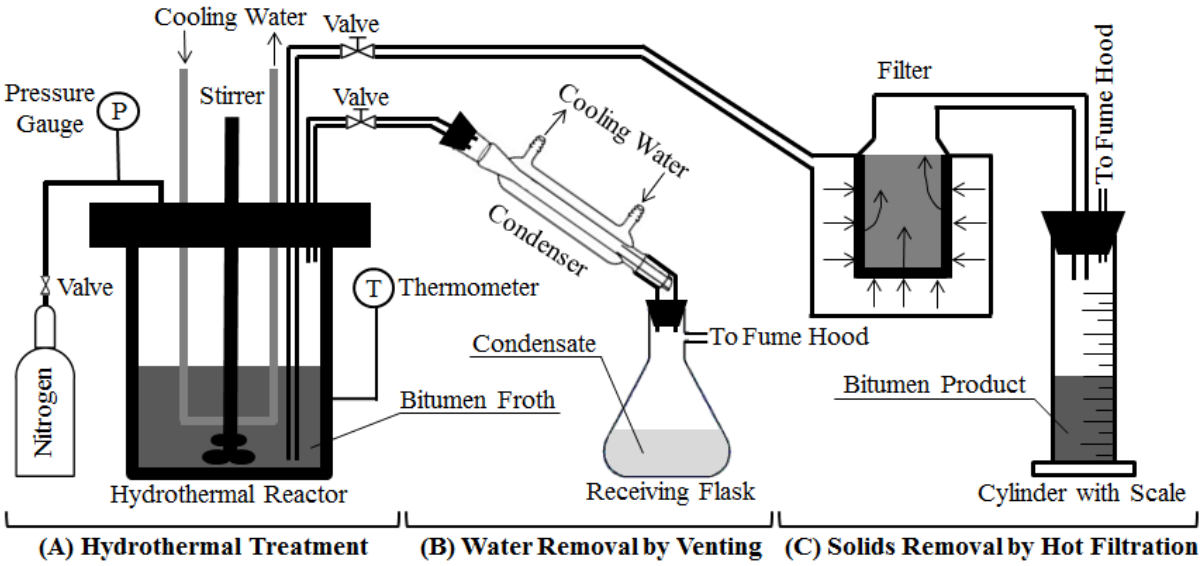

Figure 6.2 Schematics for laboratory-scale hydrothermal bitumen froth cleaning test set up. The schematics show the (A) hydrothermal treatment, (B) venting, and (C) hot filtration.

6.2.3 Filtration Test

After hydrothermal treatment and water removal, the reactor contents are called "treated bitumen mixture" (TBM). The fine solids in TBM were removed by filtration as indicated earlier, either room-temperature filtration or hot filtration.

Room-temperature filtration: The filter medium used in this method was the Millipore filter membrane (type GVWP, pore size 0.22 μm and thickness 125 μm). The filter area was 9.8 cm^2. A vacuum pump was used to generate vacuum at 55 kPa. The filtration was operated under room temperature (~25°C). To begin each filtration test, the filter assembly was set up and the vacuum pump was turned on. Five grams of bitumen froth sample or TBM were diluted by 95 mL toluene to form a suspension. The suspension was stirred at 30 rpm for 20 min and then immediately poured into the glass funnel to minimize the interference of sedimentation. The residue fine solids in the beaker were quickly rinsed off by 5 mL toluene. The solid particles were retained by the filter medium and gradually built up to form a filter cake. The total time required for all the liquid to pass through the filter was recorded as the filtration time. Three tests were performed for each sample. The filter cake was further cleaned by circa 20 mL toluene until the filtrate was colorless. The filtered solids were then placed in a vacuum oven at 65°C for 24 hours. Afterwards, the solids particles were collected as fine solids samples for later analysis.

Hot filtration: The TBM was *in-situ* filtered by hot filtration at 200°C, as illustrated in Figure 6.2C. A 0.5-μm pore size stainless steel filter (SS-6TF-05, Swagelok) was used in the hot filtration. The filter area was 12.9 cm^2. For each filtration test, the cumulative volume of the filtrate was continuously determined by a graduated cylinder. In this way, the filtration rate could be monitored. After hydrothermal treatment and venting, the TBM was cooled to 200°C and

pressurized to 1 MPa by compressed nitrogen. The valve in the filtration line was then opened and the hot bitumen subsequently flowed into the filter. All the filtration lines including the filter were fully covered by heating tapes (SWH171-020, OMEGA®) to keep the temperature at about 200°C during the entire filtration process. As the filtration proceeded, the filtrate flowed into the graduated cylinder and its volume with filtration time was recorded until no liquid came out. For comparison purposes, the bitumen froth sample was heated to hot filtration temperature (200°C) and kept for 30 min, and then filtered without going through the hydrothermal treatment. All the filtration operations followed the same procedure as above. Hot filtration took advantage of the low viscosity of the hot bitumen and aimed at removing the fine solids without using a diluent. In this study, the data from room-temperature filtration could be used to predict hot filtration performance.

6.2.4 Filterability Evaluation

Both room-temperature filtration and hot filtration steps were cake filtration operations with constant operating pressure, in the former case due to the vacuum pump and in the latter case by compressed nitrogen. In cake filtration, solids particles are retained on the filter medium, forming an increasingly thicker cake. The mechanism of flow within the cake and the filter medium, and the external conditions imposed on them are the basis for modelling a filtration process [19]. Detailed derivation of the filtration equations can be found in references [20, 21].

In the room-temperature filtration test, the suspension of toluene-diluted TBM was visible during filtration and its starting volume was constant for different runs. Therefore, the time it took for all the liquid to flow through the filter, i.e., filtration time, could be used directly as an index to evaluate the filterability. In contrast, during hot filtration the TBM was invisible and the filtration

time was ambiguous and difficult to determine accurately. Therefore, filtration time was not useful to assess the filterability in hot filtration.

The specific resistance to filtration (SRF) has been widely used to assess the filterability of solid-liquid suspension in mining, waste treatment and oil sands tailings treatment [11, 22, 23]. The procedures for SRF calculation described by Xu et al. [11] were closely followed. At constant pressure, the filtration equation [11] is described as

$$\frac{t}{V} = \frac{SRF\,\mu\omega}{2PA^2}V + \frac{SRF\,\mu L_m}{PA} \tag{6.1}$$

Where V is the volume of the filtrate (m^3), t the filtration time corresponding to V (s), SRF the specific resistance to filtration (m/kg), μ the viscosity of filtrate (Pa·s), ω the mass of solids cake formed per unit filtrate volume passing through (kg/m^3), P the pressure applied on the top of the filter cake (Pa), A the filter area (m^2) and L_m the fictitious equivalent thickness of the filter medium (kg/m^2).

According to Equation 6.1, a plot of t/V versus V would give a straight line with slope b:

$$b = \frac{SRF\,\mu\omega}{2PA^2} \tag{6.2}$$

The specific resistance to filtration (SRF) can be calculated from b through Equation 6.3.

$$SRF = \frac{2PA^2 b}{\mu\omega} \tag{6.3}$$

In the hot filtration tests of this study, the V and t are measured directly. The filter cake was assumed to be incompressible in calculating the *SRF*. The higher the *SRF*, the poorer the filterability of the particle suspension [24].

6.2.5 Analytical Methods

The residue water contents in the TBM samples were measured by Karl Fischer coulometer (Mettler Toledo DL39). The microphotographs of the bitumen froth and TBM samples were taken by a Zeiss Axiovert 200M microscope. The residue solids contents in the filtrate after hot filtration were measured by membrane filtration according to ASTM D4807-05 [25].

The fine solids samples used for detailed characterization were filtered solids (filter cake) from room-temperature filtration. The mineralogical composition of the fine solids samples was analyzed by quantitative X-ray diffraction (XRD) using RockJock version 11 software [26]. A Rigaku Ultima IV diffractometer (with Cu Kα radiation) and a graphite monochromator (operating at 44 mA and 40 kV) were employed to generate X-ray to scan the sample from 5 to 65 degrees (2θ).

The particle size distributions of the fine solids samples were determined by a G400 Mettler Toledo focused beam reflectance measurement (FBRM) particle size analyzer. The FBRM can measure the chord length of particles in an opaque suspension. Here, two samples were tested: untreated fine solids (filtered solids from original bitumen froth sample) and treated fine solids (filtered solids from TBM obtained by hydrothermal treatment at 390°C for 30 min). A 0.5 g of solids sample and 4.5 g of Athabasca bitumen (negligible solids content, courtesy of Imperial Oil Limited) were mixed into 300 mL toluene. The suspension was stirred at 300 rpm for 1 hour before the measurement and kept stirred during the

measurement. The FBRM probe has a 9.5 mm diameter flat sapphire window with a scan speed of 2 m/s and an optimum measured size range of 1 μm – 4 mm.

For contact angle measurements, each fine solids sample (~100 mg) was pressed into a 1-cm diameter pellet by an ICL 12 TON E-Z Press^{TM} pellet presser at 34 MPa. The measurements were conducted using a FTA200 contact angle goniometer equipped with an optical microscope and illumination system.

The morphology of fine solids in the original bitumen froth and TBM was analyzed by a JEOL 6301F Field Emission scanning electron microscope (SEM). The fine solids solution was prepared by dissolving 50 mg solids powder in 1 mL toluene. A droplet of the mixed solution (20 μL) was drop-casted by pipet on an aluminum SEM sample holder. After evaporation of all the toluene, the fine solids sample on the SEM sample holder was coated with carbon by a Leica EM SCD005 coater. For ultrafine particle analysis, the filtrate from hot filtration through the 0.5-μm pore sized stainless steel filter (hydrothermal treatment at 390°C for 30 min) was re-filtered by room-temperature filtration with 0.1-μm pore size filter membrane. The retained cake solids on the filter membrane were analyzed in a Tescan Vega scanning electron microscope (SEM) with energy dispersive X-ray spectrometer (EDX). The sample was coated with gold by using a Nanotek SEMprep 2 sputter coater.

The particle stacking behavior at the filter cake-filter medium interface was analyzed by the JEOL 6301F Field Emission SEM. To prepare the filter cake for analysis, one gram of the bitumen froth sample or TBM from treatment at 390°C for 30 min was diluted with 100 mL toluene. All the filtration operations followed the same procedure as in room-temperature filtration. For the bitumen froth sample, the filtration rate was very slow, but all the liquid could

pass through the filter membrane after about 2 hours, while the filtration for the TBM sample could be complete within 2 minutes. The formed filter cake was further washed by circa 20 mL toluene until the filtrate was colorless. Afterwards, the mass of the wet filter cake was immediately weighed (m_{wet}). The filter cake together with the filter membrane was then placed in an oven at 35°C for 24 hours to minimize the interference of evaporation on the filter cake structure. Care was taken not to disturb the filter cake on the filter membrane surface. The mass of the dry filter cake was also weighed (m_{dry}). The porosity of the filter cake was calculated by Equation 6.4:

$$\varepsilon = \frac{(m_{wet} - m_{dry}) \times \rho_s}{(m_{wet} - m_{dry}) \times \rho_s + \rho_t \times m_{dry}} \tag{6.4}$$

where ε is the porosity of the filter cake, m_{wet} is the mass of wet filter cake (g), m_{dry} is the mass of dry filter cake (g), ρ_s is the density of fine solids (kg/m^3), and ρ_t is the density of toluene (kg/m^3).

The filter cake after drying separated into two layers. The top layer, about 90 wt% of the total filter cake solids, was detached from the filter membrane, while a thinner bottom layer remained attached to the filter membrane. The top layer was carefully removed without disturbing the structure of the bottom layer. Then the bottom layer together with the filter membrane was subjected to SEM observation. An area of about 10 mm × 10 mm was selected for measurement. Three sides of this selected area were cut by a knife. The side that remained attached was carefully torn off and this side was used for capturing SEM images.

A Kratos AXIS 165 X-ray photoelectron spectroscopy (XPS) was used to detect the chemical composition of the sample surfaces. Pellet samples for XPS were prepared by the same method

as described above for the contact angle measurements. Monochromatic Al Kα source (hv = 1486.6 eV) was used at a power of 210 W. The analysis spot was 400 μm × 700 μm and take-off angle was 90°. Survey scan spectra (160 eV pass-energy) were obtained to detect all the elements possibly present and high resolution scan spectra (20 eV pass-energy) were also obtained for more detailed information about carbon, oxygen, aluminum and silicon. Total organic carbon contents of the fine solids samples were measured by Dumas combustion method [27]. A Costech Model EA 4010 elemental analyzer was used for the tests. The carbonates were removed by leaching with 6% HCl solution.

6.3 Results and Discussion

6.3.1 Residual Water Content

Figure 6.3 shows the residual water content after water removal under different treatment conditions. Under the studied conditions (300−420°C/30 min or 390°C/0−180 min), the different treatment temperatures and times did not change the water contents in the TBM noticeably. The original water content in the bitumen froth sample was about 14 wt%, while the residual water content in TBM was negligible (0.03 wt%). Based on these observations, the hydrothermal treatment followed by venting is an effective way to remove water from bitumen froth. Figure 6.4 shows the microphotographs of bitumen froth and typical TBM from treatment at 390°C for 30 min. A significant number of water droplets can be seen in the untreated bitumen froth sample, indicating the presence of water-in-oil emulsion (Figure 6.4A). On the other hand, no apparent water droplets were observed in TBM (Figure 6.4B). These microphotographs concur with the results of water contents measured by Karl Fischer titration (Figure 6.3).

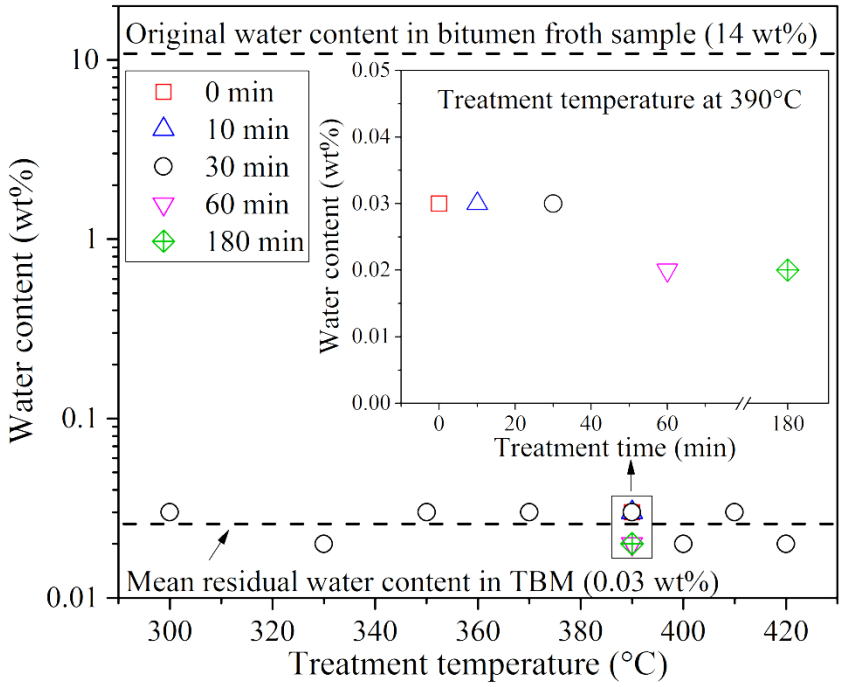

Figure 6.3 Residual water contents in TBM as a function of temperature for a treatment time of 30 min. The inset figure shows the water contents under different treatment times at 390°C.

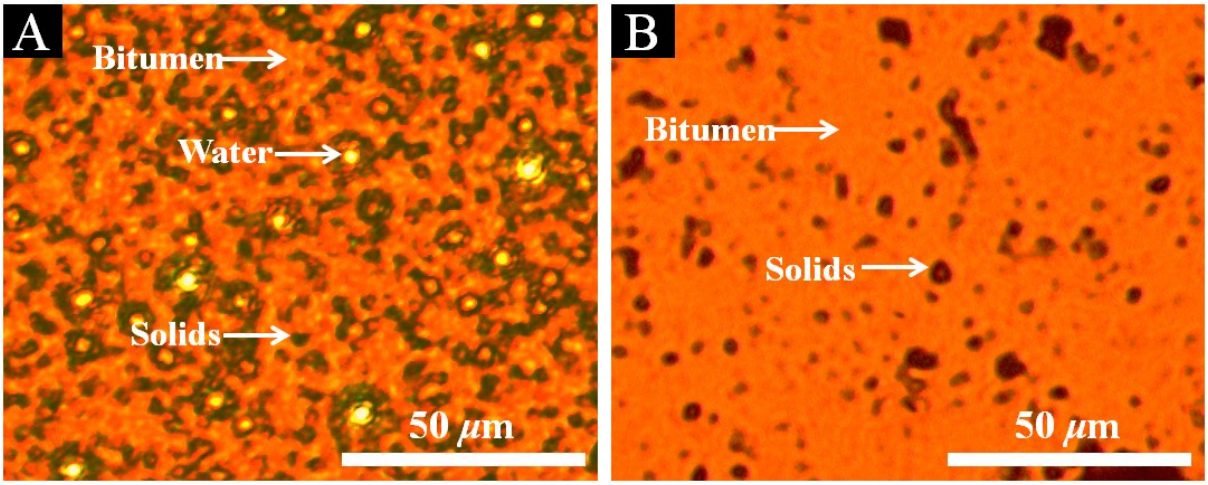

Figure 6.4 Microphotographs of (A) bitumen froth sample and (B) typical TBM. The hydrothermal treatment for the TBM in (B) was carried out at 390°C for 30 min.

6.3.2 Effect of Treatment Temperature on Filterability of Fine Solids

The room-temperature filtration behavior is illustrated in Figure 6.5. Untreated bitumen froth, i.e., original bitumen froth sample without going through hydrothermal treatment, shown in the figure as a data point at 25°C, plugged the filter membrane quickly and could not be filtered. This is shown as the data point with a filtration time of infinity at 25°C. After the hydrothermal treatment and venting, the toluene-diluted TBM became filterable. The filterability varied with different treatment temperatures. As water had been removed nearly completely, the variation in the filtration times was likely caused by an alteration of the fine solids properties. 30 min hydrothermal treatment between 300°C and 400°C followed by venting at 270°C benefited the filtration, with filtration time being lowered from infinity to 150−350 s. Hydrothermal treatment at 390°C followed by venting at 270°C gave the best filtration performance. At temperatures greater than 400°C, the filtration time increased rapidly, reaching 25 min at the treatment temperature of 420°C. This result was most likely due to the aggregation of asphaltene and the formation of fine coke particles [5, 28] that significantly slowed down the filtration. The high organic content of 420°C treated sample both on the surface (Table 5.2 and Figure 5.9) and in the bulk (31 wt%) supported the above argument.

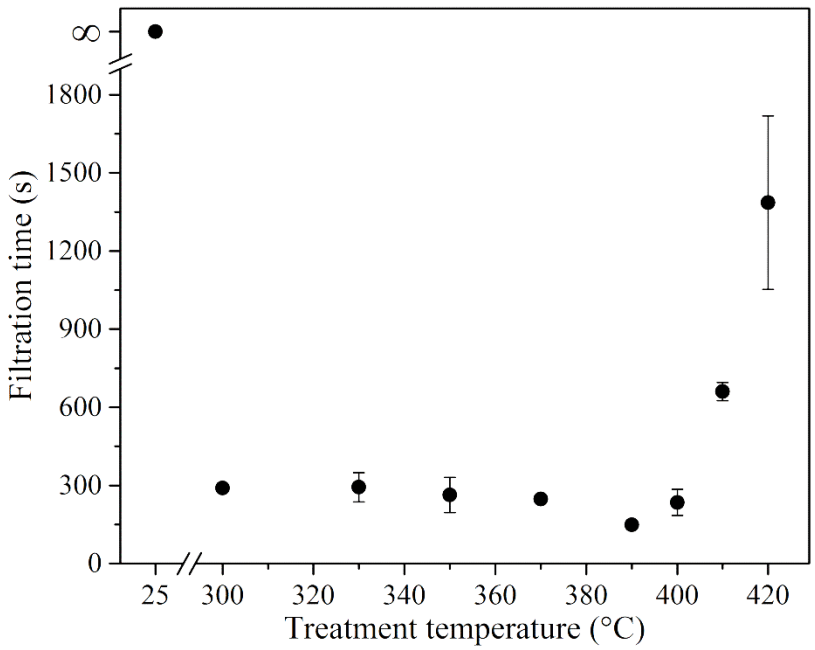

Figure 6.5 Effect of treatment temperature on the room-temperature filtration behavior (hydrothermal treatment time 30 min).

Hot filtration tests were subsequently performed based on the room-temperature filtration results. First, the repeatability of the hot filtration method was tested. The cumulative volume of filtrate was plotted versus filtration time in Figure 6.6. As can be seen, the results were repeatable. In Figure 6.7, the SRF of the hot filtration tests is plotted against the treatment temperature. The general trend of the curve is similar to that of room-temperature filtration shown in Figure 6.5. A very small amount of liquid was condensed in the experiment with dried bitumen froth sample (treated at 200°C for 30 min but not hydrothermally treated at higher temperatures). During filtration, the filter was plugged quickly and the SRF was shown as infinite. The TBM after the 30 min hydrothermal treatment at 300−390°C followed by venting at 270°C rendered the bitumen froth filterable. The higher the hydrothermal treatment temperature, the lower the SRF in the range of 300−390°C. However, when the hydrothermal treatment was carried out at

420°C, the initial hot filtration rate became slower, and eventually the filter was completely plugged. The SRF was also assigned a value of infinity. Hydrothermal treatment at 390°C for 30 min provided the lowest SRF (6.8×10^{12} m/kg). After hydrothermal treatment and hot filtration, the solids content was reduced from 8 wt% in the untreated bitumen froth to 0.08 wt% in the filtrate.

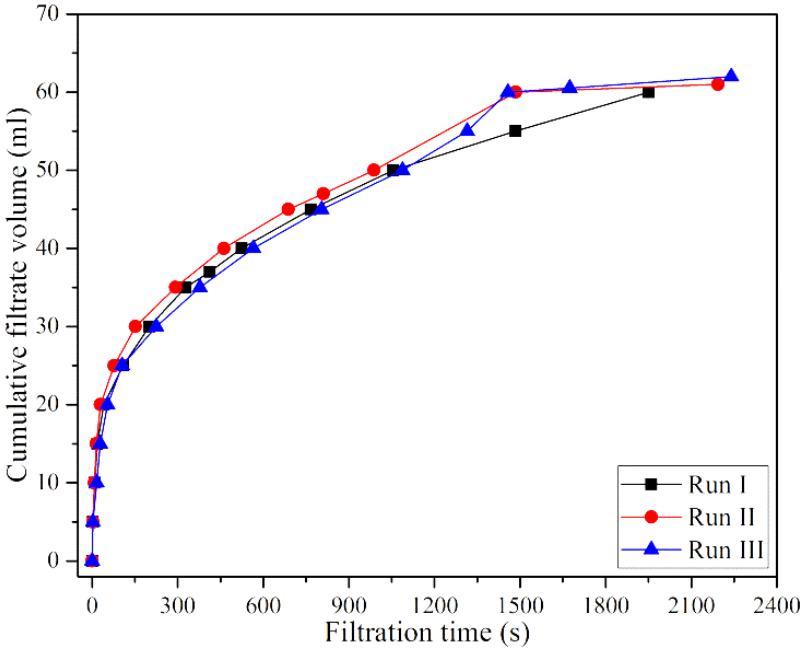

Figure 6.6 Repeatability of hot filtration method showing results from three repeat hot filtration tests (hydrothermal treatment at 390°C for 30 min).

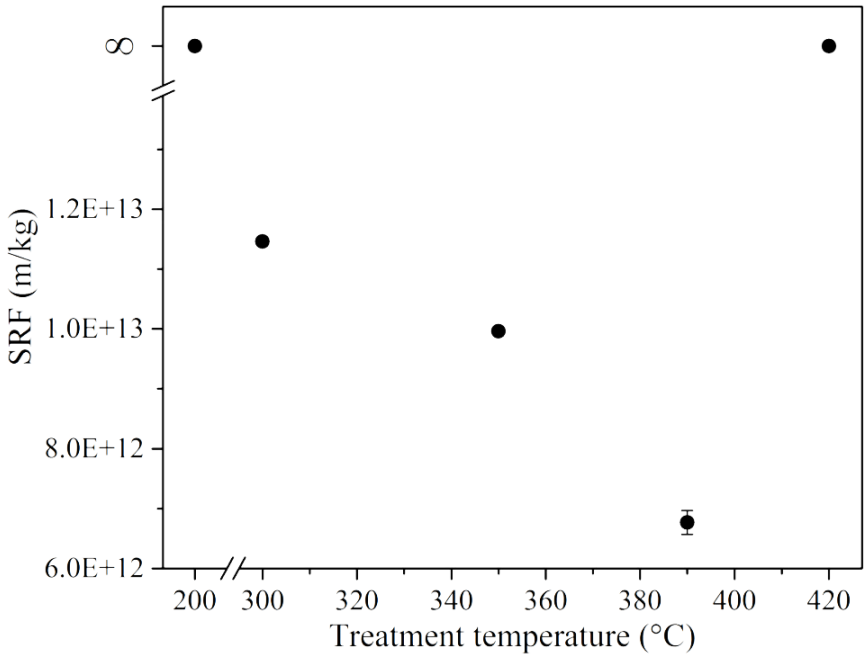

Figure 6.7 Effect of treatment temperature on the hot filtration behavior (hydrothermal treatment time 30 min). The error bar at 390°C indicates the standard deviation from three repeat tests.

6.3.3 Effect of Treatment Time on Filterability of Fine Solids

Figure 6.8 shows the effect of hydrothermal treatment time on the room-temperature filtration behavior. All the TBM samples contained negligible amount of water; therefore, the differences in the filtration performance were attributed to changes in the properties of fine solids. The data of Figure 6.8 show that the filtration time of toluene-diluted TBM from hydrothermal treatment at 390°C for 10, 30 and 60 min was between 150 and 300 s. The filtration time was longer at 550 s for toluene-diluted TBM from treatment at 390°C without any holding time (treatment time was 0 min), but still considerably shorter than the original bitumen froth that was directly diluted by toluene and filtered (which had a filtration time of infinity). Extending the treatment time to 180 min caused the filtration time to increase to about 2,700 s (45 min). From a cost perspective, lower treatment severity was more desirable as long as it could improve the filtration behavior.

Consequently, hot filtration tests were conducted at treatment times of 10 and 30 min based on the room-temperature filtration results. The hot TBM could be directly filtered by the hot filtration procedure, and the SRF at a treatment time of 30 min (6.8×10^{12} m/kg) was slightly lower than the 10 min treatment (7.5×10^{12} m/kg).

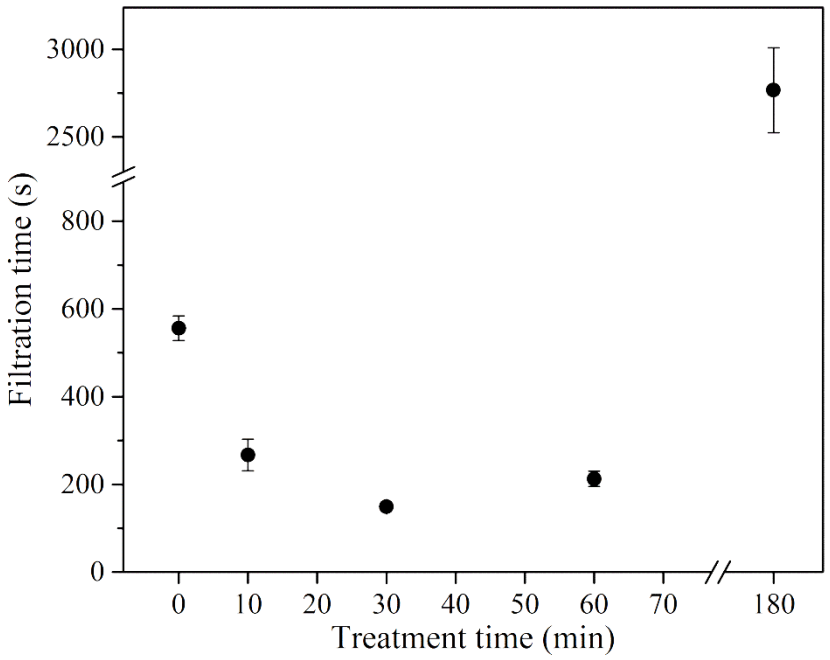

Figure 6.8 Effect of hydrothermal treatment time on the room-temperature filtration behavior (hydrothermal treatment temperature 390°C).

The laboratory filtration results suggested that hydrothermal treatment within specific range of severity (i.e. 300−400°C for 30 min or 390°C for 10−60 min) improved the filterability of the bitumen froth and thereby facilitated solids removal by filtration. Higher treatment severity (i.e. 420°C for 30 min or 390°C for 180 min) made the filterability worse again. Based on the laboratory tests, a hydrothermal treatment at 390°C for 30 min followed by venting at 270°C was found to be the optimum condition in improving filterability. The possible reasons for this

observation were analyzed by comparing the properties and stacking behavior of fine solids before and after the hydrothermal treatment, which are discussed in the following sections.

6.3.4 Characterization of Fine Solids

6.3.4.1 Mineralogy

The quantitative XRD analysis of the fine solids samples are presented in Table 6.1. Kaolinite and illite were found to be the predominant clay minerals in both untreated fine solids (filtered solids from original bitumen froth sample) and treated fine solids (filtered solids from TBM). After hydrothermal treatment (treatment at 390°C for 30 min, same for all of the following characterization work), no mineralogical changes to the clays were detected by quantitative XRD. However, a significant amount of pyrite was transformed to pyrrhotite after the hydrothermal treatment, likely due to the reaction of sulfur from pyrite with cracked hydrogen from bitumen to form hydrogen sulfide. Siderite was converted to pyrrhotite, maghemite and magnetite as shown in Table 6.1.

Table 6.1 Mineralogy of fine solids before and after hydrothermal treatment determined by quantitative XRD analysis.

Mineral	Untreated fine solids (wt%)[a]	Treated fine solids (wt%)[b]
Non-clay minerals		
Quartz	35	20
Siderite	8	1
Pyrite	7	1
Maghemite	5	9
Rutile	4	3
Anatase	1	1
Hematite	1	0
Magnetite	0	5
Pyrrhotite	0	13
Sub-total	60	52
Clay minerals		
Kaolinite	20	20
Illite	20	28
Sub-total	40	48
Total	100	100

[a] Filtered solids from original bitumen froth sample.

[b] Filtered solids from TBM obtained by hydrothermal treatment at 390°C for 30 min.

6.3.4.2 Particle Size

Figure 6.9 shows the chord length distributions of untreated and hydrothermally treated fine solids. Approximately 85% of the particles had chord length less than 10 µm for both samples. The mean chord length for untreated fine solids was 7.7 µm, while it was 6.9 µm for treated fine solids, which is not a significant change but does show that the untreated fine solids are slightly coarser. The particle size of the fine solids was not the reason for the filtration improvement. However, it should be noted that the FBRM particle size analyzer used in this study could not detect particles that are less than about 1 µm.

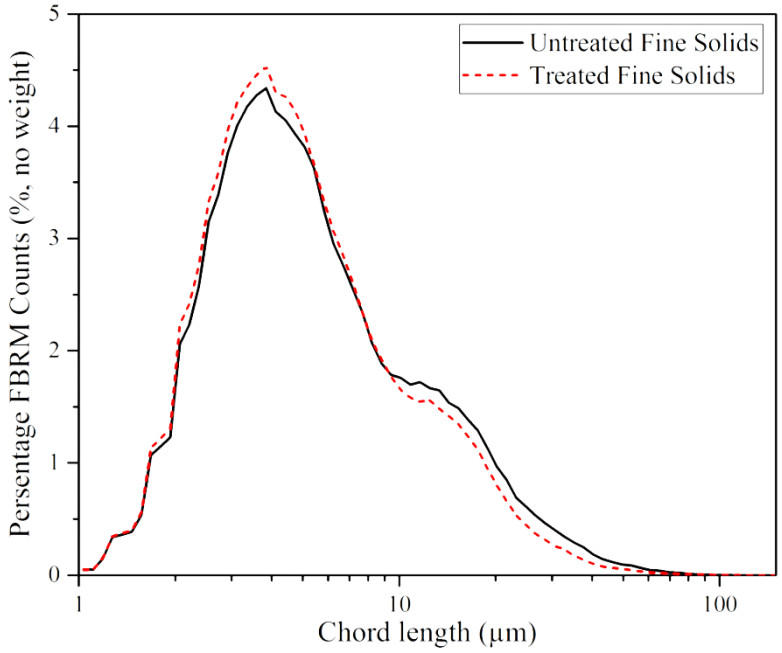

Figure 6.9 Chord length distributions for fine solids before and after hydrothermal treatment.

6.3.4.3 Wettability

After hydrothermal treatment at 390°C for 30 min, the contact angle of the fine solids increased from 57±3° to 83±2°. This result indicates that the fine solids became more hydrophobic after the

hydrothermal treatment, likely due to the accumulation of organic materials on the surface of the fine solids which modified their wettability (Chapter 5). The increase in hydrophobicity of the treated fine solids is consistent with the observations by Zhao et al. [10], where a mixture of fine solids, water and Athabasca bitumen was hydrothermally treated at 392°C for 30 min.

6.3.4.4 Morphology

Figure 6.10 shows the SEM images of fine solids before and after hydrothermal treatment. Both images show platy crystals of clay minerals. The surfaces of clay platelets before hydrothermal treatment were clean and smooth (Figure 6.10A). After hydrothermal treatment, a significant number of ultrafine particles (100−300 nm) were found to be attached on the surfaces of clay platelets, making them rough and uneven (Figure 6.10B). The observed differences in morphology were common in the two examined samples and Figures 6.10A and 6.10B show typical fields of view.

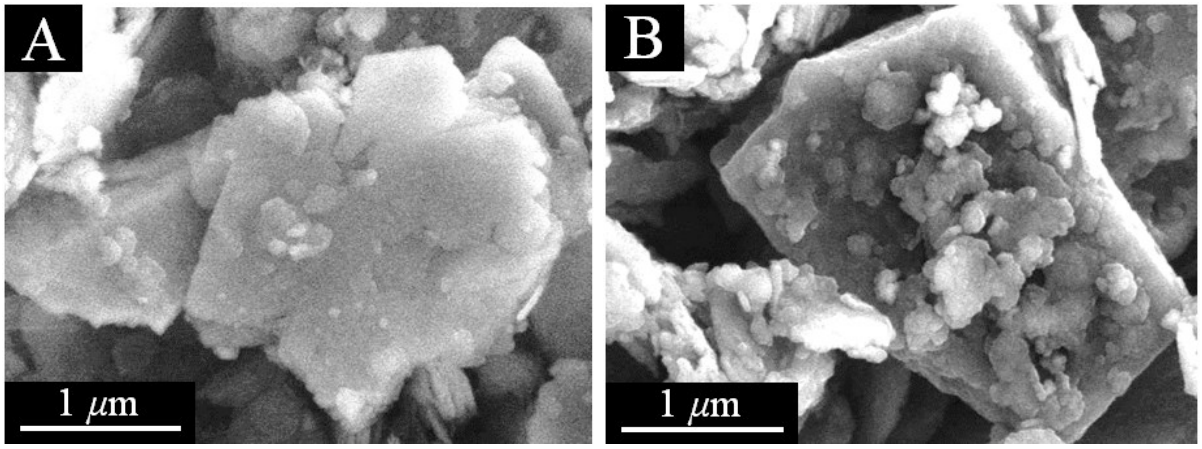

Figure 6.10 Typical SEM images of fine solids (A) before and (B) after hydrothermal treatment.

The residual solids in the filtrate of hot filtration were smaller than 0.5 μm, having passed a filter of this pore size. These residual solids, which would be expected to contain ultrafine particles as

illustrated in Figure 6.10B, were obtained by re-filtering the filtrate using a finer Millipore filter membrane. The SEM micrograph of Figure 6.11 shows these fine solids on the filter membrane. The EDX spectrum (a) at location "a" in the SEM micrograph of Figure 6.11 was dominated by the three elements in the filter membrane (carbon, fluorine and oxygen), which confirmed the area (a) was the filter membrane. In contrast, silicon, iron, and aluminum were present in area (b), which was consistent with the presence of clays and iron minerals. This result confirms that the ultrafine particles in Figure 6.10B are mineral solids, or at least include some mineral components, which is consistent with the conclusion from the AFM work as presented in Chapter 4.

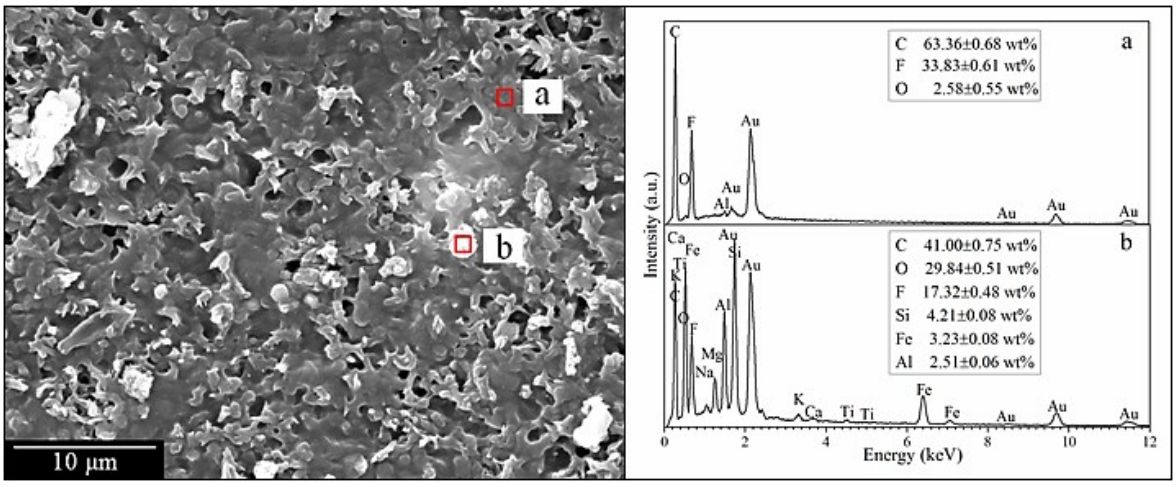

Figure 6.11 SEM image (left) of cake solids on filter membrane and the EDX spectra (right) of filter membrane (location "a" and spectrum a) and fine solids (location "b" and spectrum b). The areas for EDX analysis are indicated by square boxes. The main elements and their concentrations analyzed by EDX are listed with the spectra.

To compare the mineral types between the ultrafine particles and the whole fraction of treated fine solids from TBM, the ratios of Fe/Si and Fe/Al were measured by EDX for the whole fine

solids and the less than 0.5 μm fraction (ultrafine solids in Figure 6.11) of treated fine solids, respectively. These ratios are insensitive to any interference from the filter membrane or coating material as no Fe, Si, and Al exist in the filter membrane or coating material. As shown in Table 6.2, there was no significant difference with the ratios of Fe/Si and Fe/Al between the two samples, which confirms the mineral origin of the ultrafine particles in Figure 6.10B.

Table 6.2 Ratios of Fe/Si and Fe/Al for treated fine solids determined by EDX.

Ratio	whole fine solids	< 0.5 μm fraction
Fe/Si, wt%/wt%	1.13	1.07
Fe/Al, wt%/wt%	1.32	1.48

6.3.4.5 Particle Stacking Behavior

The image of Figure 6.12 shows the SEM micrographs of particles at the filter cake-filter medium interface. The morphology of the platy clays was consistent with the results in Figure 6.10 (clean and smooth before hydrothermal treatment, rough and uneven afterwards). The particle stacking before hydrothermal treatment was preferentially oriented (Figure 6.12A). The platy clays stacked on each other tightly and left almost no inter-particle voids, which caused low permeability. This particle stacking behavior is preferable because it is more energetically stable [29]. However, after hydrothermal treatment, the clays exhibited a randomly-oriented stacking behavior (Figure 6.12B). The attachment of ultrafine particles on the surface of clay platelets created physical barriers for tight stacking. In fact, the image in Figure 6.12B shows that the clays coated by the ultrafine particles no longer appear flaky. In this case, a more porous network resulted, which rendered the filter cake more permeable. After hydrothermal treatment, the

porosity of filter cake increased from 0.72±0.04 to 0.87±0.01 (mean ± standard deviation, estimated based on triplicate experiments), which supported the above conclusion.

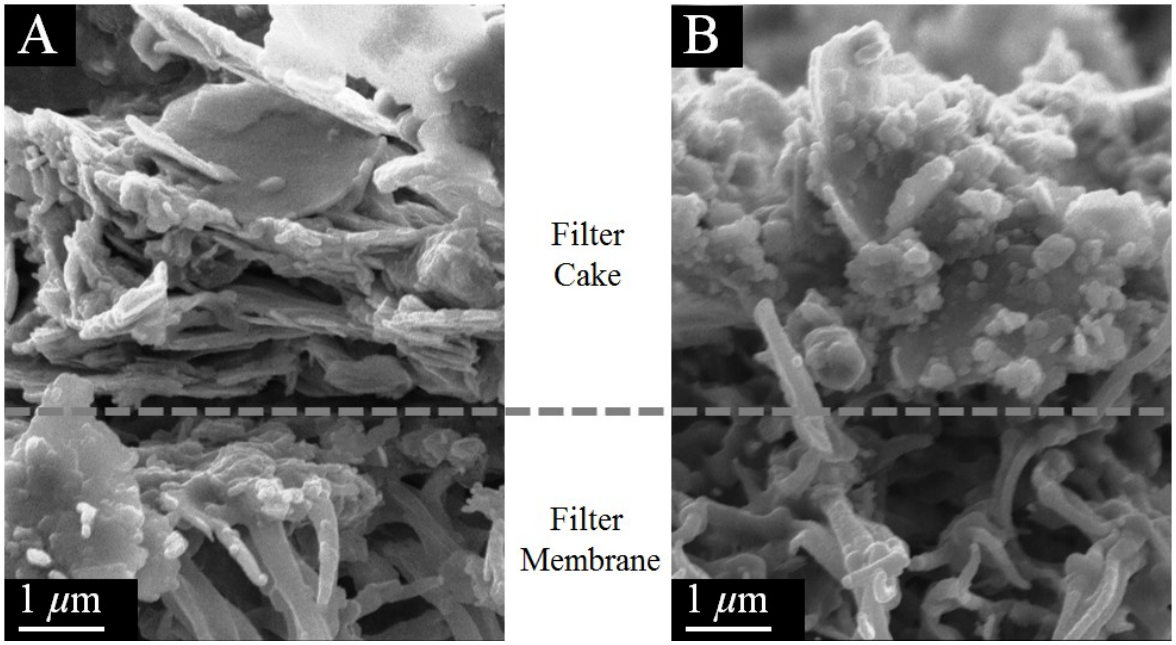

Figure 6.12 SEM images of filter cake-filter medium interface showing (A) before and (B) after hydrothermal treatment.

6.3.4.6 Associated Organics

The fine solids in bitumen froth are usually associated with significant amounts of organic matter, as discussed in literature review chapter (Section 2.1.2). These organic materials on the mineral particles dominate their behavior during processing [30, 31]. Hence, the analysis of associated organics in fine solids is important for understanding the filtration behavior. The total organic carbon content and surface elemental composition for selected elements are presented in Table 6.3. The surface elemental compositions were determined by X-ray photoelectron spectroscopy (XPS), which probes the top 2−7 nm depth of the particle surface layer. As shown in Table 6.3, the total organic carbon content of fine solids decreased from 14.7 wt% to 10.3

wt% after hydrothermal treatment; however, the surface concentration of carbon increased from 35.6 atom% to 47.7 atom%. This result implied that hydrothermal treatment reduced the total organics content of fine solids, but increased the extent of the mineral surface covered by organic material.

Table 6.3 Total organic carbon content and surface elemental composition of untreated and treated fine solids.

Sample	Total organic carbon[a] (wt%)	Surface elemental composition[b] (atom%)			
		C	O	Si	Al
Untreated fine solids	14.7±0.1	35.6	44.8	12.2	7.4
Treated fine solids	10.3±0.2	47.7	37	9.9	5.4

[a] Error estimates are standard deviations from triplicate measurements.

[b] Determined by XPS.

The presence of organic coating on bitumen-derived fine solids has been observed previously [31-33]. The signals of inorganic elements (see Si and Al in Table 6.3) were detected by XPS in both untreated and hydrothermally treated fine solids. This result was consistent with the general conclusion in prior studies [31, 34] that the organic coating on mineral surface was patchy rather than continuous. This feature rendered the fine solids in bitumen froth bi-wettable (Chapter 5). Hydrothermal treatment increased the coverage of organic matter on mineral surface. However, the surface was still not fully covered by organics even after hydrothermal treatment at 390°C for 30 min.

As mentioned in the literature review chapter (Section 2.1), Bensebaa et al. [35] found significant amount of organic matter within the bulk of oil sands fine solids by step-scan photoacoustic Fourier-transform infrared spectroscopy, and they attributed it to fine solids containing colloidal organic particles trapped inside solid particle aggregates. This suggestion provides an insight to the reduction of total organics in fine solids after hydrothermal treatment. Some organics were initially trapped inside the fine solids particle aggregates, and the adhesive effects of the trapped organics reinforce the stability of the ultrafine particles aggregates. Hydrothermal treatment altered the mineral surfaces and disrupted the aggregates, resulting in the release of the trapped organics and ultrafine particles. The release of trapped organics lowers the bulk organic contents, which is not fully compensated by the increased adsorption of the organic material on the fine solids surface. Therefore, as a whole, there is a drop in the bulk organics content but an increase in the organics on the fine solids surfaces. The release of the ultrafine particles from the aggregates accounts for the origin of the ultrafine particles in Figure 6.10B.

6.3.5 Conceptual Model

Based on the results obtained, a conceptual model for the fine solids in bitumen froth is depicted in Figure 6.13. In this model, two kinds of organics were proposed to be present in the fine solids: organic surface coating and trapped organics in the bulk aggregates. Neither of these materials are washed off by toluene. The surface organic coverage on clay particles was increased after hydrothermal treatment (Table 6.3 and Chapter 5). The release of trapped organics from the original aggregates during hydrothermal treatment also causes the release of ultrafine particles (<1 μm) which were not significant in the SEM images of the solids before hydrothermal treatment. A significant portion of these released ultrafine particles are

subsequently attached to the larger platy clay particles and this attachment disrupts the preferential oriented stacking of clays (Figure 6.12), which significantly improves the filterability of the solids. Most of the released ultrafine particles attached to the clay platelets rather than dispersing in the liquid phase, otherwise much slower filtration through the 0.22 μm pores of the filter membrane would be expected. The trapped organics in the aggregates of fine solids lowers the bitumen recovery. The removal of the trapped organics by hydrothermal treatment will potentially increase the recovery of hydrocarbons.

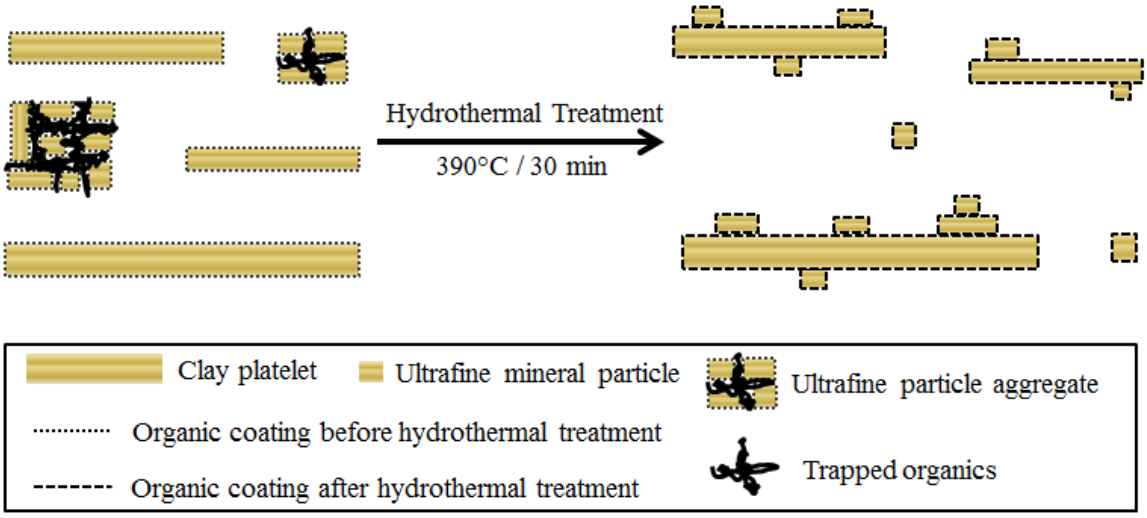

Figure 6.13 Simplified conceptual model of the fine solids in bitumen froth before and after hydrothermal treatment.

6.4 Conclusions

Fine solids removal from bitumen froth by hydrothermal treatment followed by filtration was investigated in this study. Venting at 270°C can produce an almost water-free product. The solids filterability improved significantly after hydrothermal treatment and venting, and treatment at 390°C for 30 min showed the best filtration performance in laboratory tests. The

clay mineralogy and particle size did not change noticeably, so they are not the contributors to filterability improvement. After hydrothermal treatment, the total amount of organics measured by bulk elemental analysis in the fine solids was found to be reduced, but the concentration of organics on the solids surface was found to have increased, which increased the hydrophobicity of the fine solids. The trapped organics in the oil-mineral aggregates likely act as "glue" to hold ultrafine particles together, and hydrothermal treatment may release these ultrafine particles by re-structuring the aggregates. A significant portion of these released ultrafine particles were observed attached to the larger platy particles, and this attachment disrupted the preferential oriented stacking of clays, which significantly improves the filterability of the fine solids. A combination of hydrothermal treatment and hot filtration is a viable method to remove fine solids from bitumen froth.

References

[1] S. Gao, K. Moran, Z. Xu, J. Masliyah, Role of bitumen components in stabilizing water-in-diluted oil emulsions, Energy & Fuels 23 (2009) 2606-2612.

[2] X. Wu, Investigating the stability mechanism of water-in-diluted bitumen emulsions through isolation and characterization of the stabilizing materials at the interface, Energy & Fuels 17 (2003) 179-190.

[3] N. Yan, M.R. Gray, J.H. Masliyah, On water-in-oil emulsions stabilized by fine solids, Colloids and Surfaces A: Physicochemical and Engineering Aspects 193 (2001) 97-107.

[4] F. Rao, Q. Liu, Froth treatment in Athabasca oil sands bitumen recovery process: A review, Energy & Fuels 27 (2013) 7199-7207.

[5] M.R. Gray, Upgrading oilsands bitumen and heavy oil, The University of Alberta Press, Edmonton, Alberta, 2015.

[6] U. Romanova, M. Valinasab, E. Stasiuk, H. Yarranton, The effect of oil sands bitumen extraction conditions on froth treatment performance, Journal of Canadian Petroleum Technology 45 (2006) 36-45.

[7] Y. Long, T. Dabros, H. Hamza, Stability and settling characteristics of solvent-diluted bitumen emulsions, Fuel 81 (2002) 1945-1952.

[8] G. Gu, L. Zhang, Z. Xu, J. Masliyah, Novel bitumen froth cleaning device and rag layer characterization, Energy & Fuels 21 (2007) 3462-3468.

[9] J. Masliyah, Z.J. Zhou, Z. Xu, J. Czarnecki, H. Hamza, Understanding water-based bitumen extraction from Athabasca oil sands, The Canadian Journal of Chemical Engineering 82 (2004) 628-654.

[10] J. Zhao, Q. Liu, M.R. Gray, Characterization of fine solids in Athabasca bitumen froth before and after hydrothermal treatment, Energy & Fuels 30 (2016) 1965-1971.

[11] Y. Xu, T. Dabros, J. Kan, Filterability of oil sands tailings, Process Safety and Environmental Protection 86 (2008) 268-276.

[12] T. Yoshida, C. Li, T. Takanohashi, A. Matsumura, S. Sato, I. Saito, Effect of extraction condition on "HyperCoal" production (2)−Effect of polar solvents under hot filtration, Fuel Processing Technology 86 (2004) 61-72.

[13] W. Peukert, High temperature filtration in the process industry, Filtration & Separation 35 (1998) 461-464.

[14] M. Mänttäri, A. Pihlajamäki, E. Kaipainen, M. Nyström, Effect of temperature and membrane pre-treatment by pressure on the filtration properties of nanofiltration membranes, Desalination 145 (2002) 81-86.

[15] D. Stanghelle, T. Slungaard, O.K. Sønju, Granular bed filtration of high temperature biomass gasification gas, Journal of Hazardous Materials 144 (2007) 668-672.

[16] S. Heidenreich, B. Scheibner, Hot gas filtration with ceramic filters: Experiences and new developments, Filtration & Separation 39 (2002) 22-25.

[17] B. Latella, L. Henkel, E. Mehrtens, Permeability and high temperature strength of porous mullite-alumina ceramics for hot gas filtration, Journal of Materials Science 41 (2006) 423-430.

[18] C. Lin, J. Miller, Pore structure and network analysis of filter cake, Chemical Engineering Journal 80 (2000) 221-231.

[19] C. Tien, S. Teoh, R. Tan, Cake filtration analysis−the effect of the relationship between the pore liquid pressure and the cake compressive stress, Chemical Engineering Science 56 (2001) 5361-5369.

[20] X. Cao, M. Jahazi, Examination and verification of the filtration mechanism of cake mode during the pressure filtration tests of liquid Al–Si cast alloys, Materials Science and Engineering: A 408 (2005) 234-242.

[21] F.M. Tiller, Tutorial: Interpretation of filtration data, I, Fluid/Particle Separation Journal 3 (1990) 85.

[22] R. Baskerville, J. Komorek, R. Gale, Effect of operating variables on filter press performance, Water Pollution Control 70 (1971) 400.

[23] R. Gale, R. Baskerville, Studies on the vacuum filtration of sewage sludges, Water Pollution Control 69 (1970) 574.

[24] G. Guglielmi, D. Chiarani, D.P. Saroj, G. Andreottola, Sludge filterability and dewaterability in a membrane bioreactor for municipal wastewater treatment, Desalination 250 (2010) 660-665.

[25] ASTM D 4807-05: Standard test method for sediment in crude oil by membrane filtration, Annual Book of ASTM Standards, Washington, DC, 2005.

[26] J. Środoń, V.A. Drits, D.K. McCarty, J.C. Hsieh, D.D. Eberl, Quantitative X-ray diffraction analysis of clay-bearing rocks from random preparations, Clays and Clay Minerals 49 (2001) 514-528.

[27] A. Metson, L. Blakemore, D. Rhoades, Methods for the determination of soil organic carbon: A review, and application to New Zealand soils, New Zealand Journal of Science 22 (1979) 205-228.

[28] I.A. Wiehe, A phase-separation kinetic model for coke formation, Industrial & Engineering Chemistry Research 32 (1993) 2447-2454.

[29] M. Mackley, N. Sherman, Cake filtration mechanisms in steady and unsteady flows, Journal of Membrane Science 77 (1993) 113-121.

[30] B. Sparks, L. Kotlyar, J. O'Carroll, K. Chung, Athabasca oil sands: Effect of organic coated solids on bitumen recovery and quality, Journal of Petroleum Science and Engineering 39 (2003) 417-430.

[31] F. Bensebaa, L.S. Kotlyar, B.D. Sparks, K.H. Chung, Organic coated solids in Athabasca bitumen: Characterization and process implications, Canadian Journal of Chemical Engineering 78 (2000) 610-616.

[32] L. Kotlyar, Y. Deslandes, B. Sparks, H. Hodama, R. Schutte, Characterization of colloidal solids from Athabasca fine tails, Clays and Clay Minerals 41 (1993) 341-345.

[33] S. Ren, T. Dang-Vu, H. Zhao, J. Long, Z. Xu, J. Masliyah, Effect of weathering on surface characteristics of solids and bitumen from oil sands, Energy & Fuels 23 (2008) 334-341.

[34] S. Wang, Q. Liu, X. Tan, C. Xu, M.R. Gray, Study of asphaltene adsorption on kaolinite by X-ray photoelectron spectroscopy and time-of-flight secondary ion mass spectroscopy, Energy & Fuels 27 (2013) 2465-2473.

[35] F. Bensebaa, A. Majid, Y. Deslandes, Step-scan photoacoustic Fourier transform and X-rays photoelectron spectroscopy of oil sands fine tailings: New structural insights, Spectrochimica Acta Part A: Molecular and Biomolecular Spectroscopy 57 (2001) 2695-2702.

7 Synthesis and Conclusions

7.1 Synthesis

Understanding how bitumen components associate with clay minerals and how to control or change such oil-mineral association are of vital importance in oil sands processing. This thesis work focuses on two aspects: (1) characterizing the organically-modified clay minerals extracted from bitumen froth and (2) examining the effect of hydrothermal treatment on the structures and behaviors of the mineral particles.

The asphaltene-kaolinite model system confirmed the irreversibility of adsorption of components from bitumen onto clay surfaces, i.e., circa 80% of asphaltenes remained adsorbed even after repeated toluene washing (Chapter 3). The highly irreversible adsorption characteristics indicated the high binding strength at the oil-mineral or solvent-mineral interfaces (Chapters 2 and 3) and was consistent with the presence of "toluene-unextractable-organic-matter" in oil sands fine solids (Chapters 4, 5, and 6). Here, the "toluene unextractable" organic material is defined as not removable by toluene but not necessarily insoluble by toluene, as discussed in Chapter 2. The observations in Chapter 3 convey the fundamental problems in the work of Kotlyar et al. [1-3], where all toluene-unextractable-organic-matter is defined as "humic matter" (a solubility fraction), which mis-classifies the toluene-soluble asphaltenes that irreversibly adsorb onto clay surfaces.

Both the adsorbed asphaltenes on kaolinite and the adsorbed organic matter on the fine solids in bitumen froth exhibited patchy discontinuous surface coverage. The XPS-determined surface coverage by adsorbed asphaltenes on kaolinite minerals was 17±1% (Chapter 3), while the AFM-determined surface organic coverage on basal faces of clay minerals in bitumen froth was 17±6%

(Chapter 4). As can be seen, the two values coincide nicely with each other. The random distribution of nano-scale organic and inorganic domains on the particle surfaces rendered them bi-wet and consequently enabled them to stabilize water-oil emulsions, as evidenced in Chapters 3, 4, and 5 and discussed in detail in Chapter 5. The cryo-SEM images in Chapter 5 (i.e. Figure 5.5) provided strong proof for the coating mechanism of particle-stabilized emulsions (or so-called Pickering emulsions), by clearly showing how the micron/submicron sized fine particles coated on the surface of an emulsified water droplet and thus stabilized it.

Unlike the natural kaolinite mineral that was coated by adsorbed asphaltenes, the oil sands fine solids contained organic matter trapped in the solids aggregates, in addition to the patchy organic coating on the solid surface. These trapped organics cemented the mineral solids together and strengthened the oil-mineral aggregates. Such aggregation structure in oil sands fine solids (which is analogous to soil solids [4, 5]) was rarely reported [6, 7], although the presence of an organic coating has been well recognized (Chapter 2). The QNM-AFM work in this study (Chapter 4) provided strong evidence for the presence of these trapped organics, based on the observation that the organic particles showed extremely high adhesion forces (Figures 4.5C and 4.5F). Such structure was also supported by the observed reduction in organic carbon content after hydrothermal treatment (Chapter 6), which was attributed to the disintegration of the oil-mineral aggregates, a process that released these trapped organics.

Dehydroxylation of kaolinite, which happened when the treatment temperature was higher than 400°C, enhanced its adsorption capacity for asphaltenes (Chapter 3). Such dehydroxylation reactions were insignificant during the hydrothermal treatment at 300−410°C (Figure 5.8), suggesting that the mineral dehydroxylation was not the main contributor for the increased surface organic coverage after hydrothermal treatment as observed in Chapters 5 and 6. Instead,

the increase in surface organic coating was hypothesized to be caused by the disintegration of oil-mineral aggregates into ultrafine-particle-coated platy clays: this re-structuring provided more complex morphology (Figure 6.10) and thus enabled more patchy distribution of surface zones and offered more locations for organic attachment. At the same time, this re-structuring liberated the organic components that were originally trapped in the oil-mineral aggregates, potentially increasing the hydrocarbon recovery (Chapter 6).

These structural changes would affect the particle behaviors. In this study, the emulsification and filtration behaviors were specifically investigated due to their importance in oil sands processing. Both the thermal treatment of kaolinite followed by asphaltene adsorption (Chapter 3) and hydrothermal treatment of bitumen froth (Chapters 5 and 6) enabled the manipulation of the extent of organic coating on mineral solids by controlling the treatment temperature. The varying degrees of surface organic coverage resulted in varying hydrophobicity of particles and consequently the different behaviors in emulsion stabilization (Chapters 3 and 5). In particular, hydrothermal treatment of bitumen froth at different temperatures changed the relative quantities of particles in each hydrophobicity class (from the least hydrophobic to the most hydrophobic), thereby enabling a study of the influence of hydrophobicity distribution of particle mixtures on emulsion stabilization, which has not been studied before. Interestingly, the emulsifying capacity of the heterogeneous fine particle mixtures, as indicated by the volume of the produced toluene-water emulsions, was found to be not related to an "average" hydrophobicity (i.e., the mean critical surface tension determined from the film flotation measurements); instead, the emulsifying capacity depended on the proportion of a specific sub-fraction of particles with a critical surface tension of 27–30 mN/m, i.e., particles with intermediate hydrophobicity. Furthermore, in the case of homogeneous high purity kaolinite sample (Chapter 3), the

asphaltene-coated kaolinite particles with critical surface tension of 27–30 mN/m had the strongest emulsifying capacity (Table 3.4), consistent with the conclusion from native clay minerals extracted from bitumen froth (Chapter 5).

Besides the above change in emulsification behavior which is surface-sensitive, hydrothermal treatment also altered the filtration behavior of the bitumen froth fine solids. In Chapter 6, the filterability of the fine solids was significantly enhanced after hydrothermal treatment, as indicated in both room-temperature filtration following dilution by toluene and *in-situ* hot filtration (at ~200°C). This enhancement was explained by the structural changes: the platy clay particles at the filter cake-filter medium interface turned from preferential orientation to random orientation due to the attachment of numerous ultrafine particles on the clay basal surface (Figures 6.10 and 6.12), increasing the porosity of the filter cake and thus facilitating the filtration. However, such filterability enhancement was not observed when kaolinite was treated with asphaltenes that led to a patchy asphaltene coating on the kaolinite surface (Chapter 3). Therefore, surface wettability changes were not the reasons for the enhanced filtration behaviors.

In terms of process implications, the increased asphaltene adsorption on dehydroxylated clay (Chapter 3) provided a fundamental explanation for the easy deactivation of mineral catalyst when used for thermal processing of heavy oil with high asphaltene content. The inhomogeneous spatial distribution of organic patches on the surface of oil sands fine solids (Chapter 4) made them bi-wettable (the organic patches tend to be hydrophobic and the exposed mineral regions tend to be hydrophilic). This bi-wettability of oil sands fine solids significantly contributes to the rag layer (emulsion) formation in bitumen extraction. Hydrothermal treatment at relatively high severity (>400°C) reduced the emulsifying capacity of the fine solids as compared with treatment at 390°C (Chapter 5), suggesting that severe treatment of the fine solids and thus converting the

bi-wettable fraction of particles to totally hydrophobic can reduce emulsion formation. In light of bitumen froth cleaning by hydrothermal treatment (Chapter 6), this thesis work suggests that water should be removed completely from hydrothermally-treated bitumen froth to eliminate emulsion formation.

7.2 Main Conclusions

The main conclusions of this thesis work can be summarized as follows:

(1) Dehydroxylation of kaolinite enhanced its adsorption capacity for asphaltenes. When the highest adsorption density of asphaltenes was reached on the untreated (3 mg/m^2) and dehydroxylated (7 mg/m^2) kaolinite, the XPS-determined surface coverage by the asphaltenes was 18% and 41%, respectively, which proved that the asphaltene adsorption layer was patchy and discontinuous on both materials.

(2) After saturation of kaolinite binding sites with the first asphaltene layer, at most two additional layers were adsorbed due to asphaltene-on-asphaltene deposition, forming approximately 15-nm-thick asphaltene domains. Any further adsorption became reversible, i.e., it could be removed by toluene washing.

(3) Taking advantage of the simultaneous nano-scale resolution topographic imaging and adhesion force mapping enabled by quantitative nanomechanical mapping atomic force microscopy (QNM-AFM), several different components in the bitumen froth fine solids were identified, i.e., platy clays, organic coating, trapped organics, and submicron particles, due to their variations in shapes and mechanical properties.

(4) The patchy organic coating on the clay minerals was clearly visualized on the adhesion force maps due to its relatively higher values of adhesion than the clay mineral substrate. The percent surface coverage and average adsorbed layer thickness of this organic coating on the clay basal faces were 17±6% and 1.4 nm, respectively. In addition to this organic coating, there were organic materials trapped in the oil-mineral aggregates, which were separated by ultrasonication followed by centrifugation, and they were clearly identifiable by QNM-AFM. The trapped organics was found to be softer than the asphaltene fraction of oil sands bitumen.

(5) After hydrothermal treatment at 390°C for 30 min (~17 MPa), the surface carbon concentration of the bitumen froth fine solids increased from 36 to 47 atom%, but their total (bulk) organic carbon content was reduced from 15 to 10 wt%. This observation was explained by the disintegration of oil-mineral aggregates and the formation of ultrafine-particle-coated platy clays, which provided more complex morphology for surface organic attachment (increasing surface organic concentration) and also caused a release of trapped organics (reducing total organic content).

(6) The bitumen froth fine solids were mixtures of particles with varying degrees of hydrophobicity, with critical surface tension ranging from 26 to 56 mN/m and a mean critical surface tension of 39 mN/m. Hydrothermal treatment at 300–420°C progressively shifted the hydrophobicity distribution of the fine solids, resulting in a lower mean critical surface tension to 37–30 mN/m, respectively, and a narrower critical surface tension range.

(7) The emulsifying capacity of the fine particle mixtures had no discernable relationship to the mean critical surface tension, but depended linearly and monotonically on the percentage of

particles with a critical surface tension of 27–30 mN/m. This sub-fraction of particles, with intermediate hydrophobicity, dominated the emulsification behavior of the particle mixtures.

(8) No noticeable changes were observed to the clay mineralogy and fine solids particle size after hydrothermal treatment; however, the particle stacking behavior at the filter cake-filter medium interface was significantly changed. The platy clay particles turned from preferential orientation to random orientation after the hydrothermal treatment, increasing the porosity of the filter cake and thereby improving the filterability.

(9) A combination of hydrothermal treatment of bitumen froth at 390ºC, water removal by venting at 270ºC, and solids removal by *in-situ* hot filtration at 200ºC is a viable approach in cleaning the bitumen froth. Based on the laboratory-scale tests, the use of the above approach reduced the fine solids and water contents from 8 wt% and 14 wt% to 0.08 wt% and 0.03 wt%, respectively.

7.3 Original Contributions

This study contributes to the fundamental understanding of the organically-modified clay minerals in oil sands. Their emulsification and filtration behaviors were examined systematically, providing new insights into knowledge of particle-stabilized emulsions and bitumen froth cleaning. The original contributions of this thesis work can be summarized as follows:

(1) **Thermal dehydroxylation of kaolinite enhanced its adsorption capacity for asphaltenes (Chapter 3)**

The differences in asphaltene adsorption between untreated and dehydroxylated kaolinite were compared in terms of adsorption density, percent surface coverage, and mean adsorbate domain thickness. Kaolinite dehydroxylation enhanced its adsorption capacity for asphaltenes, likely because the strained structures of the dehydroxylated kaolinite provided additional active sites for asphaltene adsorption.

(2) **The first attempt of using QNM-AFM to study the organically-modified clay minerals in oil sands (Chapter 4)**

The study of the organic coating on the clay minerals has been elusive due to the nanometer length scale and the unsuitability of sampling in high vacuum sample chambers [8-10]. In the present work, QNM-AFM was applied for the first time to study the adsorption of bitumen-derived organic matter on fine mineral solids extracted from bitumen froth. By topographic imaging and adhesion mapping, direct visualization of the organic coating on the fine mineral solids was realized; the surface coverage and average domain thickness of this organic coating were quantitatively determined; differences in mechanical property between the organic components in oil sands fine solids and the asphaltene fraction of oil sands bitumen were compared for the first time.

(3) **The first investigation of the influence of hydrophobicity distribution of heterogeneous particle mixtures on emulsion stabilization (Chapter 5)**

The emulsification behavior of heterogeneous mixtures of particles with varying hydrophobicity is rarely examined; consequently, the influence of the distribution of particle hydrophobicity on oil-water emulsion stabilization is poorly understood [11-14]. In the present work, the wettability of fine solids in bitumen froth was quantitatively characterized using critical surface tension

obtained by the film flotation technique, and the influence of hydrophobicity distribution of heterogeneous particle mixtures on their emulsification behavior was investigated for the first time. A linear correlation between the emulsifying capacity of the fine particle mixtures and the percentage of a specific sub-fraction of particles (with critical surface tension of 27−30 mN/m) was established.

(4) **Development of a novel method for cleaning bitumen froth (Chapter 6)**

A novel method for cleaning bitumen froth was developed from this work, combining hydrothermal treatment, water venting, and hot filtration. This method effectively removed the contained fine solids and water in bitumen froth and eliminated the diluent addition and recovery processes in conventional froth treatment technologies.

7.4 Recommendations for Future Work

(1) The faces and edges, or even the tetrahedral siloxane faces and the octahedral aluminum faces, of clay minerals may behave differently towards organic adsorption. Based on the present work, QNM-AFM adhesion mapping can be a useful technique in probing these differences; however, precise control of the particle orientation for AFM measurements would be a great challenge. The spatial distribution of organic coating on clay basal faces (a combined contribution from both siloxane and aluminum faces) was revealed in this study, but the distribution on clay edges remained undefined. The platy clay particles preferentially orientated on the substrate with their basal faces nearly parallel to the substrate surface, without showing their edges to AFM tip for probing.

Xu and co-workers [15-17] did some work in this regard. They used a microtome or ultramicrotome cutting technique to prepare the clay edges [15, 18], and differentiated the anisotropic basal faces of clay minerals by depositing clay particles on substrates bearing different charges (for example, when depositing kaolinite particles on silica substrate at pH ~8 (negatively charged), kaolinite would expose their negatively charged siloxane basal faces while the positively charged aluminum basal faces should preferentially attach to the surface of silica substrate) [17, 19]. However, their studies were conducted under aqueous solutions and mainly focused on the surface charge properties of clay minerals. Future studies should focus on investigating the organic adsorption on the different clay surfaces (i.e., siloxane basal faces, aluminum basal faces, and edges) under non-aqueous conditions.

(2) Non-aqueous extraction of bitumen from oil sands has attracted increasing attention from both academia and industry. In such non-aqueous extraction processes, the removal of mineral particle contamination in the extracted bitumen is a significant challenge [7, 20, 21]. A technique which can effectively remove these detrimental fine mineral particles is needed. From this point of view, the effect of both hydrothermal treatment with controlled addition of water, and solvothermal treatment under anhydrous conditions, on the filtration behavior of non-aqueous extracted bitumen should be tested. Based on the results of the present work, a process design is suggested as illustrated in Figure 7.1. After bitumen exaction from oil sands ore using organic solvents (e.g. cyclohexane) followed by solvent recovery, thermal treatment of the extracted bitumen with residual solvents would give “solvothermal” conditions. The *in-situ* hot filtration may be applied to remove the fine solids and to verify whether such solvothermal treatment can improve the filterability or not. This process would be more attractive if it could simultaneously achieve bitumen cleaning and partial upgrading.

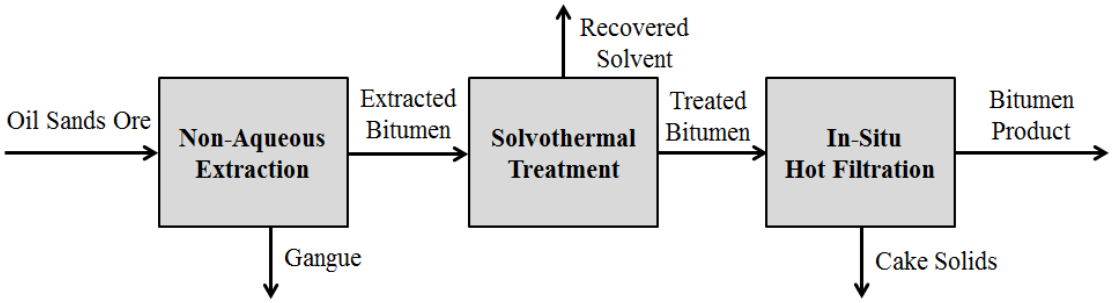

Figure 7.1 Proposed process for thermal cleaning of non-aqueous extracted bitumen via solvothermal treatment and *in-situ* hot filtration.

References

[1] L. Kotlyar, H. Kodama, B. Sparks, P. Grattan-Bellew, Non-crystalline inorganic matter-humic complexes in Athabasca oil sand and their relationship to bitumen recovery, Applied Clay Science 2 (1987) 253-271.

[2] L.S. Kotlyar, J.A. Ripmeester, B.D. Sparks, D.S. Montgomery, Characterization of oil sands solids closely associated with Athabasca bitumen, Fuel 67 (1988) 808-814.

[3] L.S. Kotlyar, J.A. Ripmeester, B.D. Sparks, D.S. Montgomery, Characterization of organic-rich solids fractions isolated from Athabasca oil sand using a cold water agitation test, Fuel 67 (1988) 221-226.

[4] J. Jastrow, Soil aggregate formation and the accrual of particulate and mineral-associated organic matter, Soil Biology and Biochemistry 28 (1996) 665-676.

[5] C.J. Bronick, R. Lal, Soil structure and management: A review, Geoderma 124 (2005) 3-22.

[6] F. Bensebaa, A. Majid, Y. Deslandes, Step-scan photoacoustic Fourier transform and X-rays photoelectron spectroscopy of oil sands fine tailings: New structural insights, Spectrochimica Acta Part A: Molecular and Biomolecular Spectroscopy 57 (2001) 2695-2702.

[7] M. Couillard, P.H. Mercier, Analytical electron microscopy of carbon-rich mineral aggregates in solvent-diluted bitumen products from mined Alberta oil sands, Energy & Fuels 30 (2016) 5513-5524.

[8] B. Sparks, L. Kotlyar, J. O'Carroll, K. Chung, Athabasca oil sands: Effect of organic coated solids on bitumen recovery and quality, Journal of Petroleum Science and Engineering 39 (2003) 417-430.

[9] F. Bensebaa, L.S. Kotlyar, B.D. Sparks, K.H. Chung, Organic coated solids in Athabasca bitumen: Characterization and process implications, Canadian Journal of Chemical Engineering 78 (2000) 610-616.

[10] A. Hooshiar, P. Uhlik, D.G. Ivey, Q. Liu, T.H. Etsell, Clay minerals in nonaqueous extraction of bitumen from Alberta oil sands: Part 2. Characterization of clay minerals, Fuel Processing Technology 96 (2012) 183-194.

[11] N. Yan, M.R. Gray, J.H. Masliyah, On water-in-oil emulsions stabilized by fine solids, Colloids and Surfaces A: Physicochemical and Engineering Aspects 193 (2001) 97-107.

[12] D.M. Sztukowski, H.W. Yarranton, Oilfield solids and water-in-oil emulsion stability, Journal of Colloid and Interface Science 285 (2005) 821-833.

[13] B. Binks, S. Lumsdon, Transitional phase inversion of solid-stabilized emulsions using particle mixtures, Langmuir 16 (2000) 3748-3756.

[14] Z.G. Cui, K.Z. Shi, Y.Z. Cui, B. Binks, Double phase inversion of emulsions stabilized by a mixture of $CaCO_3$ nanoparticles and sodium dodecyl sulphate, Colloids and Surfaces A: Physicochemical and Engineering Aspects 329 (2008) 67-74.

[15] L. Yan, A.H. Englert, J.H. Masliyah, Z. Xu, Determination of anisotropic surface characteristics of different phyllosilicates by direct force measurements, Langmuir 27 (2011) 12996-13007.

[16] L. Yan, J.H. Masliyah, Z. Xu, Understanding suspension rheology of anisotropically-charged platy minerals from direct interaction force measurement using AFM, Current Opinion in Colloid & Interface Science 18 (2013) 149-156.

[17] L. Alagha, L. Guo, M. Ghuzi, O. Molatlhegi, Z. Xu, Adsorption of hybrid polyacrylamides on anisotropic kaolinite surfaces: Effect of polymer characteristics and solution properties, Colloids and Surfaces A: Physicochemical and Engineering Aspects 498 (2016) 285-296.

[18] H. Zhao, S. Bhattacharjee, R. Chow, D. Wallace, J.H. Masliyah, Z. Xu, Probing surface charge potentials of clay basal planes and edges by direct force measurements, Langmuir 24 (2008) 12899-12910.

[19] L. Alagha, S. Wang, L. Yan, Z. Xu, J. Masliyah, Probing adsorption of polyacrylamide-based polymers on anisotropic basal planes of kaolinite using quartz crystal microbalance, Langmuir 29 (2013) 3989-3998.

[20] F. Lin, S.R. Stoyanov, Y. Xu, Recent advances in nonaqueous extraction of bitumen from mineable oil sands: A review, Organic Process Research & Development 21 (2017) 492-510.

[21] H. Nikakhtari, L. Vagi, P. Choi, Q. Liu, M.R. Gray, Solvent screening for non-aqueous extraction of Alberta oil sands, The Canadian Journal of Chemical Engineering 91 (2013) 1153-1160.

Bibliography

W.A. Abdallah, S.D. Taylor, Study of asphaltenes adsorption on metallic surface using XPS and TOF-SIMS, The Journal of physical chemistry C 112 (2008) 18963-18972.

A. Abudu, L. Goual, Adsorption of crude oil on surfaces using quartz crystal microbalance with dissipation (QCM-D) under flow conditions, Energy & Fuels 23 (2008) 1237-1248.

S. Acevedo, J. Castillo, A. Fernández, S. Goncalves, M.A. Ranaudo, A study of multilayer adsorption of asphaltenes on glass surfaces by photothermal surface deformation. Relation of this adsorption to aggregate formation in solution, Energy & Fuels 12 (1998) 386-390.

S. Acevedo, M.A. Ranaudo, C. García, J. Castillo, A. Fernández, Adsorption of asphaltenes at the toluene−silica interface: A kinetic study, Energy & Fuels 17 (2003) 257-261.

S. Acevedo, M.A. Ranaudo, C. García, J. Castillo, A. Fernández, M. Caetano, S. Goncalvez, Importance of asphaltene aggregation in solution in determining the adsorption of this sample on mineral surfaces, Colloids and Surfaces A: Physicochemical and Engineering Aspects 166 (2000) 145-152.

J.J. Adams, Asphaltene adsorption, a literature review, Energy & Fuels 28 (2014) 2831-2856.

A. Adegoroye, L. Wang, O. Omotoso, Z. Xu, J. Masliyah, Characterization of organic-coated solids isolated from different oil sands, The Canadian Journal of Chemical Engineering 88 (2010) 462-470.

Alberta Energy Regulator, 2017, Alberta energy regulator 2016/17 annual report, available at: https://www.aer.ca/documents/reports/AER2016-17AnnualReport.pdf, retrieved on 8 August 2017.

K. Akbarzadeh, A. Hammami, A. Kharrat, D. Zhang, S. Allenson, J. Creek, S. Kabir, A. Jamaluddin, A.G. Marshall, R.P. Rodgers, Asphaltenes−problematic but rich in potential, Oilfield Review 19 (2007) 22-43.

N. Akiya, P.E. Savage, Roles of water for chemical reactions in high-temperature water, Chemical Reviews 102 (2002) 2725-2750.

L. Alagha, L. Guo, M. Ghuzi, O. Molatlhegi, Z. Xu, Adsorption of hybrid polyacrylamides on anisotropic kaolinite surfaces: Effect of polymer characteristics and solution properties, Colloids and Surfaces A: Physicochemical and Engineering Aspects 498 (2016) 285-296.

L. Alagha, S. Wang, L. Yan, Z. Xu, J. Masliyah, Probing adsorption of polyacrylamide-based polymers on anisotropic basal planes of kaolinite using quartz crystal microbalance, Langmuir 29 (2013) 3989-3998.

J. An, L. Bagnell, T. Cablewski, C.R. Strauss, R.W. Trainor, Applications of high-temperature aqueous media for synthetic organic reactions, The Journal of Organic Chemistry 62 (1997) 2505-2511.

D. Andrieux, J. Jestin, N. Kervarec, R. Pichon, M. Privat, R. Olier, Adsorption mechanism of substituted pyridines on silica suspensions: An NMR study, Langmuir 20 (2004) 10591-10598.

T.S. Arnarson, R.G. Keil, Organic–mineral interactions in marine sediments studied using density fractionation and X-ray photoelectron spectroscopy, Organic Geochemistry 32 (2001) 1401-1415.

N. Ashby, B. Binks, Pickering emulsions stabilised by Laponite clay particles, Physical Chemistry Chemical Physics 2 (2000) 5640-5646.

ASTM D 4807-05: Standard test method for sediment in crude oil by membrane filtration, Annual Book of ASTM Standards, Washington, DC, 2005.

ASTM D 6560-12, Standard test method for determination of asphaltenes (heptane insolubles) in crude petroleum and petroleum products, ASTM, West Conshohocken, PA, 2012.

R. Aveyard, B.P. Binks, J.H. Clint, Emulsions stabilised solely by colloidal particles, Advances in Colloid and Interface Science 100 (2003) 503-546.

D.E. Axelson, R.J. Mikula, Z.M. Potoczny, Characterization of oil sands mineral components and clay-organic complexes, Fuel Science & Technology International 7 (1989) 659-673.

J. Bachmann, G. Arye, M. Deurer, S.K. Woche, R. Horton, K.H. Hartge, Y. Chen, Universality of a surface tension-contact angle relation for hydrophobic soils of different texture, Journal of Plant Nutrition and Soil Science 169 (2006) 745-753.

H. Barthel, B.P. Binks, A. Dyab, P. Fletcher, Multiple emulsions, US Patent 7722891, May 25, 2010.

R. Baskerville, J. Komorek, R. Gale, Effect of operating variables on filter press performance, Water Pollution Control 70 (1971) 400.

R.K. Bauer, P. de Mayo, L.V. Natarajan, W.R. Ware, Surface photochemistry: The effect of surface modification on the photophysics of naphthalene and pyrene adsorbed on silica gel, Canadian Journal of Chemistry 62 (1984) 1279-1286.

P. Bayliss, A. Levinson, Mineralogical review of the Alberta oil sand deposits (Lower Cretaceous, Mannville Group), Bulletin of Canadian Petroleum Geology 24 (1976) 211-224.

A. Benninghoven, Surface analysis by secondary ion mass spectrometry (SIMS), Surface Science 299 (1994) 246-260.

F. Bensebaa, L.S. Kotlyar, B.D. Sparks, K.H. Chung, Organic coated solids in Athabasca bitumen: Characterization and process implications, Canadian Journal of Chemical Engineering 78 (2000) 610-616.

F. Bensebaa, A. Majid, Y. Deslandes, Step-scan photoacoustic Fourier transform and X-rays photoelectron spectroscopy of oil sands fine tailings: New structural insights, Spectrochimica Acta Part A: Molecular and Biomolecular Spectroscopy 57 (2001) 2695-2702.

F. Bergaya, G. Lagaly, General introduction: Clays, clay minerals, and clay science, Developments in Clay Science 1 (2006) 1-18.

B. Bhushan, T. Kasai, G. Kulik, L. Barbieri, P. Hoffmann, AFM study of perfluoroalkylsilane and alkylsilane self-assembled monolayers for anti-stiction in MEMS/NEMS, Ultramicroscopy 105 (2005) 176-188.

C. Bich, J. Ambroise, J. Péra, Influence of degree of dehydroxylation on the pozzolanic activity of metakaolin, Applied Clay Science 44 (2009) 194-200.

B. Binks, P. Fletcher, Particles adsorbed at the oil-water interface: A theoretical comparison between spheres of uniform wettability and "Janus" particles, Langmuir 17 (2001) 4708-4710.

B. Binks, M. Kirkland, Interfacial structure of solid-stabilised emulsions studied by scanning electron microscopy, Physical Chemistry Chemical Physics 4 (2002) 3727-3733.

B. Binks, S. Lumsdon, Effects of oil type and aqueous phase composition on oil–water mixtures containing particles of intermediate hydrophobicity, Physical Chemistry Chemical Physics 2 (2000) 2959-2967.

B. Binks, S. Lumsdon, Influence of particle wettability on the type and stability of surfactant-free emulsions, Langmuir 16 (2000) 8622-8631.

B. Binks, S. Lumsdon, Transitional phase inversion of solid-stabilized emulsions using particle mixtures, Langmuir 16 (2000) 3748-3756.

B. Binks, J. Rodrigues, Types of phase inversion of silica particle stabilized emulsions containing triglyceride oil, Langmuir 19 (2003) 4905-4912.

B.P. Binks, Particles as surfactants-similarities and differences, Current Opinion in Colloid & Interface Science 7 (2002) 21-41.

G. Binnig, C. Gerber, E. Stoll, T. Albrecht, C. Quate, Atomic resolution with atomic force microscope, Europhysics Letters 3 (1987) 1281.

G. Binnig, C.F. Quate, C. Gerber, Atomic force microscope, Physical Review Letters 56 (1986) 930.

M.J. Bock, L.M. Mayer, Mesodensity organo–clay associations in a near-shore sediment, Marine Geology 163 (2000) 65-75.

D. Briggs, M. Seah, H. Bubert, Practical surface analysis. Vol. 1: Auger and X-ray photoelectron spectroscopy, Angewandte Chemie-German Edition 107 (1995) 1367.

G. Brindley, J. Kao, Relation between the structural disorder and other characteristics of kaolinites and dickites, Clays and Clay Minerals, Citeseer, 1986.

H. Brodowsky, E. Mäder, Jute fibre/epoxy composites: surface properties and interfacial adhesion, Composites Science and Technology 72 (2012) 1160-1166.

C.J. Bronick, R. Lal, Soil structure and management: A review, Geoderma 124 (2005) 3-22.

J. Brzoska, I.B. Azouz, F. Rondelez, Silanization of solid substrates: A step toward reproducibility, Langmuir 10 (1994) 4367-4373.

J. Buckley, Y. Liu, Some mechanisms of crude oil/brine/solid interactions, Journal of Petroleum Science and Engineering 20 (1998) 155-160.

K. Byrappa, T. Adschiri, Hydrothermal technology for nanotechnology, Progress in Crystal Growth and Characterization of Materials 53 (2007) 117-166.

R. Cadena-Nava, A. Cosultchi, J. Ruiz-Garcia, Asphaltene behavior at interfaces, Energy & Fuels 21 (2007) 2129-2137.

Canadian Association of Petroleum Producers CAPP, 2017, Crude oil forecast, markets and transportation, available at: http://www.capp.ca/publications-and-statistics/publications/303440, retrieved on 8 August 2017.

R.O. Canıaz, C. Erkey, Process intensification for heavy oil upgrading using supercritical water, Chemical Engineering Research and Design 92 (2014) 1845-1863.

X. Cao, M. Jahazi, Examination and verification of the filtration mechanism of cake mode during the pressure filtration tests of liquid Al–Si cast alloys, Materials Science and Engineering: A 408 (2005) 234-242.

L. Carbognani, M. Orea, M. Fonseca, Complex nature of separated solid phases from crude oils, Energy & Fuels 13 (1999) 351-358.

E. Castellini, R. Andreoli, G. Malavasi, A. Pedone, Deflocculant effects on the surface properties of kaolinite investigated through malachite green adsorption, Colloids and Surfaces A: Physicochemical and Engineering Aspects 329 (2008) 31-37.

M.L. Chacón-Patiño, C. Blanco-Tirado, J.A. Orrego-Ruiz, A. Gómez-Escudero, M.Y. Combariza, High resolution mass spectrometric view of asphaltene–SiO_2 interactions, Energy & Fuels 29 (2015) 1323-1331.

A.K. Chakraborty, New data on thermal effects of kaolinite in the high temperature region, Journal of Thermal Analysis and Calorimetry 71 (2003) 799-808.

R.J. Chalaturnyk, J. Don Scott, B. Özüm, Management of oil sands tailings, Petroleum Science and Technology 20 (2002) 1025-1046.

C. Charcosset, Preparation of emulsions and particles by membrane emulsification for the food processing industry, Journal of Food Engineering 92 (2009) 241-249.

T. Chau, A review of techniques for measurement of contact angles and their applicability on mineral surfaces, Minerals Engineering 22 (2009) 213-219.

F. Chen, J. Finch, Z. Xu, J. Czarnecki, Wettability of fine solids extracted from bitumen froth, Journal of Adhesion Science and Technology 13 (1999) 1209-1224.

H. Cheng, Q. Liu, J. Yang, S. Ma, R.L. Frost, The thermal behavior of kaolinite intercalation complexes-A review, Thermochimica Acta 545 (2012) 1-13.

Y. Chevalier, M.A. Bolzinger, Emulsions stabilized with solid nanoparticles: Pickering emulsions, Colloids and Surfaces A: Physicochemical and Engineering Aspects 439 (2013) 23-34.

T.P. Chou, G. Cao, Adhesion of sol-gel-derived organic-inorganic hybrid coatings on polyester, Journal of Sol Gel Science and Technology 27 (2003) 31-41.

S. Collins, J. Melrose, Adsorption of asphaltenes and water on reservoir rock minerals, Proceedings of the SPE Oilfield and Geothermal Chemistry Symposium, Denver, CO, June 1-3, 1983, DOI: 10.2118/11800-MS.

M. Couillard, P.H. Mercier, Analytical electron microscopy of carbon-rich mineral aggregates in solvent-diluted bitumen products from mined Alberta oil sands, Energy & Fuels 30 (2016) 5513-5524.

Z.G. Cui, K.Z. Shi, Y.Z. Cui, B. Binks, Double phase inversion of emulsions stabilized by a mixture of $CaCO_3$ nanoparticles and sodium dodecyl sulphate, Colloids and Surfaces A: Physicochemical and Engineering Aspects 329 (2008) 67-74.

E. Czarnecka, J. Gillott, Formation and characterization of clay complexes with bitumen from Athabasca oil sand, Clays and Clay minerals 28 (1980) 197-203.

J. Czarnecki, P. Tchoukov, T. Dabros, Possible role of asphaltenes in the stabilization of water-in-crude oil emulsions, Energy & Fuels 26 (2012) 5782-5786.

T. Dang-Vu, R. Jha, S.Y. Wu, D.D. Tannant, J. Masliyah, Z. Xu, Wettability determination of solids isolated from oil sands, Colloids and Surfaces A: Physicochemical and Engineering Aspects 337 (2009) 80-90.

K. Darcovich, L. Kotlyar, W. Tse, J. Ripmeester, C. Capes, B. Sparks, Wettability study of organic-rich solids separated from Athabasca oil sands, Energy & Fuels 3 (1989) 386-391.

D. Dinh, In-situ observation of heavy-oil cracking using backscattering optical techniques, University of Alberta, Master thesis, 2015.

J. Mendoza, I. Castellanos, A. Ortiz, E. Buenrostro, C. Durán, S. López, Study of monolayer to multilayer adsorption of asphaltenes on reservoir rock minerals, Colloids and Surfaces A: Physicochemical and Engineering Aspects 340 (2009) 149-154.

W.A. Deer, R.A. Howie, J. Zussman, An introduction to the rock-forming minerals, Longman, London, 1992.

M. Dejhosseini, T. Aida, M. Watanabe, S. Takami, D. Hojo, N. Aoki, T. Arita, A. Kishita, T. Adschiri, Catalytic cracking reaction of heavy oil in the presence of cerium oxide nanoparticles in supercritical water, Energy & Fuels 27 (2013) 4624-4631.

J. Diao, D. Fuerstenau, Characterization of the wettability of solid particles by film flotation 2. Theoretical analysis, Colloids and Surfaces 60 (1991) 145-160.

M.E. Dokukin, I. Sokolov, Quantitative mapping of the elastic modulus of soft materials with HarmoniX and PeakForce QNM AFM modes, Langmuir 28 (2012) 16060-16071.

F. Dongbao, J.R. Woods, J. Kung, D.M. Kingston, L.S. Kotlyar, B.D. Sparks, P.H. Mercier, T. McCracken, S. Ng, Residual organic matter associated with toluene-extracted oil sands solids and its potential role in bitumen recovery via adsorption onto clay minerals, Energy & Fuels 24 (2010) 2249-2256.

V.A. Drits, D.K. McCarty, The nature of structure-bonded H_2O in illite and leucophyllite from dehydration and dehydroxylation experiments, Clays and Clay Minerals 55 (2007) 45-58.

S. Dubey, M. Waxman, Asphaltene adsorption and desorption from mineral surfaces, SPE Reservoir Engineering 6 (1991) 389-395.

L.H. Dubois, B.R. Zegarski, Bonding of alkoxysilanes to dehydroxylated silica surfaces: A new adhesion mechanism, The Journal of Physical Chemistry 97 (1993) 1665-1670.

D. Dudášová, A. Silset, J. Sjöblom, Quartz crystal microbalance monitoring of asphaltene adsorption/deposition, Journal of Dispersion Science and Technology 29 (2008) 139-146.

L.J. Duffus, J.E. Norton, P. Smith, I.T. Norton, F. Spyropoulos, A comparative study on the capacity of a range of food-grade particles to form stable o/w and w/o Pickering emulsions, Journal of Colloid and Interface Science 473 (2016) 9-21.

R.P. Dutta, W.C. McCaffrey, M.R. Gray, K. Muehlenbachs, Thermal cracking of Athabasca bitumen: Influence of steam on reaction chemistry, Energy & Fuels 14 (2000) 671-676.

T. Eastman, D.M. Zhu, Adhesion forces between surface-modified AFM tips and a mica surface, Langmuir 12 (1996) 2859-2862.

P. Eaton, J.R. Smith, P. Graham, J.D. Smart, T.G. Nevell, J. Tsibouklis, Adhesion force mapping of polymer surfaces: Factors influencing force of adhesion, Langmuir 18 (2002) 3387-3389.

D. Eberl, User guide to RockJock-A program for determining quantitative mineralogy from X-ray diffraction data, US Geological Survey, 2003.

L. Edomwonyi-Otu, B.O. Aderemi, A.S. Ahmed, N.J. Coville, M. Maaza, Influence of thermal treatment on kankara kaolinite, Opticon1826 5 (2013) 1-5.

J.K. Edzwald, J.B. Upchurch, C.R. O'Melia, Coagulation in estuaries, Environmental Science & Technology 8 (1974) 58-63.

M. Eliyahu, S. Emmanuel, R.J. Day-Stirrat, C.I. Macaulay, Mechanical properties of organic matter in shales mapped at the nanometer scale, Marine and Petroleum Geology 59 (2015) 294-304.

K. Eusterhues, C. Rumpel, M. Kleber, I. Kögel-Knabner, Stabilisation of soil organic matter by interactions with minerals as revealed by mineral dissolution and oxidative degradation, Organic Geochemistry 34 (2003) 1591-1600.

J. Eyssautier, D. Frot, L. Barré, Structure and dynamic properties of colloidal asphaltene aggregates, Langmuir 28 (2012) 11997-12004.

O.N. Fedyaeva, A.V. Shatrova, A.A. Vostrikov, Effect of temperature on bitumen conversion in a supercritical water flow, The Journal of Supercritical Fluids 95 (2014) 437-443.

H. Fischer, H. Stadler, N. Erina, Quantitative temperature-depending mapping of mechanical properties of bitumen at the nanoscale using the AFM operated with PeakForce Tapping™ mode, Journal of microscopy 250 (2013) 210-217.

B. Fritz, Multicomponent solid solutions for clay minerals and computer modeling of weathering processes, The Chemistry of Weathering, Springer Netherlands, 1985.

C. Fromonteil, P. Bardelle, F. Cansell, Hydrolysis and oxidation of an epoxy resin in sub-and supercritical water, Industrial & Engineering Chemistry Research 39 (2000) 922-925.

R.L. Frost, E. Horvath, É. Makó, J. Kristóf, Á. Rédey, Slow transformation of mechanically dehydroxylated kaolinite to kaolinite-an aged mechanochemically activated formamide-intercalated kaolinite study, Thermochimica Acta 408 (2003) 103-113.

R.L. Frost, A.M. Vassallo, The dehydroxylation of the kaolinite clay minerals using infrared emission spectroscopy, Clays and Clay minerals 44 (1996) 635-651.

D. Fuerstenau, J. Diao, J. Hanson, Estimation of the distribution of surface sites and contact angles on coal particles from film flotation data, Energy & Fuels 4 (1990) 34-37.

D. Fuerstenau, J. Diao, M. Williams, Characterization of the wettability of solid particles by film flotation 1. Experimental investigation, Colloids and Surfaces 60 (1991) 127-144.

R. Fuhrer, I.K. Herrmann, E.K. Athanassiou, R.N. Grass, W.J. Stark, Immobilized β-cyclodextrin on surface-modified carbon-coated cobalt nanomagnets: Reversible organic contaminant adsorption and enrichment from water, Langmuir 27 (2011) 1924-1929.

M. Fuji, K. Machida, T. Takei, T. Watanabe, M. Chikazawa, Effect of wettability on adhesion force between silica particles evaluated by atomic force microscopy measurement as a function of relative humidity, Langmuir 15 (1999) 4584-4589.

S. Fujii, Y. Yokoyama, Y. Miyanari, T. Shiono, M. Ito, S.I. Yusa, Y. Nakamura, Micrometer-sized gold–silica Janus particles as particulate emulsifiers, Langmuir 29 (2013) 5457-5465.

A.J. Fuller, S. Shaw, M.B. Ward, S.J. Haigh, J.F.W. Mosselmans, C.L. Peacock, S. Stackhouse, A.J. Dent, D. Trivedi, I.T. Burke, Caesium incorporation and retention in illite interlayers, Applied Clay Science 108 (2015) 128-134.

R. Gaikwad, A. Hande, S. Das, S.K. Mitra, T. Thundat, Determination of charge on asphaltene nanoaggregates in air using electrostatic force microscopy, Langmuir 31 (2015) 679-684.

R. Gale, R. Baskerville, Studies on the vacuum filtration of sewage sludges, Water Pollution Control 69 (1970) 574.

Y.M. Ganeeva, T.N. Yusupova, G.V. Romanov, Asphaltene nano-aggregates: Structure, phase transitions and effect on petroleum systems, Russian Chemical Reviews 80 (2011) 993-1008.

S. Gao, K. Moran, Z. Xu, J. Masliyah, Role of bitumen components in stabilizing water-in-diluted oil emulsions, Energy & Fuels 23 (2009) 2606-2612.

P. Gilbert, M. Abrecht, B.H. Frazer, The organic-mineral interface in biominerals, Reviews in Mineralogy and Geochemistry 59 (2005) 157-185.

N. Glaser, D.J. Adams, A. Böker, G. Krausch, Janus particles at liquid-liquid interfaces, Langmuir 22 (2006) 5227-5229.

A. Golchin, J.A. Baldock, J. Oades, A model linking organic matter decomposition, chemistry, and aggregate dynamics, Soil Processes and the Carbon Cycle, CRC Press, Boca Raton, 1997.

M.F. González, C.S. Stull, F. López-Linares, P. Pereira-Almao, Comparing asphaltene adsorption with model heavy molecules over macroporous solid surfaces, Energy & Fuels 21 (2007) 234-241.

C. Goubault, K. Pays, D. Olea, P. Gorria, J. Bibette, V. Schmitt, F. Leal-Calderon, Shear rupturing of complex fluids: Application to the preparation of quasi-monodisperse water-in-oil-in-water double emulsions, Langmuir 17 (2001) 5184-5188.

M.R. Gray, Upgrading oilsands bitumen and heavy oil, The University of Alberta Press, Edmonton, Alberta, 2015.

M.R. Gray, R.R. Tykwinski, J.M. Stryker, X. Tan, Supramolecular assembly model for aggregation of petroleum asphaltenes, Energy & Fuels 25 (2011) 3125-3134.

R.E. Grim, Applied clay mineralogy, Geologiska Föreningen iStockholm Förhandlingar 84 (1962) 533.

B. Gu, J. Schmitt, Z. Chen, L. Liang, J.F. McCarthy, Adsorption and desorption of natural organic matter on iron oxide: Mechanisms and models, Environmental Science & Technology 28 (1994) 38-46.

G. Gu, Z. Xu, K. Nandakumar, J. Masliyah, Influence of water-soluble and water-insoluble natural surface active components on the stability of water-in-toluene-diluted bitumen emulsion, Fuel 81 (2002) 1859-1869.

G. Gu, L. Zhang, Z. Xu, J. Masliyah, Novel bitumen froth cleaning device and rag layer characterization, Energy & Fuels 21 (2007) 3462-3468.

S. Guggenheim, R. Martin, Definition of clay and clay mineral: Joint report of the AIPEA nomenclature and CMS nomenclature committees, Clays and Clay Minerals 43 (1995) 255-256.

G. Guglielmi, D. Chiarani, D.P. Saroj, G. Andreottola, Sludge filterability and dewaterability in a membrane bioreactor for municipal wastewater treatment, Desalination 250 (2010) 660-665.

Y. Guo, S. Wang, D. Xu, Y. Gong, H. Ma, X. Tang, Review of catalytic supercritical water gasification for hydrogen production from biomass, Renewable and Sustainable Energy Reviews 14 (2010) 334-343.

A. Hannisdal, M.H. Ese, P.V. Hemmingsen, J. Sjöblom, Particle-stabilized emulsions: Effect of heavy crude oil components pre-adsorbed onto stabilizing solids, Colloids and Surfaces A: Physicochemical and Engineering Aspects 276 (2006) 45-58.

D. Harbottle, Q. Chen, K. Moorthy, L. Wang, S. Xu, Q. Liu, J. Sjoblom, Z. Xu, Problematic stabilizing films in petroleum emulsions: Shear rheological response of viscoelastic asphaltene films and the effect on drop coalescence, Langmuir 30 (2014) 6730-6738.

M. Hato, Attractive forces between surfaces of controlled “hydrophobicity” across water: A possible range of “hydrophobic interactions” between macroscopic hydrophobic surfaces across water, The Journal of Physical Chemistry 100 (1996) 18530-18538.

R. Haynes, M. Beare, Influence of six crop species on aggregate stability and some labile organic matter fractions, Soil Biology and Biochemistry 29 (1997) 1647-1653.

L. He, F. Lin, X. Li, H. Sui, Z. Xu, Interfacial sciences in unconventional petroleum production: From fundamentals to applications, Chemical Society Reviews 44 (2015) 5446-5494.

C. Hedley, G. Yuan, B. Theng, Thermal analysis of montmorillonites modified with quaternary phosphonium and ammonium surfactants, Applied Clay Science 35 (2007) 180-188.

L. Heepe, S.N. Gorb, Biologically inspired mushroom-shaped adhesive microstructures, Annual Review of Materials Research 44 (2014) 173-203.

S. Heidenreich, B. Scheibner, Hot gas filtration with ceramic filters: Experiences and new developments, Filtration & Separation 39 (2002) 22-25.

L. Heller-Kallai, F. Bergaya, B. Theng, G. Lagaly, Handbook of Clay Science. Developments in Clay Science, Elsevier, Amsterdam, 2006.

M. Holuszko, J. Franzidis, E. Manlapig, M. Hampton, B. Donose, A. Nguyen, The effect of surface treatment and slime coatings on ZnS hydrophobicity, Minerals Engineering 21 (2008) 958-966.

A. Hooshiar, P. Uhlik, D.G. Ivey, Q. Liu, T.H. Etsell, Clay minerals in nonaqueous extraction of bitumen from Alberta oil sands: Part 2. Characterization of clay minerals, Fuel Processing Technology 96 (2012) 183-194.

A. Hooshiar, P. Uhlik, Q. Liu, T.H. Etsell, D.G. Ivey, Clay minerals in nonaqueous extraction of bitumen from Alberta oil sands: Part 1. Nonaqueous extraction procedure, Fuel Processing Technology 94 (2012) 80-85.

T.S. Horozov, B.P. Binks, Particle-stabilized emulsions: A bilayer or a bridging monolayer? Angewandte Chemie International Edition 45 (2006) 773-776.

Z. Hosseini-Dastgerdi, S. Tabatabaei-Nejad, E. Khodapanah, E. Sahraei, A comprehensive study on mechanism of formation and techniques to diagnose asphaltene structure; molecular and aggregates: A review, Asia-Pacific Journal of Chemical Engineering 10 (2015) 1-14.

Z.E. Ibraeva, A.A. Zhumaly, E. Blagih, S.E. Kudaibergenov, Preparation and characterization of organic-inorganic composite materials based on poly (acrylamide) hydrogels and clay minerals, Macromolecular Symposia 351 (2015) 97-111.

IFA, GESTIS Substance Database, http://gestis-en.itrust.de/nxt/gateway.dll/gestis_en/000000.xml?f=templates$fn=default.htm$vid=gestiseng:sdbeng$3.0, keyword: toluene (accessed on May 1, 2017).

IFA, GESTIS Substance Database, http://gestis-en.itrust.de/nxt/gateway.dll/gestis_en/000000.xml?f=templates$fn=default.htm$vid=gestiseng:sdbeng$3.0, keyword: water (accessed on May 1, 2017).

P. Ihalainen, J. Järnström, A. Määttänen, J. Peltonen, Nano-scale mapping of mechanical and chemical surface properties of pigment coated surfaces by torsional harmonic atomic force microscopy, Colloids and Surfaces A: Physicochemical and Engineering Aspects 373 (2011) 138-144.

D. Janssen, R. De Palma, S. Verlaak, P. Heremans, W. Dehaen, Static solvent contact angle measurements, surface free energy and wettability determination of various self-assembled monolayers on silicon dioxide, Thin Solid Films 515 (2006) 1433-1438.

J. Jastrow, Soil aggregate formation and the accrual of particulate and mineral-associated organic matter, Soil Biology and Biochemistry 28 (1996) 665-676.

T. Jiang, G.J. Hirasaki, C.A. Miller, S. Ng, Wettability alteration of clay in solid-stabilized emulsions, Energy & Fuels 25 (2011) 2551-2558.

T. Jiang, G. Li, G. Qiu, X. Fan, Z. Huang, Thermal activation and alkali dissolution of silicon from illite, Applied Clay Science 40 (2008) 81-89.

X. Jin, N.H. Wang, G. Tarjus, J. Talbot, Irreversible adsorption on nonuniform surfaces: The random site model, Journal of Physical Chemistry 97 (1993) 4256-4258.

M. Kahle, M. Kleber, R. Jahn, Carbon storage in loess derived surface soils from Central Germany: Influence of mineral phase variables, Journal of Plant Nutrition and Soil Science 165 (2002) 141-149.

H.A. Kaminsky, T.H. Etsell, D.G. Ivey, O. Omotoso, Distribution of clay minerals in the process streams produced by the extraction of bitumen from Athabasca oil sands, The Canadian Journal of Chemical Engineering 87 (2009) 85-93.

A.R. Katritzky, F.J. Luxem, M. Siskin, Aqueous high-temperature chemistry of carbo-and heterocycles. 6. Monosubstituted benzenes with two carbon atom side chains unsubstituted or oxygenated at the α-position, Energy & Fuels 4 (1990) 518-524.

G. Kayukova, A. Kiyamova, G. Romanov, Hydrothermal transformations of asphaltenes, Petroleum Chemistry 52 (2012) 5-14.

G.P. Kayukova, A.T. Gubaidullin, S.M. Petrov, G.V. Romanov, N.N. Petrukhina, A.V. Vakhin, Changes of asphaltenes' structural phase characteristics in the process of conversion of heavy oil in the hydrothermal catalytic system, Energy & Fuels 30 (2016) 773-783.

P.K. Kilpatrick, Water-in-crude oil emulsion stabilization: Review and unanswered questions, Energy & Fuels 26 (2012) 4017-4026.

W.S. Kim, I.H. Yun, J.J. Lee, H.T. Jung, Evaluation of mechanical interlock effect on adhesion strength of polymer–metal interfaces using micro-patterned surface topography, International Journal of Adhesion and Adhesives 30 (2010) 408-417.

M. Kleber, P. Sollins, R. Sutton, A conceptual model of organo-mineral interactions in soils: Self-assembly of organic molecular fragments into zonal structures on mineral surfaces, Biogeochemistry 85 (2007) 9-24.

E. Kleimenov, H. Bluhm, M. Hävecker, A. Knop-Gericke, A. Pestryakov, D. Teschner, J.A. Lopez-Sanchez, J.K. Bartley, G.J. Hutchings, R. Schlögl, XPS investigations of VPO catalysts under reaction conditions, Surface Science 575 (2005) 181-188.

L. Kotlyar, Y. Deslandes, B. Sparks, H. Hodama, R. Schutte, Characterization of colloidal solids from Athabasca fine tails, Clays and Clay Minerals 41 (1993) 341-345.

L. Kotlyar, H. Kodama, B. Sparks, P. Grattan-Bellew, Non-crystalline inorganic matter-humic complexes in Athabasca oil sand and their relationship to bitumen recovery, Applied Clay Science 2 (1987) 253-271.

L. Kotlyar, B. Sparks, J. Woods, K. Chung, Solids associated with the asphaltene fraction of oil sands bitumen, Energy & Fuels 13 (1999) 346-350.

L. Kotlyar, B. Sparks, J. Woods, S. Raymond, Y. Le Page, W. Shelfantook, Distribution and types of solids associated with bitumen, Petroleum Science and Technology 16 (1998) 1-19.

L.S. Kotlyar, J.A. Ripmeester, B.D. Sparks, D.S. Montgomery, Characterization of oil sands solids closely associated with Athabasca bitumen, Fuel 67 (1988) 808-814.

L.S. Kotlyar, J.A. Ripmeester, B.D. Sparks, D.S. Montgomery, Characterization of organic-rich solids fractions isolated from Athabasca oil sand using a cold water agitation test, Fuel 67 (1988) 221-226.

P. Kritzer, Corrosion in high-temperature and supercritical water and aqueous solutions: A review, The Journal of Supercritical Fluids 29 (2004) 1-29.

C. Laborde-Boutet, D. Dinh, F. Bender, M. Medina, W.C. McCaffrey, In situ observation of fouling behavior under thermal cracking conditions: Hue, saturation, and intensity image analyses, Energy & Fuels 30 (2015) 3666-3675.

J. Landoulsi, V. Dupres, Direct AFM force mapping of surface nanoscale organization and protein adsorption on an aluminum substrate, Physical Chemistry Chemical Physics 15 (2013) 8429-8440.

I. Lapides, S. Yariv, N. Lahav, M. Dvorachek, Stabilizing of aqueous kaolinite suspensions by thermal vapour-pressure shock explosion treatment, Thermochimica Acta 318 (1998) 251-263.

M. Larsson, M. Ahmad, Improved polymer–glass adhesion through micro-mechanical interlocking, Journal of Micromechanics and Microengineering 16 (2006) S161.

B. Latella, L. Henkel, E. Mehrtens, Permeability and high temperature strength of porous mullite-alumina ceramics for hot gas filtration, Journal of Materials Science 41 (2006) 423-430.

F. Leal-Calderon, V. Schmitt, Solid-stabilized emulsions, Current Opinion in Colloid & Interface Science 13 (2008) 217-227.

C. Lee, S.M. Kim, Y.J. Kim, Y.W. Choi, K.-Y. Suh, C. Pang, M. Choi, Robust microzip fastener: Repeatable interlocking using polymeric rectangular parallelepiped arrays, ACS Applied Materials & Interfaces 7 (2015) 2561-2568.

F. Leite, A. Riul, P. Herrmann, Mapping of adhesion forces on soil minerals in air and water by atomic force spectroscopy (AFS), Journal of Adhesion Science and Technology 17 (2003) 2141-2156.

D. Lesueur, The colloidal structure of bitumen: Consequences on the rheology and on the mechanisms of bitumen modification, Advances in Colloid and Interface Science 145 (2009) 42-82.

J.H. Levy, Effect of water vapor pressure on the dehydration and dehydroxylation of kaolinite and smectite isolated from Australian tertiary oil shales, Energy & Fuels 4 (1990) 146-151.

D. Li, A. Neumann, Contact angles on hydrophobic solid surfaces and their interpretation, Journal of Colloid and Interface Science 148 (1992) 190-200.

N. Li, B. Yan, X.M. Xiao, A review of laboratory-scale research on upgrading heavy oil in supercritical water, Energies 8 (2015) 8962-8989.

X. Li, L. He, G. Wu, W. Sun, H. Li, H. Sui, Operational parameters, evaluation methods, and fundamental mechanisms: Aspects of nonaqueous extraction of bitumen from oil sands, Energy & Fuels 26 (2012) 3553-3563.

Z. Li, D. Harbottle, E. Pensini, T. Ngai, W. Richtering, Z. Xu, Fundamental study of emulsions stabilized by soft and rigid particles, Langmuir 31 (2015) 6282-6288.

J. Liang, F. Tumpa, L.P. Estrada, M.G. El-Din, Y. Liu, Impact of ozonation on particle aggregation in mature fine tailings, Journal of Environmental Management 146 (2014) 535-542.

D. Lin-Vien, N.B. Colthup, W.G. Fateley, J.G. Grasselli, The handbook of infrared and Raman characteristic frequencies of organic molecules, Academic Press, San Diego, California, 1991.

C. Lin, J. Miller, Pore structure and network analysis of filter cake, Chemical Engineering Journal 80 (2000) 221-231.

F. Lin, S.R. Stoyanov, Y. Xu, Recent advances in non-aqueous extraction of bitumen from mineable oil sands: A review, Organic Process Research & Development 21 (2017) 492-510.

J. Liu, R. Gaikwad, A. Hande, S. Das, T. Thundat, Mapping and quantifying surface charges on clay nanoparticles, Langmuir 31 (2015) 10469-10476.

J. Liu, Z. Xu, J. Masliyah, Role of fine clays in bitumen extraction from oil sands, AIChE Journal 50 (2004) 1917-1927.

X. Liu, Q. Wu, PP/clay nanocomposites prepared by grafting-melt intercalation, Polymer 42 (2001) 10013-10019.

Y. Long, T. Dabros, H. Hamza, Stability and settling characteristics of solvent-diluted bitumen emulsions, Fuel 81 (2002) 1945-1952.

Z. Lu, J. McCaffrey, B. Brar, G. Wilk, R. Wallace, L.C. Feldman, S. Tay, SiO_2 film thickness metrology by X-ray photoelectron spectroscopy, Applied Physics Letters 71 (1997) 2764-2766.

M. Mackley, N. Sherman, Cake filtration mechanisms in steady and unsteady flows, Journal of Membrane Science 77 (1993) 113-121.

J. Madejová, FTIR techniques in clay mineral studies, Vibrational Spectroscopy 31 (2003) 1-10.

P. Maiti, K. Yamada, M. Okamoto, K. Ueda, K. Okamoto, New polylactide/layered silicate nanocomposites: Role of organoclays, Chemistry of Materials 14 (2002) 4654-4661.

A. Majid, S. Argue, V. Boyko, G. Pleizier, P. L'Ecuyer, J. Tunney, S. Lang, Characterization of sol–gel-derived nano-particles separated from oil sands fine tailings, Colloids and Surfaces A: Physicochemical and Engineering Aspects 224 (2003) 33-44.

A. Majid, J.A. Ripmeester, Isolation and characterization of humic acids from Alberta oil sands and related materials, Fuel 69 (1990) 1527-1536.

A. Majid, B.D. Sparks, J.A. Ripmeester, Characterization of solvent-insoluble organic matter isolated from Alberta oil sands, Fuel 70 (1991) 78-83.

M. Mänttäri, A. Pihlajamäki, E. Kaipainen, M. Nyström, Effect of temperature and membrane pre-treatment by pressure on the filtration properties of nanofiltration membranes, Desalination 145 (2002) 81-86.

A.W. Marczewski, M. Szymula, Adsorption of asphaltenes from toluene on mineral surface, Colloids and Surfaces A: Physicochemical and Engineering Aspects 208 (2002) 259-266.

S.J. Marshall, S.C. Bayne, R. Baier, A.P. Tomsia, G.W. Marshall, A review of adhesion science, Dental Materials 26 (2010) e11-e16.

D.E. Martínez-Tong, A. Najar, M. Soccio, A. Nogales, N. Bitinis, M. López-Manchado, T. Ezquerra, Quantitative mapping of mechanical properties in polylactic acid/natural rubber/organoclay bionanocomposites as revealed by nanoindentation with atomic force microscopy, Composites Science and Technology 104 (2014) 34-39.

J. Masliyah, J. Czarnecki, Z. Xu, Handbook on theory and practice of bitumen recovery from Athabasca oil sands, Volume I: Theoretical basis, Kingsley Knowledge Publishing, Calgary, Alberta, 2011.

J. Masliyah, Z.J. Zhou, Z. Xu, J. Czarnecki, H. Hamza, Understanding water-based bitumen extraction from Athabasca oil sands, The Canadian Journal of Chemical Engineering 82 (2004) 628-654.

L. Mayer, Extent of coverage of mineral surfaces by organic matter in marine sediments, Geochimica et Cosmochimica Acta 63 (1999) 207-215.

C.J. McConville, W.E. Lee, Microstructural development on firing illite and smectite clays compared with that in kaolinite, Journal of the American Ceramic Society 88 (2005) 2267-2276.

M. Mehranfar, R. Gaikwad, S. Das, S.K. Mitra, T. Thundat, Effect of temperature on morphologies of evaporation-triggered asphaltene nanoaggregates, Langmuir 30 (2014) 800-804.

A. Metson, L. Blakemore, D. Rhoades, Methods for the determination of soil organic carbon: A review, and application to New Zealand soils, New Zealand Journal of Science 22 (1979) 205-228.

D.M. Moore, R.C. Reynolds, X-ray diffraction and the identification and analysis of clay minerals, Oxford University Press, Oxford, 1989.

M. Morimoto, Y. Sugimoto, Y. Saotome, S. Sato, T. Takanohashi, Effect of supercritical water on upgrading reaction of oil sand bitumen, The Journal of Supercritical Fluids 55 (2010) 223-231.

M. Morimoto, Y. Sugimoto, S. Sato, T. Takanohashi, Bitumen cracking in supercritical water upflow, Energy & Fuels 28 (2014) 858-861.

T. Moriya, H. Enomoto, Conversion of polyethylene to oil using supercritical water and donation of hydrogen in supercritical water, Japanese Journal of Polymer Science and Technology 58 (2001) 661-673.

I.A. Morozov, O.K. Garishin, V.V. Shadrin, V.A. Gerasin, M.A. Guseva, Atomic force microscopy of structural-mechanical properties of polyethylene reinforced by silicate needle-shaped filler, Advances in Materials Science and Engineering 2016 (2016) Article ID 8945978.

E.M. Murphy, J.M. Zachara, S.C. Smith, Influence of mineral-bound humic substances on the sorption of hydrophobic organic compounds, Environmental Science & Technology 24 (1990) 1507-1516.

K. Nahdi, P. Llewellyn, F. Rouquérol, J. Rouquérol, N. Ariguib, M. Ayedi, Controlled rate thermal analysis of kaolinite dehydroxylation: Effect of water vapour pressure on the mechanism, Thermochimica Acta 390 (2002) 123-132.

A. Natarajan, N. Kuznicki, D. Harbottle, J. Masliyah, H. Zeng, Z. Xu, Understanding mechanisms of asphaltene adsorption from organic solvent on mica, Langmuir 30 (2014) 9370-9377.

P. Nelson, J.A. Baldock, P. Clarke, J. Oades, G. Churchman, Dispersed clay and organic matter in soil: their nature and associations, Australian Journal of Soil Research 37 (1999) 289-290.

P. Nhieu, Q. Liu, M.R. Gray, Role of water and fine solids in onset of coke formation during bitumen cracking, Fuel 166 (2016) 152-156.

H. Nikakhtari, L. Vagi, P. Choi, Q. Liu, M.R. Gray, Solvent screening for non-aqueous extraction of Alberta oil sands, The Canadian Journal of Chemical Engineering 91 (2013) 1153-1160.

H. Nikakhtari, S. Wolf, P. Choi, Q. Liu, M.R. Gray, Migration of fine solids into product bitumen from solvent extraction of alberta oilsands, Energy & Fuels 28 (2014) 2925-2932.

O. Noel, M. Brogly, G. Castelein, J. Schultz, In situ determination of the thermodynamic surface properties of chemically modified surfaces on a local scale: An attempt with the atomic force microscope, Langmuir 20 (2004) 2707-2712.

J. O'Connor, B. Sexton, R.S. Smart, Surface analysis methods in materials science, Springer-Verlag, Berlin, 2013.

O.M. Ogunsola, Decomposition of isoquinoline and quinoline by supercritical water, Journal of Hazardous Materials 74 (2000) 187-195.

M. Osacky, M. Geramian, D.G. Ivey, Q. Liu, T.H. Etsell, Mineralogical and chemical composition of petrologic end members of Alberta oil sands, Fuel 113 (2013) 148-157.

N. Osornio-Rubio, J. Torres-Ochoa, M. Palma-Tirado, H. Iménez-Islas, R. Rosas-Cedillo, J. Fierro-Gonzalez, G. Martínez-González, Study of the dehydroxylation of kaolinite and alunite from a Mexican clay with DRIFTS-MS, Clay Minerals 51 (2016) 55-68.

H. Ota, T. Akai, H. Namita, S. Yamaguchi, M. Nomura, XAFS and ToF-SIMS analysis of SEI layers on electrodes, Journal of Power Sources 119 (2003) 567-571.

E.H. Owens, K. Lee, Interaction of oil and mineral fines on shorelines: Review and assessment, Marine Pollution Bulletin 47 (2003) 397-405.

K. Pal, L.d.P. Nogueira Branco, A. Heintz, P. Choi, Q. Liu, P.R. Seidl, M.R. Gray, Performance of solvent mixtures for non-aqueous extraction of Alberta oil sands, Energy & Fuels 29 (2015) 2261-2267.

V.N. Paunov, O.J. Cayre, P.F. Noble, S.D. Stoyanov, K.P. Velikov, M. Golding, Emulsions stabilised by food colloid particles: Role of particle adsorption and wettability at the liquid interface, Journal of Colloid and Interface Science 312 (2007) 381-389.

I. Pavlovič, Z.e. Knez, M. Škerget, Hydrothermal reactions of agricultural and food processing wastes in sub-and supercritical water: A review of fundamentals, mechanisms, and state of research, Journal of Agricultural and Food Chemistry 61 (2013) 8003-8025.

W. Peukert, High temperature filtration in the process industry, Filtration & Separation 35 (1998) 461-464.

J.J. Pignatello, Soil organic matter as a nanoporous sorbent of organic pollutants, Advances in Colloid and Interface Science 76 (1998) 445-467.

B. Pittenger, N. Erina, C. Su, Quantitative mechanical property mapping at the nanoscale with PeakForce QNM. Application Note Veeco Instruments Incorporated, 2010.

G. Pletikapić, A. Berquand, T.M. Radić, V. Svetličić, Quantitative nanomechanical mapping of marine diatom in seawater using peak force tapping atomic force microscopy, Journal of Phycology 48 (2012) 174-185.

P. Ptáček, D. Kubátová, J. Havlica, J. Brandštetr, F. Šoukal, T. Opravil, Isothermal kinetic analysis of the thermal decomposition of kaolinite: The thermogravimetric study, Thermochimica Acta 501 (2010) 24-29.

H. Rahier, B. Wullaert, B. Van Mele, Influence of the degree of dehydroxylation of kaolinite on the properties of aluminosilicate glasses, Journal of Thermal Analysis and Calorimetry 62 (2000) 417-427.

P. Rahimi, T. Gentzis, C. Fairbridge, Interaction of clay additives with mesophase formed during thermal treatment of solid-free Athabasca bitumen fraction, Energy & Fuels 13 (1999) 817-825.

Y. Rahmawan, S.M. Kang, S.Y. Lee, K.Y. Suh, S. Yang, Enhanced shear adhesion by mechanical interlocking of dual-scaled elastomeric micropillars with embedded silica particles, Macromolecular Reaction Engineering 7 (2013) 616-623.

F. Rao, Q. Liu, Froth treatment in Athabasca oil sands Bitumen recovery process: A review, Energy & Fuels 27 (2013) 7199-7207.

S. Ren, T. Dang-Vu, H. Zhao, J. Long, Z. Xu, J. Masliyah, Effect of weathering on surface characteristics of solids and bitumen from oil sands, Energy & Fuels 23 (2008) 334-341.

C.A. Rezende, L.T. Lee, F. Galembeck, Surface mechanical properties of thin polymer films investigated by AFM in pulsed force mode, Langmuir 25 (2009) 9938-9946.

U. Romanova, M. Valinasab, E. Stasiuk, H. Yarranton, L. Schramm, W. Shelfantook, The effect of oil sands bitumen extraction conditions on froth treatment performance, Journal of Canadian Petroleum Technology 45 (2006) 36-45.

U.G. Romanova, H.W. Yarranton, L.L. Schramm, W.E. Shelfantook, Investigation of oil sands froth treatment, The Canadian Journal of Chemical Engineering 82 (2004) 710-721.

M. Sababi, J. Kettle, H. Rautkoski, P.M. Claesson, E. Thormann, Structural and nanomechanical properties of paperboard coatings studied by peak force tapping atomic force microscopy, ACS Applied Materials & Interfaces 4 (2012) 5534-5541.

M. Sakaguchi, K. Laursen, H. Nakagawa, K. Miura, Hydrothermal upgrading of Loy Yang Brown coal-effect of upgrading conditions on the characteristics of the products, Fuel Processing Technology 89 (2008) 391-396.

N. Sanaie, A. Watkinson, B. Bowen, K. Smith, Effect of minerals on coke precursor formation, Fuel 80 (2001) 1111-1119.

R.T. Sánchez, E. Basaldella, J. Marco, The effect of thermal and mechanical treatments on kaolinite: Characterization by XPS and IEP measurements, Journal of Colloid and Interface Science 215 (1999) 339-344.

S. Saraji, L. Goual, M. Piri, Adsorption of asphaltenes in porous media under flow conditions, Energy & Fuels 24 (2010) 6009-6017.

M. Sasaki, Z. Fang, Y. Fukushima, T. Adschiri, K. Arai, Dissolution and hydrolysis of cellulose in subcritical and supercritical water, Industrial & Engineering Chemistry Research 39 (2000) 2883-2890.

T. Sato, T. Adschiri, K. Arai, G.L. Rempel, F.T. Ng, Upgrading of asphalt with and without partial oxidation in supercritical water, Fuel 82 (2003) 1231-1239.

T. Sato, T. Tomita, P.H. Trung, N. Itoh, S. Sato, T. Takanohashi, Upgrading of bitumen in the presence of hydrogen and carbon dioxide in supercritical water, Energy & Fuels 27 (2013) 646-653.

L.L. Schramm, E.N. Stasiuk, M. MacKinnon, Surfactants in Athabasca oil sands slurry conditioning, flotation recovery, and tailings processes, Cambridge University Press, Cambridge, 2000.

H.R. Schulten, P. Leinweber, Characterization of humic and soil particles by analytical pyrolysis and computer modeling, Journal of Analytical and Applied Pyrolysis 38 (1996) 1-53.

H.R. Schulten, P. Leinweber, New insights into organic-mineral particles: Composition, properties and models of molecular structure, Biology and Fertility of Soils 30 (2000) 399-432.

H.R. Schulten, P. Leinweber, B. Theng, Characterization of organic matter in an interlayer clay-organic complex from soil by pyrolysis methylation-mass spectrometry, Geoderma 69 (1996) 105-118.

D.L. Sedin, K.L. Rowlen, Adhesion forces measured by atomic force microscopy in humid air, Analytical Chemistry 72 (2000) 2183-2189.

T. Sekine, K. Yoshida, F. Matsuzaki, T. Yanaki, M. Yamaguchi, A novel method for preparing oil-in-water-in-oil type multiple emulsions using organophilic montmorillonite clay mineral, Journal of Surfactants and Detergents 2 (1999) 309-315.

A. Shah, R. Fishwick, J. Wood, G. Leeke, S. Rigby, M. Greaves, A review of novel techniques for heavy oil and bitumen extraction and upgrading, Energy & Environmental Science 3 (2010) 700-714.

P. Shah, D. Bhalodia, P. Shelat, Nanoemulsion: A pharmaceutical review, Systematic Reviews in Pharmacy 1 (2010) 24.

S.S. Shende, S. Pendharker, Z. Jacob, N. Nazemifard, Total internal reflection fluorescence microscopy to investigate the distribution of residual bitumen in oil sands tailings, Energy & Fuels 30 (2016) 5537-5546.

H. Shulha, A. Kovalev, N. Myshkin, V.V. Tsukruk, Some aspects of AFM nanomechanical probing of surface polymer films, European Polymer Journal 40 (2004) 949-956.

A. Shvarzman, K. Kovler, G. Grader, G. Shter, The effect of dehydroxylation/amorphization degree on pozzolanic activity of kaolinite, Cement and Concrete Research 33 (2003) 405-416.

M. Siskin, A.R. Katritzky, Reactivity of organic compounds in superheated water: General background, Chemical Reviews 101 (2001) 825-836.

J. Six, G. Guggenberger, K. Paustian, L. Haumaier, E. Elliott, W. Zech, Sources and composition of soil organic matter fractions between and within soil aggregates, European Journal of Soil Science 52 (2001) 607-618.

C. Snoeyink, S. Barman, G.F. Christopher, Contact angle distribution of particles at fluid interfaces, Langmuir 31 (2015) 891-897.

R.N. Sodhi, Time-of-flight secondary ion mass spectrometry (TOF-SIMS): Versatility in chemical and imaging surface analysis, Analyst 129 (2004) 483-487.

S.P. Sohi, N. Mahieu, J.R. Arah, D.S. Powlson, B. Madari, J.L. Gaunt, A procedure for isolating soil organic matter fractions suitable for modeling, Soil Science Society of America Journal 65 (2001) 1121-1128.

R.M.Š. Sokolovic, S.M. Sokolovic, Effect of the nature of different polymeric fibers on steady-state bed coalescence of an oil-in-water emulsion, Industrial & Engineering Chemistry Research 43 (2004) 6490-6495.

B. Sparks, L. Kotlyar, J. O'Carroll, K. Chung, Athabasca oil sands: Effect of organic coated solids on bitumen recovery and quality, Journal of Petroleum Science and Engineering 39 (2003) 417-430.

J. Środoń, V.A. Drits, D.K. McCarty, J.C. Hsieh, D.D. Eberl, Quantitative X-ray diffraction analysis of clay-bearing rocks from random preparations, Clays and Clay Minerals 49 (2001) 514-528.

D. Stanghelle, T. Slungaard, O.K. Sønju, Granular bed filtration of high temperature biomass gasification gas, Journal of Hazardous Materials 144 (2007) 668-672.

T. Stifter, E. Weilandt, O. Marti, S. Hild, Influence of the topography on adhesion measured by SFM, Applied and Environmental Microbiology 66 (1998) S597-S605.

M. Subramanian, Supercritical fluid extraction of oil sand bitumens from the Uinta basin, Utah, The University of Utah, 1996.

S. Subramanian, S. Simon, B. Gao, J. Sjöblom, Asphaltene fractionation based on adsorption onto calcium carbonate: Part 1. Characterization of sub-fractions and QCM-D measurements, Colloids and Surfaces A: Physicochemical and Engineering Aspects 495 (2016) 136-148.

R.C. Surdam, L.J. Crossey, E.S. Hagen, H.P. Heasler, Organic-inorganic interactions and sandstone diagenesis, AAPG Bulletin 73 (1989) 1-23.

D.M. Sztukowski, H.W. Yarranton, Characterization and interfacial behavior of oil sands solids implicated in emulsion stability, Journal of Dispersion Science and Technology 25 (2004) 299-310.

D.M. Sztukowski, H.W. Yarranton, Oilfield solids and water-in-oil emulsion stability, Journal of Colloid and Interface Science 285 (2005) 821-833.

D.E. Tambe, M.M. Sharma, Factors controlling the stability of colloid-stabilized emulsions: I. An experimental investigation, Journal of Colloid and Interface Science 157 (1993) 244-253.

K. Tanabe, M.R. Gray, Role of fine solids in the coking of vacuum residues, Energy & Fuels 11 (1997) 1040-1043.

K. Tekin, S. Karagöz, S. Bektaş, A review of hydrothermal biomass processing, Renewable and Sustainable Energy Reviews 40 (2014) 673-687.

B.K. Theng, K.R. Tate, P. Becker-Heidmann, Towards establishing the age, location, and identity of the inert soil organic matter of a spodosol, Journal of Plant Nutrition and Soil Science 155 (1992) 181-184.

C. Tien, S. Teoh, R. Tan, Cake filtration analysis−the effect of the relationship between the pore liquid pressure and the cake compressive stress, Chemical Engineering Science 56 (2001) 5361-5369.

F.M. Tiller, Tutorial: Interpretation of filtration data, I, Fluid/Particle Separation Journal 3 (1990) 85.

M.T. Timko, A.F. Ghoniem, W.H. Green, Upgrading and desulfurization of heavy oils by supercritical water, The Journal of Supercritical Fluids 96 (2015) 114-123.

J. Tisdall, J.M. Oades, Organic matter and water-stable aggregates in soils, Journal of Soil Science 33 (1982) 141-163.

E. Tombácz, M. Szekeres, Surface charge heterogeneity of kaolinite in aqueous suspension in comparison with montmorillonite, Applied Clay Science 34 (2006) 105-124.

L. Torres, R. Iturbe, M. Snowden, B. Chowdhry, S. Leharne, Preparation of o/w emulsions stabilized by solid particles and their characterization by oscillatory rheology, Colloids and Surfaces A: Physicochemical and Engineering Aspects 302 (2007) 439-448.

Y. Tu, D. Kingston, J. Kung, L.S. Kotlyar, B.D. Sparks, K.H. Chung, Adsorption of pentane insoluble organic matter from oilsands bitumen onto clay surfaces, Petroleum Science and Technology 24 (2006) 327-338.

I. Turcotte, S.A. Quideau, S.W. Oh, Organic matter quality in reclaimed boreal forest soils following oil sands mining, Organic Geochemistry 40 (2009) 510-519.

G. Vazquez, E. Alvarez, J.M. Navaza, Surface tension of alcohol water+water from 20 to 50°C, Journal of Chemical & Engineering Data 40 (1995) 611-614.

R. Veski, V. Palu, K. Kruusement, Co-liquefaction of kukersite oil shale and pine wood in supercritical water, Oil Shale 23 (2006) 236-249.

J. Vilcáez, M. Watanabe, N. Watanabe, A. Kishita, T. Adschiri, Hydrothermal extractive upgrading of bitumen without coke formation, Fuel 102 (2012) 379-385.

S. Wahyudiono, T. Shiraishi, M. Sasaki, M. Goto, Non-catalytic liquefaction of bitumen with hydrothermal/solvothermal process, The Journal of Supercritical Fluids 60 (2011) 127-136.

A. Walther, M. Hoffmann, A.H. Müller, Emulsion polymerization using Janus particles as stabilizers, Angewandte Chemie 120 (2008) 723-726.

C. Wang, M. Geramian, Q. Liu, D.G. Ivey, T.H. Etsell, Comparison of different methods to determine the surface wettability of fine solids isolated from Alberta oil sands, Energy & Fuels 29 (2015) 3556-3565.

H. Wang, C. Li, Z. Peng, S. Zhang, Characterization and thermal behavior of kaolin, Journal of Thermal Analysis and Calorimetry 105 (2011) 157-160.

K. Wang, B. Xing, Structural and sorption characteristics of adsorbed humic acid on clay minerals, Journal of Environmental Quality 34 (2005) 342-349.

S. Wang, Q. Liu, X. Tan, C. Xu, M.R. Gray, Study of asphaltene adsorption on kaolinite by X-ray photoelectron spectroscopy and time-of-flight secondary ion mass spectroscopy, Energy & Fuels 27 (2013) 2465-2473.

S. Wang, Q. Liu, X. Tan, C. Xu, M.R. Gray, Adsorption of asphaltenes on kaolinite as an irreversible process, Colloids and Surfaces A: Physicochemical and Engineering Aspects 504 (2016) 280-286.

S. Wang, N. Segin, K. Wang, J.H. Masliyah, Z. Xu, Wettability control mechanism of highly contaminated hydrophilic silica/alumina surfaces by ethyl cellulose, The Journal of Physical Chemistry C 115 (2011) 10576-10587.

J.A. Warner, B. Forsyth, F. Zhou, J. Myers, C. Frethem, G. Haugstad, Characterization of Pebax angioplasty balloon surfaces with AFM, SEM, TEM, and SAXS, Journal of biomedical materials research. Part B, Applied biomaterials 104 (2016) 470-475.

A. Weisenhorn, P. Maivald, H.J. Butt, P. Hansma, Measuring adhesion, attraction, and repulsion between surfaces in liquids with an atomic-force microscope, Physical Review B 45 (1992) 11226.

R. Wershaw, Model for humus in soils and sediments, Environmental Science & Technology 27 (1993) 814-816.

C.P. Whitby, H.K. Anwar, J. Hughes, Destabilising Pickering emulsions by drop flocculation and adhesion, Journal of Colloid and Interface Science 465 (2016) 158-164.

C.E. White, J.L. Provis, T. Proffen, D.P. Riley, J.S. van Deventer, Combining density functional theory (DFT) and pair distribution function (PDF) analysis to solve the structure of metastable materials: The case of metakaolin, Physical Chemistry Chemical Physics 12 (2010) 3239-3245.

C.E. White, J.L. Provis, T. Proffen, D.P. Riley, J.S. van Deventer, Density functional modeling of the local structure of kaolinite subjected to thermal dehydroxylation, The Journal of Physical Chemistry A 114 (2010) 4988-4996.

A.E. Wiącek, K. Dul, Effect of surface modification on starch/phospholipid wettability, Colloids and Surfaces A: Physicochemical and Engineering Aspects 480 (2015) 351-359.

I.A. Wiehe, A phase-separation kinetic model for coke formation, Industrial & Engineering Chemistry Research 32 (1993) 2447-2454.

G. Wolansky, A. Marmur, The actual contact angle on a heterogeneous rough surface in three dimensions, Langmuir 14 (1998) 5292-5297.

X. Wu, Investigating the stability mechanism of water-in-diluted bitumen emulsions through isolation and characterization of the stabilizing materials at the interface, Energy & Fuels 17 (2003) 179-190.

X. Xiao, L. Qian, Investigation of humidity-dependent capillary force, Langmuir 16 (2000) 8153-8158.

K. Xie, K. Karan, Kinetics and thermodynamics of asphaltene adsorption on metal surfaces: A preliminary study, Energy & Fuels 19 (2005) 1252-1260.

Y. Xu, T. Dabros, J. Kan, Filterability of oil sands tailings, Process Safety and Environmental Protection 86 (2008) 268-276.

L. Yan, A.H. Englert, J.H. Masliyah, Z. Xu, Determination of anisotropic surface characteristics of different phyllosilicates by direct force measurements, Langmuir 27 (2011) 12996-13007.

L. Yan, J.H. Masliyah, Z. Xu, Understanding suspension rheology of anisotropically-charged platy minerals from direct interaction force measurement using AFM, Current Opinion in Colloid & Interface Science 18 (2013) 149-156.

N. Yan, M.R. Gray, J.H. Masliyah, On water-in-oil emulsions stabilized by fine solids, Colloids and Surfaces A: Physicochemical and Engineering Aspects 193 (2001) 97-107.

N. Yan, J.H. Masliyah, Characterization and demulsification of solids-stabilized oil-in-water emulsions Part 1. Partitioning of clay particles and preparation of emulsions, Colloids and Surfaces A: Physicochemical and Engineering Aspects 96 (1995) 229-242.

N. Yan, J.H. Masliyah, Characterization and demulsification of solids-stabilized oil-in-water emulsions Part 2. Demulsification by the addition of fresh oil, Colloids and Surfaces A: Physicochemical and Engineering Aspects 96 (1995) 243-252.

Z. Yan, J.A. Elliott, J.H. Masliyah, Roles of various bitumen components in the stability of water-in-diluted-bitumen emulsions, Journal of Colloid and Interface Science 220 (1999) 329-337.

F. Yang, P. Tchoukov, E. Pensini, T. Dabros, J. Czarnecki, J. Masliyah, Z. Xu, Asphaltene subfractions responsible for stabilizing water-in-crude oil emulsions. Part 1: Interfacial behaviors, Energy & Fuels 28 (2014) 6897-6904.

K. Yano, A. Usuki, A. Okada, T. Kurauchi, O. Kamigaito, Synthesis and properties of polyimide–clay hybrid, Journal of Polymer Science Part A: Polymer Chemistry 31 (1993) 2493-2498.

H. Yarranton, D. Ortiz, D. Barrera, E. Baydak, L. Barré, D. Frot, J. Eyssautier, H. Zeng, Z. Xu, G. Dechaine, On the size distribution of self-associated asphaltenes, Energy & Fuels 27 (2013) 5083-5106.

Y.C. Yau, D.R. Peacor, E.J. Essene, J.H. Lee, L.C. Kuo, M.A. Cosca, Hydrothermal treatment of smectite, illite, and basalt to 460°C comparison of natural with hydrothermally formed clay minerals, Clays and Clay Minerals 35 (1987) 241-250.

D. Yeskis, A.K. Van Groos, S. Guggenheim, Dehydroxylation of kaolinite, American Mineralogist 70 (1985) 1-2.

T. Yoshida, C. Li, T. Takanohashi, A. Matsumura, S. Sato, I. Saito, Effect of extraction condition on “HyperCoal” production (2)−Effect of polar solvents under hot filtration, Fuel Processing Technology 86 (2004) 61-72.

T. Young, M. Monclus, T. Burnett, W. Broughton, S. Ogin, P. Smith, The use of the PeakForce^{TM} quantitative nanomechanical mapping AFM-based method for high-resolution Young's modulus measurement of polymers, Measurement Science and Technology 22 (2011) 125703.

X. Yu, N.A. Burnham, R.B. Mallick, M. Tao, A systematic AFM-based method to measure adhesion differences between micron-sized domains in asphalt binders, Fuel 113 (2013) 443-447.

A. Zahabi, M.R. Gray, T. Dabros, Kinetics and properties of asphaltene adsorption on surfaces, Energy & Fuels 26 (2012) 1009-1018.

P. Zemenová, A. Kloužková, M. Kohoutková, R. Král, Investigation of the first and second dehydroxylation of kaolinite, Journal of Thermal Analysis and Calorimetry 116 (2014) 633-639.

L. Zhang, L. Li, S. Chen, S. Jiang, Measurements of friction and adhesion for alkyl monolayers on Si (111) by scanning force microscopy, Langmuir 18 (2002) 5448-5456.

H. Zhao, S. Bhattacharjee, R. Chow, D. Wallace, J.H. Masliyah, Z. Xu, Probing surface charge potentials of clay basal planes and edges by direct force measurements, Langmuir 24 (2008) 12899-12910.

J. Zhao, Q. Liu, M.R. Gray, Characterization of fine solids in Athabasca bitumen froth before and after hydrothermal treatment, Energy & Fuels 30 (2016) 1965-1971.

L.Q. Zhao, Z.M. Cheng, Y. Ding, P.Q. Yuan, S.X. Lu, W.K. Yuan, Experimental study on vacuum residuum upgrading through pyrolysis in supercritical water, Energy & Fuels 20 (2006) 2067-2071.

C.C. Zhu, C. Ren, X.C. Tan, G. Chen, P.Q. Yuan, Z.M. Cheng, W.K. Yuan, Initiated pyrolysis of heavy oil in the presence of near-critical water, Fuel processing technology 111 (2013) 111-117.

W.A. Zisman, Relation of the equilibrium contact angle to liquid and solid constitution, contact angle, wettability, and adhesion, Advances in Chemistry Series 43 (1964) 1-51.